

10. SITE 878¹

Shipboard Scientific Party²

HOLE 878A

Date occupied: 28 June 1992
Date departed: 12 July 1992
Time on hole: 14 days, 1 hr, 30 min
Position: 27°19.143'N, 151°53.028'E
Bottom felt (rig floor, m; drill-pipe measurement): 1337.6
Distance between rig floor and sea level (m): 15.3
Water depth (drill-pipe measurement from sea level, m): 1323.2
Total depth (rig floor, m): 2247.6
Penetration (m): 910.0
Number of cores (including cores with no recovery): 98
Total length of cored section (m): 910.0
Total core recovered (m): 265.94
Core recovery (%): 25.5
Oldest sediment cored:
Depth (mbsf): 727.5
Nature: limestone
Age: early Aptian
Hard rock:
Depth (mbsf): 727.5
Nature: basalt
Measured velocity (km/s): 2.5–5.2

HOLE 878B

Date occupied: 2 July 1992
Date departed: 2 July 1992
Time on hole: 1 hr, 30 min
Position: 27°19.143'N, 151°53.028'E
Bottom felt (rig floor, m; drill-pipe measurement): 1337.6
Distance between rig floor and sea level (m): 15.3
Water depth (drill-pipe measurement from sea level, m): 1323.2
Total depth (rig floor, m): 1343.4
Penetration (m): 5.8
Number of cores (including cores with no recovery): 1
Total length of cored section (m): 5.8
Total core recovered (m): 0.62
Core recovery (%): 10.7
Oldest sediment cored:
Depth (mbsf): 5.8
Nature: limestone
Age: Albian

HOLE 878C

Date occupied: 2 July 1992
Date departed: 2 July 1992
Time on hole: 1 hr, 30 min
Position: 27°19.143'N, 151°53.028'E
Bottom felt (rig floor, m; drill-pipe measurement): 1337.6
Distance between rig floor and sea level (m): 15.3
Water depth (drill-pipe measurement from sea level, m): 1323.0
Total depth (rig floor, m): 1343.6
Penetration (m): 6.0
Number of cores (including cores with no recovery): 1
Total length of cored section (m): 6.0
Total core recovered (m): 0.5
Core recovery (%): 8.5
Oldest sediment cored:
Depth (mbsf): 6.0
Nature: limestone
Age: Albian

Principal results: A local pre-site seismic survey of Massachusetts Institute of Technology (MIT) Guyot was conducted to determine the location of Site 878. A vibration-isolated television (VIT) survey was conducted before the mini hard-rock guide base (HRB) was set on the seafloor in preparation for a bare-rock spud. Coring at Site 878 began on 29 June 1992 and was completed on 10 July 1992, after 11.4 days. Upon completion of the drilling, a logging program, including the geophysical and geochemical tool strings and the Formation MicroScanner tool (FMS), was undertaken. After obtaining our drilling objectives and logging Hole 878A, we departed Site 878 on 12 July 1992. When departing Site 878, we deployed the 200-in.³ water gun to obtain a southeast-northwest seismic profile over MIT Guyot and across the location of Site 878.

Site 878, near proposed Site MIT-1(E) is located at 27°19.143'N, 151°53.028'E in a water depth of 1323 m, on the northeastern part of MIT Guyot near its southern edge. The MIT Guyot is an isolated feature close to the Wake Group in the 18°–28°N guyot band. The objectives at Site 878 were (1) to examine the effects of emergence and possible karsting on the platform limestone cap; (2) to establish the stratigraphy and to examine the faunas and floras of the platform facies and its changes with time; (3) to examine the diagenesis of the platform limestones; (4) to determine the age and causes of platform drowning, emergence, and subsidence history relative to sea level; (5) to establish the age and paleolatitude of the volcanic edifice; and (6) to obtain geochemical data from the volcanic edifice for comparison with other sites and the DUPAL/SOPITA anomaly.

Three holes were drilled at Site 878. Hole 878A was a multiple reentry hole; Holes 878B and 878C were single-core holes, used for the purpose of recovering the surficial hardground and pelagic sediment overlying the carbonate platform. Hole 878A was primarily cored with the rotary core barrel (RCB) to 910 mbsf total depth (TD); a Syndax diamond coring bit (DCB) was used from about 200 to 400 mbsf rather than the conventional roller-cone bit. In the upper 202 m, the average core recovery was 3.9%; however, if the first core that contains some pelagic ooze is excluded, average recovery drops to 2.29%. When coring with the DCB, recovery of

¹ Premoli Silva, I., Haggerty, J., Rack, F., et al., 1993. *Proc. ODP, Init. Repts.*, 144: College Station, TX (Ocean Drilling Program).

² Shipboard Scientific Party is as given in the list of participants preceding the contents.

the carbonate platform remained low, averaging 2.26%. The RCB coring of polymictic breccia yielded a core recovery of nearly 100%. Beneath the polymictic breccia, RCB coring was continued. Recovery of the lower platform limestone unit was about 6.5%, whereas recovery in the basalt averaged 54.7%. The recovered material included foraminifer nanofossil ooze to nanofossil ooze with manganese nodules from 0 to 3.2 mbsf; platform limestone from 3.2 to 399.7 mbsf; bluish gray clay and breccias with basalt and limestone clasts from 399.5 to 604 mbsf; platform carbonates from 604 to 722.5 mbsf; and basalt from 722.5 to 910 mbsf.

Six lithologic units were recognized at Site 878 using a combination of visual core descriptions, smear slide and thin-section data, and downhole logging data. The age of these units was based mainly on the identification of calcareous nanofossils and planktonic foraminifers in the pelagic cap as well as on larger benthic foraminifers and calcareous plankton in the platform limestone. The recognized units are from top to bottom:

Unit I (0–3.2 mbsf) consists of yellowish brown foraminifer nanofossil ooze and nanofossil ooze with manganese nodules of early Pleistocene to late Miocene age. The average carbonate content in Unit I is 70.6%. This unit is divided into three subunits on the basis of the paucity of planktonic foraminifers, the presence of chalk fragments in the intermediate subunit, and the abundance of manganese nodules and crusts in the lowermost subunit. These nodules range from submillimeter size to 5 cm. The manganese nodules and crust fragments contain phosphatized pelagic limestone fragments of latest Albian, Santonian-Campanian, late Paleocene, and early Eocene age. In addition to the abundance of manganese nodules, the insoluble residue yielded zeolites, sand-sized quartz grains, volcanic ash, goethite and hematite, and very rare marcasite. The pelagic sediment was highly disturbed; however, a disconformity spanning the early Pliocene was detected.

Unit II (3.2–236 mbsf) consists of white micritized, gastropod-rich wackestone, packstone, and mudstone; peloidal packstone with fenestral fabric; peloid-algal wackestone; and minor grainstone and rudstone of Albian to Aptian(?) age. Skeletal components in the unit include nerineid gastropods and oysters, benthic foraminifers (agglutinants, miliolids, and a few encrusting forms), and rare corals and sponge spicules. The carbonate content of Unit II is virtually 100%. Porosity varies between 7% and 15%, and is mainly moldic and intergranular in the wackestone. Grains are cemented by bladed, fine- to medium-crystalline calcite. Some fossil molds are lined by similar calcite crusts or contain geopetal sediment. Porosity increases to 25% and becomes interparticle in the grainstones. Unit II is divided into four subunits on the basis of depositional texture and variations in skeletal constituents. Subunit IIA is wackestone (with molds of nerineids) and peloidal packstone. Subunit IIB is characterized by the presence of peloids and fenestral fabrics. Subunit IIC contains gastropod-rich upper horizons and oyster-rich lower horizons. Subunit IID is characterized by mudstone coarsening upward to medium sand-sized grainstone.

Unit III (236–399.7 mbsf) primarily consists of very pale brown grainstone of fine to medium grain size, wackestone, and mudstone of late Aptian age. The carbonate content is nearly 100%. Unit III is divided into three subunits on the basis of its depositional texture and variations in the skeletal constituents. Subordinate lithologies of this unit include skeletal rudstone containing rudist, coral, and calcisponge fragments in Subunit IIIA; *Orbitolina*-rich skeletal grainstone of coarse grain size at the base of Subunit IIIB; and well-lithified skeletal foraminifer wackestone and mudstone in Subunit IIIC. These subunits display a subtle overall trend of decreasing density and increasing porosity with depth; the highest porosity (up to 40%) of this unit is in the grainstone.

Unit IV (399.7–604.3 mbsf) consists primarily of polymictic breccia with both basalt and platform limestone clasts in a white to grayish green matrix of late to possibly early Aptian age. This unit is normally magnetized with a mean inclination probably acquired at 20°S during the Aptian. Unit IV is divided into three subunits. Subunit IVA is a thin bed of bluish gray clay (max. 1.5% CaCO₃); Subunit IVB is polymictic breccia with an ash tuff bed at the top, and Subunit IVC is a polymictic breccia with steeply inclined beds, as well as slump and fluid-escape structures. Each of the two lower subunits grades from a carbonate-rich (lithoclasts and matrix), matrix-supported breccia at the bottom, to basalt-rich, clast-supported

breccia at the top. In both Subunits IVB and IVC, the carbonate content varies from 80% at the bottom to <40% at the top. In each breccia subunit, porosity linearly increases from about 20% at the bottom to 36% at the top; an equivalent decrease in sonic velocity occurs from 4.0 to 2.5 km/s over the same interval in each subunit.

The most common carbonate lithoclasts in this unit are mudstone and wackestone with miliolids. Less common lithoclasts are skeletal-peloidal wackestone and packstone, oolitic grainstone, mollusk-peloid wackestone, peloid grainstone, fenestral wackestone and packstone, and mudstone with sponge spicules. Nerineids are the most abundant macrofossils in the limestone clasts, along with rudist debris, corals, and algal-bacterial thrombolites as less common components.

Volcanic clasts, with the exception of the large basalt ones, are replaced by clay minerals; however, they retain well-preserved relict igneous textures. Three major types of basalt clasts are present: (1) scoriaceous basalt; (2) much less vesicular, microcrystalline basalt, or sometimes olivine microphyric basalt; and (3) nonvesicular basalt. Other volcanic clast types are altered, highly vesicular fragments of basalt with elongate vesicles, and altered clasts of basalt with a pumice-like texture; both types are abundant at the top of the breccia. Finally, four minute clasts of black, organic-rich material were found in the breccia.

Unit V (604.3–722.5 mbsf) consists of very pale brown skeletal grainstone, packstone, and wackestone with minor rudstone rich in nerineids, oysters, and corals of early Aptian age. This unit is mainly normally magnetized, but a reversal interval is apparently present and may correlate with Chron M0 of early Aptian age. Carbonate content is nearly 100%. Measured porosity values vary between 16% and 38%, and sonic velocity ranges from 2.2 to 4.4 km/s.

Unit V is divided into two subunits on the basis of texture and composition. Subunit VA consists of peloid foraminifer wackestone to grainstone with intervals of gastropod, oyster, and coral rudstone and some stromatoporoid boundstone. Subunit VB is composed of coarse-grained skeletal grainstone with subordinate mollusk and coral rudstone. A few highly altered basalt fragments occur near the base of this subunit; the lowermost grainstone is poorly sorted and stained reddish yellow.

The upper subunit contains peloids, miliolids, mollusks, small gastropod molds, red algae, calcisponge fragments, and a few ooid grains and lithoclasts; some fenestral fabric is present in the wackestones. Within Subunit VA, there appears to be two coarsening-upward cycles. The grainstone has up to 35% porosity, which is present as predominantly interparticle and some moldic porosity; the packstone has 5%–15% porosity as interparticle, moldic, and vuggy.

The majority of grains in Subunit VB are rounded and coated by micrite up to 200 μm thick. Skeletal constituents include red algae, codiaceans, calcisponges, corals, and stromatoporoids; molds of small gastropods are also present. Planktonic foraminifers and nanofossils occur in the lowermost part of the unit. Cement in the grainstone is patchily distributed, and porosity ranges from 20% to 35%; it is mostly primary interparticle porosity.

Unit VI (722.5–908.7 mbsf) consists of alkalic basalt flows and flow-top breccias of older than early Aptian age. Thirty-four igneous units were identified, including 24 distinct lava flows, 3 volcanoclastic units, and 2 weathering horizons. The remaining units are basalt breccias or intervals of undifferentiated, fragmented, and altered material. At least one reversed polarity interval and one normal polarity interval are recorded in Unit VI. The lower reversed polarity interval is at least as old as Chron M1, but it may represent an earlier reversed polarity interval of the Lower Cretaceous. The mean inclination of the basalt unit indicates that basement rocks acquired their magnetization at about 10°S during the Barremian.

Almost all the lava flows have well-defined vesicular and/or brecciated flow tops that grade downward into massive basalt. The flow tops are reddish or purplish in color and are altered to clay. The majority of vesicles are filled by white or pale to dark green clay. Preliminary petrographic examination suggests that all the lavas are of alkalic affinity, including basanite, alkali olivine basalt, and hawaiite. Several volcanoclastic units occur among the basalt flows. Of these, Units 4 and 9 are altered tuffs that appear to have been composed of a poorly sorted variety of vesicular and nonvesicular basalts in a finer matrix of uncertain composition. Igneous

Unit 31 is a thick (15.5 m recovered), highly altered vitric tuff, originally composed of angular, irregular, highly vesicular glassy clasts in a matrix of more finely divided glassy material. The upper 7.5 m of Igneous Unit 31 has been severely altered (bleached) to light beige clay, and the remainder is brick red in color and more lithified.

BACKGROUND AND OBJECTIVES

The Massachusetts Institute of Technology (MIT) Guyot is an isolated feature close to the Wake Group in the 18°–28°N guyot band. This guyot is interpreted to be a drowned atoll; on the basis of dredge hauls and geophysical data, the seismic facies were interpreted as a perimeter reef encircling a thick sequence of lagoonal sediments (Winterer et al., in press). The MIT Guyot probably formed on normal lithosphere in the south-central part of the Pacific at about the location of the so-called South Pacific Superswell (McNutt and Fischer, 1987; Winterer et al., in press). This guyot lies on the M29 magnetic lineation, the oldest identified in the northwestern sector of the western Pacific (Nakanishi et al., 1992a, 1992b). According to Sager et al. (in press), MIT Guyot has a magnetization that is relatively weak, partly induced, and complex. It is one of the few guyots that has a reversed polarity; this indicates that it either formed before or after the Cretaceous Long Normal at a paleolatitude of 32°S. The radiometric age of the dredged basalt is 120.3 ± 0.8 Ma (Sager et al., in press).

Using paleomagnetic and plate tectonic reconstructions backtracking MIT Guyot, Winterer et al. (in press) hypothesized that this 120-Ma (Aptian) feature rotates back to near the present-day Society Hotspot and has a depth anomaly of about 600–800 m. This depth anomaly is about 250 m smaller than the anomaly associated with present-day Tahiti (Winterer et al., in press). The elastic plate thickness beneath the northwest Pacific seamounts is less than 15 km, a figure much less than the normal thickness of oceanic lithosphere but consistent with the hypothesis that these seamounts were located on the Darwin Rise Superswell during mid-Cretaceous time. MIT Guyot was potentially built over the Darwin Rise during the oldest of three constructional volcanic episodes around 123 Ma (Winterer et al., in press). Subsequent to the volcanic constructional phase of the MIT edifice, a carbonate platform developed, possibly formed an atoll with rudist coral reefs on the perimeter, and surrounded a lagoon. Other guyots that are interpreted to have formed during late Barremian–Aptian times appear from the geophysical records to have an 800-m-thick carbonate sequence. At the close of the Albian, many of these Barremian–Aptian carbonate platforms and reefs, as well the younger ones constructed in the Albian, may have been uplifted above sea level (Winterer et al., in press). This period of uplift is required if the rough surface topography of several guyots, including MIT Guyot, is interpreted to be the result of karstification (van Waasbergen and Winterer, in press).

In addition, Winterer et al. (in press) propose that the period of uplift before the final drowning may have been caused by a major plate reorganization and a shift in the direction of plate motion from west-northwest to north-northwest in the hotspot frame of reference. The timing of these events corresponds to the time of emplacement of the Wake Seamounts and the inception of the Marshall Islands seamount chain. On the basis of geophysical models, Winterer et al. (in press) have suggested that MIT Guyot has undergone uplift and karsting of the summit region at approximately 95 Ma.

The summit surface of MIT Guyot has a rough topography, which was mapped by a Sea Beam survey during the 1988 Roundabout Leg 10 expedition of the *Thomas Washington*. On the basis of the morphologic features, the surface topography of MIT Guyot was interpreted to have formed by karstification. Some circular doline-like depressions are 500 m in diameter and more than 180 m deeper than the surrounding summit level. The floors of these depressions do not exhibit a surface connection to the flank of the guyot. Small terraces break the slopes; these are interpreted by van Waasbergen and Winterer (in press) as evidence of wave erosion during a relative lowstand of sea level.

Single-channel seismic profiles collected during the 1988 cruise by *Thomas Washington* (Roundabout Leg 10) show layered lagoonal sediments with a rough topography at the sediment-water interface. A prominent reflector at approximately 2.4 s two-way traveltime (TWT) is the acoustic basement reflector. Along the edge of the guyot, the profile displays topographic highs that may be interpreted as constructional carbonate features, potentially reefs, on the basis of the seismic subsurface characteristics. No pelagic cap appears to be present.

Drilling plans for MIT Guyot included only one lagoonal site (proposed Site MIT-1-E). The scientific objectives at Site 878 were (1) to determine the genesis of the rough surface topography in relation to the hypothesis of emergence and karsting of the platform limestone before the final drowning; (2) to establish the stratigraphy and examine the faunas and floras of the platform facies and changes with time; (3) to examine the diagenesis of the platform limestones compared to the younger carbonate platforms drilled in the Marshall Islands guyots; (4) to determine the age and causes of platform drowning, possible emergence, and subsidence history of the platform limestone relative to sea level; (5) to establish the age and paleolatitude of the volcanic edifice; and (6) to obtain geochemical data from the volcanic edifice for comparison with other sites and the DUPAL/SOPITA anomaly.

Drilling at Site 878 on MIT Guyot recovered a thin sequence of pelagic sediments, two carbonate platform sequences divided by a volcanic-limestone breccia, and a portion of the igneous edifice. The primary objectives of this site are addressed by the preliminary shipboard studies and additional shore-based studies.

OPERATIONS

Transit to Site 878

At an average speed of 11.8 kt, the first way point for the seismic survey of Site 878 was reached by 1330L (L = local time), 28 June 1992, to end the 568-nmi transit from Hole 801C. The 200-in.³ water gun was streamed and the guyot was approached from the south. The local pre-site seismic survey included a north-south crossing as well as an east-west crossing over the northeastern portion of the guyot, and an additional crossing over the proposed site before the ship turned to a reciprocal course and launched a beacon. The 3.5-kHz echo-sounder profiles showed no acoustically transparent pelagic sediment.

The 4.5 hr required for the survey of 31 nmi was used to position the hard-rock guide base (mini-HRB) on the moon-pool doors, suspend it from the traveling block by means of a double-jay running tool (“J” tool), complete its construction, and begin filling its ballast tanks with bulk barite. After the beacon drop, the vessel continued on the final leg of the survey for about 1.5 nmi before the seismic gear was retrieved. The ship returned to the drop site, the hydrophones and thrusters were lowered, and ballasting of the HRB continued.

Hole 878A

With the ship stationary over the beacon, the moon-pool doors were opened and the HRB was lowered partially into the moon pool for the final stages of ballasting. An acoustic “tilt beacon” was attached to the rim of the cone for the purposes of positioning the vessel and monitoring the attitude of the HRB relative to level. At 2000L, 28 June 1992, the HRB was lowered into the water and the pipe trip began.

The final process of lowering the HRB to the seafloor was accomplished with the top drive in the string, the motion compensator engaged, and the VIT positioned a few meters above the HRB so that sonar could be used to determine the character of the seafloor. The sonar presentation indicated that the seafloor was relatively level and smooth beneath the HRB; therefore, no additional offsetting was done before the HRB was lowered.

Just before contact was made by the legs of the base, a major hydraulic leak was discovered in the coaxial winch, which prevented

the VIT from being moved. While troubleshooting of the leak was in progress, the HRB was landed and the tilt beacon was monitored for any change in angle as the weight of the HRB was gradually applied. The angle of landing remained at about 5° as additional weight was applied. When the coaxial winch again became operational, the VIT was lowered for better viewing, the full 72,000-lb weight of the HRB was set down, and the "J" tool was released.

When the drill string had swung away from the glare of the reentry cone and base, the underwater TV could be used to survey the seafloor. A brief reconnaissance of the surrounding seafloor was undertaken. The immediate area was exceptionally flat and smooth, except for a rubbly slope a few meters east that rose 4 or 5 m to another flat bench. The location of the base appeared to be ideal for spudding, and the option of reentering it and transporting it to a more suitable site was deemed unnecessary.

The drill string and VIT were recovered to change the bottom-hole assembly (BHA). The BHA was similar to those used for earlier bare-rock spuds, except that a stabilized bit sub was installed, along with a stabilizer just above the outer core barrel (OCB) assembly. During the round trip, about 4.5 hr after the base had been set, the reading of the tilt beacon suddenly increased from about 5° to about 13°.

The HRB was reentered routinely and the bit tagged the seafloor at 1337.6 m from driller's datum or 1323 m below sea level, confirming the depth noted when the HRB was set down. No visual indication of any shifting or "punch-through" of the base was present. While the motion compensator kept the bit in contact with the seafloor, the VIT was recovered to the surface.

Hole 878A was spudded at 1100L on 29 June 1992. Even with minimum weight on bit, slow rotation, and a low circulation rate, a fairly rapid penetration rate was achieved from the seafloor to about 3.5 mbsf; however, a slower penetration rate occurred as the bit encountered harder material for the remaining 6 m of the core interval. Upon recovery, the first core barrel contained nearly 3 m of pelagic ooze and a small amount of limestone, which was jammed in the core catcher.

Coring with the RCB then continued through platform limestone, with poor core recovery (average 3.9%; see Table 1). Mud sweeps were regularly used in an attempt to keep the hole clean. Below about 40 mbsf, the familiar pattern of increased rate of penetration (ROP) and decreased core recovery returned. There was no indication that the 9¹³/₁₆-in. stabilizers above and below the OCB had any effect, positive or negative, on coring performance, and there were no torquing or sticking tendencies. By 200 mbsf, average recovery had decreased to about 2.29%. This exceptionally low recovery rate prompted us to change from a C3 cone-bit to a Syndax DCB in the hope that recovery would be improved. The round trip/reentry for bit change was made when total depth had reached 202.2 mbsf and the Rock Bit International (RBI) C-3 bit had accrued only 11.25 hr of rotation.

The round trip was routine except that about 1.5 hr were required to make up the nine 6³/₄-in. drill collars comprising the DCB BHA above the stabilized 6³/₄-in. DCB outer core barrel assembly. The HRB was readily located with the sonar and quickly brought into TV range by automatic station keeping (ASK) offsets. The near-dead-center reentry stab was made after about 15 min of maneuvering.

A clean hole was found to about 35 m above total depth, at which point a bridge had formed. The top drive was picked up and the bridge was cleared easily. When the Syndax DCB bit was in position, an inner barrel was dropped. The initial DCB core of 4.7 m was cut with minimum weight, circulation, and revolutions per minute (RPM) to "break in" the bit. The core barrel was recovered with 10 cm of grainstone core and nearly an equal amount of graphite, cored from the expendable cap that was installed to protect the bit from contact with the HRB.

The second core, cut while using more aggressive drilling parameters, also contained two pieces of core from the graphite cap, which again was nearly as much as the limestone recovered. That set the pattern for performance in the friable carbonates below. Core recovery and penetration rate were not significantly different when using

the DCB than they were when using the RCB system in the interval above. Overall progress was slower than with the RCB because the low coring circulation rates required the use of mud sweeps to clean cuttings from the large upper portion of the hole. The mud sweeps had to be circulated out for several minutes after each core was cut. Weight control was difficult because of vessel heave reaching ±1 m from swells generated by Typhoon Bobbie passing several hundred miles to the west. Holding 10,000 lb of weight on bit sometimes meant fluctuations from 4,000 to 16,000 lb.

At 404 mbsf, circulating pressure suddenly increased by about 200 psi and the ROP dropped sharply, indicating either a marked change in lithology or bit failure. After about 1 m had been penetrated under the new parameters, the core was recovered. The core liner contained the usual few pieces of limestone and one small piece of blue-green clay at the bottom. As the changes were determined to be formation related, coring continued. At the earlier sites, clays underlying the limestone sections had been only a few meters thick and had rested upon either basalt or volcanoclastic sediments. The plan was to core through the clay and sample the underlying lithology before tripping for the RCB BHA and continuing. The uppermost clay was poorly recovered, but it apparently was no more than 3 m thick. About 22 m of volcanoclastic breccia then were cored with fairly good recovery before coring was interrupted for the trip. Coring with the DCB system did not improve recovery of the platform limestones; recovery averaged 2.26% in 203 m of limestone.

Hole 878B

During the trip back to the seafloor with the RCB BHA, a 20-m ASK offset to the west was entered. A single-core hole was drilled from the seafloor to the top of the limestone in an attempt to recover pelagic ooze. The seafloor contact was noted on the weight indicator and about 5 m of soft material were penetrated before hard drilling signaled the limestone interface. After another 0.5 m had been cored, the core barrel was recovered. Unfortunately, a considerable quantity of manganiferous crust was packed into the liner above several pieces of hard limestone core. The crust had apparently jammed off sufficiently to prevent entry of any of the soft ooze and then was displaced by the limestone core.

Hole 878C

The failure to recover soft sediment in the seafloor core was attributed to a manganese crust that was better developed at Hole 878B than at the location of the HRB. The seafloor had been videotaped only to the west and east of the HRB; the outcrops began only a few meters east of the HRB. The best chance of a "window" in the crust was considered to be between Hole 878B and the HRB. An ASK offset of 6 m east was entered to put Hole 878C about 14 m west of Hole 878A. The same procedures were followed as for Hole 878B, with nearly identical results. Manganese crust was recovered, along with some limestone and no mud. No more time was allowed for the sediment-recovery attempt and preparations for reentry into Hole 878A were begun.

Continuation of Hole 878A

Hole 878A was successfully reentered with the help of the VIT at 0330L on 3 July 1992. After an apparently routine reentry, the bit met an obstruction at only 3.5 mbsf. The obstacle was quickly diagnosed as a ledge formed at the ooze/limestone interface. It was necessary to lower the VIT back to reentry depth and to make small offsets of the ship while the pipe repeatedly was raised and lowered onto the ledge. Eventually, after about 0.5 hr of effort, the drill string lined up vertically with the hole and the second stage of reentry was accomplished.

The 9⁷/₈-in. RCB bit was run into the hole to just above the point where coring had begun with the 7¹/₄-in. DCB bit. An inner core barrel

Table 1. Coring summary, Site 878.

Core no.	Date (1992)	Time (Z)	Depth (mbsf)	Cored (m)	Recovered (m)	Recovery (%)
144-878A-						
1R	29 June	0405	0-9.5	9.5	3.53	37.1
2R	29 June	0555	9.5-19.0	9.5	0.28	3.0
3R	29 June	0820	19.0-28.5	9.5	0.70	7.4
4R	29 June	0950	28.5-38.0	9.5	0.74	7.8
5R	29 June	1040	38.0-47.6	9.6	0.07	0.7
6R	29 June	1130	47.6-57.3	9.7	0.23	2.4
7R	29 June	1230	57.3-67.0	9.7	0.30	3.1
8R	29 June	1330	67.0-76.6	9.6	0.29	3.0
9R	29 June	1455	76.6-86.2	9.6	0.23	2.4
10R	29 June	1605	86.2-95.9	9.7	0.15	1.5
11R	29 June	1700	95.9-105.5	9.6	0.03	0.3
12R	29 June	1825	105.5-115.1	9.6	0.21	2.2
13R	29 June	1930	115.1-124.8	9.7	0.20	2.1
14R	29 June	2040	124.8-134.4	9.6	0.10	1.0
15R	29 June	2150	134.4-144.0	9.6	0.21	2.2
16R	29 June	1650	144.0-153.7	9.7	0.11	1.1
17R	29 June	2350	153.7-163.4	9.7	0.00	0.0
18R	30 June	0105	163.4-173.1	9.7	0.32	3.3
19R	30 June	0215	173.1-182.8	9.7	0.12	1.2
20R	30 June	0310	182.8-192.5	9.7	0.02	0.2
21R	30 June	0420	192.5-202.2	9.7	0.11	1.1
23M	30 June	1630	206.9-216.6	9.7	0.12	1.2
24M	30 June	1750	216.6-226.3	9.7	0.07	0.7
25M	30 June	1915	226.3-235.9	9.6	0.03	0.3
26M	30 June	2035	235.9-245.6	9.7	0.26	2.7
27M	30 June	2155	245.6-255.2	9.6	0.00	0.0
28M	30 June	2320	255.2-264.9	9.7	0.10	1.0
29M	1 July	0040	264.9-274.5	9.6	0.09	0.9
30M	1 July	0200	274.5-284.1	9.6	0.37	3.9
31M	1 July	0315	284.1-293.4	9.3	0.40	4.3
32M	1 July	0430	293.4-302.9	9.5	0.00	0.0
33M	1 July	0530	302.9-312.6	9.7	0.21	2.2
34M	1 July	0645	312.6-322.2	9.6	0.32	3.3
35M	1 July	0800	322.2-331.9	9.7	0.14	1.4
36M	1 July	0905	331.9-341.6	9.7	0.91	9.4
37M	1 July	1015	341.6-351.2	9.6	0.32	3.3
38M	1 July	1120	351.2-360.9	9.7	0.17	1.8
39M	1 July	1230	360.9-370.5	9.6	0.43	4.5
40M	1 July	1350	370.5-380.2	9.7	0.00	0.0
41M	1 July	1515	380.2-389.8	9.6	0.08	0.8
42M	1 July	1650	389.8-399.3	9.5	0.21	2.2
43M	1 July	1830	399.3-406.0	6.7	0.27	4.0
44M	1 July	2000	406.1-408.9	2.8	2.57	91.8
45M	1 July	2220	408.9-418.5	9.6	4.46	46.4
46M	1 July	0040	418.5-428.2	9.7	1.56	16.1
47R	3 July	0340	428.2-435.5	7.3	1.92	26.3
48R	3 July	0535	435.5-445.1	9.6	1.72	17.9
49R	3 July	0845	445.1-454.8	9.7	3.35	34.5
50R	3 July	1205	454.8-464.4	9.6	3.59	37.4
51R	3 July	1515	464.4-474.1	9.7	8.18	84.3
52R	3 July	1850	474.1-483.7	9.6	3.22	33.5
53R	3 July	2245	483.7-493.2	9.5	5.71	60.1
54R	4 July	0345	493.2-502.4	9.2	8.81	95.7
144-878A- (cont.)						
55R	4 July	0920	502.4-511.9	9.5	9.79	103.0
56R	4 July	1310	511.9-521.2	9.3	9.16	98.5
57R	4 July	1705	521.2-530.4	9.2	8.34	90.6
58R	4 July	2255	530.4-540.1	9.7	9.51	98.0
59R	5 July	0310	540.1-549.8	9.7	8.92	91.9
60R	5 July	0650	549.8-559.2	9.4	8.55	90.9
61R	5 July	0945	559.2-568.7	9.5	8.65	91.0
62R	5 July	1310	568.7-578.1	9.4	8.88	94.4
63R	5 July	2215	578.1-587.6	9.5	9.31	98.0
64R	6 July	0955	587.6-597.1	9.5	9.96	105.0
65R	6 July	1400	597.1-606.6	9.5	7.27	76.5
66R	6 July	1520	606.6-616.3	9.7	0.31	3.2
67R	6 July	1710	616.3-625.9	9.6	0.67	7.0
68R	6 July	1840	625.9-635.6	9.7	0.39	4.0
69R	6 July	1950	635.6-645.2	9.6	0.29	3.0
70R	6 July	2115	645.2-654.9	9.7	0.43	4.4
71R	6 July	2220	654.9-664.6	9.7	1.05	10.8
72R	6 July	2350	664.6-674.2	9.6	0.20	2.1
73R	7 July	0115	674.2-683.9	9.7	0.40	4.1
74R	7 July	0230	683.9-693.5	9.6	0.34	3.5
75R	7 July	0400	693.5-703.0	9.5	1.45	15.2
76R	7 July	0520	703.0-712.5	9.5	1.02	10.7
77R	7 July	0640	712.5-722.1	9.6	0.37	3.9
78R	7 July	0915	722.1-731.7	9.6	1.90	19.8
79R	7 July	1445	731.7-741.4	9.7	5.68	58.5
80R	7 July	1930	741.4-751.0	9.6	7.02	73.1
81R	7 July	2255	751.0-760.7	9.7	6.68	68.8
82R	7 July	0100	760.7-770.4	9.7	1.96	20.2
83R	8 July	0335	770.4-779.9	9.5	4.35	45.8
84R	8 July	0725	779.9-789.3	9.4	7.62	81.0
85R	8 July	1135	789.3-798.7	9.4	5.39	57.3
86R	8 July	1455	798.7-808.2	9.5	3.00	31.6
87R	8 July	2040	808.2-817.9	9.7	1.44	14.8
88R	8 July	2340	817.9-827.6	9.7	3.36	34.6
89R	9 July	0455	827.6-837.2	9.6	5.76	60.0
90R	9 July	0855	837.2-846.5	9.3	7.34	78.9
91R	9 July	1340	846.5-856.2	9.7	7.36	75.9
92R	9 July	1700	856.2-865.7	9.5	6.88	72.4
93R	9 July	1955	865.7-875.4	9.7	3.88	40.0
94R	9 July	2230	875.4-885.0	9.6	10.05	104.7
95R	10 July	0135	885.0-894.4	9.4	6.16	65.5
96R	10 July	0655	894.4-903.9	133.4	0.72	0.5
97R	10 July	1030	903.9-910.0	6.1	3.59	58.8
98R	10 July	1340	903.9-910.0	6.1	3.59	58.8
Coring totals				1043.3	265.94	25.5
144-878B-						
1R	2 July	1145	0-5.8	5.8	0.62	10.7
Coring totals				5.8	0.62	10.7
144-878C-						
1R	2 July	1340	0-6.0	6.0	0.51	8.5
Coring totals				6.0	0.5	8.5

was pumped into place and reaming of the hole began. Reaming of the interval from 202 to 428 mbsf proceeded smoothly, averaging 41 m/hr. About 9 m of "hard" fill in the bottom of the hole had to be drilled and washed out of the hole with mud. The "wash barrel" then was pulled (empty) and continuous RCB coring resumed.

The drilling in the polymictic breccia was much slower, but it produced the best core recovery and hole conditions of the entire leg. The 159.3 m of the bit run produced an average core recovery of 73.7% at an average ROP of 3.6 m/hr. Total rotating hours, including Holes 878B and 878C and the reamed interval, reached 51 hr after Core 144-878A-63R, and the drill string was tripped for a change of bit.

Upon recovery, the bit was found to be in excellent condition, with all bearing seals effective and negligible wear to the cutting structure and body. An identical bit was selected for the ensuing run and the new bit, preassembled to a second mechanical bit release (MBR), was attached to the BHA. One drill collar was added to the BHA to provide the option of using additional weight on bit (WOB) in the expected basement rocks.

After a 9-min dynamic positioning (DP) offset move, reentry was again made. The bit stopped on the ledge that had halted the previous reentry just below the HRB; the hole was found after only one pick-up and lowering of the string, however. The hole was clean to about 53 m

above total depth, at which point a minor bridge was knocked out. About 35 m of apparently fine hole fill had to be washed out of the hole with top drive circulation before the bit reached total depth. This indicated that a considerable interval of the large-diameter hole was allowing cuttings that were dislodged during the trip into Hole 878A to accumulate.

In Core 144-878A-64R, the same polymictic breccia yielded 100% recovery, but the rate of coring was only about 2.2 m/hr. A drilling break near the end of Core 144-878A-65R was found to represent limestone, and the typical pattern of high ROP/low recovery returned. After about 123 m of carbonate platform sediments had been penetrated, basaltic rocks were reached at about 727 mbsf. The lower carbonate section produced an average ROP of 21 m/hr and an average core recovery of 6.5% (see Table 1).

Hole problems started shortly after cutting began on the first full basalt core. Although the hole had been clean after the previous core, a sudden influx of cuttings or other material loaded the annulus and began "packing off" around the drill string. When the bit was lifted off bottom, the problem became worse and the string began sticking. A 20-bbl viscous mud sweep was circulated and the pipe was freed after about 1 hr; circulating pressure remained high, however, as coring resumed. When the bit was again lifted in preparation for

retrieval of the core, the sticking and packing-off tendencies returned. A sweep of extra-viscosity prehydrated bentonite mud was circulated at an increased pump rate and parameters returned to normal.

The initial hole-cleaning problems were attributed either to a hole collapse from an unstable interval of the lower carbonate sequence, or to an accumulation of cuttings from the seafloor. The difficulty in clearing the hole suggested that large particles were falling into the hole from the unstable interval; however, problems related to the basaltic "basement" rocks began almost immediately.

The basalt flow units were interbedded with horizons of altered volcanoclastic rocks and clays. Some of the clayey material was highly indurated and waxy, making it extremely difficult to drill with the tungsten-carbide insert bit. Some of the clays also proved to be unstable and water sensitive. The basalt was fractured, which caused core-jamming problems.

A short "wiper trip" was necessary to replace the knobby drilling joints after Core 144-878A-86R. Up to 40,000 lb of drag was encountered as the bit was pulled to the top of the basalt section; the clays intruded into the hole and impeded the downtrip. It was necessary to ream most of the section back to total depth and to circulate 7 m of fill from the hole with a mud sweep. Except for some unexplained elevated circulating pressures apparently caused by internal obstructions in the system (bit jets?), drilling parameters returned to normal, and fresher basalt was cored below 800 mbsf. An interval of highly altered volcanic tuff was penetrated from about 875 to 890 mbsf with excellent core recovery.

After Core 144-878A-95R at 894 mbsf, another short trip was made to replace the knobby drilling joints and to "wipe" the hole to the top of the basalt interval. Again, the upper portion of the basalt/clay section produced overpulls to 40,000 lb and obstructed the bit on attempts to lower the string. It was necessary to ream and drill through the interval from 762 to 808 mbsf, although the resistance remained after several passes. At total depth, and before coring continued, the "wash barrel" (Core 144-878A-96W) containing 72 cm of mixed lithologies was recovered. Two additional cores then were taken to 910 mbsf, at which point coring was discontinued because the allotted time for drilling had expired and the logging program had to be run (see Table 2).

A wiper trip of the entire hole up to 47 mbsf was made, with drag of up to 130,000 lb in the volcanic sequence; no significant resistance in the sediment section was encountered in either direction, however. Again, over 3 hr were required to ream through a series of solid ledges (apparently swelling clays) in the basalt interval before total depth was reached. The hole was then swept with viscous mud, and the MBR was actuated to release the bit. Because tests had shown the clays to be water reactive, the lower portion of the hole was filled with seawater "spiked" with 4% additional KCl.

The end of the pipe was withdrawn only to 806 mbsf, just below the depth of the lowermost clay ledge, in an attempt to log the lower basement part of the hole. The FMS log was deployed first because it had highest priority for that portion of the hole. The logging tool was stopped by an obstruction 27 m above total depth, but a good log of a 78-m basement interval was obtained. By the time the FMS had been recovered to the surface, the drill string had begun sticking in the hole. After the logging equipment was cleared, the pipe was worked to $\pm 60,000$ lb, and a pressure up to 1500 psi was applied to the annular seal to break the pipe free. Although the pipe came free in the hole, the risk posed to the drill string was considered to be too great for further logging, and the pipe was pulled to the upper logging depth of 46 mbsf.

The next logging attempt was with the long, heavy geophysical tool string, which found its way to 2075 m below rig floor (mbrf), about 11 m past the uppermost basalt contact. A good log was recorded all the way to drill pipe, but the quality of the sonic log was degraded by the overgauge hole (in excess of 18 in. for much of the interval). The ensuing logs—the FMS and geochemical strings—were stopped by a bridge that had formed at the top of the basalt; however, they

produced good logs throughout the entire sediment section. A delay of about 1½ hr resulted from a mechanical failure of the sensor pad/arm mechanism on the FMS tool. This failure required retrieval and repairs of the FMS tool between the two passes in the hole. A major problem was narrowly averted when the broken pad, which had become stuck at the OCB, was eventually freed by the winch operator.

The logging equipment then was rigged down and the drill string was recovered. The two positioning beacons were recalled during the pipe trip. The vessel departed the site at 2130L, 12 July 1992.

UNDERWAY AND SITE GEOPHYSICS

Introduction

MIT Guyot, centered about 27°15'N latitude and 151°50'E longitude, is located over 1000 km northwest of Site 801C (Fig. 1). To the north of MIT Guyot lie the Marcus-Wake seamounts and to the south lie the Japanese seamounts. The elongate edifice trends in a northeast-southwest direction, approaching a maximum length of over 20 km. The edifice narrows from ~6 km in the southwest to <2 km in the northeast. Magnetic anomaly M29 is found slightly south of this edifice (Nakanishi et al., 1992a, 1992b), thereby making the plate beneath MIT Guyot ~160 m.y. old.

Site Survey—Roundabout 10

The site survey work over this guyot was done during Leg 10 of the 1988 Roundabout Expedition (Roundabout 10) on the *Thomas Washington*. Geophysical data collected over MIT Guyot includes Sea Beam multibeam bathymetry, 3.5-kHz echo-sounder bathymetry, single-channel seismic records, and gravity and magnetic measurements. Dredges across the flanks and near the summit recovered basalt and limestone. Radiometric ages (⁴⁰Ar/³⁹Ar) for the basalt range between 118 and 120 Ma (R. Duncan, unpubl. data), whereas ages for the limestone are estimated as late Albian (J. Grötsch, unpubl. data).

During Roundabout 10, approximately 70% of the summit area of MIT Guyot was surveyed with Sea Beam. An overview of the morphology of all the guyots surveyed during Roundabout 10 is provided by van Waasbergen and Winterer (in press). This overview covers an area extending from the Japanese seamounts in the west through the Marcus-Wake islands to the Mid-Pacific Mountains in the east. Van Waasbergen and Winterer (in press) nominally group the guyots surveyed during Roundabout 10 according to the presumed stage of carbonate platform development before failure of the complex. The guyot classifications range from those edifices with no discernable carbonate accumulation, to those edifices topped by a completely developed atoll. In their classification scheme, MIT Guyot is a completely developed atoll which has undergone extensive subaerial erosion resulting in pronounced karst topography across the summit.

The contoured Sea Beam bathymetry (Fig. 1) shows the distribution of isolated mounds and holes across the summit of MIT. Along the northeast half of the guyot a basin or broad channel, marked by the 1320 m contour, extends across the summit. A number of isolated, 40–80 m high mounds lie to either side of this central basin. Some of the holes southwest of the central basin are over 100 m deep. As noted by van Waasbergen and Winterer (in press), these deep holes do not appear to have any surface connection to the flanks of the guyot. Consequently, they postulate that the holes are dissolution features connected to some form of subsurface drainage system.

Virtually no pelagic sediments accumulate across the top of this guyot. The seismic data collected during Roundabout 10 show two coherent reflector packets across the summit. The upper reflector packet is located at ~2.13 s two-way traveltime (TWT) beneath the proposed site location MIT-1-E (Fig. 2). This packet of reflectors remains at a relatively constant depth within the presumed carbonate platform in the direction of Profile A–A'. The lower reflector packet is located around 2.31 s TWT beneath MIT-1(E) and appears to deepen to the north (Figs. 1–2). This horizon was interpreted as the

Table 2. Well-log data, Hole 878A.

Log type	Depth (mbsf)
Natural gamma ray	17–740
Sonic	17–740
Neutron porosity (AmBe neutron source)	17–740
Lithodensity (Ce gamma-ray source)	17–740
Resistivity	17–740
*Aluminum clay (Ca neutron source)	0–740
*Gamma-ray spectrometry	0–740
Formation MicroScanner	807–885
Formation MicroScanner	40–171

Notes: Log data assume that the seafloor is at 1338.0 m, with all logs correlated and depth shifted to the gamma-ray log from the geochemical tool string.

*These logs were recorded in pipe from 0 to 17 mbsf.

top of the volcanic edifice. Van Waasbergen and Winterer (in press) claim that reflectors within the topographically high areas of the summit crop out along the flanks of these highs, thus indicating that the summit relief is erosional in origin. It is not apparent that such a truncation pattern exists with the reflectors shown in Figure 2, but it may be present in other profiles collected during Roundabout 10 and unavailable to the Leg 144 participants.

Sager et al. (in press) discuss the paleomagnetism of the Japanese and Marcus-Wake seamounts, including MIT Guyot. They note that the reversed magnetization of MIT Guyot is anomalous in relation to the majority of seamounts in these two island groups, and that the total magnetization of this guyot is relatively weak, probably partly induced, and very complex. For example, the paleomagnetic pole calculated for MIT Guyot falls far south of the assumed 125-m.y. Pacific Apparent Polar Wander Path (APWP) pole. Given the radiometric age of ~120 m.y. for this edifice, Sager et al. (in press) postulated that the anomalous paleopole position for MIT Guyot results from either significant amounts of induced or normal polarity magnetic overprinting, or that the calculated pole is simply erroneous. One of the primary objectives of drilling on MIT Guyot was to address the complex magnetization of this edifice.

Site Survey—Leg 144

After completing logging operations at Site 801C, the ship departed for MIT Guyot collecting magnetics data and 3.5- and 12-kHz echo-sounder bathymetry. Upon nearing the guyot, we deployed the seismic gear on Julian Day (JD) 180, at 0405Z (GMT) and began the site survey. The first line across MIT Guyot retraced the north-south line run during Roundabout 10 (Fig. 3). Ship speed was ~6 kt and the source was a 200-in.³ water gun. After crossing the summit, the ship turned to a heading of 225° at 0520Z, running a line parallel to the summit edge. At 0615Z, the ship changed course to 085°, beginning a west to east line which crossed the proposed site location at 0648Z. Toward the end of this line, we were informed that construction of the mini hard-rock guide base scheduled for deployment at this site was near completion. Concluding our survey, the ship looped to the north and then changed course to a heading of 230°. The site location was chosen along this line at 0738Z. Shortly after passing over the site, the ship reversed course to a heading of 050° and dropped a beacon at 0815Z on JD 180. By 0830Z the seismic gear was recovered, and by 0845Z the ship was on station.

During post-processing of the data, it became apparent that the seismic acquisition system was not functioning properly throughout the survey. A number of shots were not recorded on tape. No error message appeared at the time of acquisition, and no apparent pattern occurs in the missing shots. This incomplete data record is responsible for the “blocky” appearance of the seismic profiles shown in Figures 4–5. While on station, we determined that the recording failure was attributable either to a broken potentiometer affecting the signal received by the blast phone (thus resulting in the system not receiving

any signal that a shot had been fired) or to a gas-line problem with the water gun.

After completing the drilling at Site 878, we ran one more line across the summit of MIT Guyot. The seismic gear was deployed at ~1145Z, JD 194, on a ship's heading of 120°. After the gear was in the water, the ship changed course to a heading of 300° and we proceeded to collect data at a ship's speed of 6 kt using a 200-in.³ water gun as a source. No acquisition problems were encountered during the survey, and the seismic record collected along this line is more complete than any of the previous records over MIT Guyot (Fig. 6).

On the basis of the 3.5-kHz records, the summit of this guyot is almost completely devoid of pelagic sediment (Fig. 3) and the topography across the summit is rough. Relatively long-wavelength (>1 km) topographic features typically exhibit relief on the order of 35 m; smaller-wavelength features are commonly < 15 m high. The subsurface structure of this guyot is more difficult to interpret. The two strong, coherent reflector packets noted in the Roundabout 10 data are visible in the seismic profiles shown in Figures 4–6. Both reflector packets lose definition toward the perimeter of the summit. Along the south edge of MIT Guyot, the horizontal reflectors visible across the central portion of the summit truncate against a set of landward dipping reflectors. Areas where the reflector packets are least defined across the central portions of the summit appear to correlate with topographic depressions. Beneath Site 878, the two main reflector packets lie at 2.1 and 2.3 s TWT, respectively. The upper unit of sediments is 0.31 s TWT thick, whereas the lower unit is 0.20 s TWT thick. A number of poorly defined reflectors lie up to 0.12 s TWT beneath the top of the second reflector packet, suggesting either a thicker sediment unit overlying volcanic basement, or some change in the acoustic character of basement with depth (similar to the deep reflectors seen on Lo-En and Wodejebato guyots).

LITHOSTRATIGRAPHY

Three holes were drilled at MIT Guyot. Hole 878A ended at 910 mbsf after penetrating 3.2 m of pelagic sediment cover, 719.34 m of platform carbonates and polymictic breccia, and 187.46 m of basalt flows and flow-top breccias. Holes 878B and 878C were drilled about 10 m from Hole 878A to depths of 5.8 and 6.0 m, respectively, in an attempt to recover additional pelagic sediments. No pelagic sediments were recovered in Holes 878B or 878C; platform limestone was recovered immediately beneath the manganese-encrusted surface of the guyot in Holes 878B and 878C.

Lithologic units are identified by color, carbonate and clay content, constituent particles, lithification, sedimentary structures, and downhole log characteristics. Six lithologic units are identified at this site: Unit I, yellowish brown (10YR 5/4) foraminifer nannofossil ooze with manganese nodules and crusts; Unit II, micritized, gastropod-rich wackestone, packstone, and rudstone interlayered with grainstone and fenestral packstone; Unit III, rudstone, floatstone, and grainstone with rudist, coral, and calcisponge fragments interlayered with very fine-grained grainstone; Unit IV, polymictic breccia with volcanogenic and limestone clasts; Unit V, skeletal grainstone, packstone, and wackestone; and Unit VI, subaerial alkalic basalt flows with flow-top breccias (Table 3 and Fig. 7). Components identified in thin section are summarized for each unit and subunit in Table 4.

Each of the units was divided into subunits based on internal variations in composition. Only 2.3% of the limestone above the breccia (Units II and III) and 6.3% of the limestone between the breccia and the basalt (Unit VI) were recovered (see “Operations” section, this chapter). Therefore, the precise positions of unit and subunit boundaries are not known. We have relied on downhole logging results (especially resistivity, natural gamma, and drilling rates) for additional information about lithologic variation within the carbonate platform (see “Downhole Logging and Seismic Stratigraphy” section, this chapter).

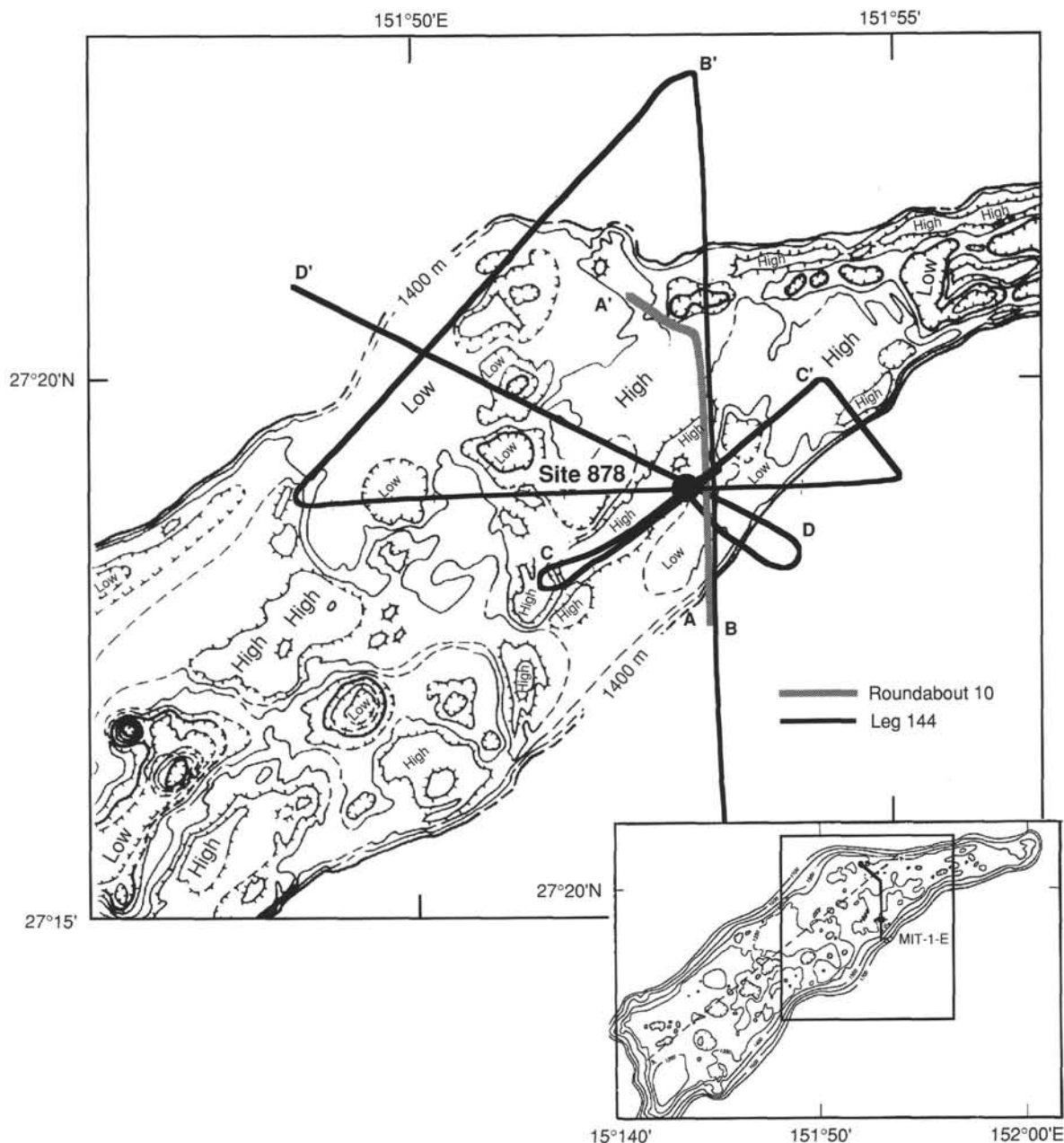


Figure 1. Sea Beam bathymetry and ship tracks across the summit of MIT Guyot. Bathymetric data was collected during Roundabout Cruise 10. For the enlarged bathymetric map, only depths shallower than 1400 m were contoured. Contour intervals in meters.

Unit I

Intervals: Hole 878A, Sections 144-878A-1R-1 to -1R-3; Hole 878B, Interval 144-878B-1R-1, 0–15 cm; Hole 878C, Interval 144-878C-1R-1, 0–23 cm
 Depth: Hole 878A, 0–3.2 mbsf; Hole 878B, 0–0.15 mbsf; Hole 878C, 0–0.23 mbsf
 Age: early Pleistocene to latest Albian

In Hole 878A, Unit I consists of yellowish brown (10YR 5/4) foraminifer nannofossil ooze that grades downhole into very pale yellowish brown (10YR 7/3) nannofossil ooze. Only traces of pelagic sediment were recovered in Holes 878B and 878C. Manganese nodules ranging from submillimeter size to 5 cm in diameter are disseminated throughout the unit (Fig. 8). The base of Unit I consists of 15–23 cm

of fragmented manganese crust and nodules recovered in Holes 878B and 878C; only few fragments of manganese crust were recovered along with limestone pebbles in Hole 878A. The very soupy sediment at the top and base of Unit I in Hole 878A may indicate mixing of lithologies in the core barrel. Changes in color, composition, and sediment consistency resulted in recognition of three subunits.

Subunit IA

Interval: Interval 144-878A-1R-1, 0–95 cm
 Depth: 0–0.95 mbsf
 Age: early Pleistocene to early late Pliocene

Subunit IA is a soupy, yellowish brown (10YR 5/4), foraminifer nannofossil ooze with disseminated manganese nodules (Fig. 8). The

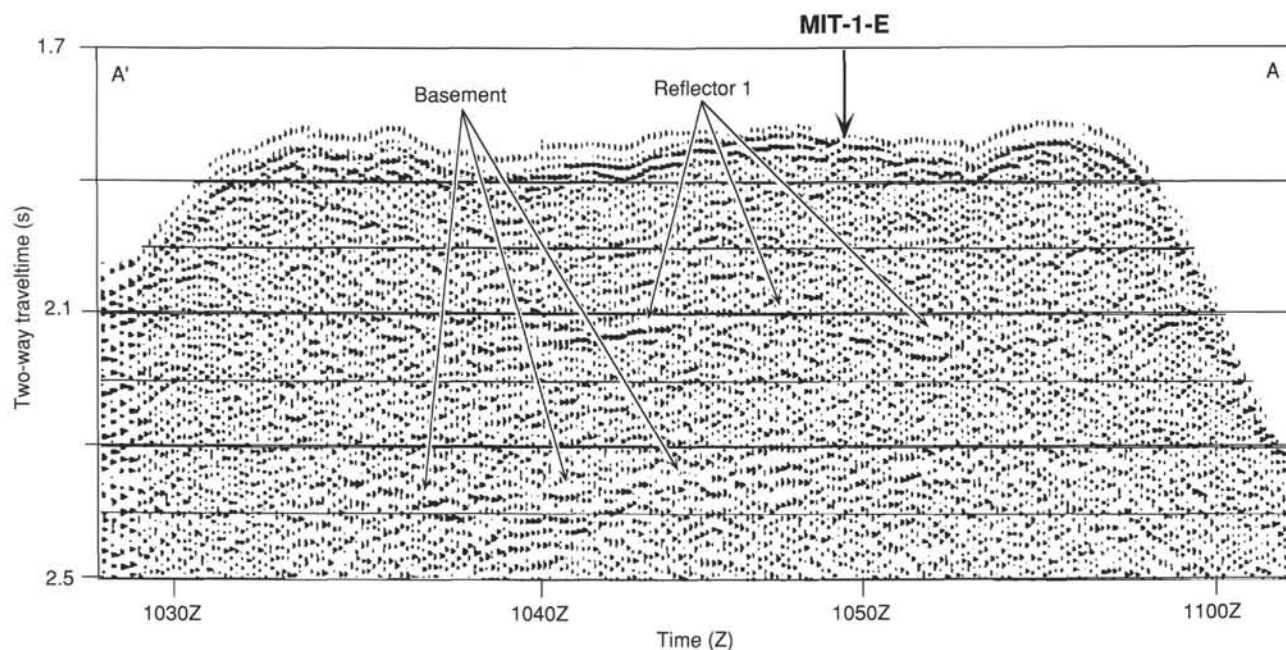


Figure 2. Seismic Profile A–A' collected during Roundabout Cruise 10. The source used for this line was an 80-in.³ water gun, and the towing speed was ~9 kt. Profile A–A' location is shown in Figure 1.

ooze consists primarily of nanofossils. Minor constituents are planktonic foraminifers, clay minerals, and sand-sized, mainly botryoidal manganese microconcretions that impart a characteristic gritty texture to the ooze. Iron-manganese nodules, 2–5 cm in diameter, float in the ooze and are most abundant in Intervals 144-878A-1R-1, 0–30 cm, and -1R-1, 70–95 cm. The nodules are black, with mostly smooth, elliptical surfaces. Others are botryoidal with surface perturbations 3 mm in height. Most of the nodules nucleated around a limestone fragment. A few appear to be massive manganese without an apparent nucleus. Some of the nodules are composite, with a nucleus of manganese-coated, phosphatized, platform limestone encased in pelagic carbonate that is coated by a manganese crust up to 5 mm thick.

The foraminifer nanofossil ooze in Subunit IA is early late Pliocene to early Pleistocene in age. Microfossils in the nuclei and cortices of the manganese nodules have been dated as latest Albian, Santonian/Campanian, late Paleocene, and early Eocene in age (see "Biostratigraphy" section, this chapter). A video survey of the seafloor at Site 878 indicates significant bathymetric relief. It is possible that the older manganese nodules have been transported from local bathymetric highs into younger sediments accumulating in local bathymetric lows.

Subunit IB

Interval: Sections 144-878A-1R-1, 95 cm, through -1R-3
 Depth: 0.95–3.2 mbsf
 Age: early late Pliocene? to late Miocene

Subunit IB is very pale brown (10YR 7/3) nanofossil ooze, with a firmer consistency than the ooze of Subunit IA. The ooze in Subunit IB is comprised of nanofossils; poorly preserved and unidentified carbonate grains; clear, bladed calcite crystals; probable fecal pellets; manganese micronodules; and zeolites. Planktonic foraminifers are extremely rare. Detrital feldspars are a trace component. Manganese nodules similar to those in Subunit IA are present at the top of the subunit, especially in Interval 144-878A-1R-2, 0–20 cm. Fine manganese micronodules are concentrated in occasional dark bands, 2–5 cm thick (e.g., Interval 144-878A-1R-2, 70–75 cm). Abundant

millimeter- to centimeter-sized clasts of semilithified fine sand are disseminated throughout Subunit IB. The sand consists of manganese micronodules, similar to those described in Subunit IA, and bladed or irregular clear crystals of calcite of uncertain origin. Mixing of the lithologies of Subunit IA and IB is apparent at the top of Subunit IB (Interval 144-878A-1R-1, 95–111 cm), and also at the base (e.g., Interval 144-878A-1R-3, 0–40 cm), where the ooze becomes soupy again, similar to Subunit IA. Mixing within these intervals is also apparent in the biostratigraphy of Unit I (see "Biostratigraphy" section, this chapter). This mixing is probably the result of drilling. Subunit IB is late Miocene to early Pliocene in age.

Subunit IC

Intervals: Hole 878B, Interval 144-878B-1R-1, 0–15 cm; Hole 878C, Interval 144-878C-1R-1, 0–23 cm
 Depth: Hole 878B, 0–0.15 mbsf; Hole 878C, 0–0.23 mbsf
 Age: early Eocene, late Paleocene, Santonian-Campanian, latest Albian

Manganese nodules and crusts were recovered overlying platform carbonates in Holes 878B and 878C. The only evidence of a similar deposit in Hole 878A is a few fragments of manganese crust mixed with limestone pebbles in Interval 144-878A-1R-CC, 4–8 cm. At Hole 878A, the manganese nodules are mixed within Subunits IA and IB (see discussion in "Subunit IA" and "Subunit IB" sections, above).

Unit II

Intervals: Hole 878A, Sections 144-878A-1R-CC to -26M-1, 17 cm; Hole 878B, Interval 144-878B-1R-1, 15–50 cm; Hole 878C, Interval 144-878C-1R-1, 23–61 cm
 Depth: Hole 878A, 3.20–236.07 mbsf; Hole 878B, 0.15–0.5 mbsf; Hole 878C, 0.23–0.61 mbsf
 Age: late Aptian? to Albian

Unit II is composed of white (10YR 8/2) wackestone, packstone, and rudstone with intervals of grainstone and fenestral packstone. Gastropods, mostly molds, are common to abundant, especially in the

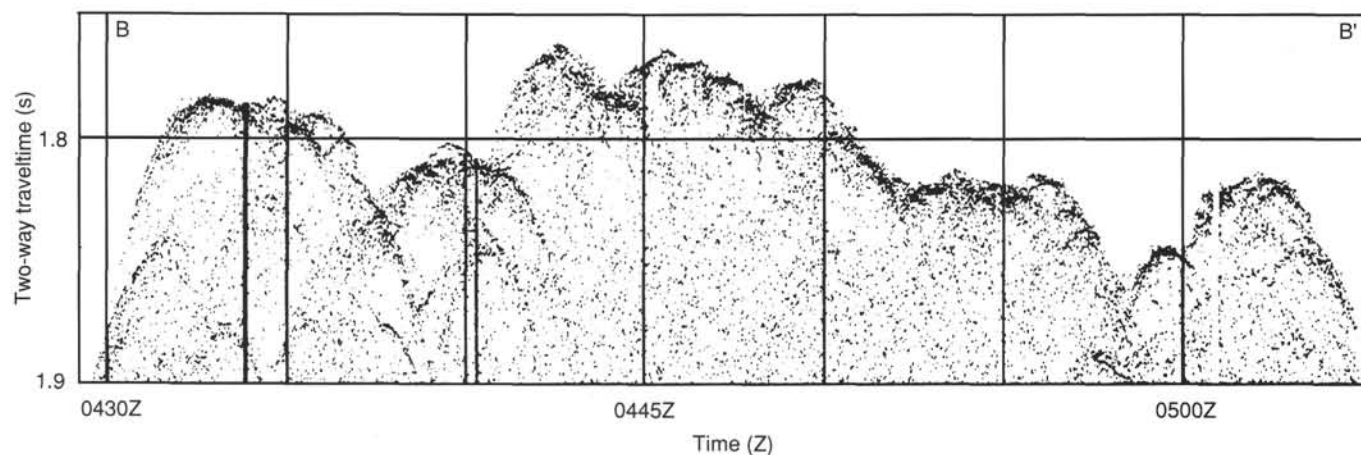


Figure 3. Profile B-B' of 3.5-kHz echo-sounder collected during Leg 144 over MIT Guyot. Profile B-B' location is shown in Figure 1.

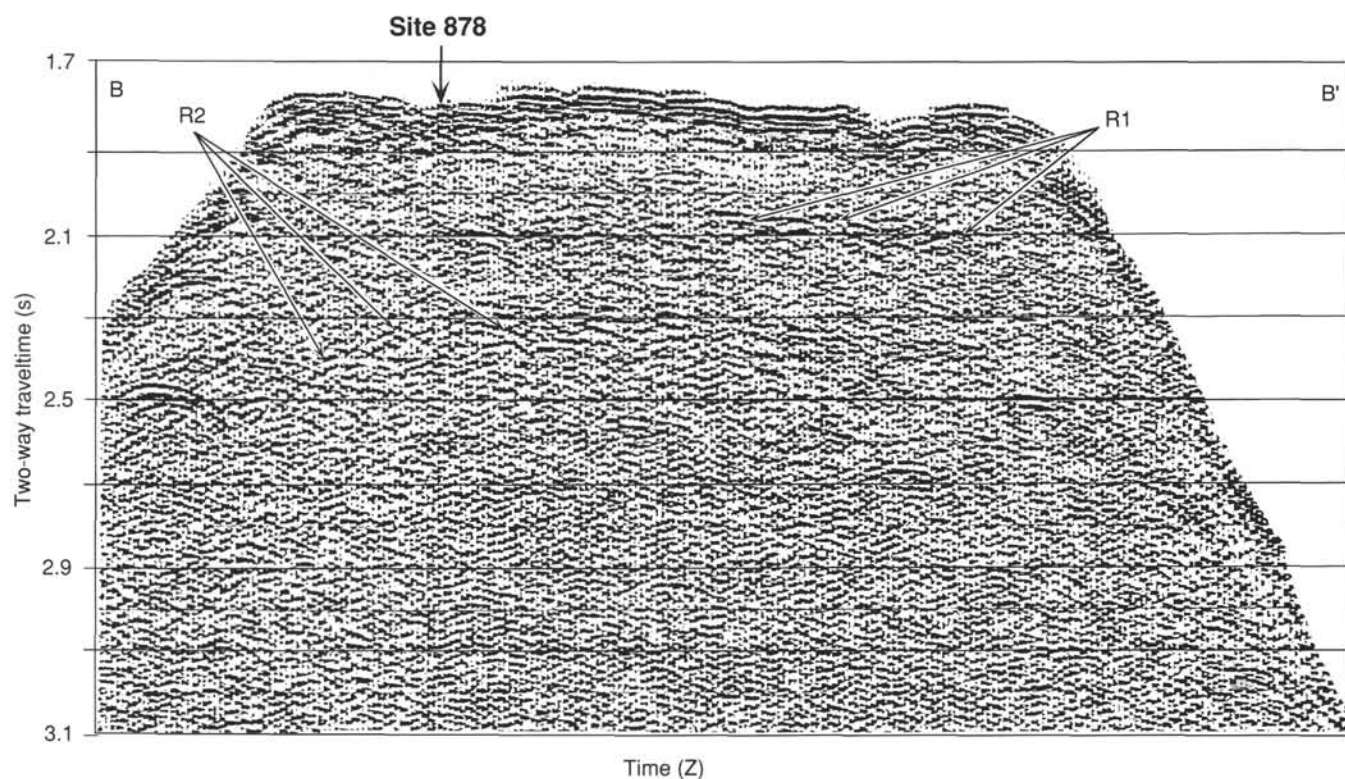


Figure 4. Single-channel seismic Profile B-B' collected during Leg 144 over MIT Guyot. Reflectors R1 and R2 correspond to Reflector 1 and basement horizons shown in Figure 2. Profile B-B' location is shown in Figure 1.

upper half of the unit; oysters are locally abundant. Compositional and textural variations permit subdivision of Unit II into four subunits.

Subunit IIA

Intervals: Hole 878A, Sections 144-878A-1R-CC to -8R-1, 26 cm; Hole 878B, Interval 144-878B-1R-1, 15–50 cm; Hole 878C, Interval 144-878C-1R-1, 23–61 cm
 Depth: Hole 878A, 3.2–67.26 cm; Hole 878B, 0.15–0.5 mbsf; Hole 878C, 0.23–0.61 mbsf
 Age: Albian

White (10YR 8/2) wackestone and peloid packstone with molds and recrystallized fragments of nerineid gastropods are the dominant

lithologies in Subunit IIA (Fig. 9). Thin beds of friable, coarse-grained grainstone (Interval 144-878A-3R-1, 0–10 cm) and intraclast packstone (Interval 144-878A-6R-1, 0–1 cm) are rare. The peloid packstone is poorly sorted; most skeletal grains are coarse-sand size. A characteristic feature of Subunit IIA is pervasive recrystallization of grains. The top of Subunit IIA and several lower horizons have a chalky aspects. Macrofossils in the limestones are represented by molds of high-spired nerineid gastropods as long as 4 cm long and bivalves as long as 0.5–2.0 cm. Fragments of corals are rare (Interval 144-878A-7R-1, 0–33 cm); a bored fragment of oyster shell, 2 cm in length, is present in Section 144-878A-6R-1, 20 cm. Other constituents, identified in the thin section, include benthic foraminifers (dominantly miliolids and *Vercorsella*), echinoderm debris, thin bivalve

shell fragments, sponge spicules, calcisponge fragments, cyanobacteria (*Ortonella*), and worm tubes. Encrusting red algae are common in the skeletal wackestone of Core 144-878A-7R, but rare elsewhere. Nonskeletal components include peloids and rare superficial ooids. Porosity is mainly moldic and interparticle, varying between 5% and 15%. Some of the molds are sparsely coated by bladed sparry calcite. Yellow, orange, or pink stains are common on the walls of some pores throughout the subunit. Filled borings of clionid sponges and cyanobacteria are common in molds.

Subunit IIB

Interval: Sections 144-878A-8R-1, 26 cm, to -10R-1, 0 cm
Depth: 67.26–86.2 mbsf
Age: Albian

Subunit IIB consists of very pale brown (10YR 7/3) to light brown (10YR 8/2) peloid packstone, peloid algal wackestone, and minor medium- to coarse-grained grainstone. Fenestrae, parallel to bedding, are common in the packstone of Intervals 144-878A-8R-1, 26–29 cm, and -9R-1, 26–43 cm (Fig. 10). The fenestral voids are lined with light brown (5YR 5/6), bladed, very fine to medium crystalline calcite crusts. The dominant grains are peloids with subordinate bivalve shell debris, codiacean algae(?), red algae, and benthic foraminifers. Skeletal grains are heavily micritized. Porosity in this subunit, ranging from 5% to 20%, includes fenestral, cement-reduced moldic, and solution-enlarged interparticle in the packstone and grainstone, and vuggy micropores in the wackestone.

Subunit IIC

Interval: Sections 144-878A-10R-1, to -22M-1, 0 cm
Depth: 86.2–202.2 mbsf
Age: late Aptian or Albian

Subunit IIC is white (10YR 8/1) skeletal wackestone with intervals of skeletal packstone, grainstone, and rudstone. Most of the skeletal grains in the subunit are micritized, which obscures their origin. Porosity averages <10%. Recognizable skeletal components consist of fragments of bivalves, calcisponges, cyanobacteria (*Ortonella*), rare miliolid and encrusting foraminifers, ostracodes, and polychaete worm tubes; molds of gastropods are also common. Oyster shells are especially common in wackestone from Intervals 144-878A-16R-1, 0–2 cm, -18R-1, 31–40 cm, and -19R-1, 13–19 cm (Fig. 11). Thin, straight to slightly curved tubes are molds of sponge spicules. The wackestone and packstone are commonly bioturbated; burrows are partially filled by pelleted mud. Grainstone is rare (Intervals 144-878A-12R-1, 20–34 cm, and -18-1, 40–44 cm). Grain-size distribution in the grainstone is bimodal; the average size is medium sand (0.25–0.5 mm), with larger grains to 2.6 mm. The coarser fraction of the grainstone consists of gastropod shell molds, well-preserved *Ortonella*, a few bivalve shells, rare foraminifers, and rounded micritic intraclasts.

Subunit IID

Interval: Sections 144-878A-22M-1, to -26M-1, 17 cm
Depth: 202.2–236.07 mbsf
Age: late Aptian or Albian

The top of Subunit IID is skeletal peloid grainstone successively overlain by skeletal packstone, mudstone, and wackestone at the base. The grainstone is well sorted, medium sand sized, and friable, with abundant peloids, very rare larger foraminifers, and green algae debris. Interparticle porosity in the grainstone is about 25%.

The underlying packstone is also friable and contains molds of nerineid gastropods in addition to other constituents similar to those in the overlying grainstone of this subunit. Grapstones are a minor com-

ponent. Calcite cement is rare as finely crystalline, bladed crusts. Burrows are rare; some are stained pale yellow (2.5Y 7/4) by iron hydroxide.

The mudstone and wackestone at the base of Subunit IID is bioturbated, with packstone filling burrows in the mudstone. Burrows in the basal wackestone, which are mostly empty, are enlarged by solution; most are empty, but a few are filled by soft, chalky carbonate. Small benthic foraminifers, gastropod molds, and thin bivalve shell fragments can be recognized in both lithologies. Slightly curved, open tubes, 50 μ m in diameter and >1 mm long, in the matrix are molds of sponge spicules. Planktonic foraminifers were identified in the wackestone from Interval 144-878A-26M-1, 4–12 cm, at the base of Subunit IID (see “Biostratigraphy” section, this chapter).

Unit III

Interval: Sections 144-878A-26M-1, 17 cm, to -43M-1, 44 cm
Depth: 236.07–399.74 mbsf
Age: late Aptian

Changes in grain size, color, and major constituents are the main criteria for separating Units II and III. Grainstone, rudstone, and coarser grained packstone are the dominant lithofacies; the characteristic of Unit III is very pale brown (10YR 7/3). Minor changes in fossil content and grain size distinguish three subdivisions of the unit.

Subunit IIIA

Interval: Sections 144-878A-26M-1, 17 cm, to -34M-1, 5 cm
Depth: 236.07–312.65 mbsf
Age: late Aptian

Fine- to medium-grained skeletal grainstone with intervals of skeletal rudstone and packstone comprise Subunit IIIA. Debris of rudists, corals, stromatoporoids, gastropods, and calcisponges, as large as 3 cm, characterize all lithologies of this subunit (Fig. 12). Other constituents are larger foraminifers (orbitolinids), encrusting foraminifers, and red algae. A few rhodoliths are present at the base of the subunit (Intervals 144-878A-33M-1, 14–18 cm, and -34M-1, 0–6 cm). Grains are highly micritized; many are preserved only by micrite envelopes. Many of the mollusk fragments are recrystallized (Fig. 13). The porosity of the mollusk rudstone in Interval 144-878A-31M-1, 0–44 cm, is highly variable, from near 0% to 15%; it includes molds with a few interparticle, intraparticle, and shelter pores. Cement typically comprises two generations: inclusion-rich, finely crystalline, fibrous, isopachous rim cement overlain by equant, clear, coarsely crystalline calcite.

The rudstone and packstone of Subunit IIIA was recovered in Cores 144-878A-26M and -28M (no recovery in Core 144-878A-27M), and again in Core 144-878A-31M; these occurrences correspond to peaks in resistivity recorded during downhole logging. Fine- to medium-grained grainstone was recovered in Cores 144-878A-29M, -30M, and -33M (no recovery in Core 144-878A-32M); these occurrences correspond to lower resistivity than that recorded for the rudstone and packstone horizons (see “Downhole Measurements and Seismic Stratigraphy” section, this chapter).

Subunit IIIB

Interval: Sections 144-878A-34M-1, 5 cm, to -42M-1, 0 cm
Depth: 312.65–389.8 mbsf
Age: late Aptian

The fine-grained grainstone of Subunit IIIB is very similar to the fine-grained grainstone of Subunit IIIA; however, it lacks the occasional large (>2 mm) skeletal debris characteristic of Subunit IIIA. Subunit IIIB grainstone is friable as a result of sparse cementation or leaching. The grainstone is well sorted and fine to medium sand size. Peloids are common; most are probably skeletal grains, micritized

Table 3. Lithostratigraphic summary, Site 878.

Unit/subunit	Cores	Depth (mbsf)	Age	Description
Subunit IA	144-878A-1R-1, 0 cm, to -1R-1, 95 cm	0–0.95	early Pliocene to early late Pleistocene	Foraminifer nanofossil ooze with manganese nodules.
Subunit IB	144-878A-1R-1, 95 cm, to -1R-CC, 0 cm	0.95–3.20	early late Pliocene to early Miocene	Nannofossil ooze with chalk fragments and manganese nodules.
Subunit IC	144-878A-CC (fragments) 144-878B-1R-1, 0–15 cm 144-878C-1R-1, 0–23 cm	Uncertain 0–0.15 0–0.23	latest Albian, Santonian-Campanian, early Eocene, late Paleocene	Manganese nodules and crust.
Subunit IIA	144-878A-1R-CC, 0 cm, to -8R-1, 26 cm 144-878B-1R-1, 15–50 cm 144-878C-1R-1, 23–61 cm	3.20–67.26 0.15–0.53 0.23–0.61	Albian	Wackestone and peloid packstone with molds and recrystallized fragments of nerineid gastropods (as large as 4 cm) abundant in upper half.
Subunit IIB	144-878A-8R-1, 26 cm, to -10R-1, 0 cm	67.26–86.2	Albian	Peloidal packstone with fenestral fabric, peloid-algal wackestone, and minor grainstone.
Subunit IIC	144-878A-10R-1, 0 cm, to -22M-1, 0 cm	86.2–202.2	late Aptian or Albian	Skeletal wackestone with minor packstone, grainstone, and rudstone that is gastropod-rich in upper horizons and oyster-rich in lower horizons.
Subunit IID	144-878A-22M-1, 0 cm, to -26M-1, 17 cm	202.2–236.07	late Aptian or Albian	Mudstone coarsening upward to wackestone, packstone with gastropods, and medium sand-sized grainstone.
Subunit IIIA	144-878A-26M-1, 17 cm, to -34M-1, 5 cm	236.07–312.65	late Aptian or Albian	Fine- to medium-grained grainstone with intervals of skeletal rudstone containing rudist, coral, and calcisponge fragments.
Subunit IIIB	144-878A-34M-1, 5 cm, to -42M-1, 0 cm	312.65–389.8	late Aptian or Albian	Friable fine to medium grainstone with coarse <i>Orbitolina</i> -rich skeletal grainstone at the base of the subunit.
Subunit IIIC	144-878A-42M-1, 0 cm, to -43M-1, 44 cm	389.8–399.74	late Aptian	Well-lithified skeletal foraminifer wackestone and mudstone.
Subunit IVA	144-878A-43M-1, 44 cm, to -44M-1, 0 cm	399.74–406.1	late Aptian	Bluish gray clay.
Subunit IVB	144-878A-44M-1, 0 cm, to -56R-2, 140 cm	406.1–514.74	late Aptian	Breccia with highly vesicular, glassy basalt and limestone clasts in a predominantly carbonate matrix; ash tuff beds at top; partly oxidized at top; volcanics decrease toward base.
Subunit IVC	144-878A-56R-2, 140 cm, to -65R-6, 22 cm	514.74–604.3	early to late Aptian	Breccia with alternating carbonate-rich (light) and volcanic-rich (dark) intervals; steeply inclined beds; slump and fluid escape structures common; volcanics decrease toward base.
Subunit VA	144-878A-65R-6, 22 cm, to -76R-1, 0 cm	604.3–703.0	early Aptian	Peloid foraminifer wackestone, packstone, and grainstone with intervals of gastropod, oyster, and coral rudstone.
Subunit VB	144-878A-76R-1, 0 cm, to -78R-1, 44 cm	703.0–722.54	early Aptian	Coarse-grained skeletal grainstone with minor mollusk coral rudstone.
Unit VI	144-878A-78R-1, 44 cm, to -98R-3, 101 cm	722.54–907.8	?	Alkalic basalt flows and flow-top breccias.

beyond recognition. A few grains have micrite coatings as well. The few recognizable bioclasts, most of which have micrite envelopes, are molluscan shell fragments, worm tubes, poorly preserved larger foraminifers (orbitolinids), and bivalves. *Orbitolina* concentration is locally up to 15% of the rock (Interval 144-878A-37M-1, 27–40 cm). Echinoderm fragments and oncooids are rare. Planktonic foraminifers and nanofossils were recovered from Interval 144-878A-41M-7, 4–8 cm, near the base of the subunit (see “Biostratigraphy” section, this chapter). The cement consists of medium crystalline, bladed crusts and very coarse equant overgrowths on echinoderms. The porosity is primary interparticle, which ranges from 5% to 15%.

Subunit IIIC

Interval: Sections 144-878A-42M-1, to -43M-1, 44 cm
Depth: 389.8–399.74 mbsf
Age: late Aptian

Subunit IIIC consists of light gray (10YR 7/2) to very pale brown (10YR 7/3) foraminifer peloidal wackestone and mudstone. Constituents of this subunit include benthic foraminifers (mostly miliolids), ostracodes, a few corals, molluscan fragments (including nerineid gastro-

pods), rare cyanobacterial bushes (*Ortonella*), silt-sized peloids, and a few recrystallized oncooids. Bioturbation is common; some burrows are stained pale yellowish orange (10YR 8/6). Subunit IIIC is well lithified and porosity is low. Subunit IIIC can easily be identified in the downhole logs as a sharp increase in resistivity and bulk density. The top of Subunit IIIC may also correspond to the first major seismic reflector at the site (see “Downhole Measurements and Seismic Stratigraphy” section, this chapter).

Unit IV

Interval: Sections 144-878A-43M-1, 44 cm, to -65R-6, 22 cm
Depth: 399.74–604.3 mbsf
Age: early to late Aptian

Polymictic breccia of glassy, highly vesicular basalt and platform limestone clasts in a dominantly carbonate matrix comprises Unit IV (Fig. 14). The breccia, 204.56 m thick, is predominantly light greenish gray (5GY 7/1), but it varies in color depending on the proportions of dark greenish gray volcanic clasts (5GY 4/1), very pale brown limestone clasts (10YR 8/3), and light gray (N7), pale green (10G 7/2), to white (N8) matrix. The contact between Unit IV and Unit III (platform

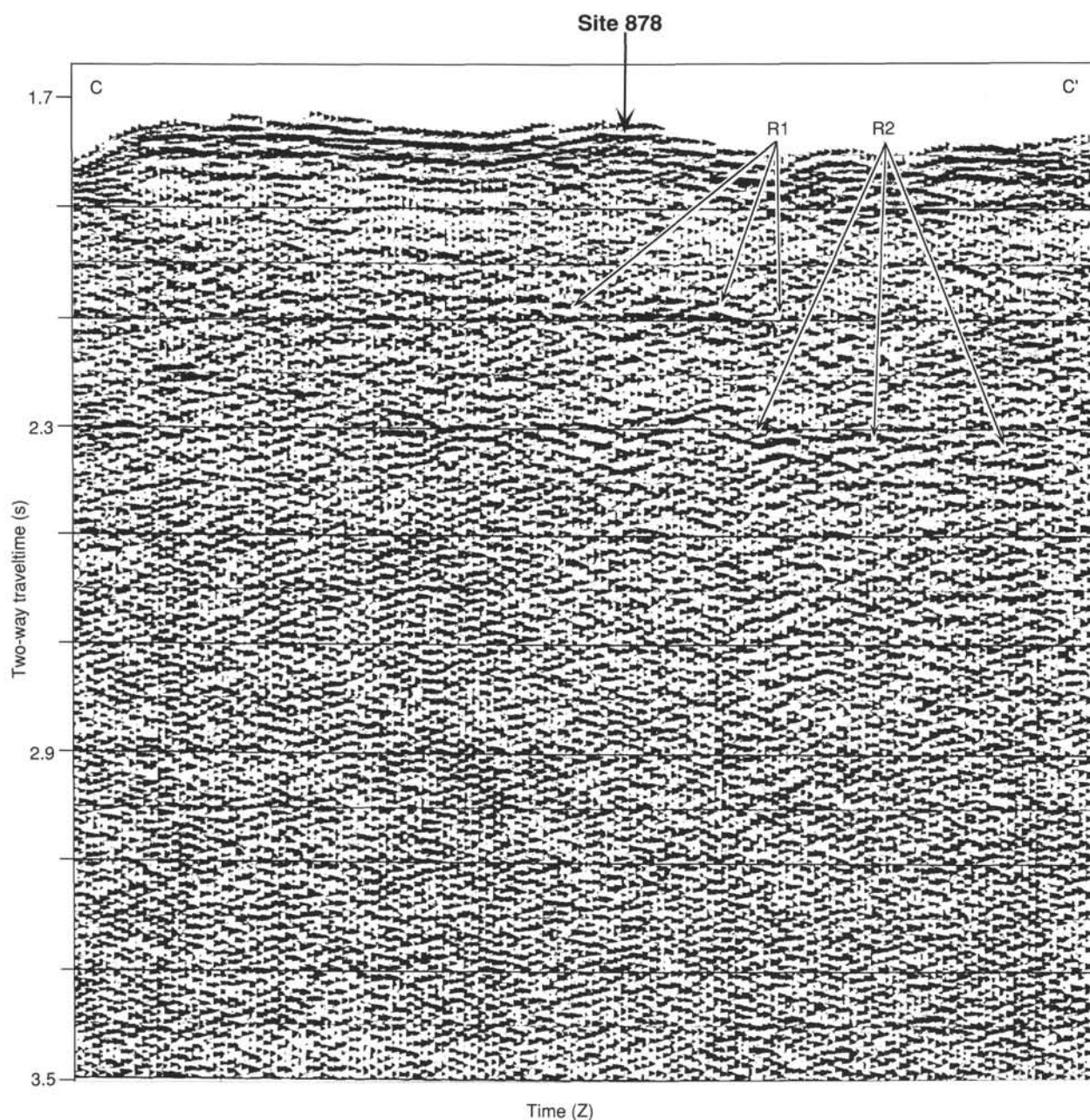


Figure 5. Single-channel seismic Profile C–C' collected during Leg 144. Profile C–C' location is shown in Figure 1.

carbonates) was not recovered; an abrupt decrease in drilling rate, an increase in resistivity, and an increase in natural gamma suggest that the boundary is sharp (see "Downhole Measurements and Seismic Stratigraphy" section, this chapter).

Because little variation exists throughout Unit IV in the composition of volcanic clasts, limestone clasts, and matrix, they are described for the whole unit in this section.

Most volcanic clasts fall within the size range of 0.6–2 cm; clasts from 2 to 5 cm are rare. One clast, 25 cm in length, was recovered (Interval 144-878A-46M-1, 109–132 cm). The volcanic clasts are angular to subangular and equant, although a few are elongate, arcuate, or irregular (Fig. 14). Three types of volcanic clasts are present based on texture and composition.

The dominant volcanic lithology, referred to below as type 1, is altered, aphyric scoriaceous basalt. Vesicles typically comprise 50% of individual clasts and are variably tubular, elliptical, or spherical;

50%–60% of the vesicles are empty. The most common vesicle fill is clear calcite, locally stained yellow, probably by iron oxides; other vesicle fills include zeolites and orange chabazite (see "Igneous Petrology" section, this chapter). Clinopyroxene phenocrysts are rare. Type 1 clasts are generally dark greenish gray (5GY 4/1), probably altered from black basalt.

Light gray (N7), highly altered basalt, with fewer vesicles (20%–30%) than type 1 clasts are designated type 2 clasts. Vesicles are typically spherical, but some are irregular. They are partly or completely filled by clear calcite or lined by clay. The primary mineralogy is uncertain, except for about 5% microphenocrysts, with 0.1–0.5 mm prismatic outlines resembling clinopyroxenes, now replaced by greenish black (5GY 2/1) clay (see "Igneous Petrology" section, this chapter).

A third rare type of volcanic clast is dark gray altered basalt with reddish iron staining and olivine phenocrysts about 0.1 mm in diameter, altered to iddingsite. There are a few larger (3–25 cm) clasts of

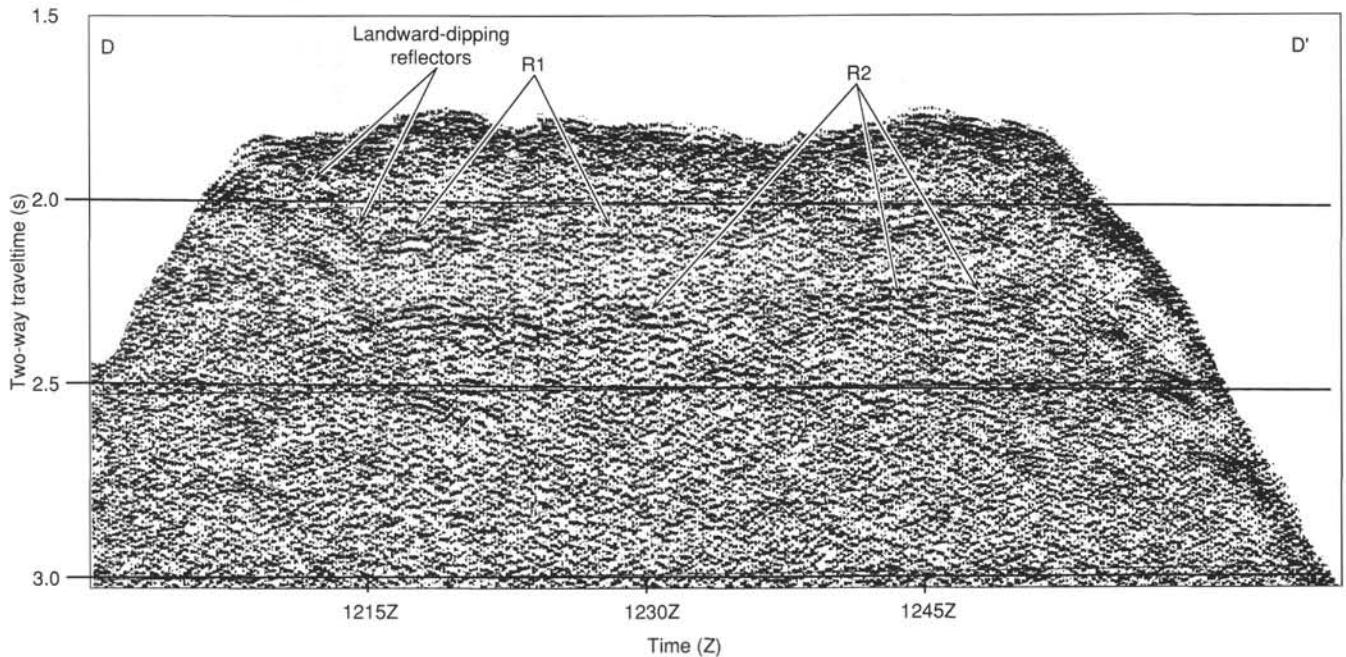


Figure 6. Single-channel seismic Profile D-D' collected during the departure from Site 878 to Site 879. Profile D-D' location is shown in Figure 1. Reflectors R1 and R2 as in Figure 4.

fresh microcrystalline, slightly vesicular basalt (2%–3%) with 5%–10% olivine microphenocrysts, 0.1–1 mm in diameter, and rare plagioclase laths (e.g., Interval 144-878A-46M, 109–132 cm, and Sections 144-878A-55R-2 to -55R-4). These latter clasts may be preexisting basalt that was fragmented by the eruption and redeposited in the breccia.

The second category of clasts in the breccias of Unit IV is comprised of very pale brown (10YR 8/3) limestone with varied textures and compositions. These clasts are equant to ovoid, mostly rounded, but some are subrounded to subangular. Many have embayed outlines reflecting preexisting molds and vugs. Size is most commonly 0.8–2.0 cm in diameter, generally coarser grained than adjacent basalt clasts (Fig. 15). Not uncommonly, limestone clasts are 3–5 cm in diameter; one clast, or bed, is 25 cm in length (Interval 144-878A-63R-4, 62–87 cm). The limestone clasts are a mixture of various lithologic types with no apparent trends throughout the unit. The most common lithologies are mudstone and wackestone with miliolids; less common are skeletal-peloidal wackestone and packstone, oolitic grainstone, molluscan-peloidal wackestone, peloid grainstone, fenestral wackestone and packstone, and mudstone with sponge spicules. Nerineids are the most abundant macrofossil in the limestone clasts; rudist debris, corals, and thrombolites are less common. Porosity within the limestone clasts is ubiquitously low, nearly all pore space has been filled by clear, medium to very coarsely crystalline, equant or bladed calcite. Some of the cement is stained yellow near the top of the unit.

In general, volcanic clasts dominate in the breccia, comprising variably 95% to 50% of clasts greater than 2 mm in size. The breccia matrix, on the other hand, is dominantly carbonate, a mixture of silt- or sand-sized limestone lithoclasts, peloids, rare ooids, very rare molluscan debris, trace miliolid foraminifers, and lime mud. All interparticle space is filled by lime mud. Silt- to sand-sized volcaniclastic fragments, similar to the clasts described above, are mixed with the dominantly carbonate matrix in variable amounts, but seldom more than 25% of the total matrix. Matrix is typically 40%–70% of the volume, and, as this implies, the breccia is matrix supported. Numerous intervals, a few centimeters to a few decimeters thick, are clast supported, however (Figs. 14–15).

Variations in the proportion of volcanic clasts, limestone clasts, and matrix are used in defining Subunits IVB and IVC within the breccia portion of Unit IV. In general, an increase in the volcanic component occurs toward the top of each subunit. Other distinctive features of the subunits are described below.

Subunit IVA

Interval: Sections 144-878A-43M-1, 44 cm, to -44M-1, 0 cm
Depth: 399.74–406.1 mbsf
Age: late Aptian

Subunit IVA is dark greenish gray (5G 4/1) clay, of which only 2 cm was recovered; the subunit boundaries are defined here by the base of Unit III and the top of the volcanic breccia. Reduced penetration rates relative to the overlying limestone and a spike in natural gamma radiation (see "Downhole Measurements and Seismic Stratigraphy" section, this chapter) indicate that most of the interval drilled for Core 144-878A-43M may be clay. The origin of Subunit IVA is not established yet, but it may simply represent the alteration of a volcanic-rich layer at the top of the polymictic breccia. Pyrite is disseminated in the clay. A few grains of peloid wackestone were recovered mixed with the clay; there is, however, no way to determine whether these were emplaced by drilling.

Subunit IVB

Interval: Sections 144-878A-44M-1, to -56R-2, 140 cm
Depth: 406.1–514.74 mbsf
Age: early-late Aptian

Subunit IVB is a polymictic breccia of volcanic and limestone clasts in a detrital carbonate matrix. The contact between Subunits IVA and IVB was not recovered.

The upper portion of Subunit IVB (Cores 144-878A-44M to -49R) has a higher concentration of volcanic fragments, among the clasts and within the matrix, than the lower portion. It is, therefore, darker in color. Pyrite is abundant in Section 144-878A-44M-1, but it is

absent elsewhere in the subunit. Above Core 144-878A-50R, the typical color is greenish gray (5GY 6/4). From Core 144-878A-50R to Section 144-878A-56R-2, 140 cm, the breccia changes from light greenish gray (10G 4/2) to white (10YR 8/2) with a few greenish gray clasts. The breccia is generally matrix supported, but small intervals are clast supported, especially in the upper half. Locally, matrix is absent and sand- and gravel-sized volcanic clasts are cemented by sparry calcite. Yellow, coarsely crystalline, bladed, and equant cement locally fills intergranular space in the breccia in Cores 144-878A-44M and -45M (e.g., Intervals 144-878A-44M-2, 0–21 cm, and -45M-2, 89–93 cm), but it is rare below this level. The upper portion of Subunit IVB also had a faster drilling rate than the rest of the subunit; this faster rate may be related to the high percentage of altered, highly vesicular, glassy basalt fragments.

The abundance of volcanic components decreases from the middle of Subunit IVB to the base (Core 144-878A-50R to Section 144-878A-56R-2, 140 cm); consistent with this trend, the carbonate content of the breccia matrix increases from the middle of Subunit IVB to the base (see “Organic Geochemistry” section, this chapter); the geochemical log Ca/Fe ratio also increases from the top to the base of Subunit VB (see “Downhole Measurements and Seismic Stratigraphy” section, this chapter). Because the carbonate components in the breccia are well cemented and have low porosity, the drilling rate decreased and resistivity increased (see “Downhole Logging and Seismic Stratigraphy” section, this chapter) from the middle of Subunit IVB to the base.

Two dark greenish gray (5GY 5/4), highly altered beds (Intervals 144-878A-44M-1, 26–76 cm, and -44M-1, 148–151 cm) consist exclusively of very angular, highly vesicular, glassy clasts (Fig. 16). The clasts are elongated horizontally; they appear to have been flattened. The vesicles are also elongated horizontally, typically 0.1 × 0.3 mm in diameter. No phenocrysts are visible. The matrix apparently consists of angular glassy fragments. The overall texture of these beds is reminiscent of an ash-flow tuff; however, the thinness of the beds and the sharp contacts with the breccia make an ash-flow origin unlikely. Elongation of shards and vesicles may suggest a siliceous (trachyte?) lava. Some clasts, especially in Interval 144-878A-44M-1, 148–151 cm, appear to be altered pumice, suggesting the presence of trachytic lavas. Fine pyrite is disseminated throughout all lithologies in Section 144-878A-44M-1, but it is not present elsewhere in the breccia.

Elongate vesicles are common near the top of Subunit IVB in type 1 volcanic clasts. They become less common in the lower half of Subunit IVB and are rare in Subunit IVC. Overall, a wider variety of volcanic clasts is present in the upper half of Subunit IVB (Cores 144-878A-44M to -45M) than in the lower half.

Another distinctive feature at the top of Subunit IVB is the reddish brown coloration (2.5YR 5/4) between Sections 144-878A-44M-2, 21 cm, and -45M-4. The breccia composition in this interval is similar to the rest of Subunit IV, except for the iron-oxide staining of the matrix and a greater number of gray basalt clasts with olivine phenocrysts altered to iddingsite. Cores 144-878A-46M to -49R are the same greenish gray color as Section 144-878A-44M-1.

Some of the larger clasts, both volcanic and limestone, are coated by thin (2–4 mm thick), light gray (N7) laminae consisting of glassy volcanic fragments and carbonate debris of silt to fine sand size (e.g., Sample 144-878A-46M-1, 77–79 cm). The origin of this coating is uncertain, but one possibility is that these coatings may have been acquired by larger clasts thrown through a cloud of volcanic and carbonate debris.

Variations in grain size and changes in composition of the average clasts delineate vague beds, 1–3 cm thick, throughout most of Subunit IVB. Bedding attitude varies from horizontal to inclinations of 30° in Core 144-878A-49R and as high as 40° in Section 144-878A-54R-3 (Fig. 14). Small-scale crossbedding occurs in several intervals (e.g., Interval 144-878A-51R-4, 98–129 cm). Several intervals of normal and reverse grading, without sharp contacts, are apparent in the

breccia (e.g., upward coarsening in Interval 144-878A-51R-4, 25–95 cm, and upward fining in Interval 144-878A-51R-6, 70–141 cm).

Subunit IVC

Interval: Sections 144-878A-56R-2, 140 cm, to -65R-6, 22 cm
Depth: 514.74–604.3 mbsf
Age: early-late Aptian

The boundary between Subunits IVB and IVC, both polymictic breccias, is marked by an abrupt color change from light gray (10YR 7/1) to greenish gray (5G 6/1) in Section 144-878A-56R-2, 140 cm. Beds dip 45° below the contact and 15° above the contact. The relative strike of beds above and below the contact differs about 90°. The contact between Subunits IVB and IVC is also marked by a sharp downhole decrease in resistivity and in the Ca/Fe ratio (see “Downhole Measurements and Seismic Stratigraphy” section, this chapter) and an increase in the drilling rate (Fig. 7).

The overall variation in the breccia within Subunit IVC is similar to that within Subunit IVB; volcanic clasts are dominant in the upper half and decrease in abundance toward the base of the subunit. Some alternation occurs between volcanic-rich and -poor horizons throughout the subunit, but carbonate is dominant in the matrix and clasts below Section 144-878A-62R-7. Above Section 144-878A-62R-7, the breccia is varying shades of greenish gray (e.g., 5GY 6/1), gray (e.g., 2.5Y 7/2), and olive gray (5Y 5/2); below this section, the breccia is light gray (N7) because of a decrease in the abundance of volcanic clasts to about 10%–30%, an increase in the size and number of limestone clasts (commonly 1–4 cm in length), and an increased abundance of carbonate matrix. Analyses of bulk carbonate content demonstrate the increase of carbonate in the matrix from the top to the bottom of Subunit IVC (see “Organic Geochemistry” section, this chapter). Resistivity also increases downhole as the abundance of porous, altered vesicular basalt decreases (see “Downhole Measurements and Seismic Stratigraphy” section, this chapter). No sharp boundary is present between the upper volcanic-rich portion and the lower carbonate-rich portion of Subunit IVC.

The volcanic component throughout Subunit IVC is dominated by scoriaceous basalt clasts similar to those of Subunit IVB. The vesicles in these clasts are almost exclusively spherical and only rarely tubular. Some of the clasts are completely altered to clay.

The limestone clasts in Subunit IVC are similar to those of Subunit IVB, except for an increase in the number of gray clasts. The gray color is apparently the result of pyrite, which is found in as many as 5% of the limestone clasts (see “Organic Geochemistry” section, this chapter). Several different lithologies are stained, including miliolid wackestone, peloid packstone, and ooid grainstone. Interval 144-878A-63R-4, 63–87 cm, is a bed, or large clast, cut by several stylonites of very pale brown packstone with a nodular aspect. The contact between the nodular(?) packstone and the breccia is irregular; breccia matrix fills some voids in the limestone.

One characteristic feature of Subunit IVC is inclined bedding angles as steep as 28° to 62° within Cores 144-878A-57R through -62R (Fig. 17). The bedding is recognizable as an alternation of coarser and finer grained intervals on a 2–10 cm scale. Coarse beds are composed of granule- to pebble-sized clasts, whereas the fine beds are coarse sand. Some crossbedding is apparent (Interval 144-878A-65R-2, 114–120 cm; Fig. 15). Bedding inclination is commonly easier to recognize in round cores, in which true dips can also be measured. The steepest inclinations measured were 62° in Core 144-878A-57R, 55°–60° in Core 144-878A-58R, 45° in Core 144-878A-59R, and 55° in Core 144-878A-60R. Rapid changes in the dip orientation within a continuous cylinder and the presence of curved, convolute, and truncated beds strongly suggest that the steep bedding is the result of slumping (Fig. 17). Numerous irregular “veins” of carbonate matrix with steep and irregular boundaries cut through beds of the breccia in the base of Subunit IVC (e.g., Intervals 144-878A-62R-1, 83–110 cm; -62R-2, 103–145 cm; -62R-3, 35–65 cm; and -62R-4, 45–75 cm;

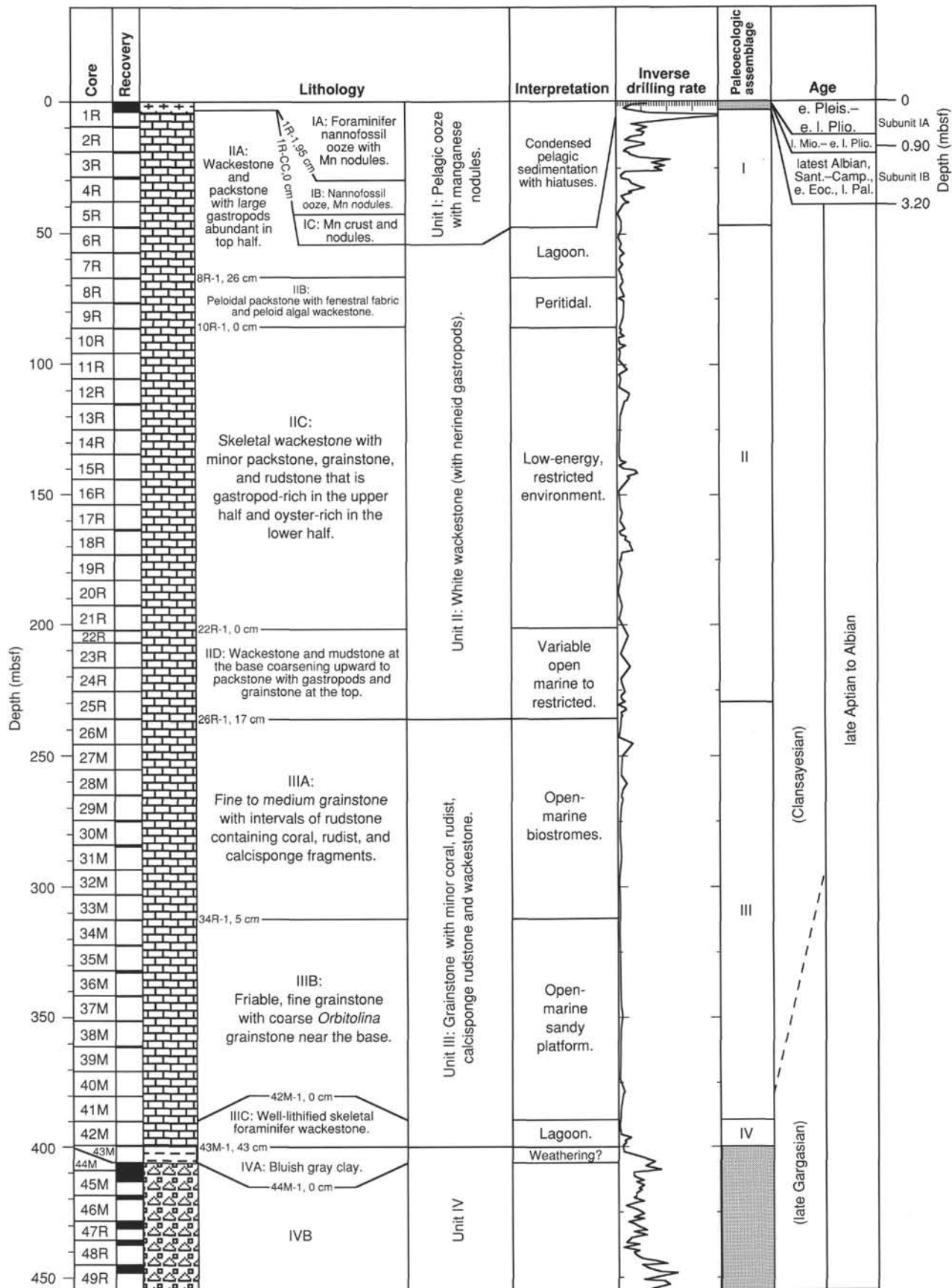


Figure 7. Lithostratigraphic summary and interpretation, Site 878, MIT Guyot.

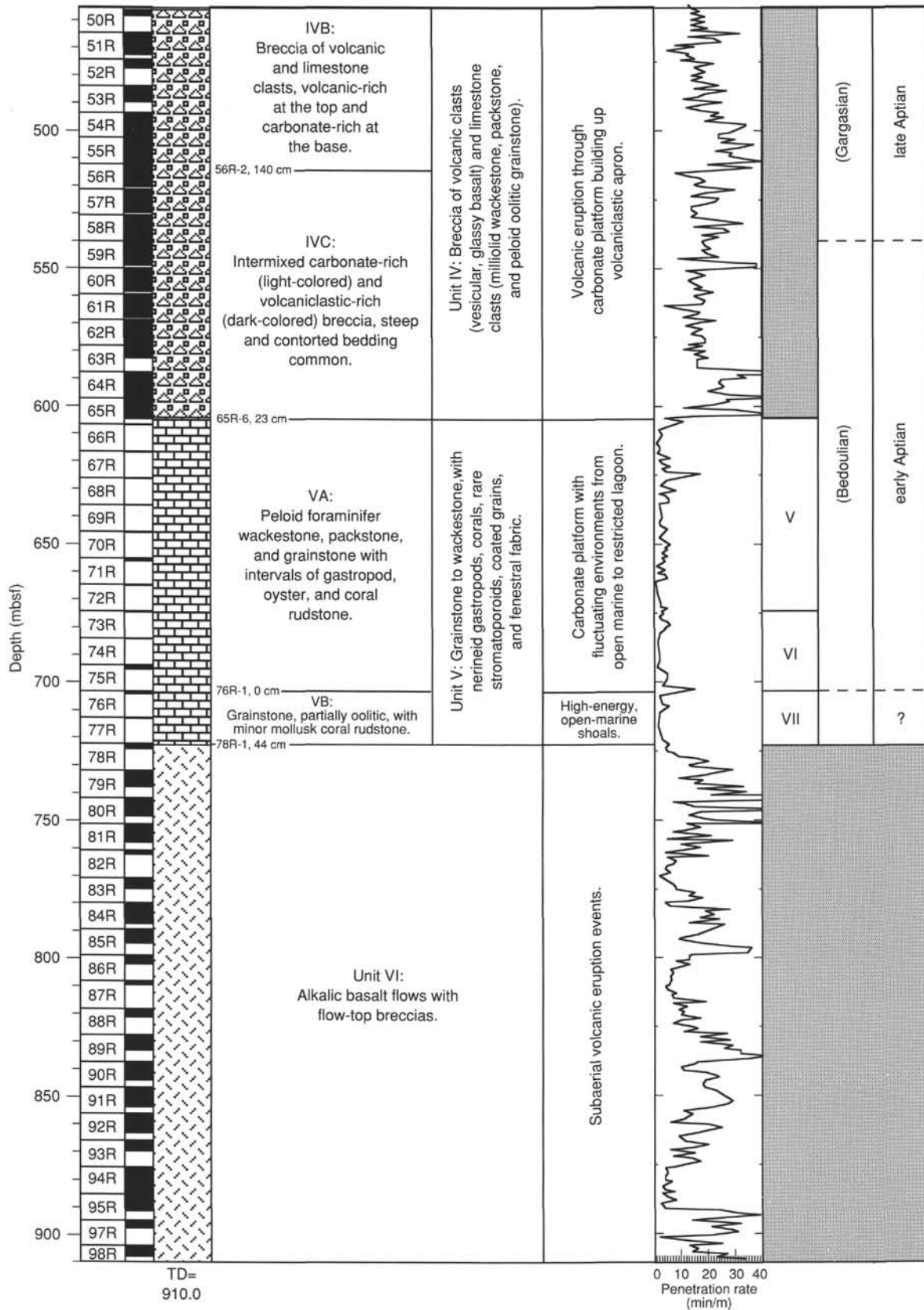


Figure 7 (continued).

Table 4. Summary of components recognized in thin section samples from limestones and volcanic limestone breccias at Site 878.

Unit/subunit	Total porosity (%)	Cement (%)	Volcanic clasts (%)	Limestone clasts (%)	Inorganic calcite (%)	Pellets (%)	Peloids (%)	Ooids (%)	Oncoliths (%)	Lithoclasts (%)	Intraclasts (%)	Micrite (%)	Foraminifers (%)	Benthic foraminifers (%)	Ostracodes (%)	Echinoderms (%)	Calcareous sponges (%)	Corals (%)	Gastropods (%)	Rudists (%)	Other bivalves (%)	Red algae (%)	Green algae (%)	Others (%)	
Subunit IIA average	7.64	3.46	0	0	0	7.27	15.00	0	5.45	0	1.09	48.82	0.45	4.00	0.18	0.84	0.02	0	0.09	0.73	3.19	0	1.18	0.18	
Subunit IIB average	17.50	27.50				0	37.00	0	0	0	0	7.50	0	2.50	0	0	0	0	0	0	7.00	1.00	0	0	
Subunit IIC average	9.45	7.45				1.00	12.91	0	0	0	0.03	55.45	0.91	0.92	0.64	0.10	3.45	0	0.27	0	1.91	0.01	4.00	1.64	
Unit average	9.29	7.30				3.79	15.88	0	2.50	0	0.51	48.42	0.63	2.46	0.38	0.43	1.59	0	0.17	0.33	2.92	0.09	2.38	0.83	
Unit SD	8.09	9.49				11.43	16.92	0	8.47	0	1.44	35.74	1.06	4.15	0.82	0.88	7.75	0	0.48	1.17	4.00	0.41	5.99	2.24	
Subunit IID average	19.67	1.33				0	33.67	0	0	0	0	35.67	3.33	2.67	0	0	0	0	1.00	0	0.03	0	0	1.67	
Subunit IIIA average	18.60	19.00				0	10.20	0	4.80	0.20	0	5.00	0	7.60	0	2.60	8.00	0	0.40	0	18.40	0	0.40	0.40	
Subunit IIIB average	22.25	5.75				0	36.25	0	4.25	0	0	11.25	0	6.50	0	4.25	0	0	0	0	9.25	0	0.25	0	
Subunit IIIC average	7.50	1.50				0	17.75	0	0	0	0	59.75	0	10.00	0	0	0	0	0.25	0	1.50	0	2.25	1.00	
Unit average	16.94	8.00				0	23.00	0	2.56	0.06	0	26.00	0.63	7.00	0	1.88	2.50	0	0.38	0	8.44	0	0.75	0.69	
Unit SD	12.55	12.55				0	21.10	0	6.00	0.25	0	30.25	2.50	9.36	0	2.28	10.00	0	0.89	0	10.28	0	2.27	1.40	
Subunit IVB average																									
Breccia only	0.63	5.74	28.95	12.21	0	0	19.84	2.38	0.06	0.47	0	25.58	0.68	0.11	0	0.01	0.05	0	0.01	0.11	1.32	0	0.01	1.69	
Carbonate only	3.90	12.30	0	0	0	0.40	22.00	2.51	1.00	0	1.50	39.40	5.10	3.50	0.15	0.10	0.10	1.00	0.20	0.10	1.30	0.10	0.20	5.40	
Subunit IVC average																									
Breccia only	2.32	3.21	18.79	27.26	0	0.16	19.05	1.68	0.53	0	0.53	24.16	0	0.53	0	0	0	0	0	0	0.58	0	0.16	0.79	
Unit average breccia only	1.47	4.47	23.87	19.74	0	0.08	19.45	2.03	0.29	0.24	0.26	24.87	0.34	0.32	0	0.01	0.03	0	0	0.06	0.95	0	0.08	1.24	
Unit SD breccia only	2.35	8.15	11.17	19.88	0	0.49	10.74	1.89	1.63	1.46	1.62	15.99	0.67	0.93	0	0.02	0.16	0	0.02	0.23	2.49	0	0.27	2.43	
Carbonate only	1.50	10.50	0	0	0	0	27.50	7.50	0	0	1.00	30.00	10.00	1.00	0.50	0	0	2.00	0.05	0	2.50	1.00	0	5.00	
Unit average carbonate only	3.50	12.00	0	0	0	0.33	22.92	3.34	0.83	0	1.42	37.83	5.92	3.08	0.21	0.08	0.08	1.17	0.18	0.08	1.50	0.25	0.17	5.33	
Unit SD carbonate only	8.51	11.99	0	0	0	1.15	14.37	6.85	2.89	0	3.09	21.86	7.18	10.07	0.37	0.29	0.29	3.01	0.39	0.29	2.94	0.62	0.58	8.30	
Subunit VA average	15.23	3.08	0	0	1.92	0	23.31	5.70	4.15	0	4.54	23.46	1.15	1.85	0.31	3.08	0.15	0	0	0.31	7.69	1.15	0	1.17	
Subunit VB average	35.00	17.00	0	0	0	0	28.50	0	0	0	6.50	1.00	0	0.10	0	2.50	0.55	0	0	0	6.50	2.55	0	0	
Unit average	17.87	4.93	0	0	1.67	0	24.00	4.94	3.60	0	4.80	20.47	1.00	1.62	0.27	3.00	0.21	0	0	0.27	7.53	1.34	0	1.00	
Unit SD	10.33	6.83	0	0	4.50	0	17.72	11.15	8.93	0	8.42	22.96	3.87	3.80	1.03	3.53	0.56	0	0	1.03	5.57	2.77	0	2.42	

Note: SD = standard deviation.

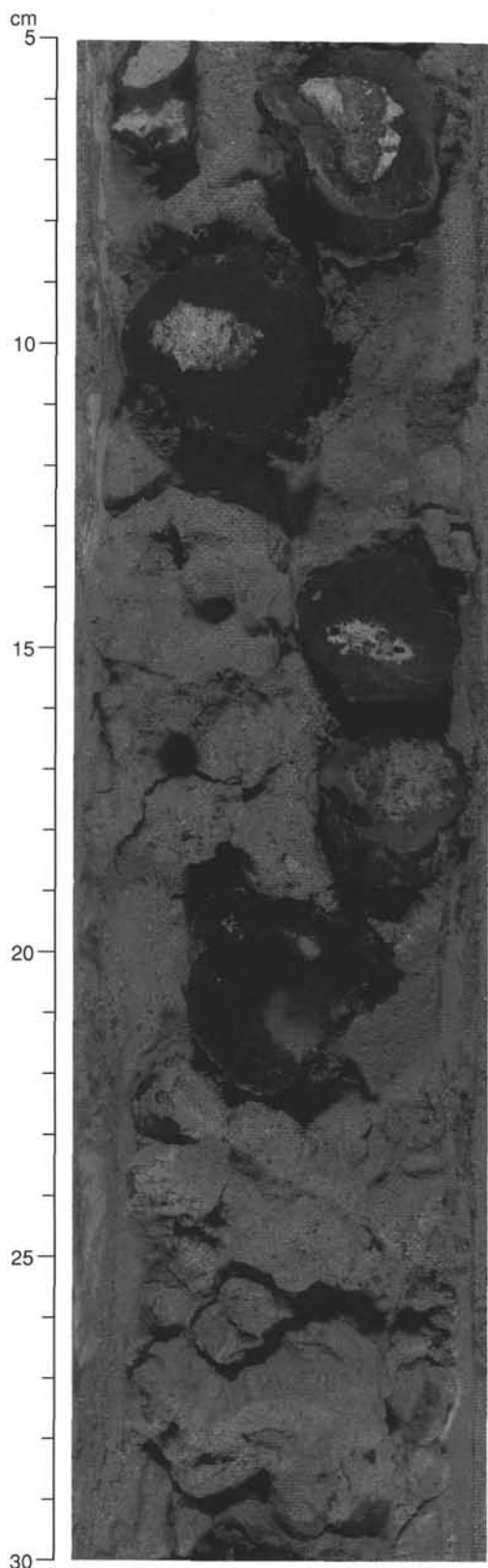


Figure 8. Close-up photograph of manganese nodules in foraminifer nannofossil ooze typical of Subunit IA (Interval 144-878A-1R-1, 5–30 cm).

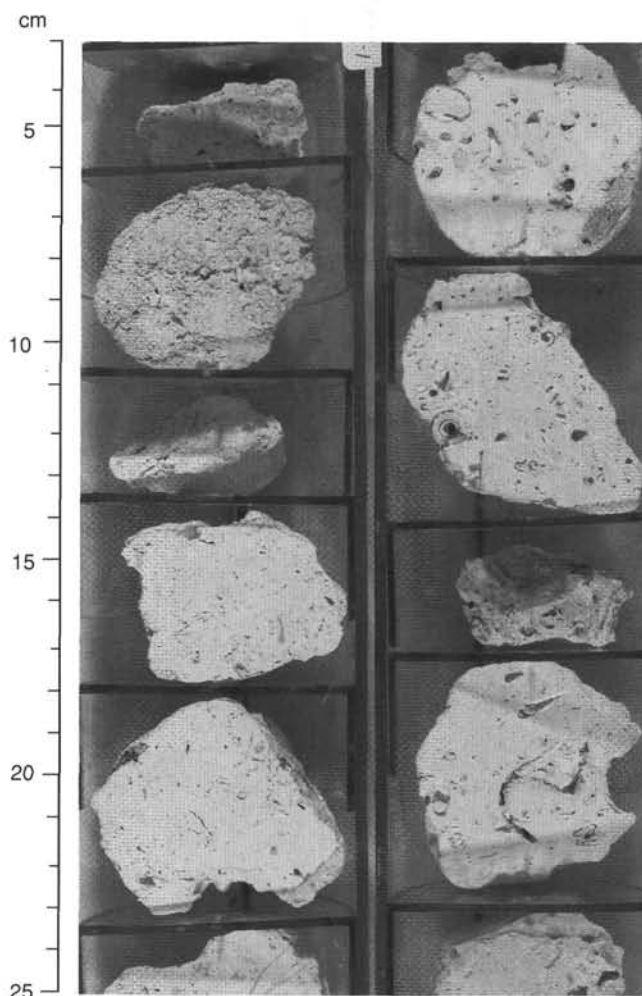


Figure 9. Close-up photograph of gastropod wackestone and packstone typical of Subunit IIA (Intervals 144-878A-2R, 3–25 cm [right], and -3R, 3–25 cm [left]).

Fig. 18). These are interpreted as fluid-escape structures. As in Subunit IVB, numerous normal and reverse graded intervals are present in Subunit IVC (e.g., Interval 144-878A-61R-5, 14–26 cm).

Toward the base of Subunit IVC, coarse sand laminae and beds up to 10 cm thick become common. Below Core 144-878A-60R, bed inclination generally decreases to only 5° at the base of the subunit. Downhole logging documented that the hole has a general inclination of 5° (see “Downhole Measurements and Seismic Stratigraphy” section, this chapter); this means most beds near the base of Subunit IVC are horizontal. Such an observation is significant because it suggests that the substratum upon which the breccia was deposited is horizontal. Only a few beds within Section 144-878A-64R-1 are inclined 18°; a possible contorted bed is present in Section 144-878A-64R-6.

The lowermost breccia (Core 144-878A-65R) shows that the base of Subunit IVC has been altered. A sharp contact at Section 144-878A-65R-5, 31 cm, separates light gray (N7), carbonate-rich breccia with dark greenish gray volcanic clasts, typical of the lower portion of Subunit IVC, from a yellow (10YR 7/6) breccia in which volcanic clasts are altered into clayey aggregates. In Interval 144-878A-65R-5, 44–60 cm, some vesicular basalt clasts have large vesicles, several millimeters in diameter, with reddish rims. In some of the clasts, vesicles are elongated. At the base of Subunit IVC (Interval 144-878A-65R-6, 8–22 cm), volcanics are coarse sand size and comprise only 10% of the sediment volume. Limestone clasts are 1.0–1.5 cm in size

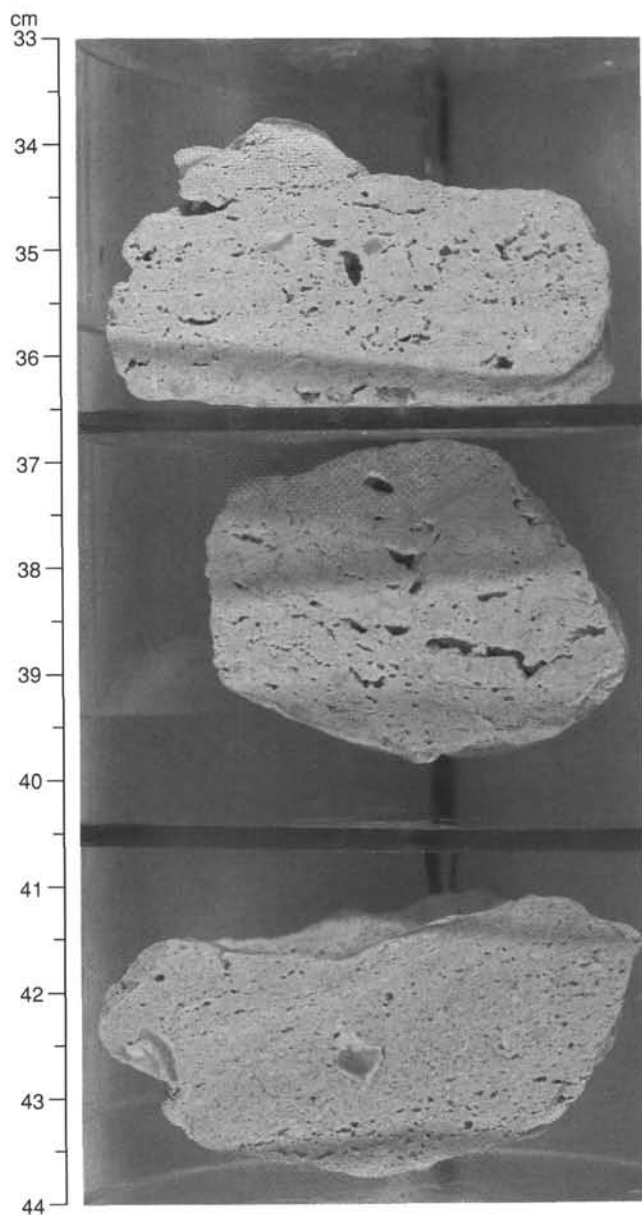


Figure 10. Close-up photograph of packstone with fenestral fabric from Subunit IIB (Interval 144-878A-9R-1, 33–44 cm).

and include oolitic grainstone, miliolid packstone, and silt-sized peloid packstone. The contact between the breccia and the underlying limestone was recovered at Section 144-878A-65R-6, 22 cm.

Unit V

Interval: Sections 144-878A-65R-6, 22 cm, to -78R-1, 44 cm
 Depth: 604.3–722.54 mbsf
 Age: early Aptian

Unit V consists of 118.34 m of very pale brown (10YR 8/3), skeletal grainstone, packstone, and wackestone with intervals of rudstone that contain large nerineids and corals. Two subunits are differentiated, based on changes in texture and composition. Given the overall low recovery of the subunit, precise relationships between the different lithologies cannot be defined.

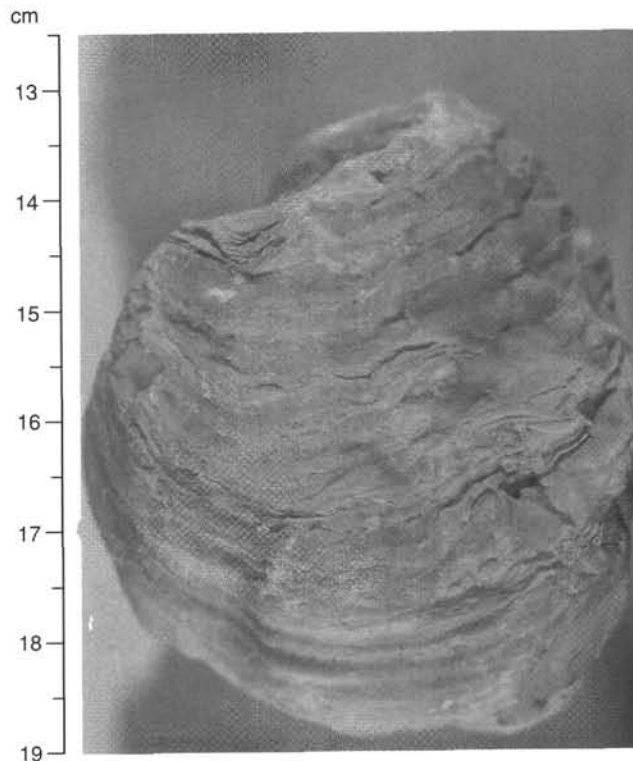


Figure 11. Close-up photograph of whole oyster shell from the lower half of Subunit IIC (Interval 144-878A-19R-1, 12–19 cm).

Subunit VA

Interval: Sections 144-878A-65R-6, 22 cm, to -76R-1, 0 cm
 Depth: 604.3–703.0 mbsf
 Age: early Aptian

Subunit VA consists of peloid and foraminifer wackestone, packstone, and grainstone with intervals of gastropod, oyster, and coral rudstone and some stromatoporoid boundstone. The variation of lithologies within the Subunit VA suggests two broad textural trends with a boundary between Cores 144-878A-70R and -71R. Lithology changes within each trend from mudstone and wackestone at the base to rudstone and grainstone at the top. However, because of a recovery rate of <7% (see “Operations” section, this chapter), these trends are not precisely defined and should be considered interpretative.

At the top of the upper trend, the grainstone is composed of peloids of medium sand size with a few ooids and coated grains. Rare components are lithoclasts, miliolids and other foraminifers, echinoderms, coral(?), oysters, and rudist(?) fragments. The grains are well sorted. Porosity is up to 35%, mostly interparticle with some molds. Cement is very patchy, coarse, equant calcite. In thin section, some cement appears to be concentrated as bridges between grains with local curved (meniscus) boundaries (e.g., thin-section Sample 144-878A-66R-1, 10–15 cm).

Packstone is peloidal and skeletal-peloid, with grains of fine sand to silt size. The dominant constituents are peloids, miliolids, mollusks, small gastropod molds, a few red algae, and calcisponge fragments. Rare components are ooid grains and lithoclasts. Packstone forms the matrix surrounding nerineids and oysters in the rudstone (Intervals 144-878A-67R-1, 54–79 cm, and -68R-1, 20–25 cm). The oyster rudstone contains many coated grains with dense, laminated, coatings that resemble coralline algae. Such grains occur throughout Unit V, but their possible algal origin is difficult to confirm, even in thin

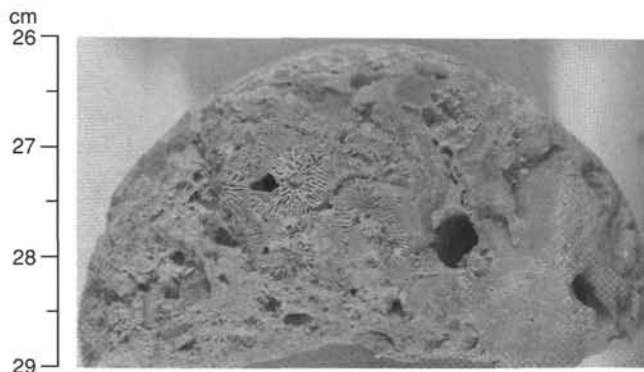


Figure 12. Close-up photograph of coral fragment typical of rudstone intervals in Subunit IIIA (Interval 144-878A-31M-1, 26–29 cm).

section. Minor components of the rudstone are calcisponges, squamariacean red algae, and corals. Porosity in the packstone is intergranular, moldic, and vuggy; it ranges from 5% to 15%.

Miliolid foraminifers, peloids, molluscan shell fragments (some rudists), and molluscan molds (few gastropods) are the dominant constituents in the wackestone from the upper trend in Subunit VA (e.g., Intervals 144-878A-69R-1, 0–19 cm, and -70R-1, 20–44 cm). Other minor constituents include ooids, red algae, and stromatoporoid fragments; some stromatoporoid boundstone was recovered from within the wackestone and packstone of Subunit VA (Interval 144-878A-70R-1, 15–22 cm). Porosity in the wackestone is mostly solution-enlarged interparticle, some moldic after gastropods, and some is possibly fenestral (Interval 144-878A-70R-1, 22–40 cm). The sparse cements are crusts of finely crystalline, bladed calcite. Some orange and yellow staining is present in the pore spaces. The peloid wackestone and mudstone at the base of the upper trend (Core 144-878A-70R, 44–57 cm) is very pale brown (10YR 8/3), with a few discernable grains, including peloids and rare gastropods. Some of the grains are stained pale yellowish orange (10YR 8/6) in Interval 144-878A-70R-1, 53–57 cm.

The lower trend in Subunit VA (Cores 144-878A-71R to -75R) is similar to the upper trend. Coarser, grainier facies, such as skeletal rudstone and medium to coarse grainstone, alternate with packstone in the upper half of the trend. Finer grained facies (silt-sized packstone and wackestone) occur at the base of the trend.

At the top of the lower trend, 23 cm of skeletal packstone (Interval 144-878A-71R-1, 0–23 cm) overlies 107 cm of bedded, skeletal grainstone (Interval 144-878A-71R-1, 23–130 cm) that fines from very coarse sand at the base to medium sand at the top (Fig. 19). The grains are well sorted and rounded with micrite envelopes or coatings 50–150 μm thick. Skeletal components include a few bivalves, red algae, corals, calcisponges, and gastropods. The grainstone has 35%–40% porosity, mostly interparticle, with minor vugs and molds. Interparticle cement is finely crystalline, equant to bladed calcite, whereas the cement in molds is coarsely crystalline. The grainstone is laminated in gently inclined beds (5%–10%); the apparent bed inclination may be a product of hole deviation (see “Downhole Measurements and Seismic Stratigraphy” section, this chapter).

Rudstone with grainstone and packstone matrix was recovered in Intervals 144-878A-73R-1, 0–24 cm, and -74R-1, 0–19 cm. The rudstone contains coral molds, recrystallized coral colonies up to 4 cm in diameter, large (1.5 cm diameter) nerineids (Fig. 20), 1-cm-sized lithoclasts and calcisponge fragments. Grains in the rudstone matrix are commonly ovoid to spherical, up to 1 mm in size, but recrystallized beyond recognition. Corals and gastropod molds were heavily bored; bores were filled and preserved as the shells were dissolved to form molds. Some molds are lined with medium to coarse, bladed and equant, clear calcite. The gastropod rudstone in Interval 144-878A-74R-1, 8–19 cm, is a coquina; nerineids and molds up to 1.5 cm in

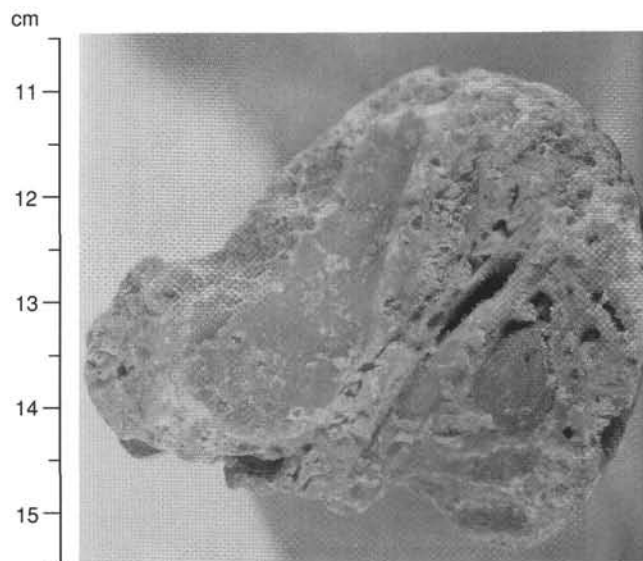


Figure 13. Close-up core photograph showing the recrystallization, cementation, and porosity typical of rudstone intervals in Subunit IIIA (Interval 144-878A-31M-1, 11–15 cm).

diameter make up 70% of some samples (Fig. 20). The gastropods and molds are surrounded by wackestone to packstone matrix. Intergranular porosity of the matrix is 10%–15%. Micritization is pervasive; one coral fragment at Section 144-878A-74R-1, 37 cm, has been completely micritized.

Other lithologies at the top of the lower trend in Subunit VA include ooid-peloid grainstone, minor fenestral wackestone (Interval 144-878A-72R-1, 0–6 cm), and algal-stromatoporoid boundstone (Interval 144-878A-72R-1, 13–18 cm). Fenestrae in the wackestone (Interval 144-878A-72R-1, 0–6 cm) are lined by crusts of clear, coarsely crystalline, bladed calcite, some of which are stained orange.

The basal part of the lower trend in Subunit VA (Interval 144-878A-74R-1, 19–41 cm, and Core 144-878A-75R) consists of white, fine-grained packstone to wackestone. The grains are mostly unidentified except for a few thin molluscan shell fragments, rare benthic foraminifers, rare coral fragments, 0.5–1.0 cm in size, and few planktonic foraminifers and nannofossils (see “Biostratigraphy” section, this chapter). Some mottling may be the result of burrowing. Porosity, about 10%, is moldic and vuggy; some pore space is stained orange. Little visible cement is evident. There are stylolites in Intervals 144-878A-75R-1, 32–38 cm, and -75R-2, 0–5 cm. Sections 144-878A-75R-1, 118 cm, to -75R-2, 35 cm, have wavy ripple laminae that resemble flaser bedding (Fig. 21). No visible difference is present between grains in adjacent laminae; the color variation may be related to local variation in cement.

Subunit VB

Interval: Sections 144-878A-76R-1, 0 cm, to -78R-1, 44 cm
Depth: 703.0–722.54 mbsf
Age: early Aptian

Subunit VB is dominated by very pale brown (10YR 7/4), coarse-grained, skeletal grainstone with minor molluscan coral rudstone. A majority of grains are rounded and coated by micrite up to 200 μm thick. Skeletal constituents include molds of small gastropods, red algae, cyanobacterial bushes (*Ortonella*), calcisponges, corals, and stromatoporoids. A few highly altered granules of basalt were found within the grainstone in Cores 144-878A-76R and -78R. Cement in the grainstone is patchily distributed, with porosity ranging from 20% to 35%. About two-thirds of the porosity is primary interparticle. Some

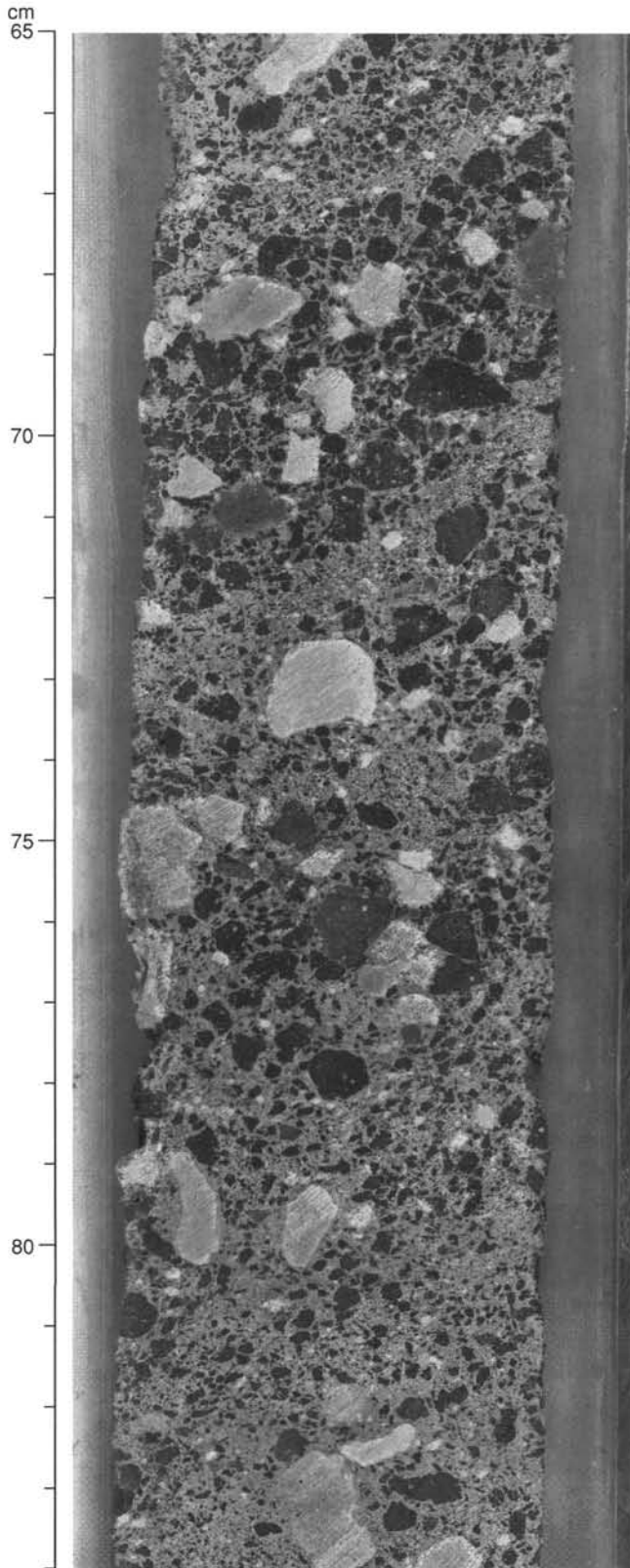


Figure 14. Close-up core photograph of polymictic breccia typical of Unit IV (Interval 144-878A-54R-3, 65–84 cm).

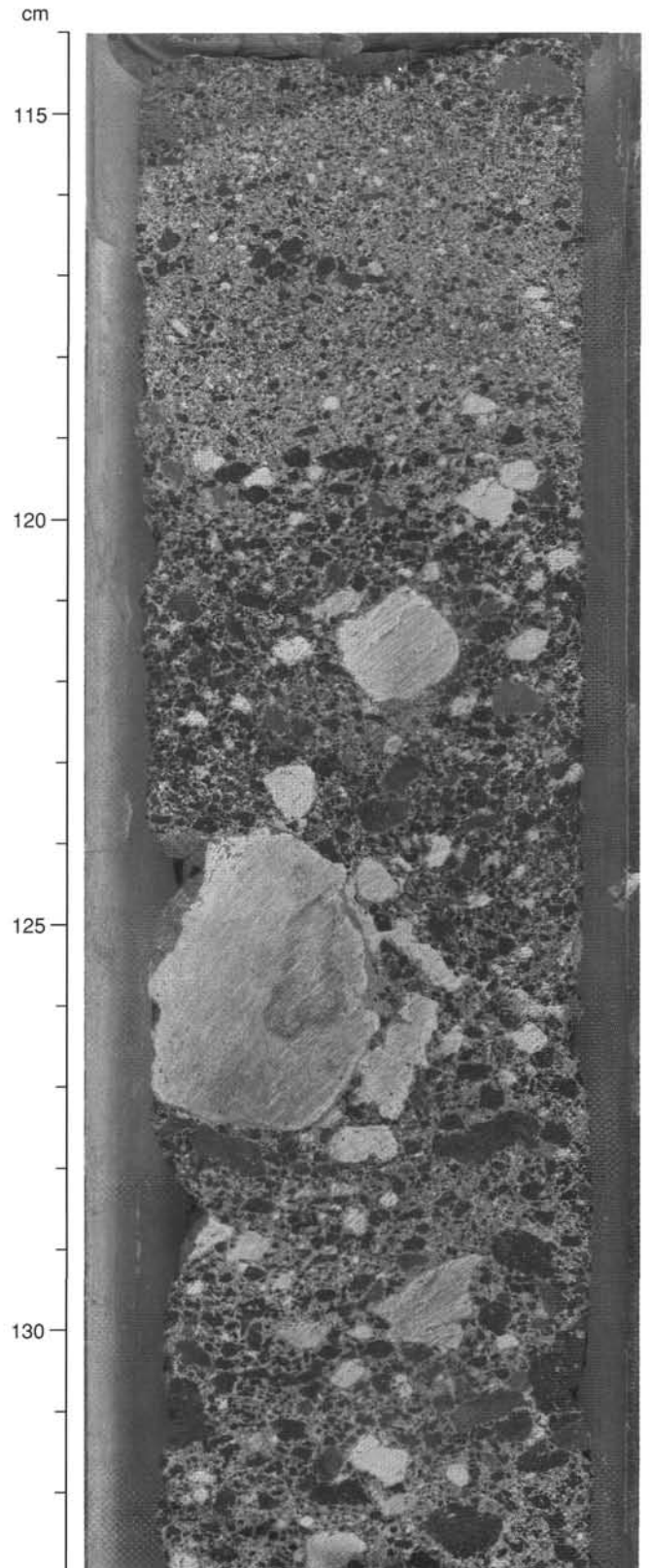


Figure 15. Close-up core photograph of polymictic breccia in Subunit IVC with large, rounded limestone clasts (Interval 144-878A-65R-2, 120–133 cm) and cross-bedding in a sandy bed (Interval 144-878A-65R-2, 114–120 cm).

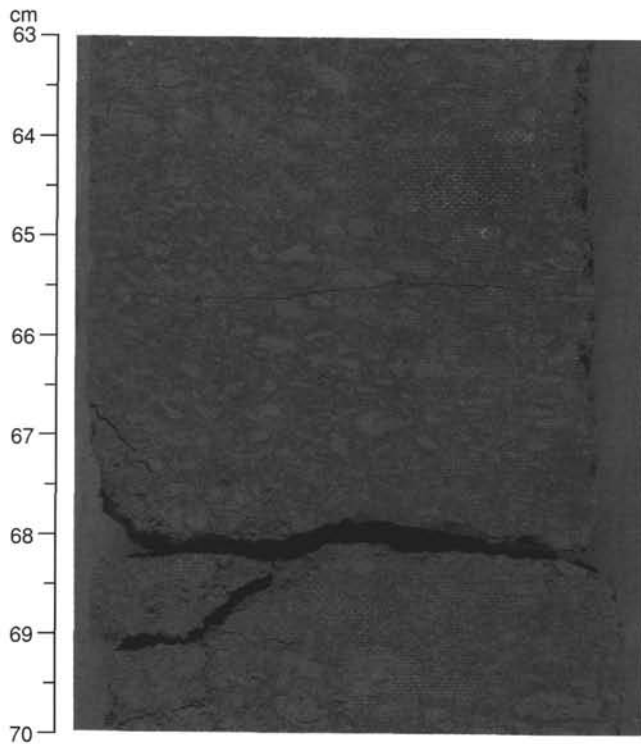


Figure 16. Close-up core photograph of bedded, highly altered, elongated, glassy, vesicular clasts that may be an ash flow tuff at the top of Subunit IVB (Interval 144-878A-44M-1, 63–70 cm).

of the beds within Interval 144-878A-77R-1, 47–52 cm, show low-angle cross-stratification. A low-relief stylolite can be seen in Section 144-878A-76R-1, 53 cm. Skeletal fragments in rudstone intervals (Intervals 144-878A-76R-1, 64–74 cm, and -76R-1, 100–121 cm) are up to 4 cm in size and consist of colonial coral, stromatoporoid fragments, and gastropod molds. The coral rudstone is cemented by cloudy isopachous calcite.

Above the contact with basalt (Section 144-878A-78R-1, 43 cm), the grainstone is stained reddish yellow (5YR 6/6), is leached, and has variably high intergranular porosity (15%–30%). The grainstone is poorly sorted, with grains ranging from 0.25 to 4.0 mm. The grains include common red algae fragments and many fragments of corals. Some of the grains are coated by micrite. Calcite cement is sparse and mainly isopachous. The contact with the underlying basalt (Core 144-878A-78R-1, 44 cm) is sharp. The top of the basalt underlying the carbonates has been completely altered into purple claystone with iron oxide veins.

Unit VI

Interval: Sections 144-878A-78R-1, 44 cm, to -98R-3, 101 cm

Depth: 722.54–907.8 mbsf

Age: early Aptian or older

Subunit VI consists of 185.34 m of alkalic basalt flows with flow-top breccias. See “Igneous Petrology” section, this chapter, for a detailed discussion of Unit VI.

Preliminary Interpretation of Depositional History

This interpretation of depositional history at MIT Guyot is speculative because of the very low core recovery in the carbonate sequences.

The top of volcanic basement at MIT Guyot consists of multiple lava flows with flow-top breccias, indicating subaerial eruption. Unit

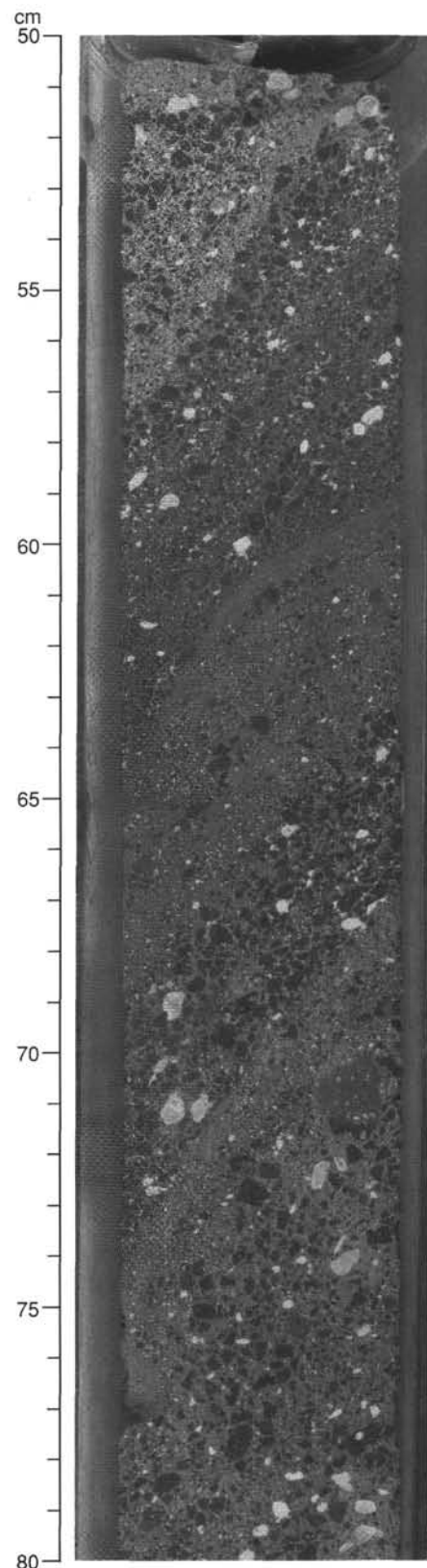


Figure 17. Close-up core photograph of steeply inclined beds in the polymictic breccia of Subunit IVC (Interval 144-878A-57R-3, 50–80 cm). Note the truncation of beds in Interval 144-878A-57R-3, 59–60 cm.

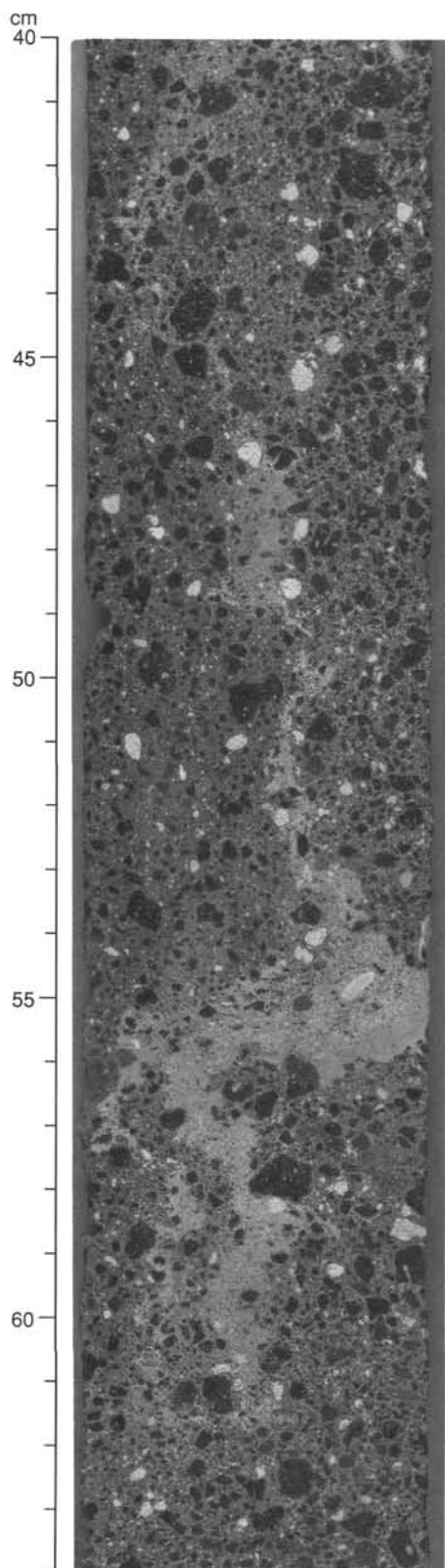


Figure 18. Close-up core photograph of fluid escape structure in polymictic breccia from Subunit IVC (Interval 144-878A-62R-3, 40–64 cm).

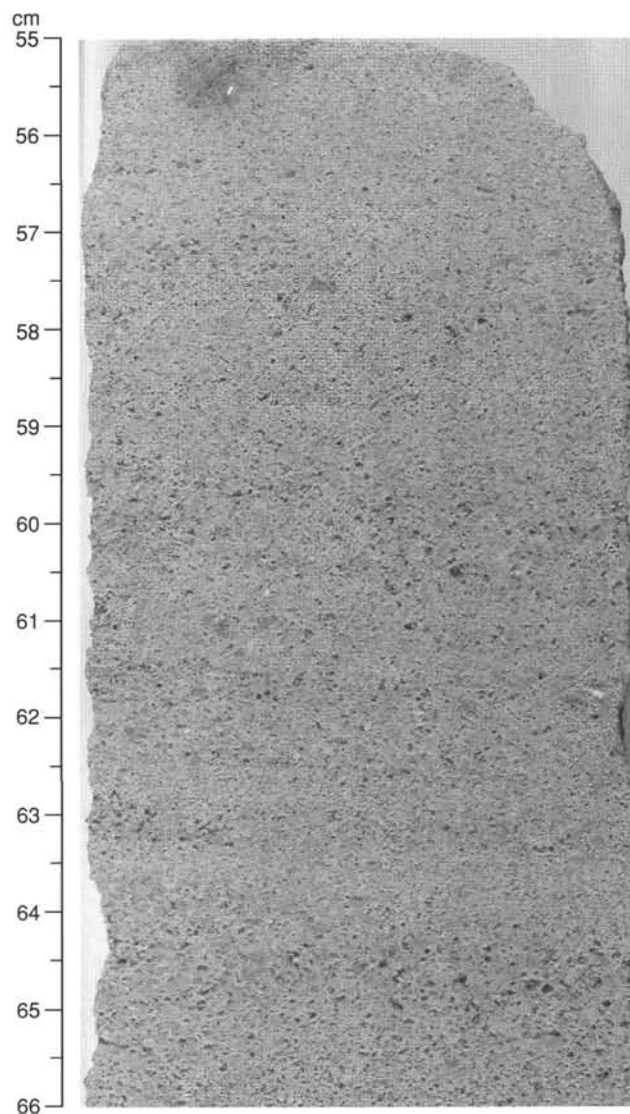


Figure 19. Close-up core photograph of bedding in the grainstones from Subunit VA (Interval 144-878A-71R-1, 55–66 cm).

tops are variably altered by weathering and/or hydrothermal activity (see “Igneous Petrology” section, this chapter). Subaerial eruption is further indicated by the lack of marine sediment intercalated between basalt flows.

The limestones that overlie basalt (Subunit VB) are well sorted and partly oolitic; they include debris of red algae, bivalves, gastropods, bryozoans, echinoderms, and corals. Subunit VB is a high-energy, open-marine, transgressive sand deposit. Corals and stromatoporoid debris suggest that bioherms were locally established on the guyot during the flooding of basement and the deposition of Subunit VB.

Planktonic foraminifers and nannofossils in fine-grained lithologies (wackestone) at the base of Subunit VA (Core 144-878A-75R) indicate a change from a high-energy, open-marine setting (Subunit VB) to a quieter, deeper, unrestricted marine environment. Increases in the grain size and abundance of coral, stromatoporoid, calcisponge, and gastropod debris from Cores 144-878A-74R to -72R reflect a coarsening and shoaling upward trend. During this shoaling interval, favorable conditions for colonization of the guyot by reef-building biota were established, although these biota are only represented by redeposited detritus at Site 878. The presence of ooid-peloid grain-

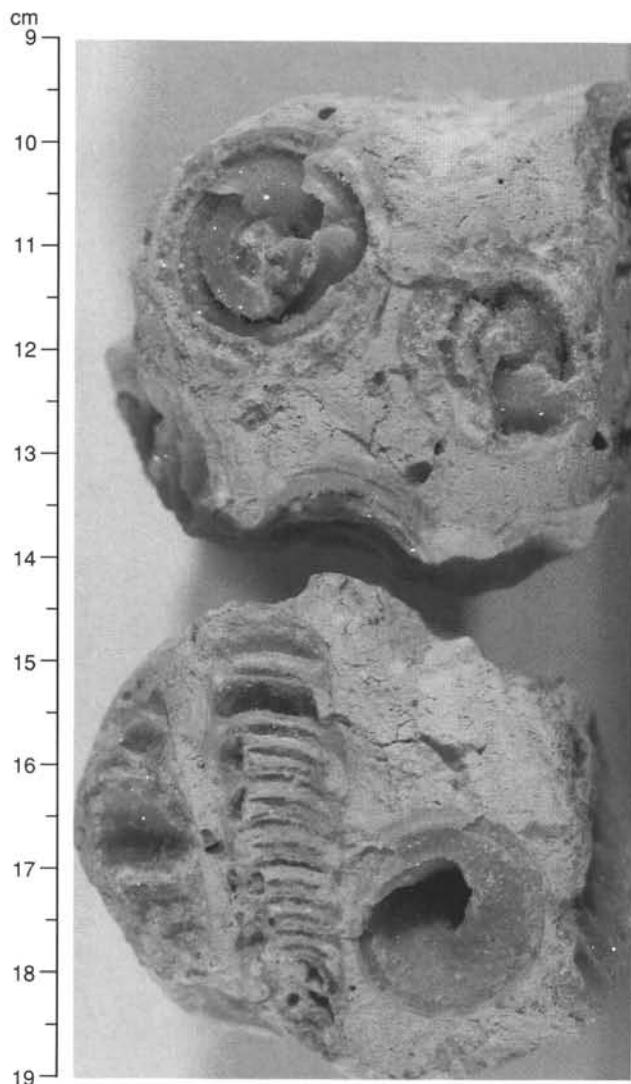


Figure 20. Close-up core photograph of large nerineids from Subunit VA (Interval 144-878A-74R-1, 9–19 cm).

stone and packstone above the rudstone in the lower portion of Subunit VA indicates a high-energy, shallow depositional environment near the top of the trend (Cores 144-878A-71R and -72R). Further shoaling with peritidal deposition is indicated by fenestral fabric in the fine-grained packstone in Section 144-878A-72R-1.

Mudstone and wackestone in Core 144-878A-70R, at the bottom of the second textural trend, indicate a return to a quieter depositional environment. The mudstone and wackestone are both bioturbated. The middle part of the trend is represented by nerineid gastropod rudstone and oyster-gastropod coquina, both with a wackestone to packstone matrix (Cores 144-878A-66R to -68R); the environment of deposition was probably normal marine, variably low to high energy. The top of this second textural trend is marked by coated grain and oolitic grainstones deposited in a shallow, high-energy environment.

Development of the carbonate platform was interrupted by one or more volcanic eruptions that broke through the platform. The platform carbonates were fragmented, mixed with volcanics, and redeposited on top of an undisturbed portion of the platform. The presence of coated-grain oolitic grainstones at the top of the platform (Unit VA) suggests that the initial breccia may have been deposited in a shallow, high-energy environment.

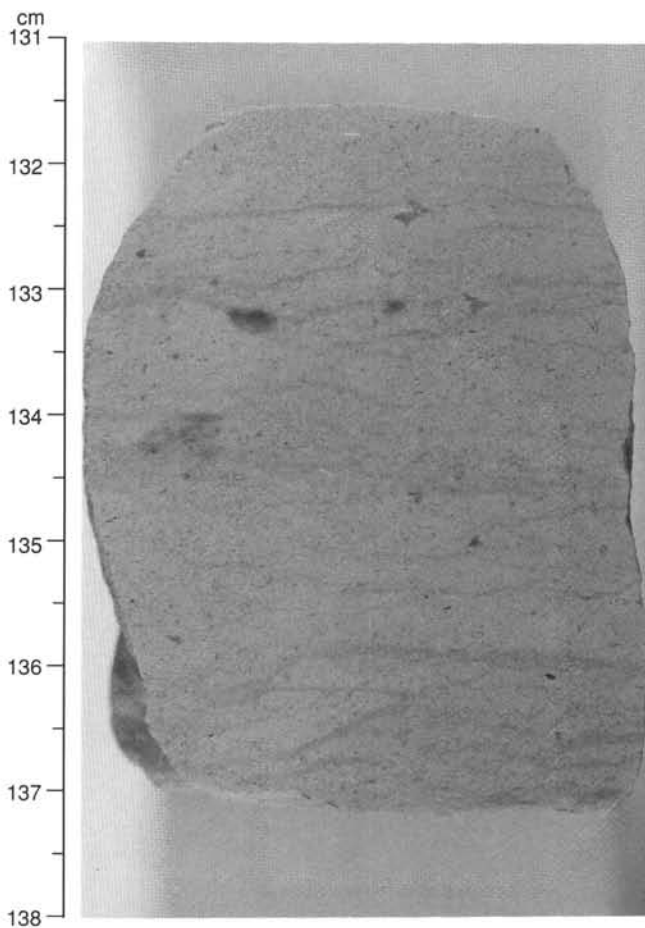


Figure 21. Close-up core photograph of wavy laminae that may be flaser bedding near the base of Subunit VA (Interval 144-878A-75R-1, 131–138 cm).

The breccia consists of two distinct intervals in which the percentage of volcanic component increases upward (see description of Subunits IVB and IVC, above). These parallel trends observed in the breccia may be related to separate eruptive events; the two subunits are separated by a sharp, unconformable contact that appears to be erosional. During each eruptive cycle, initial ejecta may have been dominated by preexisting (accidental) material, both limestone and lava. As the vent became established, progressively more “juvenile” material, derived from new lava, was incorporated into the eruptive products (see “Igneous Petrology” section, this chapter).

The size of volcanic fragments rarely exceeds an average of 2 cm, indicating that deposition was not immediately adjacent to the volcanic center. Not a single carbonate bed was found intercalated within the breccia, where recovery was nearly complete. The lack of such sediments indicates that deposition of the breccia occurred in a very short time, or that it was subaerial, or both. The only suggestion of subaerial exposure is oxidation at the top of Subunit IVB; this could be the result of subaerial exposure or from percolation of oxygenated ground water. No evidence exists for weathered surfaces in the breccia. The presence of contorted bedding and fluid escape structures supports rapid deposition and extensive slumping during the construction of Subunit VC.

The breccia was submerged and shallow-water carbonates were deposited during late Aptian to Albian time (see “Biostratigraphy” section, this chapter). The cause of submergence could be one or more of the following processes: isostatic adjustment, thermal subsidence, eustatic rise, or faulting of the edifice.

The clay interval penetrated at the top of the breccia could represent a weathered surface of the breccia or a sedimentary deposit. The abundance of pyrite in the clay and in the first section of breccia precludes weathering in an oxygenated environment.

The clay is overlain by 10 m of mudstone and wackestone (Subunit IIIC), with faunas typical of a restricted or poorly oxygenated marine environment. A major change took place in the depositional environment between Subunits IIIC and IIIB. Planktonic foraminifers were recovered at the base of Subunit IIIB, and the grainstones in Subunit IIIB have faunas and textures typical of moderate-energy, open-marine environment; Subunit IIIA consists of more grainstone with at least two intervals of coral, rudist, and calcisponge-rich rudstone with a packstone matrix. We interpret the sequence of lithologies in Subunits IIIB and IIIC as (1) flooding (deepening) of a quiet lagoonal environment (base of Subunit IIIB over Subunit IIIC), (2) establishment of an open-marine sandy platform (Subunit IIIB), followed by (3) growth of one or more bioherms near the site (Subunit IIIA).

The bioturbated wackestone at the base of Subunit IID, which contains both benthic and planktonic foraminifers (see "Biostratigraphy" section, this chapter), was deposited in a low-energy, open-marine, subtidal environment. The succession of facies in Subunit IID from wackestone and mudstone to packstone containing nerineid gastropods and then to well-sorted grainstone with larger foraminifers at the top of the subunit indicates progression from lower to higher energy environments. Subunit IIC is mostly skeletal wackestone deposited in a low-energy, restricted environment. Minor skeletal peloid packstone and rudstone with a mixture of fragmented and whole oysters, nerineid gastropods, benthic foraminifers, ostracodes, and sponge spicules indicate that the deposition of Subunit IIC was punctuated by intervals of storm deposition.

Subunit IIB consists of peloid algal wackestone and a few intervals of peloid packstone with fenestral fabric and isopachous, bladed sparry calcite cement (Sections 144-878A-10R-1, 0 cm, to -8R-1, 26 cm). This packstone is interpreted as a peritidal deposit.

The overlying Subunit IIA is dominated by wackestone and peloid packstone with nerineid gastropods, especially common at the top, ostracodes, and benthic foraminifers. These may be lagoonal deposits interspersed with storm deposits.

Based on the ages of sediments from the nuclei of manganese nodules in Unit I, MIT Guyot drowned by latest Albian time. The pelagic sediments from latest Albian to middle Eocene age are preserved only as nuclei in manganese nodules (see "Biostratigraphy" section, this chapter). The accumulation of pelagic sediment at Site 878A (Subunit IA and IB) did not begin until late Miocene time and continued at least until early Pleistocene. These sediments are confined to surface depressions on the top of the guyot. Manganese nodules within the pelagic cover, some of which are significantly older than the surrounding sediment, likely were eroded from surrounding elevated surfaces.

BIOSTRATIGRAPHY

Introduction

Three holes were drilled at Site 878 on MIT Guyot. Hole 878A penetrated a thin pelagic section overlying a very thick sequence of platform limestones and breccia atop basaltic basement. Holes 878B and 878C were drilled to core a more complete pelagic sequence and manganese crust, but only manganese nodules, with a superficial cover of nanofossil ooze, and the top of the platform limestones were recovered.

Age dating of the pelagic sediments is based on calcareous nanofossils and planktonic foraminifers. Paleoenvironmental interpretations are supplemented by studies of palynomorphs and siliceous microfossils.

Benthic foraminifers are encountered frequently through the platform limestones and breccia and provide the basis for the biostratigraphy and paleoenvironmental reconstruction. Calcareous nanofossils and planktonic foraminifers occur at three levels within the platform carbonates, allowing more precise biostratigraphic control.

Calcareous Nanofossils

Pelagic Sediments

The interval from Sections 144-878A-1R-1 through -1R-3 consists of intermixed foraminifer nanofossil ooze, nanofossil ooze, and manganese nodules (Fig. 22). The material in Sections 144-878A-1R-1 and -1R-3, is largely soupy and structureless, whereas that in Section 144-878A-1R-2 is coherent and only moderately disturbed. Nanofossil biostratigraphy indicates that these sections contain ooze of at least three ages, although only the material in Section 144-878A-1R-2 is relatively untainted by mixing and/or reworking.

Section 144-878A-1R-1 consists of a soupy ooze containing mixed nanofossil assemblages. The degree of mixing varies within this section. One slide (from Sample 144-878A-1R-1, 30–31 cm) contains a relatively small proportion (<3%) of taxa such as discoasters that could have been derived from the underlying upper Miocene (Subzone CN9b). If these are discounted as reworked or mixed, the remaining taxa yield biostratigraphically coherent assemblages of early Pleistocene and late Pliocene age. Samples 144-878A-1R-1, 4–5 cm, to -1R-1, 56–57 cm, contain abundant *Pseudoemiliana lacunosa* and *Gephyrocapsa caribbeanica* and common *Calcidiscus macintyreii* in combination with rare *Helicosphaera sellii* and *Gephyrocapsa oceanica*, suggesting the *H. sellii* and *C. macintyreii* zones of early Pleistocene age.

The occurrence of *Discoaster tamalis* in Samples 144-878A-1R-1, 92–93 cm, and -1R-2, 5–6 cm, indicates that at least some of this interval has been derived from the upper part of the *Reticulofenestra pseudumbilica* Zone (CN11) or the *D. tamalis* Zone (CN12a) of early late Pliocene age.

The untainted ooze in Section 144-878A-1R-2 contains abundant, well-preserved nanofossils including *Discoaster quinqueramus*, *D. berggrenii*, *D. brouweri*, *D. pentaradiatus*, *Amaurolithus primus*, *A. delicatus*, *A. amplificus*, and *Reticulofenestra pseudumbilica*. This assemblage is definitive of the *A. primus* Subzone (CN9b) of late Miocene age. The assemblage is characterized by the abundance of *Discoaster intercalaris*, *D. mendomobensis*, and *D. surculus* and the absence of *Sphenolithus* spp., *Pontosphaera* spp., and *Hayaster perplexus*. *Triquetrorhabdulus rugosus* is very rare. This assemblage is similar to coeval ones from Shatsky Rise (Bukry, 1978) and is indicative of cool surface waters.

The soupy ooze in Sections 144-878A-1R-3 contains a mixture of assemblages similar to that in Section 144-878A-1R-1. The oldest marker species observed indicates Subzone CN9b of late Miocene age.

In Holes 878B and 878C, only minute amounts of nanofossil ooze adhering to the surface of manganese nodules was recovered. Nanofossil ooze on the surface of a manganese nodule in Sample 144-878B-1R-1, 7–9 cm, contains an assemblage with *Calcidiscus macintyreii*, rare *Gephyrocapsa oceanica*, and abundant small reticulofenestrids. This assemblage identifies the *Calcidiscus macintyreii* Zone of early Pleistocene age. Nanofossil ooze adhering to a manganese nodule in Sample 144-878C-1R-1, 17–22 cm, contains *Discoaster tamalis*, *D. pentaradiatus*, *D. blackstockae*, and *D. brouweri*, indicating the *D. tamalis* Subzone (CN12a) of late Pliocene age. Specimens of *D. quinqueramus*, *D. berggrenii*, and *T. rugosus* are reworked into this assemblage.

Manganese Nodules

Sample 144-878A-1R-1, 6–8 cm, consists of a manganese nodule with a complex pelagic sediment nucleus containing moderately preserved, phosphatized nanofossils (Fig. 22). The assemblage includes *Micula decussata*, *M. concava*, *Reinhardtites anthophorus*, and *Placozygus fibuliformis*. Two specimens questionably identified as *Eprolithus floralis* were observed. Assuming that the identification of *E. floralis* is correct, the assemblage can be assigned to the combined *Reinhardtites anthophorus*–*Lucianorhabdus cayeuxii* zones (CC15–16) of late early through late Santonian age. Planktonic foraminifer assemblages of late Santonian to early Campanian age and of late

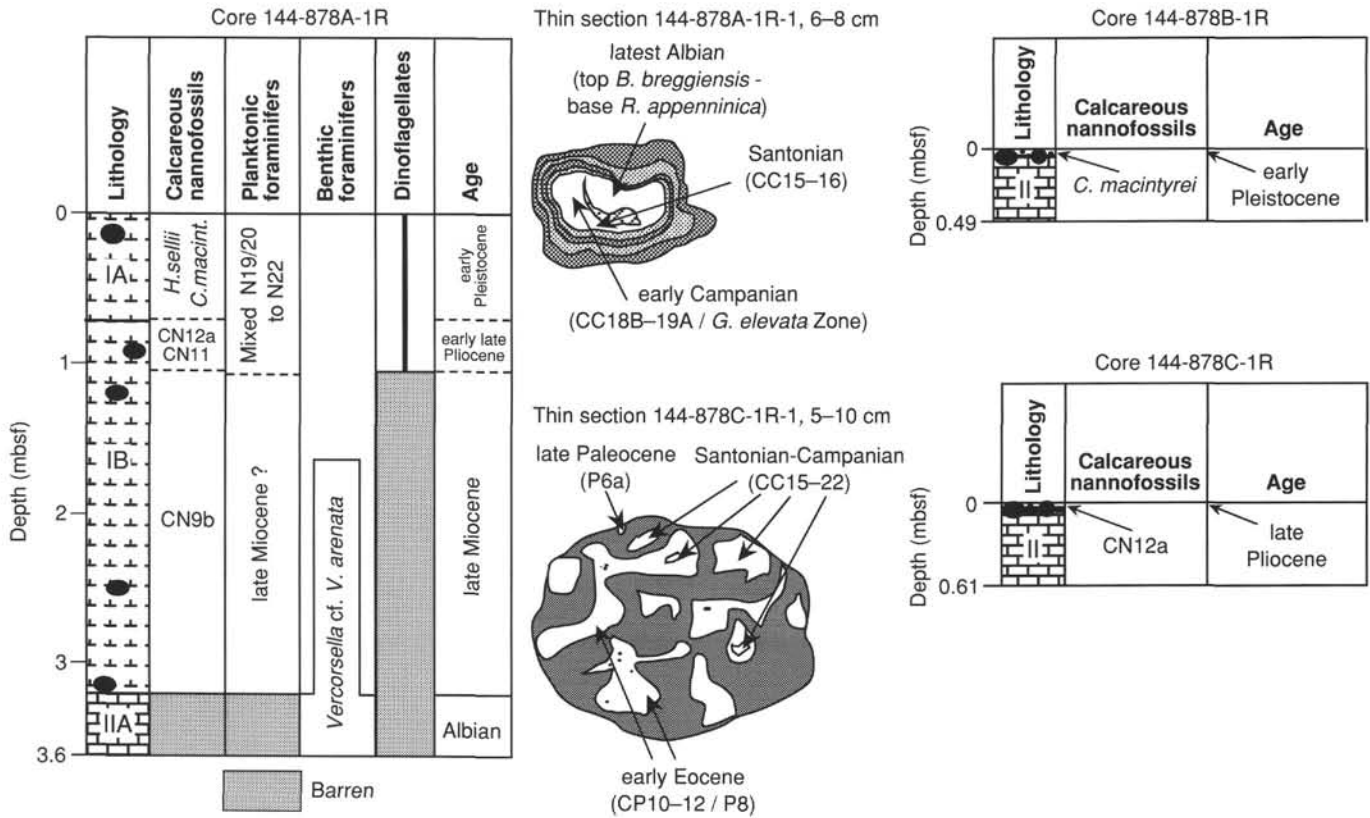


Figure 22. Calcareous plankton biostratigraphy of the pelagic sediments and some manganese nodules recovered in Holes 878A, 878B, and 878C.

Albian age were identified in this sample (see below). No evidence of the upper Albian could be identified by nannofossils.

A manganese nodule (Sample 144-878C-1R-1, 5–10 cm) contains phosphatized nannofossils, indicating at least three generations of pelagic fill. The older fill contains *Reinhardtites anthophorus*, *Micula decussata*, *M. concava*, and *Placozygus* sp., indicating a Santonian to early Campanian age. The younger fill contains *Discoaster lodoensis*, *D. barbadiensis*, *D. kuepperii*, and *Chiasmolithus grandis*, indicating an assignment to Zone CP10 to Subzone CP12a (early to early middle Eocene in age). Planktonic foraminifer assemblages have been identified as belonging to Zone P8 (see below), which limit biozone assignment to nannofossil Zone CP10 or CP11 of early Eocene age.

Platform Carbonates

Three samples from the platform carbonate sequence yielded nannofossils in thin section (Fig. 23).

Sample 144-878A-41M-1, 4–8 cm, in the upper platform carbonate sequence (Lithologic Subunit IIIB), contains a sparse but well-preserved nannofossil assemblage that includes *Nannoconus truitii frequens*, *N. inconspicuus*, *N. steinmannii*, *Rucinolithus irregularis*, *R. terebrodentarius*, and *Eprolithus floralis*. The assemblage is dominated by *N. truitii frequens*, indicating the *N. truitii* Acme (Mutterlose, 1991) within the *Rhagodiscus angustus* Zone (upper part of Zone CC7) of late Aptian age.

Sample 144-878A-75R-1, 141–143 cm, in the lower platform carbonate sequence (Lithologic Subunit VA), contains common nannofossils including *N. globulus*, *N. wassallii*, *N. circularis*, *N. bucheri*, *N. steinmannii*, *N. colomii*, *N. truitii frequens*, *Rucinolithus irregularis*, and *R. terebrodentarius*. A similar assemblage was observed also in Sample 144-878A-75R-2, 0–4 cm, but preservation is poorer and abundance lower. Based on the dominance of nannoconids, both samples are attributable to the lower portion of the *Chiastozygus*

litterarius Zone (lowermost part of Zone CC7) of early Aptian age (Coccioni et al., 1992).

Planktonic Foraminifers

Pelagic Sediments

The dark brown ooze recovered at Hole 878A was sampled for planktonic foraminifers. Samples were taken from the muddy water that flowed from each section as they were split as well as from the consolidated core. The sediment appears highly disturbed in Section 144-878A-1R-1, but it is better consolidated in Sections 144-878A-1R-2 and -1R-3. The planktonic foraminifer biostratigraphy is shown in Figure 22.

Sample 144-878A-1R-1, 38–40 cm, was the highest sample studied; it yielded common planktonic foraminifers from a mixed fauna that contains both Pliocene and Pleistocene species (Zones N19/20 to N22). The assemblage includes *Truncorotalia truncatulinoides*, *T. tosaensis*, *Sphaeroidinella dehiscens*, *Sphaeroidinellopsis seminulina*, *Globorotalia tumida*, and *G. tumida flexuosa*. A similar assemblage was found in Sample 144-878A-1R-1, 100–102 cm, and also in the water that flowed from Sections 144-878A-1R-1 to -1R-3, indicating that the planktonic foraminifers in this water were mainly contaminants from the top of the hole.

Sample 144-878A-1R-2, 31–33 cm, contains a few poorly preserved planktonic foraminifers including *Globorotalia tumida*, *Orbulina universa*, *Sphaeroidinella dehiscens*, and *Sphaeroidinellopsis seminulina*. Planktonic foraminifers are also rare and poorly preserved in Samples 144-878A-1R-2, 75–77 cm, -1R-2, 125–127 cm, -1R-3, 15–17 cm, and -1R-3, 40–42 cm. Occasional, better preserved individuals recovered from these samples are probably downhole contaminants, but the majority of specimens encountered belong to either the thick-walled *Globigerina nepenthes* group or the cortex-bearing species *Sphaeroidinellopsis seminulina*, indicating that these

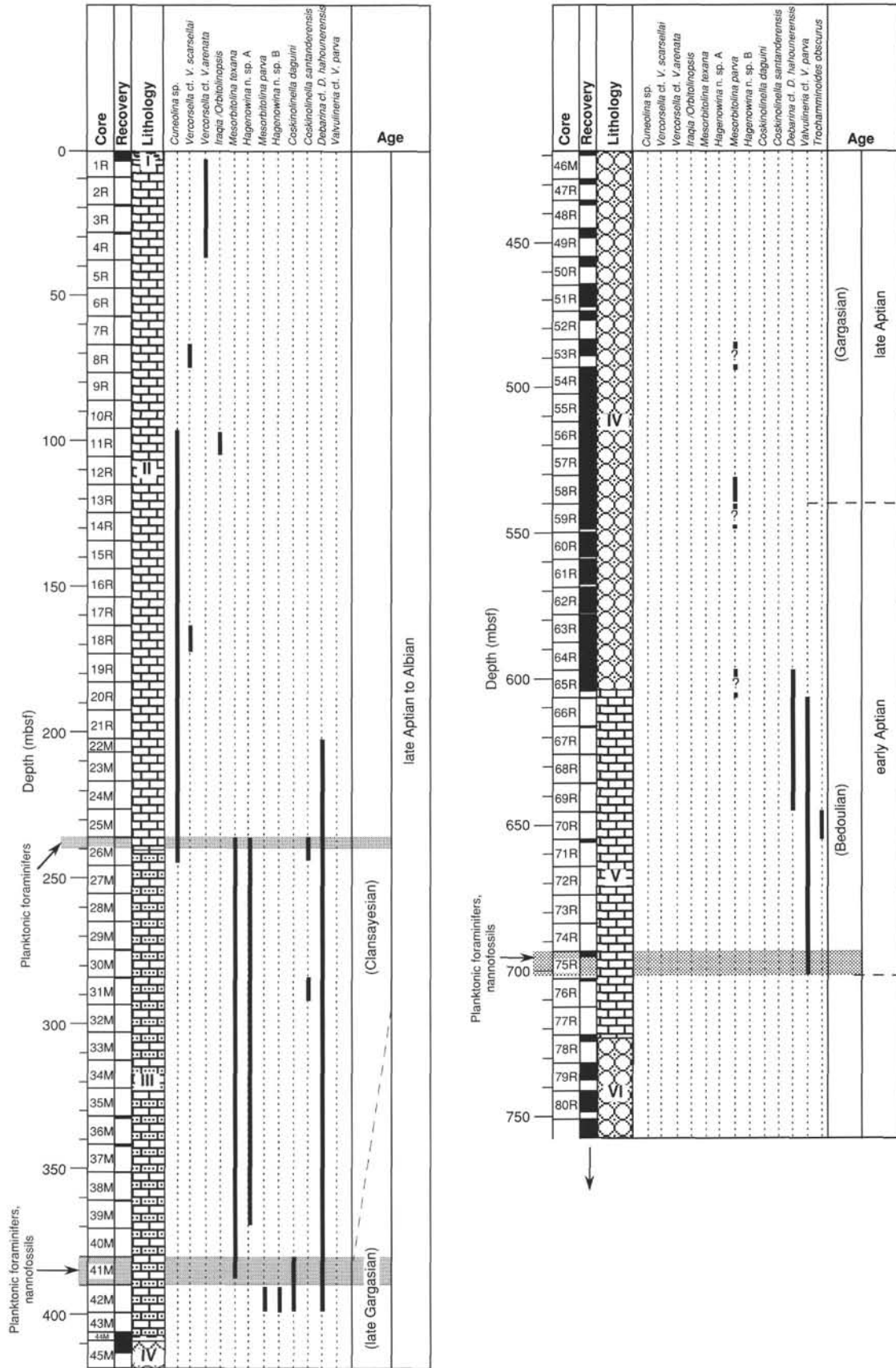


Figure 23. Biostratigraphy based on benthic foraminifers in Hole 878A. The occurrence of planktonic foraminifers and nannofossils is also reported.

individuals are probably in place and are perhaps all that remain of the fauna after dissolution. These samples contain frequent manganese micronodules, echinoid fragments, fish otoliths, pellets, and some benthic foraminifers. *G. nepenthes* and *S. seminulina* are long-ranging species and suggest a middle Miocene to early Pliocene age. However, nannofossils from this interval indicate a late Miocene age (see Fig. 22).

Manganese Nodules

A manganese nodule in Sample 144-878A-1R-1, 6–8 cm, contains pelagic sediment with planktonic foraminifers (Fig. 22), rare sponge spicules, and radiolarians. In the central portion of the nodule, the occurrence of *Planomalina praebuxtorfi* and *Heterohelix moremani* suggests the top of the *Biticinella breggiensis*/base of *Rotalipora appenninica* zones of latest Albian age. In the surrounding sediment, the planktonic foraminifer assemblage includes *Globotruncana tricarinata*, *Globotruncana linneiana*, *Globotruncana elevata*, *Contusotruncana fornicata*, *Globigerinelloides ultramicrus*, *Marginotruncana coronata*, *Archaeoglobigerina blowi*, and *Heterohelix reussi*, indicating the *Globotruncana elevata* Zone of early Campanian age.

Sample 144-878C-1R-1, 5–10 cm, consists of a manganese nodule with complex infillings that indicate at least two generations of pelagic sediments. The older sediment contains *Morozovella velascoensis*, *M. gracilis*, *M. marginodentata*, and *M. aequa*, indicating Subzone P6a of latest Paleocene age. The younger fill contains common *Morozovella gracilis*, along with *Morozovella aragonensis*, "*Globigerinatheka*" *senni*, and *Acarinina intermedia*, which have been assigned to the lower portion of Zone P8 of middle early Eocene age.

Platform Carbonates

Planktonic foraminifers occur in two samples from the upper platform carbonate sequence (Lithologic Unit III) and in one sample from the lower platform carbonate sequence (Lithologic Unit V) (Fig. 23).

Sample 144-878A-26M-1, 4–12 cm, contains a sparse and poorly preserved assemblage including *Hedbergella delrioensis* and large forms resembling either *Ticinella roberti* or high-spined specimens of *Hedbergella trocoidea*. The uncertain species identification suggests either the *Ticinella bejaouensis* Zone of late Aptian age or the *Biticinella breggiensis* Zone of late Albian age.

Rare planktonic foraminifers were observed in Sample 144-878A-41M-1, 4–8 cm. The assemblage includes unidentifiable specimens in addition to *Hedbergella gorbachickae* and *Hedbergella delrioensis*, indicating a late Aptian to Albian age.

Sample 144-878A-75R-1, 141–143 cm, in the lower platform carbonate sequence, contains common small-sized hedbergellids including *Hedbergella aptica* and *Hedbergella sigali*. Most specimens are unidentifiable; no *Globigerinelloides* were observed. This assemblage is most probably of early Aptian age.

Benthic Foraminifers

The 720-m-thick sequence of platform limestones and breccias (Lithologic Units II–V) recovered in Hole 878A contain sparse benthic foraminifers. Figure 23 illustrates the distribution of the stratigraphically important taxa. This range chart is based on observation of thin sections and specimens isolated from the saw cuttings of each section of the split cores. It should be considered preliminary.

The interval between Cores 144-878A-1R and -40M yielded few *Cuneolina* n. sp. (primitive form), few *Vercorsella* sp. cf. *V. scarsellai*, few to common *Vercorsella* sp. cf. *V. arenata*, common *Mesorbitolina texana*, rare *Coskinolinella santanderensis*, rare *Debarina* sp. cf. *D. hahounerensis*, a single specimen of *Iraquia/Orbitolinopsis*, and few *Hagenowina* n. sp. A. These species are indicative of a late Aptian to Albian age. The Aptian/Albian boundary was not recognized because of the absence of marker species. Within the upper Aptian, the

Clansayesian/Gargasian boundary is placed between the last occurrence of *Coskinolinella daguini* (Section 144-878A-41M-1) and the first occurrence of *Coskinolinella santanderensis* (Section 144-878A-31M-1). Benthic foraminifers are rare in Cores 144-878A-42M through -77R. *Mesorbitolina parva*, *Hagenowina* n. sp. B, *Coskinolinella daguini*, and *Debarina* sp. cf. *D. hahounerensis* co-occur in Core 144-878A-42R, supporting a late Aptian age (Gargasian).

Only a single specimen of *Mesorbitolina parva* occurs in Core 144-878A-58R, at the base of which the early/late Aptian (Bedoulian/Gargasian) boundary is tentatively placed. Specimens of *Mesorbitolina* resembling *M. parva* were observed in Cores 144-878A-59R and -65R.

In Cores 144-878A-66R through -75R, *Debarina* sp. cf. *D. hahounerensis*, *Trochamminoides obscurus*, and *Valvulineria* sp. cf. *V. parva* were the only taxa observed. This interval is attributed to the early Aptian (Bedoulian) based on the absence of *Mesorbitolina parva*. *Trochamminoides obscurus* is known only from the lowermost Aptian.

Paleoenvironment of Platform Carbonates

The distribution and relative abundance of benthic foraminifers, sponge spicules, bryozoans, echinoderms, corals, rudists, ostracodes, and planktonic foraminifers were analyzed in thin sections from the upper sequence of platform limestones (Lithologic Units II and III) and the lower sequence of platform limestones (Lithologic Unit V). The data are illustrated in Figures 24–25, in which the open-marine indicators appear to the left and those indicative of more restricted environments are plotted to the right. The identified paleoecologic assemblages and the changes in paleoenvironments are also reported.

Four paleoecologic assemblages (numbered I–IV) were tentatively differentiated within the upper sequence of platform limestones (Fig. 24) and three paleoecologic assemblages (numbered V–VII) were preliminarily distinguished within the lower part of the sequence (Fig. 25). They are described below, from top to bottom.

Paleoecologic Assemblage I (interval from Sample 144-878A-1R-CC, 0–4 cm, to Section 144-878A-5R-1) is characterized by relatively abundant *Vercorsella* sp. cf. *V. arenata*, *Pseudotriloculina*, miliolids, and ostracodes, along with few echinoderm fragments and sponge spicules. Forms indicative of fully oxygenated marine conditions are rare. Paleoecologic Assemblage I is interpreted as being representative of medium to poorly oxygenated marine environments, to restricted at the top. Sample 144-878A-2R-1, 25–27 cm, contains rare specimens of *Vercorsella* sp. cf. *V. arenata*, *Pseudotriloculina*, and abundant miliolids and may represent a relatively better oxygenated marine environment.

Paleoecologic Assemblage II (Interval from Sections 144-878A-6R-1 to -25R-1) contains abundant *Pseudotriloculina*, *Ortonella*, and ostracodes, as well as less frequent *Cuneolina* sp., *Vercorsella* sp., *Valvulineria*, miliolids, and sponge spicules. *Vercorsella* sp. cf. *V. arenata* was not observed in this interval. Paleoecologic Assemblage II is interpreted as reflecting fluctuations from restricted to poorly oxygenated marine environments. Relative changes are based mainly on the distribution of ostracodes and the relative abundance of benthic foraminifers.

Paleoecologic Assemblage III (interval from Samples 144-878A-26M-1, 4–12 cm, to -41M-1, 4–8 cm) is remarkably different from Paleoecologic Assemblage II. It is characterized by common fragments of echinoderms, corals, bryozoans, and rudists, and few specimens of *Mesorbitolina* and miliolids. No forms associated with restricted environments were encountered in this interval. Rare specimens of *Cuneolina* sp., *Vercorsella*, *Gavelinella*, and *Valvulineria* were observed only in Core 144-878A-26M. Paleoecologic Assemblage III indicates the most oxygenated marine conditions during the deposition of the upper sequence of platform limestones. This interval is bounded by layers containing planktonic foraminifers (Cores 144-878A-26M and -41M) and calcareous nannofossils (Core 144-878A-41M), which indicate a pelagic influence.

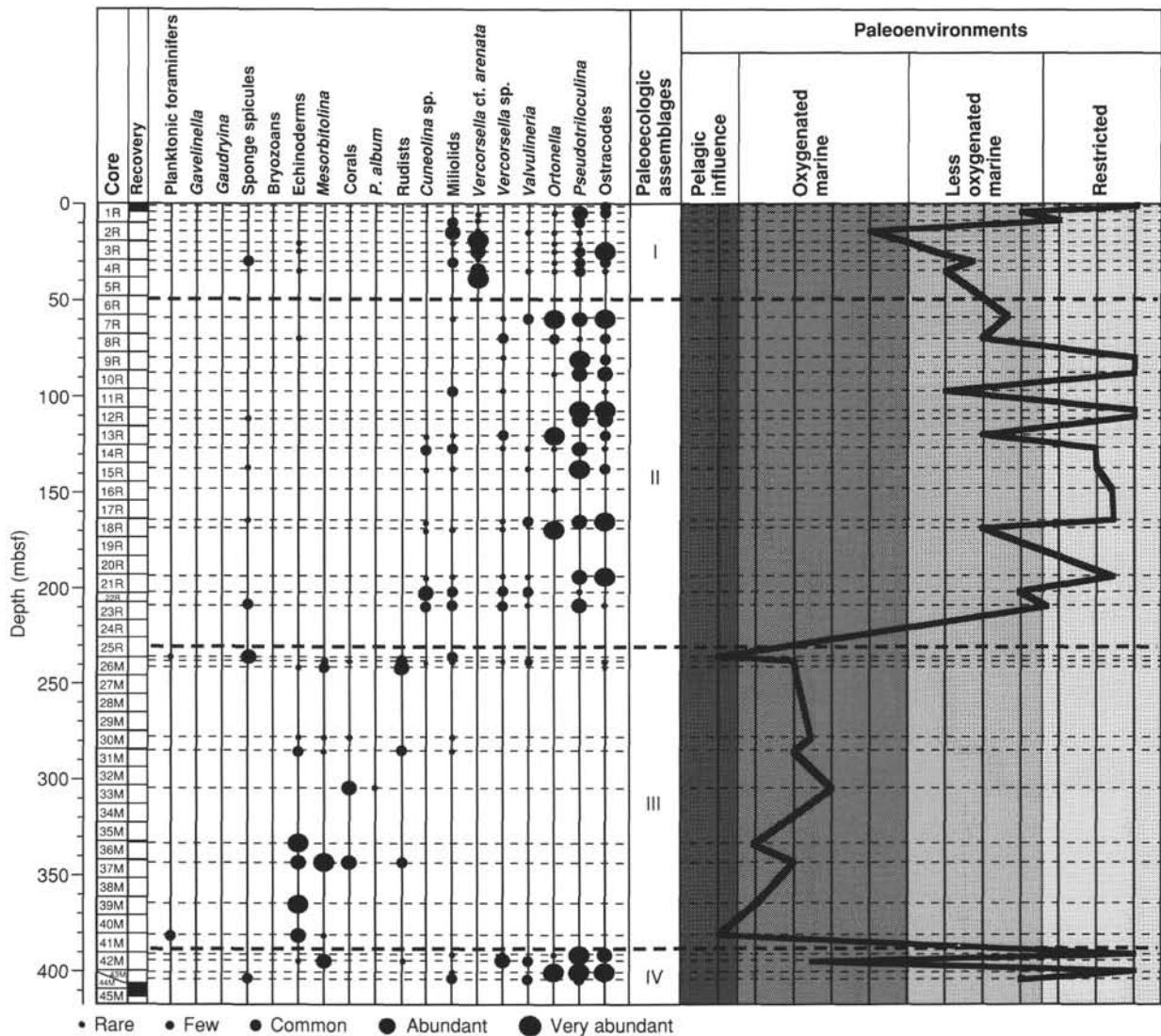


Figure 24. Distribution of microfossils and paleoecologic assemblages in the upper platform limestones (Lithologic Units II and III), Hole 878A. Microfossils are arranged from marine (left) to more restricted environmental indicators (right) on which the paleoenvironmental interpretation was based (Arnaud-Vanneau, 1980).

Paleoecologic Assemblage IV (Interval from Samples 144-878A-42M-1, 11–15 cm, to -44M-1, 33–36 cm) records a marked change in composition; this assemblage displays some similarities with Paleoecologic Assemblage II. The most abundant components are ostracodes, *Pseudotriloculina*, *Ortonella*, *Vercorsella* sp., *Mesorbitolina*, miliolids, and sponge spicules; rudist fragments are rare. The forms indicative of fully oxygenated marine conditions are rare. This assemblage is interpreted as representing fluctuations from more to less oxygenated conditions.

Paleoecologic Assemblage V (Interval from Samples 144-878A-65R-6, 35–37 cm, to -72R-1, 7–10 cm) is characterized by relatively abundant miliolids, ostracodes, fragments of rudists and echinoderms, few to common *Vercorsella* sp. and *Valvulineria*, rare *Pseudotriloculina*, few *Pseudolithothamnium album*, and rare *Gaudryina*. This interval begins under oxygenated marine conditions and passed through more poorly oxygenated conditions before it returned to more oxygenated marine conditions at the bottom of the interval (Fig. 25).

Paleoecologic Assemblage VI (Interval from Samples 144-878A-73R-1, 37–41 cm, to -75R-2, 0–4 cm) is characterized by low diversity and low abundance of *Valvulineria*, *Gavelinella*, ostracodes, sponge

spicules, and fragments of echinoderms. Forms indicative of restricted conditions were not observed. This assemblage is interpreted as being representative of oxygenated marine conditions. Planktonic foraminifers and calcareous nanofossils occur at the base of the interval (Core 144-878A-75R) and indicate an open-marine influence.

Paleoecologic Assemblage VII (Interval from Samples 144-878A-76R-1, 12–14 cm, to -77R-1, 48–52 cm) contains relatively abundant fragments of rudists along with coral and echinoderm debris. Rare bryozoans and *Pseudolithothamnium album* also occur, whereas taxa indicative of restricted environments are absent. A fully oxygenated marine environment is suggested.

Assemblages typical of restricted environments are missing in the lower part of the carbonate sequence of platform limestones, whereas the upper part of the sequence platform carbonates, on the other hand, contains forms indicative of restricted conditions both at its top (Paleoecologic Assemblages I and II) and in the lower part (Assemblage IV). Layers containing planktonic foraminifers (Cores 144-878A-26M, -41M, and -75R) and calcareous nanofossils (Cores 144-878A-41M and -75R) occur in the upper and lower sequences of platform limestones, indicating periods of pelagic input.

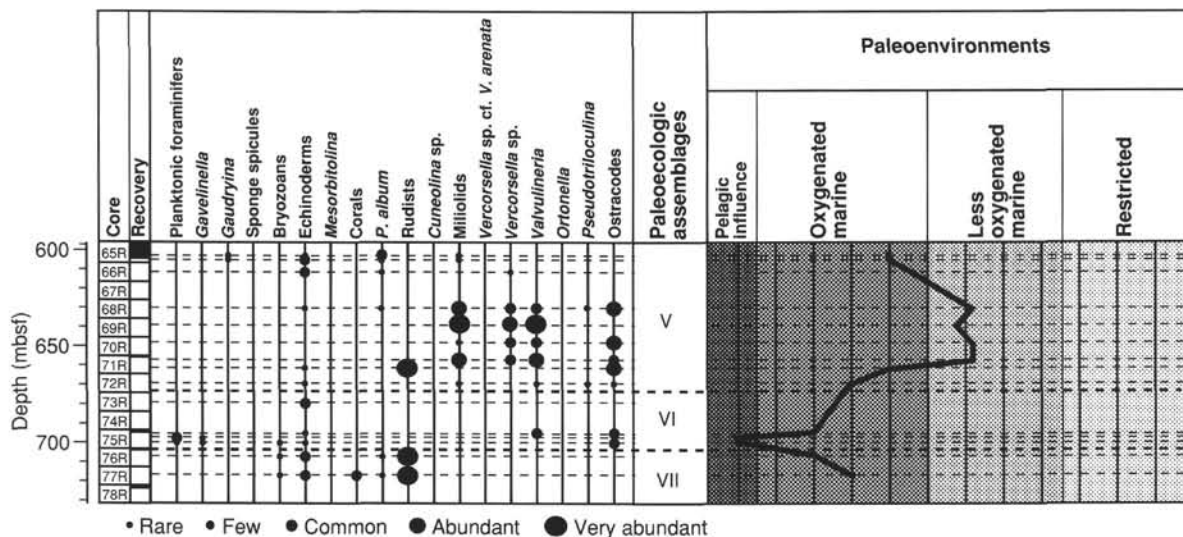


Figure 25. Distribution of microfossils and paleoecologic assemblages in the lower platform limestones (Lithologic Unit V). See Figure 24 caption for explanation.

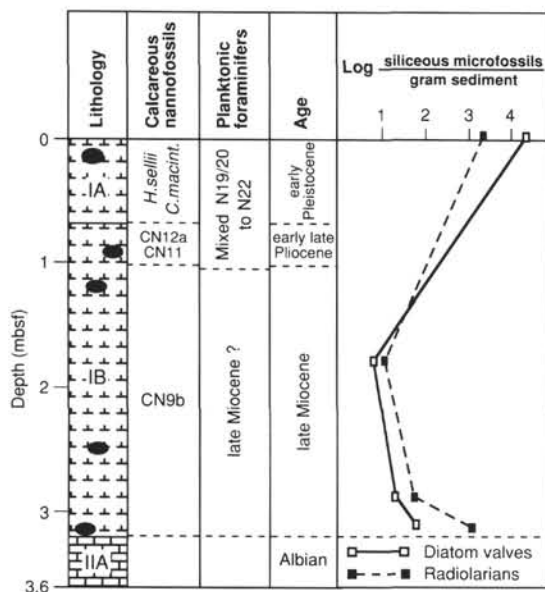


Figure 26. Distribution of siliceous microfossils in the pelagic sediments recovered in Core 144-878A-1R.

Siliceous Microfossils and Their Diagenetic Products

Pelagic Sediments

Four samples from Core 144-878A-1R were quantitatively analyzed for the HCl-insoluble residue (>2 μm) (Fig. 26). The samples were collected from the Pleistocene through late Miocene pelagic ooze, as dated by calcareous nannofossils and planktonic foraminifers. Siliceous microfossils are present within the pelagic sediments, but they fluctuate in abundance and preservation. Diverse and well-preserved radiolarians and diatoms occur at the top of Core 144-878A-1R. In Sections 144-878A-1R-2 and -1R-3, siliceous microfossils are very rare, but they increase again in abundance in Sample 144-878A-1R-CC.

The diatom assemblage occurring in Sample 144-878A-1R-1, 1–3 cm, includes *Azpeitia nodulifer*, *Nitzschia marina*, *Hemidiscus cuneiformis*, *Thalassiosira leptopus*, and *T. eccentrica*. Sample 144-878A-1R-CC contains a similar assemblage, but *Thalassiosira eccentrica* is more abundant. In addition, *Thalassiosira oestrupii*, *Azpeitia crenulatus*, and *Azpeitia africanus* were observed. Both assemblages indicate a Miocene to Pleistocene age.

The relative increase in abundance of diatoms at the base of the pelagic sequence may reflect a de facto higher abundance or, conversely, downhole contamination. The excellent preservation of all the diatom valves suggests that they are Pleistocene forms mixed through the ooze. Considerable mixing of sediment is also documented by calcareous nannofossils (see above).

The radiolarian assemblage observed at the top of the pelagic sediments is characterized by relatively high diversity. Taxa include *Anthocyrthidium angulare*, *Spongaster tetras*, *Centrobotrys thermophila*, and *Theocorythium trachelium*, indicating a Pleistocene age. In Section 144-878A-1R-3, *Lithopera bacca* and *Theocorythium vetulum* were encountered. The latter species also occurs in Sample 144-878A-1R-CC.

Zeolites are present in the four samples analyzed. They are interpreted as the result of silica precipitation from pore water after dissolution of siliceous microfossils. Phillipsite occurs with abundances of approximately 10^7 crystals per gram of sediment, whereas clinoptilolite is less abundant.

Volcanic Limestone Breccia

Three samples from clasts of the polymictic breccia (Lithologic Unit IV) were investigated for siliceous microfossils. Sample 144-878A-43M-1, 44–47 cm, at the top of the volcanoclastic sequence, consists of a greenish gray clay barren of siliceous microfossils.

Limestone clasts and the matrix from Samples 144-878A-50R-CC and -53R-CC were analyzed separately. Rare recrystallized centric diatoms probably belonging to the genus *Paralia* were observed.

Palynomorphs

Pelagic Sediments

A 20-cm³ sample of fluid sediment, obtained from spillage during the splitting of Section 144-878A-1R-1, was treated with HCl and HF and then sieved at 20 μm. A late Pliocene to early Pleistocene age is

suggested for this section, based on planktonic foraminifers and nannofossils. About half of the residue was mounted on a single microscope slide for analysis. The >20 µm organic fraction is lean and dominated by single- and multichambered spheroidal objects (foraminifer linings?) and fluffy amorphous matter. Dinoflagellates are present in moderate numbers and are fairly well preserved. All specimens on the slide were counted and are attributed to the following taxa (numbers of specimens in parentheses): *Impagidinium aculeatum* (74), *I. patulum* (19), *I. paradoxum* (7), *Nematosphaeropsis lemniscata* (5), *Spiniferites* spp. (3), *Impagidinium japonicum* (3), *I. velorum* (2), and *I. striatum*? (2). The dinoflagellates constitute a low-diversity assemblage of oceanic character. The outer neritic to oceanic genus *Impagidinium* (93% of total) dominates the assemblage; the high number of *Impagidinium aculeatum* specimens (64% of total) indicate warm to tropical surface waters. All species recorded have long stratigraphic ranges within the upper Cenozoic. Terrigenous organic material is extremely rare and is represented by occasional fragments of woody tissues and rare bisaccate (*Pinus*) pollen.

The presence of late Cenozoic dinoflagellates in moderate numbers at the remote location of MIT Guyot suggests local productivity as a source rather than long-distance current transport from some far continental shelf. By late Cenozoic times, no islands were apparently in the vicinity of MIT Guyot that could provide either nutrients or a shelf environment for dinoflagellate growth. Perhaps upwelling caused by MIT Guyot itself (the "guyot effect") provided a favorable environment for these oceanic dinoflagellates.

Volcanic Limestone Breccia

Four 10-cm³ samples (Samples 144-878A-46M-2, 37-44 cm, -55R-6, 24-26 cm, -57R-5, 139-141 cm, and -58R-7, 74-76 cm) of fine-grained limestone clasts from the polymictic breccia were examined. Samples were digested in HCl; both unsieved and >20-µm fractions of the residues were searched. The organic material is lean and consists of amorphogen and occasional algal? cells, but no dinoflagellates were found.

Sample 144-878A-43M-CC is a medium greenish gray clay. About 2 cm³ were examined after HF and HCl treatment. The residue consists mainly of opaque minerals and sparse light brown amorphous (organic?) material. No palynomorphs were seen.

Sample 144-878A-54R-1, 8-9 cm, is a small, black, organic-rich fragment entombed within the breccia unit. The sample (about 2 cm³) was first crushed and dried for geochemical determinations; a subsample was then mounted in glycerine jelly for palynologic analysis. This subsample revealed the presence of exclusively woody plant tissues of yellowish brown (~10YR 5/8) color, suggesting a sub-bituminous rank of coalification. The sample evidently did not reach temperatures above, or much above, a level expected from burial depth alone. Geochemical results are consistent with this conclusion (see "Organic Geochemistry" section, this chapter).

Summary

At Site 878, a carbonate platform was established on basaltic basement during the early Aptian. The fossil evidence in the lower sequence of platform carbonates indicates that this early Aptian platform developed in a fully oxygenated marine environment with at least one episode of pelagic influence (Cores 144-878A-75R and -76R) early in its development. A period of less oxygenated marine conditions (Cores 144-878A-67R through -71R) occurred upward, but floral and faunal components of true restricted conditions were not observed.

Carbonate platform development was abruptly interrupted by volcanism during the late early Aptian, which resulted in a thick sequence of volcanoclastic sediments. The breccia contains clasts of platform carbonates, whose origins are still uncertain and whose ages are poorly constrained. Fragments of woody plant material of sub-

bituminous rank imply the presence of nearby islands at some point in the development of the ancient platform.

The age of the upper platform carbonate sequence is well constrained in its lower part but relatively poorly constrained in its upper part. Little age information, other than a generalized late Aptian to Albian assignment, is presently possible for the platform carbonates in Cores 144-878A-1R through -25M. Core 144-878A-26M contains rare, poorly preserved planktonic foraminifers that may be either late Aptian or late Albian in age. However, the occurrence of these planktonic forms with the benthic foraminifer *Coskolinella santanderensis*, which ranges from the upper Aptian to the middle Albian, implies that this interval is late Aptian in age. The consistent occurrence of upper Aptian benthic foraminifers from Cores 144-878A-26M through -43M, coupled with the occurrence of mid-Aptian calcareous nannofossils and planktonic foraminifers in Core 144-878A-41M, constrain the lower portion of the upper platform carbonate sequence to a late Aptian age.

Benthic foraminifer assemblages indicate that the upper carbonate platform at Site 878 was initially characterized by restricted to poorly oxygenated marine conditions (Cores 144-878A-42M to -45M), which rapidly became fully oxygenated marine conditions (Cores 144-878A-26M to -41M), with episodes of pelagic influence at the beginning and end of this phase. A significant change occurred in the late Aptian-early Albian?, with the onset of alternating poorly oxygenated marine and restricted environmental conditions (Cores 144-878A-1R to -25M). The evidence suggests that the platform was quite restricted before its demise, although it is uncertain how much (if any) of the uppermost carbonate sequence was removed by post-drowning erosion.

Manganese nodules within and below the ooze sequence contain nuclei that record several episodes of calcareous pelagic sedimentation. The oldest material consists of phosphatized pelagic limestone with planktonic foraminifers of latest Albian age. This assemblage establishes a minimum age for the drowning of the underlying carbonate platform. A second generation of pelagic limestone is composed of fully phosphatized nannofossils and planktonic foraminifers of late Santonian to early Campanian age. A third episode of pelagic sedimentation is recorded in another nodule that bears planktonic foraminifers and nannofossils of latest Paleocene age. Finally, nannofossils and planktonic foraminifers of middle early Eocene age are contained in phosphatized limestone within a manganese nodule.

A thin (approximately 3 m), manganese-nodule-bearing nannofossil ooze was recovered from Hole 878A; it contains calcareous microplankton of latest Miocene, late Pliocene, and early Pleistocene age. Only the upper Miocene ooze was sufficiently consolidated to maintain its paleontologic integrity. The soupy Pliocene and Pleistocene ooze was slightly to heavily contaminated with upper Miocene microfossils. The Pliocene-Pleistocene ooze contains well-preserved diatoms, radiolarians, and dinoflagellates, in addition to calcareous microplankton fossils, implying relatively high local productivity during its deposition. The upper Miocene ooze contains well-preserved calcareous nannofossils but severely dissolved planktonic foraminifers. In addition, it contains manganese nodules and micronodules, echinoderm fragments, fish otoliths, and benthic foraminifers, including common *Uvigerina*. This indicates deposition in a low oxygen environment at, or near, the late Miocene oxygen minimum.

PALEOMAGNETISM

Susceptibility

The susceptibility of limestone cores from Hole 878A was not measured because of the low average recovery (<5%). Susceptibility was measured at an interval of 5 cm for most whole cores from the volcanic limestone breccia sequence (406-604 mbsf) and the volcanic basement (722.5-908 mbsf). The archive halves of cores from volcanic basement were remeasured after the cores were split and final curated positions had been established. In contrast to the data from the whole cores, measurements from the archive half cores are di-

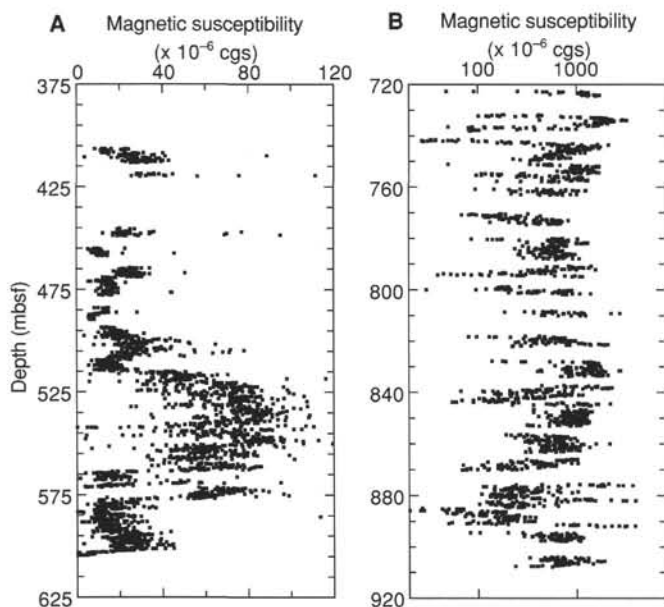


Figure 27. Magnetic susceptibility variations within the volcanoclastic sequence (A) and volcanic basement (B) of Hole 878A. Note change in depth scale.

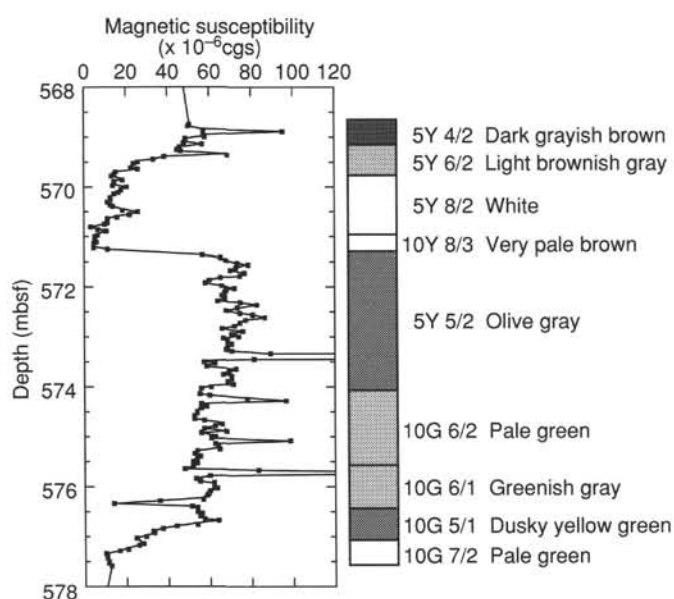


Figure 28. Comparison of magnetic susceptibility and color variations in a representative core (144-878A-62R) from the volcanoclastic sequence. Colors are from the visual core descriptions.

rectly comparable to other data (e.g., remanence measurements, shipboard descriptions) from the curated archive half cores. Susceptibility within the volcanic basement ranges from 50×10^{-6} to about 5000×10^{-6} cgs (Fig. 27). In addition to longer wavelength variations, small-scale variability may often be related to features within flows (e.g., low susceptibility at flow-top boundaries).

Susceptibility in the volcanic limestone breccia sequence is generally $<100 \times 10^{-6}$ cgs. Occasional higher values (not shown) also occur and can usually be attributed to the presence of larger volcanic clasts (Fig. 27). The marked increase in susceptibility near 515 mbsf corresponds to a relatively sharp contact (Section 144-878A-56R-2, 140 cm) between lighter (more carbonate-rich unit) and underlying

darker volcanoclastic sediments. Similarly high susceptibility values persist to a depth of about 577 mbsf.

The variations within the polymictic breccia unit probably reflect fluctuations in the proportion of volcanic material, although susceptibility is also a function of such parameters as grain size and mineralogy. Results from Core 144-878A-62R illustrate the correspondence between susceptibility fluctuations and the color of the core/proportion of volcanic material (Fig. 28; see also "Lithostratigraphy" section, this chapter). The upper part of this core is dark grayish brown and contains about two-thirds volcanic material. From 569.4 to 571.3 mbsf, the color becomes progressively lighter, with the low susceptibility at 570.9 to 571.3 mbsf corresponding to a nearly pure carbonate interval. With the exception of the lowermost 50 cm, the remaining portion of the core has various shades of gray and green and a significant percentage (30%–40%) of volcanic clasts. Insofar as the susceptibility variations reflect the proportion of volcanic material, the fluctuations shown in Figure 27 may be interpreted in terms of multiple depositional pulses.

Remanence Measurements

Remanence measurements included whole-core measurements of the entire volcanic limestone breccia sequence and portions of volcanic basement and discrete sample measurements of a few large pieces from the archive halves of the lower Aptian limestone sequence (604.3–722.5 mbsf). While on site at Hole 878A, all three RF amplifiers on the cryogenic magnetometer were temporarily out of order. After extensive repair and tuning, the 2G magnetometer performed well for the remainder of the site. An additional benefit of this maintenance was the better agreement (1%–2%) between the sensors in the X-Y plane and the Z-axis sensor, obviating the need for correction of demagnetization results (see "Paleomagnetism" section, "Explanatory Notes" chapter, this volume).

Cores from the polymictic breccia unit (406.1–604.3 mbsf) were measured at 5-cm intervals for both the natural remanent magnetization (NRM) and the magnetization after demagnetization at 15 mT. Recovery in this unit was high, providing a nearly continuous record of magnetization below about 490 mbsf (Fig. 29). Although declinations are generally randomly distributed as expected for rotary drilled sediments, long drilling cylinders have internally consistent declinations. Inclinations are generally negative and most lie between -25° to -45° . The similarity of inclination values in cores with steeply dipping and near-horizontal bedding (see "Lithostratigraphy" section, this chapter) indicates that the remanence was acquired after deposition. Inclination values that deviate from this range can generally be attributed either to edge effects associated with the ends of drilling cylinders or to isolated volcanic clasts, which apparently maintain an original, predepositional remanence. Assuming that such effects are randomly distributed, we calculate a mean NRM inclination of -36° ($N = 2870$). The magnetization intensity is generally between 1 and 50 mA/m, although lower values (e.g., 0.05 mA/m near 490 mbsf) also occur. Intensity variations correlate well with the susceptibility values, providing further support for the interpretation of susceptibility fluctuations in terms of the proportion of volcanic material.

Fifty-six discrete samples from the volcanic limestone breccia sequence were demagnetized (Table 5). About 10% of these samples yielded no stable characteristic remanence direction, possibly because of the presence of isolated basaltic clasts with a preexisting remanence direction. The majority of samples, however, have a nearly univectorial magnetization (Figs. 30–31) and very consistent negative inclinations. The mean inclination (-39°) calculated from the discrete sample data is similar to that estimated from the whole-core data (-36°). The simplest explanation of these data is that they represent a normal polarity magnetization acquired in the Southern Hemisphere.

Five of the longest pieces of limestone from the archive halves of Cores 144-878A-71R through -76R were demagnetized (to a peak field of 15 mT) and measured in discrete sample mode. The magneti-

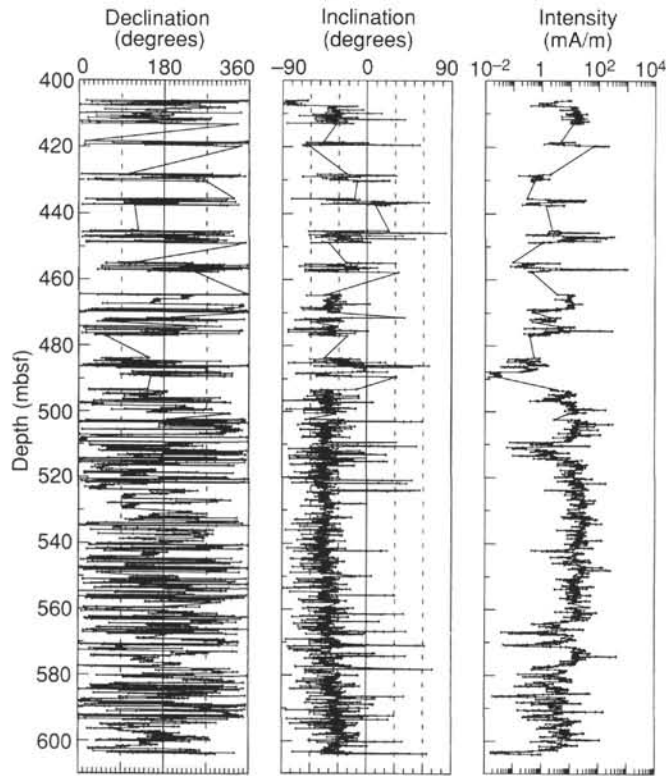


Figure 29. Declination, inclination, and intensity variations in volcanoclastic sediments from Site 878.

zation of these limestone samples was typically <0.5 mA/m, and only two samples yielded apparently reliable results (Fig. 32). The inclinations of both samples are positive (about 10°–30°), which may be interpreted as a Southern Hemisphere reversed magnetization.

Remanence measurements of cores from the volcanic basement included both discrete samples ($N = 26$) and whole-core measurements with the 2G pass-through magnetometer. The latter measurement is not routinely made on basalt cores because the high magnetization (typically several A/m) and large volume may exceed the upper limit of the 2G magnetometer. The upper limit of the magnetometer on extended range is approximately 0.15 emu (total magnetic moment), which corresponds to a magnetization of about 0.4 A/m for a half core (Boillot, Winterer, Meyer, et al., 1987). Basalt cores with a magnetization of ~0.5 A/m were measured during Leg 115 with some limited success (Backman, Duncan, et al., 1988). Higher magnetizations can theoretically be measured on range one when the flux counters are working properly (the maximum counter value of 9999 corresponds approximately to a magnetization of 20 A/m). We were able to measure archive halves of basalt cores with magnetizations approaching 10 A/m, with the counters returning to zero, or near zero, from counter values of more than 3000. This success must be, in large part, a result of the complete tuning procedure done by the electronic technicians.

Discrete sample data from the volcanic basement section indicate that both normal and reversed polarity flows are present (Table 6). Samples from Cores 144-878A-78R to -84R have negative inclinations (normal), and samples from Core 144-878A-85R and below generally have positive inclinations (reversed). However, pass-through magnetometer measurements of the red clay interval within Section 144-878A-85R-3 indicate a normal polarity in the otherwise reserved polarity interval. In addition, a single discrete sample from Core 144-878A-88R with normal polarity magnetization occurs within the lower reversed interval. The simplest explanation of these data is that

Table 5. Results of demagnetization of discrete samples from volcanoclastic unit (406–604 mbsf), Hole 878A.

Core, section, interval (cm)	Inclination (degree)
144-878A-	
44M-1, 126–128	—*
44M-2, 34–36	–34.8
45M-1, 21–23	–38.3
45M-2, 67–69	–23.8
45M-3, 97–99	–38.7
46M-1, 44–46	–46.5
46M-1, 112–114	–54.7
47R-2, 27–29	—*
48R-1, 1–3	–35.2
49R-2, 18–20	–33.6
50R-2, 66–68	–46.6
51R-1, 29–31	–31.3
51R-3, 28–30	–39.7
51R-4, 114–116	—*
51R-5, 9–11	–36.8
51R-6, 74–76	–37.5
52R-1, 141–143	–41.6
52R-2, 92–94	–36.6
53R-1, 96–98	–59.7
53R-2, 70–72	–32.6
53R-3, 70–72	—*
53R-4, 49–51	—*
54R-1, 61–63	–62.7
54R-2, 75–77	–39.8
54R-3, 104–106	–40.8
54R-6, 24–26	–42.7
55R-2, 118–120	–40.0
55R-4, 110–112	–28.4
55R-6, 104–106	14.5*
56R-2, 56–58	–43.4
56R-3, 78–80	–38.9
56R-6, 28–30	–40.5
57R-1, 37–39	–41.9
57R-3, 63–65	–44.4
57R-5, 102–104	–34.2
58R-3, 96–98	–36.2
58R-5, 53–55	–45.4
58R-7, 88–90	–43.6
59R-3, 40–42	–44.6
59R-4, 76–78	–39.8
59R-5, 37–39	–37.0
59R-7, 38–40	–37.0
60R-2, 60–62	–44.9
60R-3, 106–108	–39.5
60R-5, 22–24	–33.9
60R-6, 27–29	–38.1
61R-2, 13–15	2.7*
61R-4, 96–98	–34.7
62R-2, 78–80	–55.1
62R-4, 46–48	–40.5
63R-1, 77–79	–31.1
63R-6, 37–39	–29.9
64R-1, 13–15	–23.4
64R-5, 77–79	–32.0
65R-3, 70–72	–29.1
65R-5, 23–25	–28.4

Notes: Dash (—) indicates an unstable remanence, and an asterisk (*) indicates that the sample was excluded from calculation of mean inclination.

they represent one reversed and one normal polarity interval, with the complications near the reversal boundary caused either by remagnetization effects or possibly by transitional fields.

Nearly univectorial demagnetization behavior occurs in both normal and reversed polarity flows, although many samples from the lower portion of the sequence have a significant low-stability component (Figs. 33–34). This low-stability component has a negative inclination, indicating that it is not of recent origin. The magnitude of this low-stability component is often sufficient to obscure the polarity of the NRM (e.g., sample in lower part of Figs. 33–34). Stable characteristic magnetization directions were determined in all but five of the discrete samples, and the final few demagnetization steps were used in these cases to estimate the direction (Table 6). Excluding the

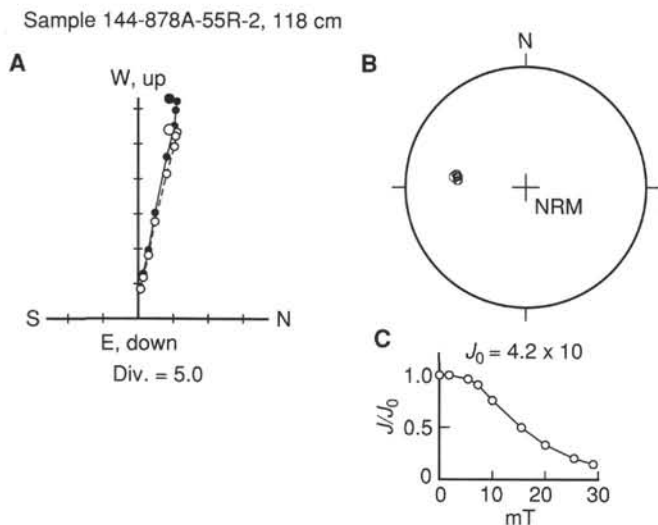


Figure 30. Alternating-field (AF) demagnetization results for volcanoclastic Sample 144-878A-55R-2, 118 cm. Demagnetization fields are 0, 2.5, 5, 7.5, 10, 15, 20, 25, and 29 mT. **A.** Orthogonal vector plot of progressive AF demagnetization. Closed (open) circles represent horizontal (vertical) component of the magnetization. **B.** Stereonet plot of vector endpoints after progressive demagnetization. **C.** Variation of intensity (calculated as mA m^{-1}) after progressive AF demagnetization.

two samples with near-horizontal inclinations, the normal and reversed polarity samples yield mean inclinations of -20.0° ($N = 13$) and $+23.4^\circ$ ($N = 11$), respectively.

Results from pass-through measurements of Cores 144-878A-78R to -98R (after 15-mT demagnetization) are shown in Figure 35. Two features of the data are noteworthy. First, the majority of the inclinations cluster about -10° to -40° apart from the shallow negative inclinations from Core 144-878A-89R (near 830 mbsf). Comparison with discrete sample data indicates that 15 mT is insufficient to isolate the characteristic magnetization in samples from Core 144-878A-89R. Thus, the data are entirely consistent with a reversed polarity magnetization acquired in the Southern Hemisphere. Second, the measured magnetizations span more than 2 orders of magnitude. Although the section contains abundant volcanoclastic/pyroclastic material, some of the lowest magnetizations (0.1 Am^{-1}) are associated with basalts (Core 144-878A-94R; near 850 mbsf). The altered pyroclastic rocks from Cores 144-878A-94R and -95R have magnetizations in excess of 1 Am^{-1} , similar to that of some basalts.

Reversal Sequence

Although no firm magnetostratigraphy can be established, we suggest the following tentative correlation of the sequence of reversals in the sediments and volcanic basement with the magnetic reversal time scale. The polymictic breccia unit is constrained by biostratigraphy to be of middle Aptian age ("Biostratigraphy" section, this chapter). This age suggests that the normal polarity recorded in the volcanoclastic unit corresponds to Chron C34N (Cretaceous Long Normal; Harland et al., 1990). Provided that the reversed polarity magnetization of the limestone samples from Core 144-878A-75R can be confirmed with shore-based measurements, a correlation with Chron M0 is suggested by the early Aptian biostratigraphic age. A minimum of one reversed polarity interval and one normal polarity interval has been recorded in cores from the volcanic basement. The lower reversed polarity interval must be at least as old as Chron M1 and may represent an earlier reversed polarity interval (Barremian).

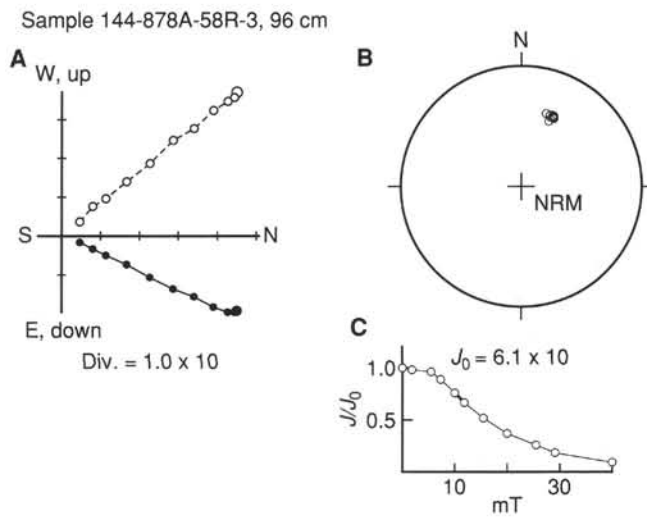


Figure 31. Alternating-field (AF) demagnetization results for volcanoclastic Sample 144-878A-58R-3, 96 cm. Demagnetization fields are 0, 2.5, 5, 7.5, 10, 12.5, 15, 20, 25, 29 and 40 mT. Other plot conventions are as in Figure 30.

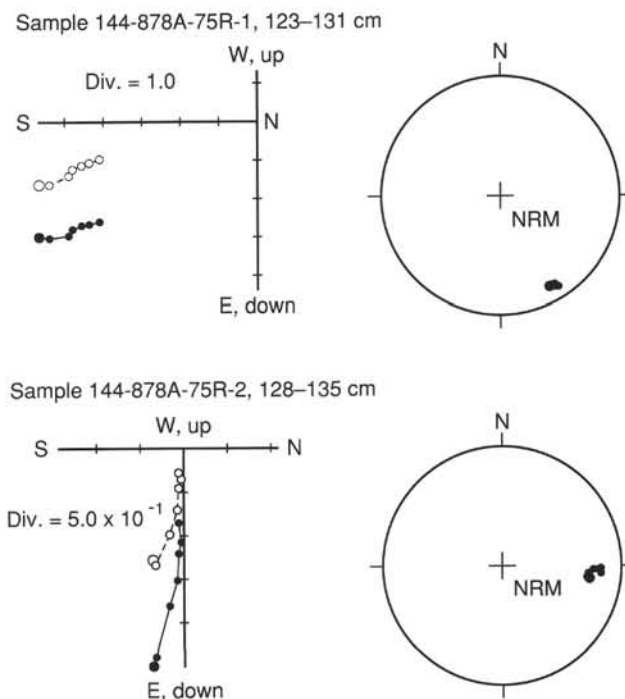


Figure 32. Alternating-field (AF) demagnetization results for limestone Samples 144-878A-75R-1, 123–131 cm, and -75R-2, 128–135 cm. Demagnetization fields are 0, 2, 5, 7, 10, 12, and 15 mT. Other plot conventions are as in Figure 30.

Paleolatitude

The mean inclination of the volcanic limestone breccia sequence indicates that the latitude of the MIT Guyot in the Aptian was about 20°S . The mean inclination of the volcanic basement indicates that the latitude of the guyot during the Barremian was about 10°S . These paleolatitudes may be taken as minimum estimates, as downhole measurements indicate that Hole 878A deviates from vertical by

Table 6. Results of demagnetization of discrete samples from volcanic basement from Hole 878A.

Core, section, interval (cm)	Inclination (degrees)	Polarity
144-878A-		
78R-2, 71	-18.8	N
80R-3, 28	-15.2	N
80R-5, 26	-12.7	N
81R-1, 15	-12.5	N
81R-3, 35	-15.9	N
81R-4, 58	-18.2	N
81R-5, 84	-12.2	N
82R-2, 81	-14.3	N
83R-3, 67	-39.1	N
84R-1, 13	-41.6	N
84R-5, 87	-21.4	N
84R-6, 70	-22.5	N
85R-2, 90	+23.1	R
86R-3, 43	+27.3	R
88R-3, 4	-15.4	N
89R-4, 45	+19.8	R*
90R-1, 105	+2.1	R?
91R-1, 103	+38.9	R*
92R-1, 101	+16.6	R
92R-2, 4	-0.9	?
92R-4, 83	+14.7	R
93R-1, 15	+21.0	R
93R-2, 123	+21.1	R
95R-6, 2	+18.7	R*
97R-2, 128	+21.1	R*
98R-3, 46	+35.6	R*

Note: An asterisk (*) indicates single demagnetization step or great circle path. N = normal, and R = reversed, and ? = uncertain polarity.

3°–5° along an azimuth of 180°. The inclination difference between the basement and volcanoclastic sediments may imply that the Pacific Plate moved southward between the Barremian and the Aptian. The southward motion of the Pacific Plate from the Barremian to the Aptian is consistent with the results from Leg 129 (Larson et al., 1992).

INORGANIC GEOCHEMISTRY

Interstitial Waters

Interstitial waters were squeezed from three core samples in Hole 878A. One sample was located in the pelagic material and two from clay-rich samples associated with the basalts. No interstitial water samples were taken from the limestone units. These samples were analyzed according to the methods outlined in the "Explanatory Notes" chapter (this volume); however, sodium could not be measured because of technical difficulties, and fluoride, silica, and ammonium could not be measured because of a terminal disfunction with the spectrophotometer. These measurements will have to be run onshore. Shipboard interstitial water data from Site 878 are presented in Table 7.

Salinity and Chlorinity

Pore-water salinity and chlorinity of samples from Hole 878A range from 35‰ to 36‰ and from 540 to 572 mM, respectively. These data are consistent with normal seawater values (Fig. 36 and Table 7).

Alkalinity, pH, Calcium, Magnesium, Potassium, Rubidium, Strontium, and Lithium

The pH and alkalinity values of interstitial water samples from Hole 878A both decrease with depth: pH from 7.73 to 7.48 and alkalinity from 2.84 to 0.82 mM (Fig. 36). Calcium contents increase from 10.95 to 58.52 mM, and magnesium concentrations decline from 49.82 to 24.75 mM with sample depth. Strontium concentrations increase from 100 μM at 2.56 mbsf to 266 μM at 800 mbsf. Potassium and rubidium contents of the interstitial water decrease downhole; potassium contents decline nearly three times (6.16 to 2.30 mM), whereas rubidium values show a twelvefold change (2.16–0.18 μM;

Sample 144-878A-84R-1, 13 cm

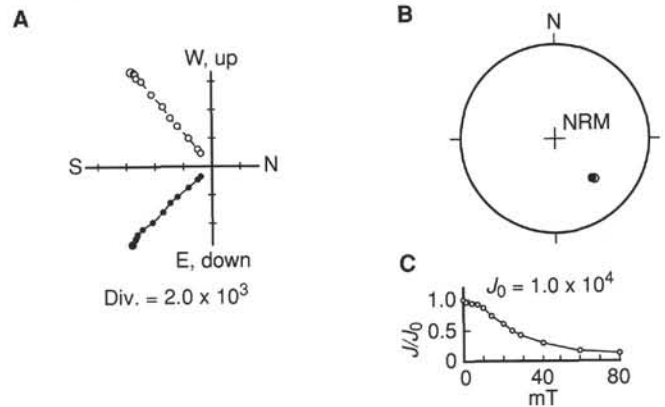


Figure 33. Alternating-field (AF) demagnetization results for basalt Sample 144-878A-84R-1, 13 cm. Demagnetization fields are 0, 2.5, 5, 7.5, 10, 15, 25, 29, 40, 60, and 80 mT. Other plot conventions are as in Figure 30.

Fig. 36). Rubidium concentrations in the pore waters of Sample 144-878A-1R-2, 143–150 cm, are elevated over surface seawater contents (2.16 vs. 1.40 μM). All of the above concentration changes are consistent with inferred chemical exchanges between the pore waters and the clay-rich altered basalt (Table 7).

Sulfate and Lithium

Sulfate and lithium concentrations increase in Sample 144-878A-79R-CC and then decline markedly in Sample 144-878A-86R-1, 118–129 cm. Typically, decreases in sulfate content are attributed to the chemical reduction of sulfate to sulfide. Sulfate contents from the pelagic sediment are about 3 mM below seawater concentrations (28.9 mM) in Sample 144-878A-1R-2, 143–150 cm, suggesting that pore waters are mildly reducing in nature. Lithium concentrations in the interstitial water increase from 26 μM in seawater to 35 μM in Sample 144-878A-79R-1, and then drop to 9 μM in Sample 144-878A-86R-1 (Table 7). The specific chemical reactions responsible for this decline in lithium content are known to be related to the low-temperature diagenetic reactions that take place within basaltic material (Holland, 1984).

Summary

Site 878 data are consistent with chemical exchange between weathered basalt (clays) and their interstitial waters. Interstitial waters from pelagic sediments are more clearly reductive compared with previous sites studied during Leg 144.

ORGANIC GEOCHEMISTRY

Introduction

Site 878 was drilled on MIT Guyot. The type of rocks encountered at the site were (from top to bottom): pelagic cap (Lithologic Unit I; see "Lithostratigraphy" section, this chapter), platform limestone (Unit II and III), volcanic limestone breccia (Unit IV), platform limestone (Unit V), and basalt (Unit VI).

The analytical program for Hole 878A included headspace gas analysis, chemical analysis, and pyrolysis. One sample from the pelagic cap was analyzed to determine the content of light hydrocarbon gases. One hundred and two samples from the carbonate rocks and the volcanoclastic limestone breccia were analyzed for inorganic carbon (IC). Of these, forty-six samples were selected for total organic carbon (TOC), nitrogen (N), and total sulfur (TS) analyses. One sample from the breccia was analyzed for organic matter type by

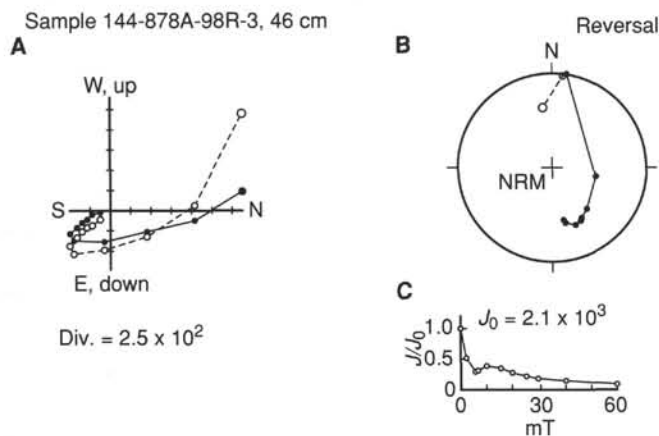


Figure 34. Alternating-field (AF) demagnetization results for basalt Sample 144-878A-98R-3, 46 cm. Demagnetization fields are 2.5, 5, 7.5, 10, 15, 25, 29, 40, and 60 mT. Other plot conventions are as in Figure 30.

pyrolysis. The procedures used for the analytical program are described in the "Organic Geochemistry" section of the "Explanatory Notes" chapter (this volume).

Volatile Hydrocarbons

The shipboard safety and pollution monitoring program requires measurements of light hydrocarbon gases (C_1 to C_3) in cores immediately after retrieval onto the core deck. One sample from the pelagic cap (Sample 144-878A-1R-3, 0–5 cm) was analyzed to determine the content of light hydrocarbon gases. Methane content (1.9 ppm) was indistinguishable from the laboratory background (Table 8). The sample contained no heavier hydrocarbons. As light hydrocarbon gases were not considered a safety hazard at this site, no sampling for headspace gas was attempted in the indurated rocks encountered deeper in the hole.

Carbonate Carbon

Inorganic carbon (IC) content was measured in 102 samples from Holes 878A with the Coulometrics carbon dioxide coulometer; the results are reported as weight% calcium carbonate. Sampling was performed in such a way as to obtain representative material of both lithotypes and from different depths. One hundred microsamples from the limestone and breccia (approximately 100 mg each) were collected with a hand drilling using a standard 5-mm drill bit. Sampling levels were identical to those used for the physical properties analyses. In the breccia, samples were mostly obtained from the matrix. Two samples from the red clay interlayering the basalt flows were collected from the squeeze-cake left after interstitial water sampling. No samples were taken from the basalt. Results of the inorganic carbon analyses are given in Tables 9–10, and the calcium carbonate data are shown in Figure 37.

The pelagic cap sediments encountered in Hole 878A (Lithologic Unit I) had carbonate contents of between 65% and 72% (average $CaCO_3 = 70.6\%$). These values were considerably lower than those observed in the pelagic caps from Sites 871, 872, and 873. The platform limestone from Lithologic Units II, III, and V had carbonate contents close to 100% (average $CaCO_3$ for all three units = 98.6%). In the breccia (Lithologic Unit IV), carbonate content was highly variable. The lowest values were found in the green tuff horizon at the top of the unit (Interval 144-878A-44M-1, 27–77 cm: $CaCO_3$ from 0.8% to 1.5%). Carbonate content in the matrix varied from 20% to 80%. The large variability in carbonate content can partly be ascribed to difficulties in sampling matrix material totally free of clasts of

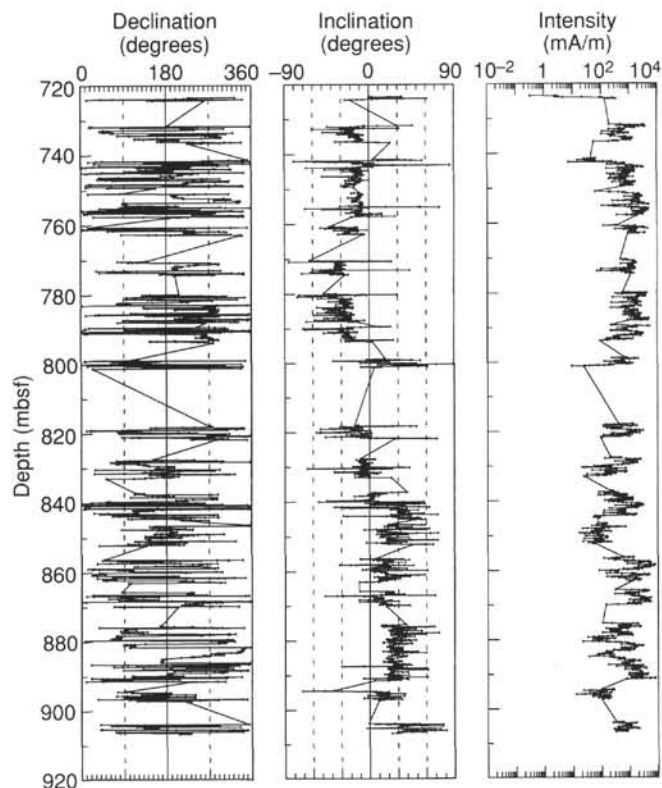


Figure 35. Declination, inclination, and intensity variations in the lower portion of the volcanic basement (Cores 144-878A-78R to -98R).

limestone or lava. However, apart from this sampling "noise," two cycles from high to low carbonate values were observed in the matrix, one ranging from the bottom of the breccia at 603 m to about 515 m, and one from about 515 m to the top of the breccia at 406 m. In both cycles, carbonate content decreased from about 80% at the bottom to <40% at the top. The cycles probably reflected two separate eruptive events (see "Igneous Petrology" section, this volume).

The red clay from the basalt in Unit V was virtually carbonate free.

Organic Carbon and Total Sulfur

The content of total carbon (TC), nitrogen (N), and total sulfur (TS) was determined using the Carlo Erba Model NA1500 elemental analyzer. Total organic carbon (TOC) values were calculated from the difference between TC and IC. Detection limits for TOC, N, and TS are 0.2%, 0.02%, and 0.02%, respectively. Analyses were performed on 46 samples of the samples used for carbonate carbon determinations. The results of the TOC, N, and TS analyses are given in Tables 9–10.

Very low TOC values were found in the pelagic cap sediments and the platform limestone (Lithologic Units I, II, III, and V; average TOC = 0.2%). In the same units, nitrogen and sulfur concentrations were below detection limits. The top of the breccia (Lithologic Unit IV, Samples 144-878A-44M-1, 11–14 cm, to -44M-1, 126–128 cm) was characterized by increased sulfur concentrations, reaching peak values of 6.5% total sulfur in the green tuff. The high sulfur values were found in an interval already described as carrying millimeter-sized, euhedral pyrite crystals and pyrite rims around clasts. Below this interval, no sulfur was detected. The sulfur enrichment cannot be explained by processes related to early diagenetic sulfate reduction of organic matter, as was the case for Sites 871, 874 and 878. Rather, sulfide-rich solutions of volcanic origin were the source for pyrite precipitation in this case.

Table 7. Surface seawater and interstitial water geochemical data, Hole 878A.

Core, section, section (cm)	Depth (mbsf)	pH	Alkalinity (mM)	Salinity (g/kg)	Cl ⁻ (mM)	Mg ²⁺ (mM)	Ca ²⁺ (mM)	SO ₄ ²⁻ (mM)	K ⁺ (mM)	Rb ⁺ (μM)	Sr ⁺ (μM)	Li (μM)
Surface seawater	0	8.23	2.45	35.0	562	54.02	10.53	28.9	10.00	1.40	91	26
144-878A-												
1R-2, 143-150	2.56	7.73	2.84	35.0	540	49.82	10.95	26.2	6.16	2.16	100	32
79R-CC, 18-27	735.83	7.61	1.60	35.0	564	46.20	13.93	28.4	3.83	0.65	106	35
86R-1, 118-129	800.04	7.48	0.82	36.0	572	24.75	58.52	11.9	2.30	0.18	266	9

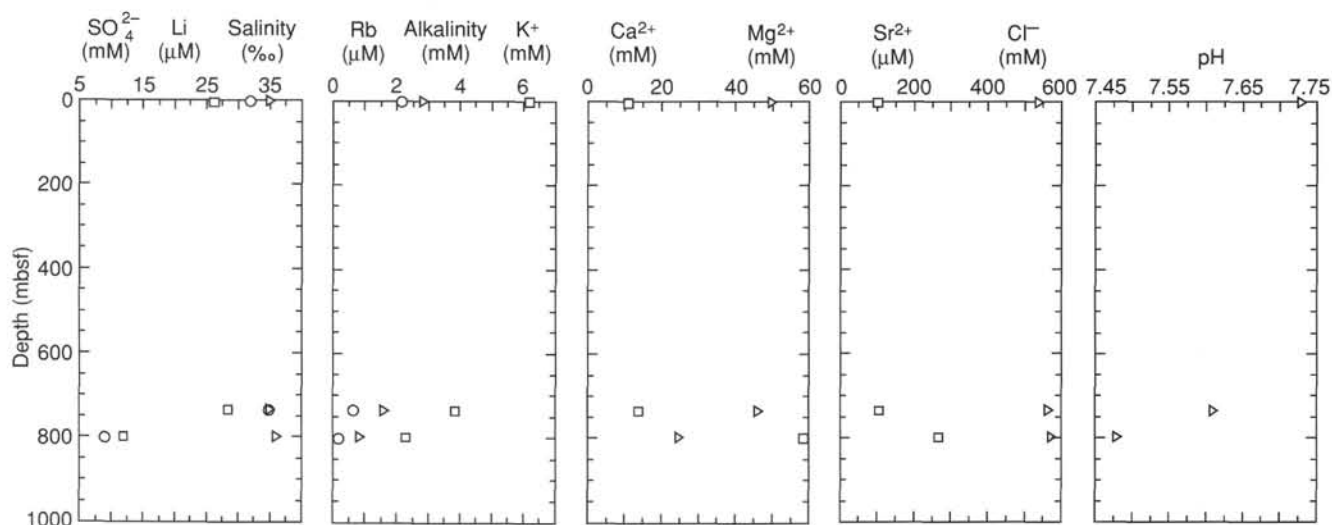


Figure 36. Concentrations of interstitial pore-water parameters vs. depth, Hole 878A.

No enrichment in organic carbon or nitrogen was observed within the breccia except for four millimeter-sized "clasts" of black peaty clay. The red clay between the basalt flows in Lithologic Unit VI was free of organic carbon, nitrogen, and sulfur.

Organic Matter Type and Thermal Maturation Level

Shipboard geochemical characterization of organic matter is normally performed by Rock-Eval (RE) and pyrolysis gas chromatographic (Py-GC) analysis. Only samples containing >1% organic matter are considered suitable for these types of analyses. During the time spent at Site 878, the Rock-Eval instrument was out of order, and organic matter characterization was confined to the Geofina instrument.

Only one sample from Hole 878A was analyzed by pyrolysis. This sample represented the largest of the four organic clasts found in the breccia. Visual inspection demonstrated the sample to be dominated by woody material (see "Biostratigraphy" section, this chapter). The amount of sample material was not large enough for both pyrolysis and TOC determination. It was not possible, therefore, to calculate a hydrogen index value from the Geofina analysis, and the only parameter obtained was T_{max} . The measured value of 428°C corresponded to marginally mature organic matter with regard to thermal influence. This value was slightly higher than those observed at the previous guyots and cannot be explained by burial alone. Thus, marginal heating from the volcanic events cannot be excluded. The organic maturity levels determined by geochemical methods are in agreement with the palynologic observations (see "Biostratigraphy" section, this volume).

Interpretation of Organic Facies and Depositional Environments

Very little can be said about the organic facies represented in Hole 878A. In all types of depositional environments found at the site,

preservation potential for organic matter was extremely poor, and no organic carbon enrichments were observed. The only exceptions were the four minute clasts of black organic-rich material found in the breccia. These clasts indicate that a terrestrially influenced, organic-rich facies must have occurred somewhere within the sedimentary sequence below the breccia.

Conclusions

The following conclusions can be made regarding the organic geochemistry at Site 878:

1. No volatile hydrocarbons were encountered at the site.
2. The pelagic cap sediments and the shallow-water limestone (Lithologic Units I, II, III, and V) had calcium carbonate contents above 95%. Only very low concentrations of organic matter and sulfur were encountered. The units were deposited under oxic conditions.
3. The volcanic limestone breccia (Lithologic Unit IV) contained two cycles of upward-decreasing carbonate content, probably reflecting two eruptive events.
4. A marked sulfur enrichment was found in the topmost part of the breccia. The enrichment corresponded to an occurrence of euhedral pyrite crystals probably related to H₂S-rich volcanic solutions formed during the eruptions.
5. The breccia had very low concentrations of organic carbon.
6. Organic matter from a minute, organic-rich clast in the breccia was marginally mature with regard to thermal influence ($T_{max} = 428^{\circ}\text{C}$). This maturity level cannot be explained from burial depths alone.

IGNEOUS PETROLOGY

Introduction

At Site 878 on MIT Guyot, basalt was first encountered at 722.5 mbsf in Hole 878A, beneath the limestone of Lithologic Unit V.

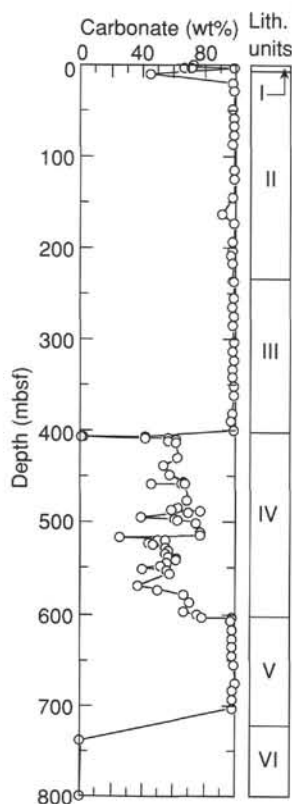


Figure 37. Carbonate content of sediments in Hole 878A, calculated as calcium carbonate. Also shown are the major lithologic units, as given in the "Lithostratigraphy" section (this chapter).

Below this depth, drilling continued for 187.5 m, ending at 910.0 mbsf. Recovery in this basement interval averaged 56%.

The basement section, designated as Lithologic Unit VI, consists of interlayered basalt, basalt breccia, tuff, and claystone weathering horizons. We have divided this section into 35 igneous units including 24 lava flows (Fig. 38). The 24 flows represent at least 3 distinct periods of volcanism separated by periods of weathering. The upper volcanic interval consists of 2 hawaiite flows. These are underlain by a sequence of altered and oxidized volcanoclastic breccias, tuffs, and sandstones that mark the younger of the two weathering intervals. The middle volcanic interval consists of 7 basanitoid flows and a thick breccia deposit. Below the basanitoids, the older weathering interval is represented by a thick claystone weathering profile (Unit 17) that retains relict textures of basalt and basalt breccia. The lower volcanic interval contains 15 flows and 1 thick breccia deposit. The upper 3 flows of this sequence are also basanitoids, and all of the lower flows that have been examined petrographically are alkali olivine basalts.

An oxidized flow-top breccia was recovered with almost every massive flow, indicating that the entire sequence is subaerial. Except in the uppermost three flows, calcite veins are rare, in contrast to their abundance in all other Leg 144 basalt cores. All the igneous units have been considerably altered, resulting in the replacement of matrix and phenocrysts by clay. This type of alteration must have occurred at low temperatures. In contrast, Unit 31, a thick volcanic breccia, is severely altered, with an upper bleached subunit (Subunit 31A) and a lower, oxidized subunit (Subunit 31B); it appears to have been subjected to hydrothermal alteration. Furthermore, serpentine slickensides occur on two steeply dipping (70°) fractures in Sections 144-878A-89R-2 and -89R-3. These may also reflect relatively high temperature, hydrous alteration.

Table 8. Results of headspace gas analyses, Hole 878A.

Core, section, interval (cm)	Methane (ppm)	Ethane (ppm)	Propane (ppm)	Lithology
144-878A-1R-3, 0-5	1.9	None	None	Pelagic ooze
Laboratory background	2.2	None	None	
Core deck background	1.7	None	None	
Sea air background	1.8	None	None	

Note: None = no gas detected.

We have divided the basalt flows and basalt breccias into seven petrographic types (Table 11). In most cases, sets of several successive flows belong to one type.

Petrographic Types

Type 1

Type 1 volcanic flows include the hawaiite flows of Units 1 and 2. Both flows contain moderately abundant plagioclase, olivine, and clinopyroxene phenocrysts that have been replaced by clay. Each flow is severely altered in the top 50 cm (soft, friable, with widely varying colors); below each altered zone the flows are dark to light gray and much harder. In Unit 2 narrow bands (0.5–1.0 cm) of iron-stain material, comprising 20%–25% of the rock, occur throughout the matrix in the lower part of the flow. Both units contain up to 5% <2-mm-wide, calcite-filled veins. Few veins occur elsewhere in the basalts.

In thin section, olivine microphenocrysts, 5%–10% in abundance and 0.1–2.0 mm in diameter, are set in a pilotaxitic to intergranular groundmass dominated by weak flow-oriented plagioclase laths. Between the plagioclase laths, relatively scarce (10%), greenish, granular, clinopyroxene and anhedral magnetite grains are set among interstitial areas of feldspar partially replaced by pale green clay. The interstitial feldspar is predominantly plagioclase, but alkali feldspar may also be present. Acicular apatite and tiny bladed ilmenite are minor phases.

Type 1 flows are separated from those of Type 2 by a sequence of very altered breccias, tuffs, and volcanogenic sandstones (Units 3–7). Extensive oxidation and clay development has occurred, obscuring texture, filling vesicles, and pseudomorphing olivine. Unit 3 consists of subangular, vesicular basalt clasts, 0.5–6.0 cm in diameter, in a matrix comprised of volcanogenic, sand-sized fragments and authigenic clay. Unit 4 is a lithic tuff consisting of nonvesicular basalt clasts and olivine and clinopyroxene crystal fragments. The clasts, which are subangular to subrounded in shape, are 0.2–0.6 cm in diameter. Unit 5 is a volcanogenic sandstone, altered and oxidized so severely that few sand-sized grains can be distinguished from the authigenic matrix. Unit 6 consists of two pieces of olivine-phyric, vesicular basalt. Unit 7 is a coarse basalt breccia with an average clast size larger than 6 cm.

Type 2

Basanitoid lavas of Type 2 are characterized by their fine grain size, intergranular texture, and a predominance of titanite. Units 8 and 10 are separated by two small pieces of lithic (Unit 9) tuff that occur at the top of Core 144-878A-81R, and that are likely to have fallen from the vicinity of Unit 4. If this is so, then Units 8 and 10 are likely to be a single thick (>10 m) flow. This is supported by their very similar petrographic character and by the observation that no flow-top breccia was recovered from Unit 10. Unit 11 is approximately 5 m thick, Unit 15 is about 9 m thick, and Unit 16 is about 3 m thick. Units 8, 11, and 15 each have thin (50 cm recovered) flow-top breccias.

In hand specimen, Units 8, 10, 11, and 16 each have 10%–20%, euhedral, rounded or broken, olivine grains, usually pseudomorphed by iddingsite but occasionally by green clay. Unit 15 has 15%, broken, olivine grains that are unaltered in certain intervals (e.g., Interval

Table 9. Results of geochemical analyses, Hole 878A

Core, section, interval (cm)	Depth (mbsf)	IC (wt%)	CaCO ₃ (wt%)	TC (wt%)	TOC (wt%)	N (wt%)	TS (wt%)	Lithology
144-878A-								
1R-1, 0-5	0	8.71	72.55	ND	ND	ND	ND	Nannofossil foraminifer ooze
1R-2, 143-150	2.49	8.06	67.14	8.34	0.28	0	0	Nannofossil ooze
1R-3, 0-5	2.56	8.65	72.06	ND	ND	ND	ND	Nannofossil ooze
1R-CC, 22-25	3.37	11.87	98.88	12.01	0.14	0	0	Wackestone
2R-1, 26-27	9.76	5.44	45.32	6.46	1.02	0.01	0	Phosphatized packstone
3R-1, 59-61	19.59	11.86	98.79	ND	ND	ND	ND	Wackestone
4R-1, 26-29	28.76	11.88	98.96	ND	ND	ND	ND	Wackestone
6R-1, 16-20	47.76	11.85	98.71	12.54	0.69	0	0	Wackestone
7R-1, 22-28	57.52	11.88	98.96	ND	ND	ND	ND	Wackestone
8R-1, 5-10	67.05	11.87	98.88	ND	ND	ND	ND	Wackestone
9R-1, 12-14	76.72	11.87	98.88	ND	ND	ND	ND	Wackestone
10R-1, 0-4	86.20	11.85	98.71	12.29	0.44	0	0	Wackestone
13R-1, 8-12	115.18	11.89	99.04	11.96	0.07	0.01	0	Floatstone
14R-1, 14-18	124.94	11.90	99.13	ND	ND	ND	ND	Wackestone
16R-1, 8-12	144.08	11.86	98.79	11.85	0	0	0	Packstone
18R-1, 21-24	163.61	10.96	91.30	11.90	0.94	0.01	0.17	Wackestone
19R-1, 9-12	173.19	11.93	99.38	ND	ND	ND	ND	Wackestone
21R-1, 4-7	192.54	11.84	98.63	ND	ND	ND	ND	Wackestone
22M-1, 10-12	202.30	11.84	98.63	11.49	0.01	0	0	Grainstone
23M-1, 16-22	207.06	11.74	97.79	ND	ND	ND	ND	Packstone
24M-1, 4-9	216.64	11.84	98.63	ND	ND	ND	ND	Wackestone
26M-1, 4-12	235.94	11.83	98.54	ND	ND	ND	ND	Wackestone
26M-1, 13-16	236.03	11.89	99.04	11.76	0	0	0	Rudstone
26M-1, 31-34	236.21	11.88	98.96	ND	ND	ND	ND	Rudstone
28M-1, 0-8	255.20	11.87	98.88	ND	ND	ND	ND	Rudstone
29M-1, 0-6	264.90	11.85	98.71	ND	ND	ND	ND	Grainstone
30M-1, 43-54	274.93	11.88	98.96	11.96	0.08	0.01	0.02	Grainstone
31M-1, 30-32	284.40	11.81	98.38	ND	ND	ND	ND	Rudstone
33M-1, 0-7	302.90	11.90	99.13	ND	ND	ND	ND	Grainstone
34M-1, 18-21	312.78	11.84	98.63	11.93	0.09	0	0	Grainstone
35M-1, 7-11	322.27	11.91	99.21	ND	ND	ND	ND	Grainstone
36M-1, 18-20	332.08	11.85	98.71	ND	ND	ND	ND	Grainstone
37M-1, 0-3	341.60	11.82	98.46	11.48	0	0.01	0	Grainstone
38M-1, 7-10	351.27	11.89	99.04	ND	ND	ND	ND	Grainstone
39M-1, 36-39	361.26	11.90	99.13	11.92	0.02	0	0	Grainstone
41M-1, 4-8	380.24	11.83	98.54	ND	ND	ND	ND	Grainstone
42M-1, 16-21	407.36	11.68	97.29	ND	ND	ND	ND	Mudstone
43M-1, 21-29	399.51	11.87	98.88	11.97	0.10	0.01	0	Wackestone
44M-1, 11-14	406.21	5.10	42.48	5.14	0.04	0	4.23	Volcanic breccia, matrix
44M-1, 27-28	406.37	0.13	1.50	0.12	0	0	6.52	Tuff
44M-1, 47-49	406.57	0.10	0.83	0.16	0.06	0	2.43	Tuff
44M-1, 126-128	407.36	5.03	41.90	5.07	0.04	0	1.94	Volcanic breccia, matrix
44M-2, 34-36	407.94	6.84	56.98	7.25	0.41	0	0	Volcanic breccia, matrix
45M-1, 21-24	409.11	7.45	62.06	7.46	0.01	0.01	0	Volcanic breccia, matrix
45M-2, 67-69	410.95	6.80	56.64	7.25	0.45	0	0	Volcanic breccia, matrix
45M-3, 97-100	412.67	7.40	61.64	8.09	0.69	0	0	Volcanic breccia, matrix
46M-2, 21-23	420.06	10.90	90.80	ND	ND	ND	ND	Volcanic breccia, matrix
47R-1, 79-82	428.99	7.60	63.31	ND	ND	ND	ND	Volcanic breccia, matrix
48R-2, 66-69	437.63	6.51	54.23	6.52	0.01	0.01	0	Volcanic breccia, matrix
49R-2, 18-20	446.80	6.91	57.56	ND	ND	ND	ND	Volcanic breccia, matrix
50R-1, 51-53	455.31	8.02	66.81	ND	ND	ND	ND	Volcanic breccia, matrix
50R-2, 66-68	456.94	7.87	65.56	ND	ND	ND	ND	Volcanic breccia, matrix
50R-2, 135-137	457.63	5.56	46.31	ND	ND	ND	ND	Volcanic breccia, matrix

144-878A-84R-4, 96-106 cm), but otherwise are pseudomorphed by iddingsite. Also, Unit 15 contains 1% subhedral prisms of small (0.1-0.2 mm) clinopyroxene grains that are unaltered in the same intervals in which olivine is fresh and which are otherwise pseudomorphed by dark green clay. Veins are sparse and thin (<1% in abundance and <2 mm in diameter). They are filled with calcite and lesser amounts of green clay.

In thin section, Type 2 basalts are seen to contain abundant (5%-20%) olivine microphenocrysts ranging from larger (~1 mm), euhedral shapes to smaller (>0.2 mm), anhedral, apparently broken grains that are set in an intergranular matrix dominated by clusters of subhedral titanite. In some flows, a few large, broken and partially resorbed prisms of clinopyroxene and/or plagioclase are also present. Additional groundmass phases include plagioclase laths, interstitial patches of plagioclase (and nepheline?), and abundant (~10%), subhedral to euhedral magnetite cubes. Green clay has replaced the original mesostasis and colorless clay or zeolite with mottled extinction, and low birefringence has replaced some of the interstitial feldspar.

Below the lowermost Type 2 lava flow is Unit 17, an 8-m-thick tropical weathering profile that is now preserved as claystone. Parts of the claystone retain relict textures of basalt and volcanic breccia,

including sharp clast boundaries and dark yellowish orange (10YR 6/6) spots (0.2-3.0 mm in diameter) that are probably iddingsite pseudomorphs after olivine. This unit represents a time interval during which no basalt flowed over this locality.

Type 3

Type 3 volcanic flows include Unit 12, a basanitoid breccia, and Units 18, 20, and 21, which are basanitoid lava flows. They are characterized by a predominance of plagioclase over titanite and by finer and more abundant titanomagnetite than Type 2 lavas.

Unit 12, a 10-m-thick breccia of Type 3 basanitoid clasts, lies between two Type 2 lava flows. The clasts are subrounded and 5 mm to >5 cm in diameter. The lava is aphanitic with <3% euhedral olivine grains that are 0.5-2.0 mm in diameter and pseudomorphed by iddingsite. The clasts are highly vesicular with 20%-40%, irregular vesicles, <1-3 mm in diameter. The matrix consists of sand- and granule-sized, vesicular basalt grains with interstitial clay. The breccia is strongly oxidized and moderately altered to clay.

Unit 18 is a lava flow approximately 15 m thick. The core is very friable, indicating extensive replacement of the matrix by clay. No

Table 9 (Continued).

Core, section, interval (cm)	Depth (mbsf)	IC (wt%)	CaCO ₃ (wt%)	TC (wt%)	TOC (wt%)	N (wt%)	TS (wt%)	Lithology
144-878A- (cont.)								
50R-3, 27-29	458.06	8.12	67.64	ND	ND	ND	ND	Volcanic breccia, matrix
52R-2, 92-94	476.50	8.30	69.14	ND	ND	ND	ND	Volcanic breccia, matrix
53R-1, 96-98	484.66	7.56	62.97	8.02	0.46	0.01	0	Volcanic breccia, matrix
53R-2, 70-73	485.71	7.11	59.23	ND	ND	ND	ND	Volcanic breccia, matrix
53R-3, 70-73	487.16	9.36	77.97	ND	ND	ND	ND	Volcanic breccia, matrix
53R-4, 49-52	488.40	8.38	69.81	ND	ND	ND	ND	Volcanic breccia, matrix
54R-1, 61-63	493.81	4.70	39.15	3.31	0	0	0.01	Volcanic breccia, matrix
54R-2, 75-77	495.32	7.35	61.23	ND	ND	ND	ND	Volcanic breccia, matrix
54R-3, 104-106	496.89	7.50	62.48	ND	ND	ND	ND	Volcanic breccia, matrix
54R-6, 24-26	499.95	8.95	74.55	ND	ND	ND	ND	Volcanic breccia, matrix
55R-6, 24-26	509.61	11.72	97.63	ND	ND	ND	ND	Volcanic breccia, clast
55R-6, 104-106	510.41	9.35	77.89	ND	ND	ND	ND	Volcanic breccia, matrix
56R-2, 56-58	513.90	9.33	77.72	ND	ND	ND	ND	Volcanic breccia, matrix
56R-3, 78-80	515.58	3.12	25.99	ND	ND	ND	ND	Volcanic breccia, matrix
56R-5, 74-76	518.46	6.07	50.56	ND	ND	ND	ND	Volcanic breccia, matrix
56R-6, 28-30	519.20	6.55	54.56	ND	ND	ND	ND	Volcanic breccia, matrix
57R-1, 37-39	521.57	5.30	44.15	5.54	0.24	0	0	Volcanic breccia, matrix
57R-3, 63-65	524.42	5.65	47.06	ND	ND	ND	ND	Volcanic breccia, matrix
57R-5, 102-104	527.71	6.61	55.06	ND	ND	ND	ND	Volcanic breccia, matrix
58R-1, 120-122	530.52	6.87	57.23	ND	ND	ND	ND	Volcanic breccia, matrix
58R-3, 96-98	534.30	6.57	54.73	ND	ND	ND	ND	Volcanic breccia, matrix
58R-5, 53-55	536.48	6.83	56.89	ND	ND	ND	ND	Volcanic breccia, matrix
58R-7, 88-90	539.35	7.39	61.56	ND	ND	ND	ND	Volcanic breccia, matrix
59R-1, 1-23	540.10	7.41	61.73	ND	ND	ND	ND	Volcanic breccia, matrix
59R-4, 76-78	544.10	6.69	55.73	ND	ND	ND	ND	Volcanic breccia, matrix
59R-7, 38-40	547.75	6.21	51.73	ND	ND	ND	ND	Volcanic breccia, matrix
60R-1, 127-129	549.80	4.83	40.23	4.74	0	0.01	0	Volcanic breccia, matrix
60R-3, 106-108	552.61	6.68	55.64	ND	ND	ND	ND	Volcanic breccia, matrix
60R-5, 63-65	555.04	7.00	58.31	ND	ND	ND	ND	Volcanic breccia, matrix
62R-1, 18-20	568.70	4.50	37.49	ND	ND	ND	ND	Volcanic breccia, matrix
62R-2, 95-102	570.76	11.66	97.13	ND	ND	ND	ND	Volcanic breccia, clast
62R-4, 45-74	573.25	6.06	50.48	ND	ND	ND	ND	Volcanic breccia, matrix
63R-1, 77-79	578.87	8.00	66.64	8.26	0.26	0.01	0	Volcanic breccia, matrix
64R-1, 13-15	587.73	8.47	70.56	ND	ND	ND	ND	Volcanic breccia, matrix
65R-1, 51-54	597.61	8.00	66.64	8.08	0.08	0.01	0	Volcanic breccia, matrix
65R-3, 70-72	600.78	9.04	75.30	ND	ND	ND	ND	Volcanic breccia, matrix
65R-5, 84-86	603.42	9.49	79.05	ND	ND	ND	ND	Volcanic breccia, matrix
65R-6, 41-45	604.49	11.80	98.29	11.61	0	0.01	0	Limestone breccia
66R-1, 10-16	606.70	11.74	97.79	ND	ND	ND	ND	Grainstone
67R-1, 31-37	616.61	11.81	98.38	ND	ND	ND	ND	Grainstone
68R-1, 40-45	626.30	11.80	98.29	11.86	0.05	0.01	0	Wackestone
69R-1, 36-38	635.96	11.77	98.04	ND	ND	ND	ND	Packstone
70R-1, 45-50	645.65	11.82	98.46	ND	ND	ND	ND	Mudstone
71R-1, 66-68	655.56	11.88	98.96	10.06	0	0	0	Grainstone
73R-1, 41-49	674.61	12.00	99.96	ND	ND	ND	ND	Grainstone
74R-1, 22-29	684.12	11.83	98.54	12.39	0.55	0.01	0	Packstone
75R-1, 122-124	694.42	11.85	98.71	ND	ND	ND	ND	Packstone
76R-1, 12-14	703.12	11.86	98.79	ND	ND	ND	ND	Grainstone
79R-CC, 18-27	738.13	0.03	0.25	0.06	0.03	0	0	Reddish clay
86R-1, 118-129	799.81	0.02	0.17	ND	ND	ND	ND	Reddish clay

Notes: IC = inorganic carbon, CaCO₃ = carbonate carbon calculated as calcium carbonate, TC = total carbon, TOC = total organic carbon, N = nitrogen, and TS = total sulfur. All numbers are in weight percent. ND = no determination.

flow-top breccia was recovered. Unit 20 is approximately 12 m thick; half of this is flow-top breccia. Unit 21 is also approximately 12 m thick, but no flow-top breccia was recovered. The latter two flows are relatively unaltered.

Each unit contains 5%–10% olivine with lesser clinopyroxene phenocrysts. Olivine grains are euhedral to round, 0.5–3.0 mm in diameter, and pseudomorphed by iddingsite and lesser brown clay. Clinopyroxene prisms are commonly unaltered. Units 20 and 21 contain abundant (20%), anhedral, olivine microphenocrysts that are visible in hand specimen as tiny iddingsite pseudomorphs after olivine.

In thin section, olivine microphenocrysts range from larger (~1 mm) euhedral shapes to smaller (>0.2 mm) anhedral, apparently broken grains that are set in an intergranular matrix dominated by plagioclase laths. Plagioclase also occurs as interstitial patches with clusters of subhedral titanite. In some flows, a few large broken or resorbed prisms of clinopyroxene and/or plagioclase (not visible in hand specimen) are also present. Additional groundmass phases include abundant (~10%), fine-grained, subhedral to euhedral magnetite cubes. Green clay has replaced the original mesostasis; and colorless clay (or zeolite), with mottled, low birefringence, has replaced some of the feldspar.

Type 4

Type 4 volcanic flows of Units 22 and 23 are characterized by sparse olivine, clinopyroxene, plagioclase, and biotite phenocrysts in an intersertal groundmass dominated by plagioclase. There is no thin section of Unit 22, but it has visible plagioclase phenocrysts that group it as Type 4 rather than as Type 3.

Unit 22 is approximately 4 m thick; half of this is flow-top breccia. Unit 23 is approximately 11 m thick with about 50 cm of flow-top breccia. Except for Sections 144-878A-90R-5 and -90R-6, within Unit 23, olivine abundances are low (3–5%) and clinopyroxene and plagioclase abundances are very low (typically <1%). Olivine and clinopyroxene grains are <0.5–4.0 mm in diameter and subhedral to rounded. Olivine is occasionally unaltered but usually iddingsitized. Clinopyroxene usually has clay along fine fractures, but it is otherwise unaltered. Clinopyroxene and olivine sometimes occur together in glomerocrysts up to 7 mm in diameter. The occurrence of glomerocrysts and the rounded shapes of individual crystals suggest that the larger clinopyroxene and olivine grains are xenocrysts. Plagioclase, in 1–4 mm long laths, is sometimes fresh and sometimes pseudo-morphed by white clay or zeolite. Unit 23 contains sparse, subangular,

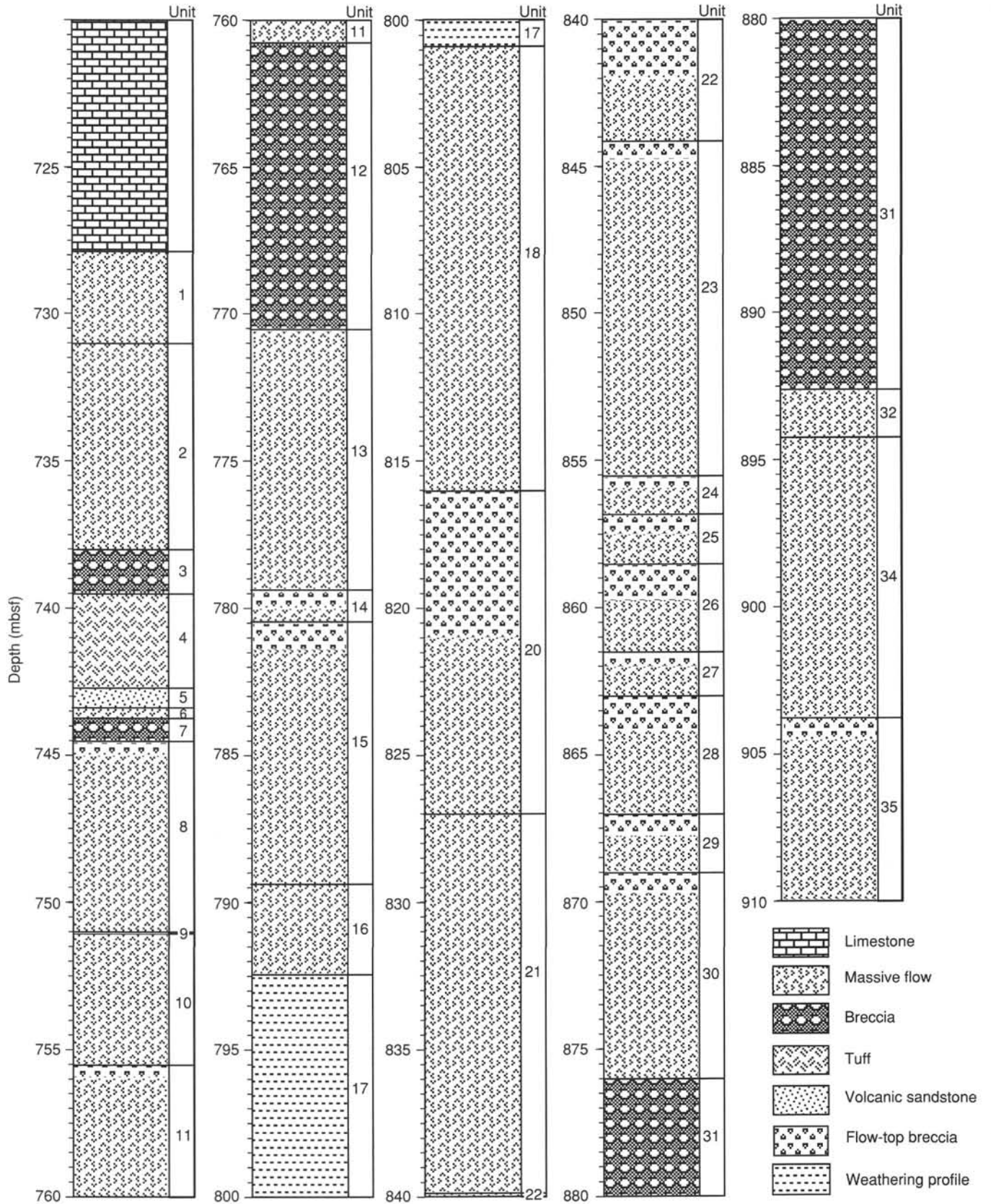


Figure 38. Lithostratigraphy of the igneous units in Hole 878A, as defined in the text. Note that the flow-top breccia and the massive flow material blend into one another.

Table 10. Averages of geochemical results from Hole 878A.

Units	CaCO ₃ (wt%)	TOC (wt%)	N (wt%)	TS (wt%)	General lithology
I					Pelagic ooze
Average	70.58	0.28	0	0	
SD	2.99				
N	3	1	1	1	
II					Limestone
Average	98.87	0.37	0	0.02	
SD	0.09	0.42	0	0.06	
N	9	9	9	9	
III					Limestone
Average	98.46	0.06	0	0	
SD	1.5	0.04	0	0.01	
N	27	5	5	5	
IV					Breccia
Average	58.47	0.18	0	1.01	
SD	18.28	0.22	0	1.98	
N	51	15	15	15	
V					Limestone
Average	98.57	0.15	0	0	
SD	0.57	0.27	0	0	
N	11	4	4	4	
VI					Clay in basalt
Average	0.21	0.03	0	0	
SD					
N	2	2	2	2	

Notes: SD = standard deviation, and N = number of samples.

ultramafic xenoliths, as large as 4 cm in diameter, composed of fresh clinopyroxene and iddingsitized olivine. Both units are strongly altered, although the center part of the thick massive Unit 23 has remained relatively fresh.

In thin section, Type 4 lavas are seen to contain up to 15% olivine and sparse (<5% total) phenocrysts of biotite, plagioclase, and clinopyroxene. The groundmass is intersertal and dominated by laths and interstitial patches of plagioclase with granular olivine (replaced by green/brown clay), titanite, and subhedral to anhedral, bladed or granular ilmenite. Apatite needles are abundant. Green clay has replaced the mesostasis, and colorless clay or zeolite with mottled, low birefringence, has replaced some of the feldspar.

Type 5

Type 5 volcanic flows, which include the alkali basalts of Units 25, 26, 27, and 30, are characterized by a distinctive intersertal texture dominated by randomly oriented, bladed ilmenite in a matrix of plagioclase laths and lesser granular titanite.

Units 24–30 form a series of thin flows that are <4 m thick, except for Unit 30, which is approximately 7 m thick. Each flow has a 50- to 75-cm-thick flow-top breccia. Units 24 and 28 are identical in appearance to the other units, but no thin sections were made. The flow-top breccias are clast supported with subangular to subround clasts, 0.5–10.0 cm in diameter. The basalt comprising the clasts is aphanitic with <3% iddingsite pseudomorphs of olivine, 1–3 mm in diameter. The colors and vesicularity of both clasts and flows vary widely, but all flow-top breccias are oxidized. The matrix around the clasts consists of sand- and granule-sized basalt fragments and interstitial authigenic clay, which varies in color in shades of white, red, and green. Some flow-top breccias have been so extensively replaced by clay that clast-matrix boundaries are obscured.

The massive portion of each flow is microcrystalline with iddingsitized olivine phenocrysts or xenocrysts, typically up to 5 mm in diameter and euhedral to round or broken. Each also contains variable (<1%–5%) abundances of partially fresh, rounded clinopyroxene phenocrysts or xenocrysts, 1–5 mm in diameter. Unit 28 has scattered, tiny (<1 cm), altered xenoliths. Unit 30 has <1% 1- to 3-mm-long laths of altered plagioclase that typically occur in glomerocrysts with clinopyroxene.

In thin section, it is apparent that olivine, the sole phenocryst phase, occurs in two distinct size ranges. Larger (1–3 mm), subhe-

Table 11. Summary of igneous units, Hole 878A.

Unit	Type	Sample number	Description
Upper volcanic interval:			
1	I	144-878A-78R-1, 44 cm, to -78R-2, 88 cm	Hawaiite
2	I	144-878A-79R-1, 0 cm, to -79R-4, 4, 51 cm	Hawaiite
Upper weathering interval:			
3	NA	144-878A-79R-4, 51 cm, to -79R-5, 70 cm	Basalt breccia
4	NA	144-878A-79R-5, 70 cm, to -80R-1, 87 cm	Lithic tuff
5	NA	144-878A-80R-1, 87–144 cm	Volcanogenic sandstone
6	NA	144-878A-80R-1, 144 cm, to -80R-2, 7 cm	Olivine basalt
7	NA	144-878A-80R-2, 7–74 cm	Basalt breccia
Middle volcanic interval:			
8	2	144-878A-80R-2, 74 cm, to -80R-6, 120 cm	Basanitoid
9	NA	144-878A-81R-1, 0–6 cm	Lithic tuff
10	2	144-878A-81R-1, 6 cm, to -81R-3, 103 cm	Basanitoid
11	2	144-878A-81R-3, 103 cm, to -82R-1, 0 cm	Basanitoid
12	3	144-878A-82R-1, 0 cm, to -83R-1, 3 cm	Basalt breccia
13	NA	144-878A-83R-1, 3 cm, to -83R-4, 41 cm	Olivine basalt
14	NA	144-878A-84R-1, 0–19 cm	Olivine basalt
15	2	144-878A-84R-1, 19 cm, to -85R-1, 0 cm	Basanitoid
16	2	144-878A-85R-1, 0 cm, to -85R-2, 134 cm	Basanitoid
Lower weathering interval:			
17	NA	144-878A-85R-2, 134 cm, to -86R-2, 16 cm	Claystone
Lower volcanic interval:			
18	3	144-878A-86R-2, 16 cm, to -86R-3, 47 cm	Basanitoid
19	NA	144-878A-87R-1, 0–67 cm	Wash-core pieces
20	3	144-878A-88R-1, 0 cm, to -89R-1, 0 cm	Basanitoid
21	3	144-878A-89R-1, 0 cm, to -90R-2, 70 cm	Basanitoid
22	4	144-878A-90R-2, 70 cm, to -90R-4, 145 cm	Alkali olivine basalt
23	4	144-878A-90R-4, 145 cm, to -92R-1, 0 cm	Alkali olivine basalt
24	5	144-878A-92R-1, 0–16 cm	Alkali olivine basalt
25	5	144-878A-92R-1, 16 cm, to -92R-2, 104 cm	Alkali olivine basalt
26	5	144-878A-92R-2, 104 cm, to -92R-4, 101 cm	Alkali olivine basalt
27	5	144-878A-92R-4, 101 cm, to -92R-5, 86 cm	Alkali olivine basalt
28	5	144-878A-92R-5, 86 cm, to -93R-1, 71 cm	Alkali olivine basalt
29	5	144-878A-93R-1, 71 cm, to -93R-2, 63 cm	Alkali olivine basalt
30	5	144-878A-93R-2, 63 cm, to -94R-1, 58 cm	Alkali olivine basalt
31	NA	144-878A-94R-1, 58 cm, to -95R-5, 83 cm	Basalt breccia
32	6	144-878A-95R-5, 83 cm, to -95R-6, 58 cm	Alkali olivine basalt
33	NA	144-878A-96R-1, 0 cm, to -97R-1, 19 cm	Wash-core pieces
34	6	144-878A-97R-1, 19 cm, to -98R-1, 0 cm	Alkali olivine basalt
35	7	144-878A-98R-1, 0 cm, to -98R-3, 67 cm	Alkali olivine basalt

Note: NA = not attributed.

dral, partially resorbed xenocrysts of olivine make up approximately 1% of the lava, whereas much smaller (0.05–0.20 mm), anhedral grains make up as much as 10%. The groundmass is dominated by plagioclase laths and bladed ilmenite grains forming a randomly oriented meshwork. Within this meshwork, granular titanite, interstitial plagioclase (and/or alkali feldspar), and pale green clay, which has replaced the mesostasis, occur. Trace amounts of biotite and apatite are also present.

Beneath the lowermost Type 5 lava, Unit 31 is an extremely altered volcanic breccia, approximately 17 m thick. Subunit 31A is predominantly very pale brown (10YB 8/4) with some dark reddish brown clasts. Clasts are 1 mm to 3 cm in size, irregularly shaped, and highly angular to subrounded. Clast outlines are often diffuse, attesting to extensive clay replacement. This subunit has been severely bleached and altered to a dense claystone. It is soapy to the touch, expands and disintegrates in fresh water, and becomes fragmented as it dries. Subunit 31B has variable but strong oxidative coloration, ranging from weak red (5R 3/4) to dark reddish brown (2.5YR 3/4). In many intervals this coloration obscures the original texture, but Subunit 31B appears to be a continuation of Subunit 31A where relict texture is visible. Relative to Subunit 31A, Subunit 31B is harder and more abrasive to the touch. Sparse, fresh clinopyroxene grains, 1–4 mm in diameter, appear in certain intervals. These are rounded and thus likely to be xenocrysts.

Type 6

Type 6 volcanic flows include the alkali basalts of Units 32 and 34. They are characterized by abundant (15–20%), fine-grained, granular oxide minerals whose proportions vary to produce color banding parallel to flow structure in Sample 144-878A-97R-1, 28–31

cm, and irregular dark and light patches in Sample 144-878A-97R-2, 123–125 cm.

No thin section was made of Unit 32, but it appears similar in hand specimen and has been grouped in this type. It is possible that Units 32 and 34 are a single flow, because Unit 33, which is located between them, is a wash-core containing only uphole rubble. Unit 32 is approximately 2 m thick, and Unit 34 is approximately 10 m thick; neither has a flow-top breccia. Each unit contains <2% iddingsite pseudomorphs of euhedral to anhedral olivine (0.5–2.0 mm in diameter) and 1%–2% subhedral prisms of fresh clinopyroxene (<1 mm in Unit 32; 0.5–3.0 mm in Unit 34). In Unit 34, plagioclase laths can be observed in places. They are 0–5 mm long and occur in glomerocrysts with clinopyroxene. Unit 32 is mottled in medium gray (N5) and weak red (10R 5/2) colors, and the intensity of the red mottling decreases downsection. Unit 34 is medium gray (N5) but iron-stained to red (2.5YR 5/6) within 1 cm of fractures.

Unit 34 is a very fine-grained, intergranular basalt with regions of oriented, slightly larger plagioclase laths. Unusually abundant (~1%) biotite phenocrysts and sparse (5%) olivine phenocrysts, 0.05–0.50 mm in diameter, are set in a matrix dominated by abundant (15%–20%), fine, granular ilmenite, plagioclase laths, and granular titanite with minor green/brown clay that is replacing mesostasis. A weak lamination is created by concentrations of larger plagioclase laths into narrow, flow-parallel bands.

Type 7

The only Type 7 volcanic flow is Unit 35, an alkali olivine basalt characterized by abundant olivine phenocrysts in an intergranular groundmass that is dominated by plagioclase. Approximately 6 m of this flow had been drilled when drilling in the hole ended at 910.0 mbsf. The unit has about 50 cm of flow-top breccia. The massive part of the flow contains about 5%, 1–5 mm, xenocrystic olivines that are iddingsitized, altered to green or brown clay, or fresh in different areas of the core (Core 144-878A-98R). Sparse clinopyroxene grains, intergrown with plagioclase, were seen in hand specimen but do not appear in the thin section. Alteration decreases progressively downhole, and the lowermost recovered section (Section 144-878A-98R-3) appears to be very fresh, except along fractures and in iron-stained patches.

Olivine (3%), the only phenocryst phase, ranges in size from 3 mm to <0.5 mm. The larger phenocrysts have rounded, anhedral shapes and are largely fresh. Smaller grains and the rims of larger grains are replaced by green/brown clay. The groundmass is dominated by laths and interstitial patches of plagioclase. The interstitial patches may also include alkali feldspar and/or nepheline. Clinopyroxene is relatively scarce (~10%) and occurs as green, subhedral prisms. Magnetite cubes (10%) and traces of apatite are also present.

Summary

The basement section of Hole 878A records three distinct periods of subaerial volcanism with intervening weathering intervals. A fourth, near-shore, shallow marine volcanic episode is recorded by the polymictic breccias of Lithologic Unit IV.

Period 1

Two thick (>6 m) alkali olivine basalt flows were erupted (Units 34 and 35). Next, an approximately 17-m-thick, apparently continuous, volcanic breccia was deposited (Unit 31). Subsequently, a series of 12 flows was erupted. These represent 3 distinct lava types. First, 7 alkali olivine basalt flows were erupted (Units 24–30). These formed thin (typically <4 m thick) flows, each with a less than 1-m-thick flow-top breccia. Second, 2 alkali olivine basalt flows, petrographically distinct from the previous 7 flows, were erupted (Units 22 and 23). These are somewhat thicker, and each also has a flow-top breccia. Third, 3 plagioclase-rich basanitoid lavas formed

thick (11–15 m) flows (Units 18, 20, and 21). Obviously, more flows and breccias were subsequently erupted and deposited, because these 14 flows and 1 breccia deposit are overlain by an 8-m-thick weathering profile that retains relict textures of basalts and breccias.

Period 2

Seven flows erupted and one breccia unit was emplaced. The breccia, Unit 12, consists of clasts of petrographic Type 3 basalt; all other Type 3 lavas lie below the weathering horizon. However, five of the six Type 2 flows (Units 8, 10, 11, 15, and 16) are also basanitoids, differing from Type 3 only in having a higher content of groundmass titanite relative to plagioclase. The weathering horizon represents a time interval during which no lavas flowed across Site 878 but not necessarily a period of no volcanic activity on MIT Guyot. Two flows (Units 13 and 14) that erupted during this period of volcanism are extremely altered, and their petrographic type has not been identified. This cycle of volcanism ended with the deposition of thin (<4 m) volcanic breccias, tuffs, and sandstones (Units 3–7). These units were subsequently oxidized and extensively replaced by clay minerals.

Period 3

The extensive weathering of the volcanic breccia, tuffs, and sandstones, the abrupt change in lava composition, and the relative freshness of Units 1 and 2 suggest that a significant period of time passed before Type 1 lavas were erupted. Type 1 lavas are of hawaiite composition; these lavas formed two flows of moderate thickness (<7 m).

Period 4

Following the onset of marine conditions and the deposition of a thick carbonate platform (see “Lithostratigraphy” section, this chapter), submarine eruptions broke through the platform and formed a thick polymictic breccia deposit (Lithologic Unit IV) composed of clasts of limestone, of the erupting lava, and of preexisting basalts such as hawaiites similar to the Type 1 lavas.

By analogy with Hawaiian examples, basanitoid lava are usually thought of as belonging to a posterosional stage. However, because a well-established magma system is required for the formation of fractionated lavas, the hawaiites, which overlie the basanitoids, seem more likely to have been part of a major edifice-building phase of volcanism. Therefore, the basalts sampled in Hole 878A most likely represent upper shield or alkalic-cap stages of volcanism. Given that all known lavas from the SOPITA region are more enriched than Hawaiian lavas, it is likely that, in any specific volcanic stage, more alkalic lava types such as basanites may appear. The explosive eruptions that formed the polymictic breccia may represent a posterosional stage of volcanism because a significant amount of time must have elapsed while MIT Guyot subsided and developed a carbonate platform.

Relative to lava from the previous sites, (1) Hole 878A volcanics may be unique in representing more than one magmatic lineage; (2) Site 878 is the only site with significant basalt recovery at which calcite veins are not prevalent; and (3) Sites 878 and 871 both have anomalously thick (>3 m, up to 10 m) basanite flows. At Site 871 we argue that these must be ponded because basanitoid lavas have insufficient viscosity to otherwise form thick flows. However, the large number of basanitoid lavas suggests the possibility that MIT Volcano was erupting large quantities of basanitoid lava during the upper shield stage of volcanism.

PHYSICAL PROPERTIES

Introduction

The objectives of the physical properties measurement program at Site 878 were (1) to measure standard shipboard physical properties and (2) to differentiate the downhole changes in lithology by means

Table 12. Index properties data, Hole 878A.

Core, section, interval (cm)	Depth (mbsf)	Wet-bulk density (g/cm ³)	Dry-bulk density (g/cm ³)	Grain density (g/cm ³)	Porosity (%)	Water content (% dry wt)	Void ratio
144-878A-							
1R-1, 55-59	0.55	1.63	0.92	2.92	70.3	78.7	2.36
1R-1, 56-60	0.56	1.96	1.22	4.49	72.5	60.9	2.64
1R-1, 108-109	1.08	1.64	0.95	2.88	67.0	71.9	2.03
1R-2, 75-76	1.81	1.73	1.07	2.81	64.5	62.0	1.82
1R-3, 55-56	3.11	1.80	1.18	2.93	60.9	52.9	1.55
1R-CC, 22-25	3.37	2.44	2.23	2.75	20.7	9.5	0.26
2R-1, 26-27	9.76	2.58	2.40	2.78	17.8	7.6	0.22
3R-1, 59-61	19.59	2.76	2.63	2.83	13.1	5.1	0.15
4R-1, 26-29	28.76	2.76	2.66	2.75	10.6	4.1	0.12
6R-1, 16-2	47.76	2.64	2.46	2.79	17.5	7.3	0.21
7R-1, 22-28	57.52	2.62	2.46	2.78	14.9	6.2	0.17
8R-1, 5-10	67.05	2.69	2.56	2.80	12.5	5.0	0.14
8R-1, 33-36	67.33	2.70	2.61	2.74	8.4	3.3	0.09
9R-1, 12-14	76.72	2.66	2.53	2.78	13.1	5.3	0.15
10R-1, 1-4	86.21	2.59	2.41	2.81	17.2	7.3	0.21
12R-1, 4-10	105.54	2.58	2.36	2.76	20.8	9.0	0.26
13R-1, 8-12	115.18	2.40	2.10	2.74	28.8	14.0	0.40
14R-1, 14-18	124.94	2.66	2.52	2.72	13.6	5.5	0.16
15R-1, 28-31	134.68	2.57	2.40	2.77	16.7	7.1	0.20
16R-1, 8-12	144.08	2.45	2.22	2.74	22.7	10.5	0.29
18R-1, 21-24	163.61	2.72	2.60	2.76	12.1	4.8	0.14
19R-1, 9-12	173.19	2.49	2.28	2.74	20.7	9.3	0.26
21R-1, 4-7	192.54	2.61	2.47	2.70	13.6	5.6	0.16
22M-1, 10-12	202.30	2.13	1.70	2.77	41.8	25.1	0.72
23M-1, 16-22	207.06	2.69	2.53	2.79	16.4	6.7	0.20
24M-1, 4-9	216.64	2.64	2.48	2.74	15.3	6.3	0.18
26M-1, 4-12	235.94	2.70	2.57	2.77	12.7	5.1	0.15
26M-1, 13-16	236.03	2.58	2.40	2.76	16.9	7.2	0.20
26M-1, 31-34	236.21	2.87	2.80	2.71	6.9	2.5	0.07
28M-1, 1-8	255.21	2.46	2.17	2.77	28.4	13.4	0.40
29M-1, 1-6	264.91	2.37	2.07	2.75	28.8	14.2	0.40
30M-1, 43-45	274.93	2.27	1.91	2.74	35.5	19.1	0.55
31M-1, 30-32	284.40	2.76	2.72	2.72	3.8	1.4	0.04
33M-1, 1-7	302.91	2.29	1.98	2.78	30.4	15.8	0.44
34M-1, 18-21	312.78	2.23	1.87	2.78	35.0	19.1	0.54
35M-1, 7-11	322.27	2.13	1.72	2.79	39.7	23.6	0.66
36M-1, 18-20	332.08	2.12	1.70	2.73	41.0	24.7	0.69
37M-1, 1-3	341.61	2.15	1.72	2.74	41.9	25.0	0.72
38M-1, 7-10	351.27	2.20	1.81	2.79	37.5	21.2	0.60
39M-1, 36-39	361.26	2.25	1.85	2.80	39.6	21.9	0.65
41M-1, 4-8	380.24	2.23	1.84	2.84	37.6	20.9	0.60
42M-1, 16-21	389.96	2.70	2.59	2.75	10.6	4.2	0.12
43M-1, 21-29	399.51	2.61	2.45	2.77	15.3	6.4	0.18
44M-1, 11-14	406.21	2.45	2.09	2.93	35.4	17.4	0.55
44M-1, 47-49	406.57	2.00	1.43	3.37	55.9	40.0	1.27
44M-1, 126-128	407.36	2.29	1.90	3.02	38.2	20.6	0.62
44M-2, 34-36	407.94	2.29	1.94	2.97	34.5	18.2	0.53
45M-1, 21-24	409.11	2.35	2.01	2.94	33.1	16.9	0.49
45M-2, 67-69	410.95	2.32	1.96	2.95	36.0	18.9	0.56
45M-3, 97-100	412.67	2.42	2.08	2.92	33.1	16.3	0.49
45M-3, 97-100	412.67	2.30	1.91	2.74	38.7	20.8	0.63
45M-4, 56-58	413.76	2.74	2.65	2.73	9.1	3.5	0.10
46M-1, 44-46	418.94	2.41	2.05	2.82	35.9	18.0	0.56
46M-1, 112-114	419.62	2.96	2.86	2.85	9.5	3.4	0.10
46M-2, 21-23	420.07	2.45	2.14	2.76	30.0	14.3	0.43
46M-2, 37-44	420.23	2.87	2.85	2.73	2.7	1.0	0.03
47R-1, 79-82	428.99	2.30	1.98	2.83	31.3	16.2	0.46
48R-1, 66-69	436.16	2.22	1.87	2.81	34.2	18.8	0.52
49R-1, 85-87	445.95	2.38	2.06	2.88	30.8	15.3	0.45
49R-2, 18-20	446.80	2.35	2.06	2.93	28.1	14.0	0.39
49R-2, 121-123	447.83	2.33	2.02	2.81	29.8	15.1	0.42
50R-1, 51-53	455.31	2.39	2.12	2.78	26.6	12.9	0.36
50R-2, 66-68	456.94	2.36	2.09	2.86	26.0	12.7	0.35
50R-2, 135-137	457.63	2.33	2.02	2.78	30.3	15.3	0.43
50R-3, 27-29	458.06	2.31	2.01	2.80	29.3	15.0	0.42
51R-1, 29-31	464.69	2.36	2.07	2.77	28.0	13.8	0.39
51R-3, 28-30	467.54	2.35	2.08	2.76	27.2	13.4	0.37
51R-4, 114-116	469.74	2.30	2.01	2.77	28.7	14.7	0.40
51R-5, 9-11	470.06	2.41	2.20	2.75	21.1	9.8	0.27
51R-6, 74-76	472.11	2.32	2.05	2.79	26.1	13.1	0.35
52R-1, 141-143	475.51	2.40	2.15	2.75	24.0	11.5	0.32
52R-2, 92-94	476.50	2.34	2.11	2.81	22.4	10.9	0.29
53R-1, 96-98	484.66	2.58	2.30	2.82	27.9	12.4	0.35
53R-2, 70-73	485.71	2.47	2.21	2.80	25.9	12.0	0.39
53R-3, 70-73	487.16	2.65	2.47	2.79	18.1	7.5	0.22
53R-4, 49-52	488.40	2.56	2.36	2.77	20.3	8.8	0.25
53R-4, 49-52	488.40	2.49	2.33	2.75	15.8	6.9	0.19
54R-1, 61-63	493.81	2.40	2.15	2.79	25.2	12.1	0.34
54R-2, 75-77	495.32	2.38	2.12	2.79	25.1	12.2	0.34
54R-3, 104-106	496.88	2.42	2.18	2.82	23.0	10.8	0.30
54R-6, 24-26	499.95	2.38	2.11	2.83	26.3	12.8	0.36
55R-2, 118-121	504.95	2.57	2.30	2.77	25.7	11.4	0.35
55R-4, 110-112	507.74	2.54	2.30	2.76	22.9	10.2	0.30
55R-6, 24-26	509.61	2.80	2.78	2.70	2.0	0.7	0.02
55R-6, 104-106	510.41	2.45	2.25	2.77	20.0	9.1	0.25
56R-2, 56-58	513.90	2.49	2.29	2.76	19.2	8.6	0.24
56R-3, 78-80	515.58	2.24	1.92	2.83	31.6	16.9	0.46
56R-5, 74-76	518.46	2.35	2.08	2.75	26.6	13.1	0.36
56R-6, 28-30	519.20	2.35	2.08	2.79	26.6	13.1	0.36
144-878A- (cont.)							
57R-1, 37-39	521.57	2.39	2.13	2.80	25.3	12.2	0.34
57R-3, 63-65	524.42	2.38	2.12	2.79	25.7	12.4	0.35
57R-5, 102-104	527.71	2.38	2.14	2.74	24.1	11.6	0.32
57R-5, 139-141	528.08	2.76	2.72	2.70	4.2	1.6	0.04
58R-1, 120-122	531.60	2.41	2.15	2.75	25.4	12.1	0.34
58R-3, 96-98	534.30	2.41	2.16	2.74	24.1	11.4	0.32
58R-5, 53-55	536.48	2.37	2.11	2.74	25.5	12.4	0.34
58R-7, 40-42	538.87	2.42	2.12	2.77	29.3	14.2	0.41
58R-7, 74-76	539.21	2.79	2.78	2.70	1.4	0.5	0.01
58R-7, 88-90	539.55	2.42	2.17	2.77	24.0	11.3	0.32
59R-7, 23-25	540.33	2.49	2.22	2.79	26.1	12.0	0.35
59R-1, 23-25	540.33	2.41	2.15	2.75	25.2	12.0	0.34
59R-2, 65-67	542.25	2.78	2.77	2.69	1.3	0.5	0.01
59R-2, 84-86	542.44	2.77	2.72	2.74	4.5	1.7	0.05
59R-3, 40-42	543.04	2.48	2.22	2.80	25.1	11.6	0.34
59R-4, 76-78	544.86	2.56	2.31	2.83	24.5	10.9	0.33
59R-5, 37-39	545.67	2.46	2.20	2.78	26.1	12.2	0.35
59R-5, 49-51	545.79	2.67	2.58	2.71	8.0	3.2	0.09
59R-6, 44-46	546.78	2.44	2.17	2.79	26.7	12.6	0.36
59R-6, 44-46	546.78	2.45	2.20	2.75	24.7	11.5	0.33
59R-7, 38-40	548.13	2.49	2.22	2.79	26.1	12.0	0.35
59R-7, 70-72	548.45	2.73	2.63	2.74	9.6	3.7	0.11
60R-1, 64-66	550.44	2.43	2.18	2.76	25.3	11.9	0.34
60R-1, 67-69	550.47	2.58	2.42	2.71	15.2	6.4	0.18
60R-1, 127-129	551.07	2.40	2.10	2.75	28.6	13.9	0.40
60R-1, 132-134	551.12	2.73	2.66	2.71	7.0	2.7	0.08
60R-2, 60-62	551.77	2.54	2.27	2.85	26.2	11.8	0.36
60R-2, 60-62	551.77	2.41	2.15	2.75	25.2	12.0	0.34
60R-3, 106-108	553.67	2.46	2.20	2.76	24.6	11.4	0.33
60R-3, 106-108	553.67	2.43	2.18	2.56	24.2	11.4	0.32
60R-4, 116-118	554.94	2.51	2.26	2.77	25.2	11.5	0.34
60R-4, 116-118	554.94	2.37	2.08	2.75	29.0	14.3	0.41
60R-5, 63-65	555.67	2.45	2.22	2.74	22.0	10.1	0.28
61R-2, 13-15	560.84	2.43	2.17	2.79	25.0	11.8	0.33
61R-3, 67-69	562.88	2.74	2.65	2.71	8.7	3.4	0.10
61R-4, 96-98	564.63	2.39	2.13	2.79	24.8	11.9	0.33
61R-5, 88-89	566.01	2.26	1.83	2.86	42.0	23.5	0.72
61R-6, 121-123	567.67	2.57	2.41	2.72	15.9	6.8	0.19
62R-1, 18-20	568.88	2.35	2.07	2.72	27.8	13.8	0.39
62R-2, 78-80	570.59	2.45	2.23	2.74	20.9	9.6	0.26
62R-2, 122-124	571.03	2.68	2.59	2.73	8.8	3.5	0.10
62R-4, 46-48	573.26	2.42	2.16	2.80	25.5	12.1	0.34
62R-6, 75-77	576.34	2.78	2.76	2.70	2.9	1.1	0.03
62R-7, 34-36	577.43	2.56	2.38	2.72	17.5	7.5	0.21
63R-1, 77-79	578.87	2.47	2.26	2.74	21.0	9.5	0.27
63R-1, 131-133	579.41	2.51	2.29	2.73	20.9	9.4	0.26
63R-4, 42-44	582.96	2.55	2.37	2.72	17.5	7.6	0.21
63R-4, 68-70	583.22	2.74	2.69	2.69	5.5	2.1	0.06
63R-6, 37-39	585.36	2.52	2.31	2.74	20.1	8.9	0.25
64R-1, 13-15	587.73	2.56	2.36	2.76	18.7	8.1	0.23
64R-1, 69-71	588.29	2.77	2.74	2.70	2.5	0.9	0.03
6							

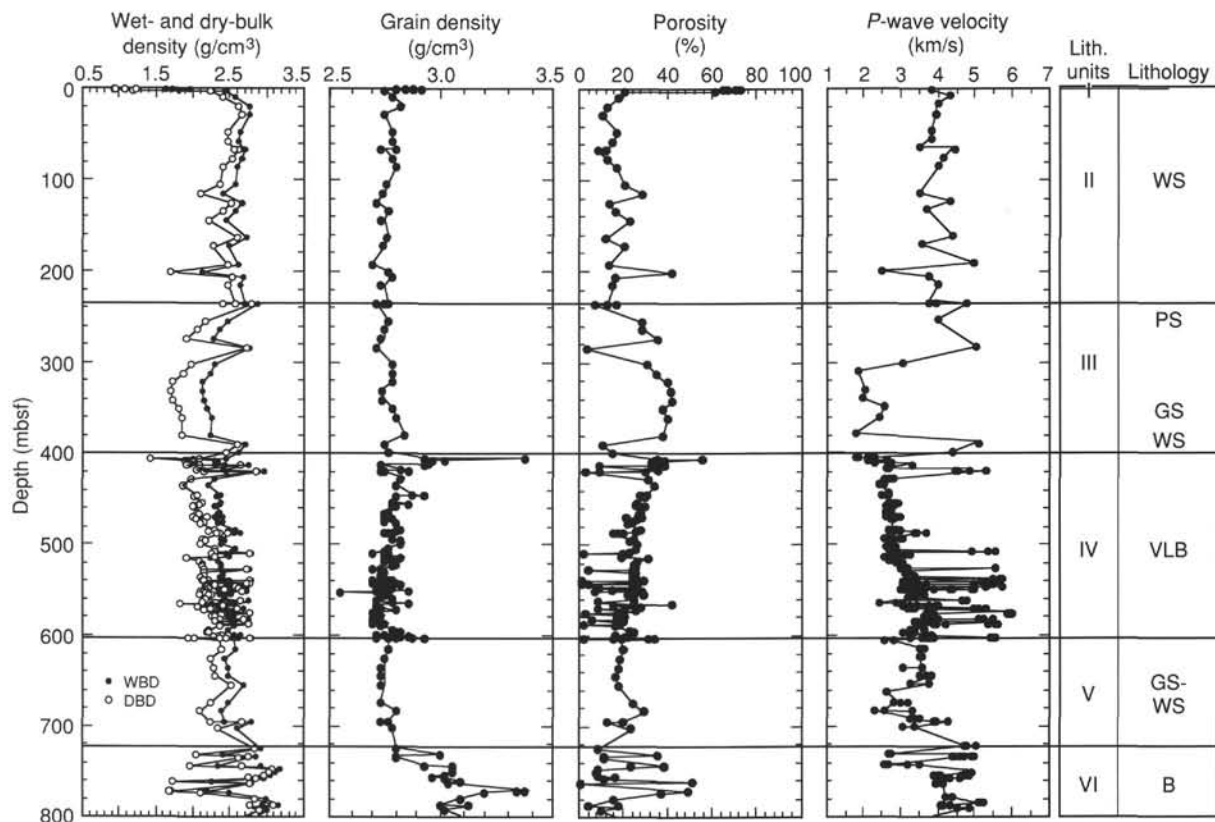


Figure 39. Measurements of index properties (wet- and dry-bulk density, grain density, and porosity) and compressional wave velocity vs. depth, Hole 878A. WS = wackestone, PS = packstone, GS = grainstone, VLB = volcanic limestone breccia, and B = basalt.

packstone (235–400 mbsf), a thin band of bluish gray clay (400–406 mbsf), greenish to whitish breccia of volcanic clasts, limestone and scoria (406–604 mbsf), and white to pale brown grainstone, packstone, and wackestone (604–723 mbsf). Below 723 mbsf, there are a series of basalt flows, volcanic breccia, and minor clay horizons, derived from the weathering of the basalts. The upper surface of limestone is covered either by a thick manganese crust (Holes 878B and 878C) or by a thin pelagic drape of nanofossil foraminifer ooze that is early Pleistocene to late Miocene in age and which contains manganese nodules with Albian, Santonian, and Campanian age nuclei (Hole 878A).

Index Properties and Sonic Velocity

Measurements of both index properties and sonic velocity were conducted on most of the samples. Wet and dry weights and volumes were used to calculate wet- and dry-bulk density, grain density, porosity, and water content (see “Explanatory Notes” chapter, this volume). The results, corrected for 3.5% salt, are given in Table 12 and Figure 39. Hole 878A is the deepest hole drilled during Leg 144. Consequently, the number of samples and the amount of physical properties data collected are the highest of any site drilled during Leg 144.

Pelagic Nanofossil Foraminifer Ooze

In Hole 878A, Lithologic Unit I consists of nanofossil foraminifer clayey ooze and manganese nodules. The porosity of the ooze is 60%–70% overall, but it reaches 73% in the upper part of Section 144-878A-1R-1 (manganese nodule). The grain density of the manganese nodule in Sample 144-878A-1R-1, 56–60 cm, is 4.5 g/cm³, which is the highest value measured in the entire core.

Upper Limestone

The upper limestone sequence at Site 878 is comprised of two lithologic units (Units II and III). Wet- and dry-bulk densities in the uppermost limestone sequence (3–400 mbsf) are variable, with a slightly decreasing overall trend with depth, ranging from 2.1 to 2.8 g/cm³ and from 1.7 to 2.7 g/cm³, respectively. Porosity values show a high scatter, ranging from about 5% to 40%; the highest porosities in this unit are found in the grainstone from 312 to 390 mbsf (Lithologic Subunit IIIB). The sonic velocity values measured in this unit range from 1.8 to 2.5 km/s. Between 200 and 400 mbsf, good correlation is seen between lithologic changes and changes in physical properties, in particular the bulk density and porosity values. Three cycles of sedimentation (Lithologic Subunits IIIA, IIIB, and IIIC) are reflected in clear downhole trends of decreasing density and increasing porosity, respectively (see Fig. 39 and Table 12).

Clay

The greenish clayey layer of altered basaltic glass from 400 to 406 mbsf (Lithologic Subunit IVA) has 60% porosity. Wet- and dry-bulk density are 2.0 and 1.4 g/cm³, respectively. The grain density measured in the clay is very high, approximately 3.4 g/cm³. This clay layer appears to contain a high proportion of swelling clay minerals.

Volcanic Limestone Breccia

The volcanic limestone breccias between 406 and 604 mbsf show a general linear decrease in porosity from about 36% at the top to 20% at the base of the unit. An increasing trend in sonic velocity, from 2.0 to 4.0 km/s, was observed over the same interval (Fig. 39). These

changes in properties correlate with changes in Lithologic Subunits IVB and IVC, each of which shows an increase in the matrix carbonate content with depth ("Organic Geochemistry" section, this chapter). The greater vesicularity of Subunit IVB contributes to a slightly higher porosity in this subunit. Superimposed on the general trend is a slight increase in porosity, from approximately 20% to 28% at 513 mbsf. This change occurs near the boundary between the two inferred volcanic events (Lithologic Subunits IVB and IVC).

The highest sonic velocities (5.0–6.0 km/s) were measured on isolated, dense, limestone clasts selected from the breccia (Fig. 39). These clasts have undergone extensive diagenesis in which cements have reduced the pore space (see "Lithostratigraphy" section, this chapter) and, hence, have particularly low measured porosities and high measured velocities.

Lower Limestone

Porosity values in the lowermost limestone layer (604–725 mbsf, Lithologic Unit V) vary from 16% to 38%. Wet- and dry-bulk density values in this unit range from 2.3 to 2.8 g/cm³ and from 2.2 to 2.7 g/cm³, respectively. These values are consistent with the wackestone and grainstone lithology. Sonic velocity ranges from 2.2 to 4.4 km/s within this unit.

Basalts

In the basalt below 723 mbsf (Lithologic Unit VI), porosity varies from near 0% to 50%; the sonic velocity variation lies between 2.5 and 5.2 km/s, depending primarily on the degree of weathering, but in part also on the texture and composition. Dense basalt, when relatively fresh, has more or less identical dry, wet, and grain densities, which are equal to approximately 3.0 g/cm³.

Compressional Wave Anisotropy

Hamilton Frame velocity measurements on oriented sample cubes in three orthogonal directions were only conducted below 400 mbsf, because of the higher recovery in this part of the hole. The data given in Table 13 and shown in Figure 40 are scattered in the volcanic limestone breccia, but the trend is toward positive values of anisotropy. In the lower limestone, sonic velocity anisotropy tends more to negative values, indicating higher vertical than horizontal compressional wave velocity. No consistent trend in compressional wave anisotropy is present in the basalt.

Relationship of Physical Properties to Lithology

A comparison between index properties, sonic velocity, and lithology reveals that a particular range of physical properties values can be clearly correlated with the various lithologic units at Site 878. Grain density values are consistently between 2.7 and 2.8 g/cm³ in the limestones and the volcanic limestone breccia. Values higher than 3.0 g/cm³ are found in the manganese oxide, volcanic clay, and the basalt. Porosity and water content are inversely related to wet- and dry-bulk densities and to sonic velocity. Sonic velocities are between 1.6 and 6 km/s; porosities below 15% are typical for dense wackestone and packstone facies and for fresh dense basalt, whereas lower sonic velocities and higher porosities (to about 40%, or higher) are typical for grainstone facies and weathered basalt.

With the exception of the variations discussed earlier, clear linear decreases in porosity and water content, and equivalent increases in wet- and dry-bulk density and velocity are seen between 340 and 640 mbsf. These span the breccia and parts of both the upper and lower limestones. These trends are the result of lithologic variations superimposed on gravitational compaction. Within the lower breccias, stylolites and clast deformation are seen; these affect the properties of the limestone clasts. The effect of cementation reducing pore space within the limestone breccia clasts ("Lithostratigraphy" section, this

chapter) is clearly seen in the profile of velocity vs. depth (Fig. 39), in which velocities are 50% higher than the mean values for the main limestone sequences.

DOWNHOLE MEASUREMENTS AND SEISMIC STRATIGRAPHY

Log Types, Processing, and Reliability

The complete carbonate platform and a portion of the lower igneous complex were logged in Hole 878A in the northeastern portion of MIT Guyot. The carbonate platform sequence was logged using the geophysical (two passes), Formation MicroScanner (FMS; two passes), and geochemical tool strings from approximately the seafloor to 740 mbsf. This interval corresponds to Cores 144-878A-1R through -79R, although the uppermost 17 m was logged from within the drill pipe. Because of deteriorating hole conditions within the volcanic flow sequence, the lower igneous complex could only be logged by the FMS (two passes) from approximately 807 to 885 mbsf, corresponding to Cores 144-878A-87R through -94R, before logging operations ended. The spacing of tools on the various logging tool strings implies that the lower boundary of logging data from each tool varies (see diagram of tool strings in "Explanatory Notes" chapter, this volume). These logs are valuable for interpreting the sedimentary succession and for identifying possible discontinuities within the carbonate platform series, because core recovery within the upper 400 m averaged only 2% and within the lower 140 m averaged only 6%. In particular, the FMS provides high-resolution resistivity imagery of the borehole wall within the carbonate platform succession.

Logging depths were calibrated to cored intervals by using the known position of the end of the drill pipe during logging (1354.8 m below the rig floor [mbrf], or 17.2 mbsf), as detected by measurements of iron content by the geochemistry tool string. The midpoint of the sharp change in iron content was at a logging depth of 1353.5 mbrf, implying that 1.3 m should be added to geochemistry logging depths to convert to drilled depths. The geochemical and FMS runs were calibrated to the geochemical run by using a sharp narrow peak in natural gamma-ray radiation (100 API units) recorded by the natural gamma-ray tool (NGT) run on each string. This gamma-ray radiation spike centered at 406.4 mbsf (corrected depth) is caused by a clay layer at the top of the volcanic-limestone breccia unit (Lithologic Subunit IVA; Fig. 41). From this intra-run calibration, additional corrections were made to the main geophysics run (an additional +1.0 m) and to the two FMS runs (+0.6 and -0.7 m, respectively). During the drilling and logging operations, the daily tide range was less than 1 m in this region (Hydrographer of the Navy, 1991); thus, we did not compute differential tide corrections for the intercalibration of logging and drilling depths. These depth conversions should place features observed in the logs to within a few tens of centimeters of corresponding features in the cored intervals.

The caliper log of the borehole diameter (Fig. 41) indicates that the borehole widened to 45 cm (18 in.) or greater through most of the two carbonate series (Lithologic Units II–III and V) and the uppermost 50 m of the volcanoclastic limestone breccia (Lithologic Unit III). Within these intervals, the FMS pads were no longer in complete contact with the borehole walls, and one or more of the four traces may be incoherent (see "Explanatory Notes" chapter, this volume). However, there is a 4° to 5° dip of the borehole to the south (approximately toward 170°), enabling contact of at least two of the FMS pads through most of these "washout" intervals. The lithodensity tool was not in complete contact against the borehole wall where borehole diameter exceeded 45 cm (18 in.), resulting in unreliably low values.

General Log-facies Comparison

The lithologic units and a few of the subunits defined on the basis of the limited core recovery are recognized in the composite logs, but some major features observed in the logging measurements were

Table 13. Compressional wave velocity data, Hole 878A.

Core, section, interval (cm)	Depth (mbsf)	Distance (mm)	Axes of measurement	Traveltime (μm)	Corrected traveltime (μm)	Measured velocity (m/s)	Velocity anisotropy index
144-878A-							
1R-CC, 22-25	3.37	20.26		8.29	5.29	3829.87	
2R-1, 26-27	9.76	12.56		5.90	2.90	4331.03	
3R-1, 59-61	19.59	7.68		4.93	1.93	3979.28	
4R-1, 26-29	28.76	11.98		6.04	3.04	3940.79	
6R-1, 16-20	47.76	9.35		5.44	2.44	3831.97	
7R-1, 22-28	57.52	11.18		5.95	2.95	3789.83	
8R-1, 5-10	67.05	8.39		5.40	2.40	3495.83	
8R-1, 33-36	67.33	10.23		5.31	2.31	4428.57	
9R-1, 12-14	76.72	12.73		6.07	3.07	4146.58	
10R-1, 1-4	86.21	13.32		6.33	3.33	4000.00	
13R-1, 8-12	115.18	13.70		6.92	3.92	3494.90	
14R-1, 14-18	124.94	21.67		7.97	4.97	4360.16	
15R-1, 28-31	134.68	20.30		8.50	5.50	3690.91	
18R-1, 21-24	163.61	19.41		7.44	4.44	4371.62	
19R-1, 9-12	173.19	15.66		7.38	4.38	3575.34	
21R-1, 4-7	192.54	14.12		5.84	2.84	4971.83	
22M-1, 10-12	202.30	20.61		11.32	8.32	2477.16	
23M-1, 16-22	207.06	11.62		6.07	3.07	3785.02	
24M-1, 4-9	216.64	11.42		5.83	2.83	4035.34	
26M-1, 4-12	235.94	6.45		4.72	1.72	3750.00	
26M-1, 13-16	236.03	18.12		7.59	4.59	3947.71	
26M-1, 31-34	236.21	23.39		7.92	4.92	4754.07	
28M-1, 1-8	255.21	21.39		8.37	5.37	3983.24	
31M-1, 30-32	284.40	19.35		6.85	3.85	5025.97	
33M-1, 1-7	302.91	21.37		10.03	7.03	3039.83	
34M-1, 18-21	312.78	11.48		9.27	6.27	1830.94	
36M-1, 18-20	332.08	15.14		10.40	7.40	2045.95	
37M-1, 1-3	341.61	11.15		8.58	5.58	1998.21	
38M-1, 7-10	351.27	21.04		11.28	8.28	2541.06	
39M-1, 36-39	361.26	21.16		11.65	8.65	2446.24	
41M-1, 4-8	380.24	6.69		6.71	3.71	1803.24	
42M-1, 16-21	389.96	20.62		7.04	4.04	5103.96	
43M-1, 21-29	399.51	21.45		7.91	4.91	4368.64	
44M-1, 11-14	406.21	21.40	a	12.50	9.50	2252.63	
44M-1, 11-14	406.21	21.35	b	12.33	9.33	2288.32	
44M-1, 47-49	406.57	22.92	a	15.25	12.25	1871.02	
44M-1, 47-49	406.57	21.09	b	14.75	11.75	1794.89	
44M-1, 126-128	407.36	21.16	a	12.47	9.47	2234.42	
44M-1, 126-128	407.36	21.37	b	12.37	9.37	2280.68	
44M-1, 126-128	407.36	21.41	c	13.20	10.20	2099.02	0.07
44M-2, 34-36	407.94	21.37	b	12.69	9.69	2205.37	
44M-2, 34-36	407.94	21.40	c	13.16	10.16	2106.30	0.08
45M-1, 21-24	409.11	20.63		10.86	7.86	2624.68	
45M-2, 67-69	410.95	18.12	a	11.03	8.03	2256.54	
45M-2, 67-69	410.95	21.35	b	12.42	9.42	2266.45	
45M-2, 67-69	410.95	21.40	c	12.44	9.44	2266.95	0
45M-3, 97-100	412.67	23.08	a	11.56	8.56	2696.26	
45M-3, 97-100	412.67	21.44	b	10.93	7.93	2703.66	
45M-3, 97-100	412.67	21.41	c	11.09	8.09	2646.48	0.02
45M-4, 56-58	413.76	12.94		6.94	3.94	3284.26	
46M-1, 44-46	418.94	22.90	a	11.69	8.69	2635.21	
46M-1, 44-46	418.94	21.46	b	11.02	8.02	2675.81	
46M-1, 44-46	418.94	21.41	c	11.05	8.05	2659.63	0
46M-1, 112-114	419.62	21.49		7.43	4.43	4851.02	
46M-1, 112-114	419.62	21.33		7.72	4.72	4519.07	
46M-1, 112-114	419.62	20.79		7.60	4.60	4519.57	
46M-2, 21-23	420.07	21.39		7.83	4.83	4428.57	
46M-2, 21-23	420.07	19.71		7.05	4.05	4866.67	
46M-2, 21-23	420.07	21.38		7.77	4.77	4482.18	
46M-2, 37-44	420.23	14.04		5.67	2.67	5258.43	
47R-1, 49-82	428.69	21.24	a	10.73	7.73	2747.74	
47R-1, 49-82	428.69	21.37	b	10.60	7.60	2811.84	
47R-1, 49-82	428.69	21.34	c	10.57	7.57	2819.02	-0.01
47R-2, 27-29	429.97	21.31	a	10.87	7.87	2707.75	
47R-2, 27-29	429.97	20.84	b	11.10	8.10	2572.84	
47R-2, 27-29	429.97	21.47	c	10.97	7.97	2693.85	-0.02
48R-1, 1-4	435.51	21.37	a	11.34	8.34	2562.35	
48R-1, 1-4	435.51	22.17	b	11.64	8.64	2565.97	
48R-1, 1-4	435.51	21.60	c	11.61	8.61	2508.71	0.02
48R-1, 66-69	436.16	22.15	a	11.73	8.73	2537.23	
48R-1, 66-69	436.16	21.32	b	11.55	8.55	2493.57	
48R-1, 66-69	436.16	21.42	c	11.76	8.76	2445.21	0.03
49R-1, 85-87	445.95	20.59	a	10.62	7.62	2702.10	
49R-1, 85-87	445.95	21.26	b	10.99	7.99	2660.83	
49R-1, 85-87	445.95	21.35	c	11.01	8.01	2665.42	0.01
49R-2, 18-20	446.80	19.41	a	10.77	7.77	2498.07	
49R-2, 18-20	446.80	21.30	b	11.19	8.19	2600.73	
49R-2, 18-20	446.80	21.41	c	11.22	8.22	2604.62	-0.02
49R-2, 121-123	447.83	20.98	a	10.85	7.85	2672.61	
49R-2, 121-123	447.83	21.54	b	11.03	8.03	2682.44	
49R-2, 121-123	447.83	21.33	c	10.92	7.92	2693.18	-0.01

Table 13 (Continued).

Core, section, interval (cm)	Depth (mbsf)	Distance (mm)	Axes of measurement	Traveltime (μ m)	Corrected traveltime (μ m)	Measured velocity (m/s)	Velocity anisotropy index
144-878A- (cont.)							
50R-1, 51-53	455.31	21.11	a	10.67	7.67	2752.28	
50R-1, 51-53	455.31	21.33	b	10.55	7.55	2825.17	
50R-1, 51-53	455.31	21.38	c	10.60	7.60	2813.16	-0.01
50R-2, 66-68	456.94	19.42	a	10.05	7.05	2754.61	
50R-2, 66-68	456.94	21.35	b	10.32	7.32	2916.67	
50R-2, 66-68	456.94	21.38	c	10.51	7.51	2846.87	0
50R-2, 135-137	457.63	20.44	a	10.54	7.54	2710.88	
50R-2, 135-137	457.63	21.36	b	10.68	7.68	2781.25	
50R-2, 135-137	457.63	21.67	c	11.06	8.06	2688.59	0.02
50R-3, 27-29	458.06	22.90	a	11.23	8.23	2782.50	
50R-3, 27-29	458.06	21.38	b	10.56	7.56	2828.04	
50R-3, 27-29	458.06	21.28	c	11.11	8.11	2623.92	0.07
51R-1, 29-31	464.69	21.20	a	11.06	8.06	2630.27	
51R-1, 29-31	464.69	21.27	b	11.10	8.10	2625.93	
51R-1, 29-31	464.69	21.58	c	10.88	7.88	2738.58	-0.04
51R-3, 28-30	467.54	21.66	a	11.24	8.24	2628.64	
51R-3, 28-30	467.54	21.30	b	11.17	8.17	2607.10	
51R-3, 28-30	467.54	21.52	c	10.95	7.95	2706.92	-0.03
51R-4, 114-116	469.74	21.25	a	10.84	7.84	2710.46	
51R-4, 114-116	469.74	21.34	b	11.03	8.03	2657.53	
51R-4, 114-116	469.74	21.45	c	10.93	7.93	2704.92	-0.01
51R-5, 9-11	470.06	21.38	a	10.57	7.57	2824.31	
51R-5, 9-11	470.06	21.35	b	10.19	7.19	2969.40	
51R-5, 9-11	470.06	21.57	c	10.38	7.38	2922.76	-0.01
51R-6, 74-76	472.11	21.29	a	10.97	7.97	2671.27	
51R-6, 74-76	472.11	21.35	b	10.87	7.87	2712.83	
51R-6, 74-76	472.11	21.36	c	11.24	8.24	2592.23	0.04
52R-1, 141-143	475.51	21.63	a	10.95	7.95	2720.76	
52R-1, 141-143	475.51	21.31	b	10.59	7.59	2807.64	
52R-1, 141-143	475.51	21.28	c	10.59	7.59	2803.69	-0.01
53R-1, 96-98	484.66	21.36	a	10.71	7.71	2770.43	
53R-1, 96-98	484.66	19.01	b	10.18	7.18	2647.63	
53R-1, 96-98	484.66	21.36	c	10.97	7.97	2680.05	0.01
53R-2, 70-73	485.71	21.82	a	10.47	7.47	2921.02	
53R-2, 70-73	485.71	21.47	b	10.16	7.16	2998.60	
53R-2, 70-73	485.71	13.97	c	7.88	4.88	2862.71	0.03
53R-4, 49-52	488.40	23.82	a	9.47	6.47	3681.61	
53R-4, 49-52	488.40	21.33	b	9.28	6.28	3396.50	
53R-4, 49-52	488.40	21.39	c	9.26	6.26	3416.93	0.04
54R-1, 61-63	493.81	17.09	a	9.08	6.08	2810.86	
54R-1, 61-63	493.81	21.34	b	9.94	6.94	3074.93	
54R-1, 61-63	493.81	21.39	c	10.23	7.23	2958.51	-0.01
54R-2, 75-77	495.32	19.07	a	10.44	7.44	2563.17	
54R-2, 75-77	495.32	21.36	b	10.90	7.90	2703.80	
54R-2, 75-77	495.32	21.40	c	11.29	8.29	2581.42	0.02
54R-3, 104-106	496.88	19.26	a	10.06	7.06	2728.05	
54R-3, 104-106	496.88	21.37	b	10.64	7.64	2797.12	
54R-3, 104-106	496.88	21.42	c	10.69	7.69	2785.44	-0.01
54R-6, 24-26	499.95	17.73	a	9.59	6.59	2690.44	
54R-6, 24-26	499.95	21.31	b	10.84	7.84	2718.11	
54R-6, 24-26	499.95	21.32	c	10.88	7.88	2705.58	0
55R-2, 118-121	504.95	20.22	a	10.04	7.04	2872.16	
55R-2, 118-121	504.95	21.06	b	10.99	7.99	2635.80	
55R-2, 118-121	504.95	21.14	c	10.99	7.99	2645.81	0.04
55R-4, 110-112	507.74	21.83	a	10.88	7.88	2770.31	
55R-4, 110-112	507.74	21.23	b	10.40	7.40	2868.92	
55R-4, 110-112	507.74	21.38	c	10.99	7.99	2675.85	0.05
55R-6, 24-26	509.61	20.16	a	6.63	3.63	5553.72	
55R-6, 24-26	509.61	21.85	b	7.08	4.08	5355.39	
55R-6, 24-26	509.61	21.51	c	7.37	4.37	4922.20	0.10
55R-6, 104-106	510.41	18.80	a	9.86	6.86	2740.53	
55R-6, 104-106	510.41	21.25	b	10.50	7.50	2833.33	
55R-6, 104-106	510.41	21.38	c	10.61	7.61	2809.46	-0.01
56R-2, 56-58	513.90	19.79	a	9.33	6.33	3126.38	
56R-2, 56-58	513.90	21.35	b	9.62	6.62	3225.08	
56R-2, 56-58	513.90	21.40	c	10.21	7.21	2968.10	0.07
56R-3, 78-80	515.58	21.65	a	11.48	8.48	2553.07	
56R-3, 78-80	515.58	21.37	b	10.96	7.96	2684.67	
56R-3, 78-80	515.58	21.33	c	11.25	8.25	2585.46	0.01
56R-5, 74-76	518.46	21.62	a	10.52	7.52	2875.00	
56R-5, 74-76	518.46	21.34	b	10.30	7.30	2923.29	
56R-5, 74-76	518.46	21.38	c	10.57	7.57	2824.31	0.03
56R-6, 28-30	519.20	21.36	a	10.87	7.87	2714.10	
56R-6, 28-30	519.20	21.42	b	10.58	7.58	2825.86	
56R-6, 28-30	519.20	21.38	c	10.95	7.95	2689.31	0.03
57R-1, 37-39	521.57	21.03	a	9.95	6.95	3025.90	
57R-1, 37-39	521.57	21.34	b	9.96	6.96	3066.09	
57R-1, 37-39	521.57	21.32	c	10.43	7.43	2869.45	0.06
57R-3, 63-65	524.42	21.72	a	10.22	7.22	3008.31	
57R-3, 63-65	524.42	21.32	b	9.96	6.96	3063.22	
57R-3, 63-65	524.42	21.35	c	10.21	7.21	2961.17	0.02
57R-5, 102-104	527.71	21.29	a	9.81	6.81	3126.29	

Table 13 (Continued).

Core, section, interval (cm)	Depth (mbsf)	Distance (mm)	Axes of measurement	Traveltime (μm)	Corrected traveltime (μm)	Measured velocity (m/s)	Velocity anisotropy index
144-878A- (cont.)							
57R-5, 102-104	527.71	22.39	b	10.04	7.04	3180.40	
57R-5, 102-104	527.71	21.51	c	10.13	7.13	3016.83	0.04
57R-5, 139-141	528.08	21.24		6.85	3.85	5516.88	
58R-1, 120-122	531.60	21.41	a	9.68	6.68	3205.09	
58R-1, 120-122	531.60	19.73	b	9.37	6.37	3097.33	
58R-1, 120-122	531.60	21.40	c	9.76	6.76	3165.68	0
58R-3, 96-98	534.30	20.86	a	9.42	6.42	3249.22	
58R-3, 96-98	534.30	21.57	b	9.77	6.77	3186.12	
58R-3, 96-98	534.30	21.38	c	9.85	6.85	3121.17	0.03
58R-5, 53-55	536.48	21.37	a	9.37	6.37	3354.79	
58R-5, 53-55	536.48	21.94	b	9.73	6.73	3260.03	
58R-5, 53-55	536.48	21.46	c	9.79	6.79	3160.53	0.05
58R-7, 74-76	539.21	21.29	a	6.72	3.72	5723.12	
58R-7, 74-76	539.21	20.44	b	6.71	3.71	5509.43	
58R-7, 74-76	539.21	21.62	c	6.81	3.81	5674.54	-0.01
58R-7, 88-90	539.35	21.38	a	9.39	6.39	3345.85	
58R-7, 88-90	539.35	21.49	b	9.27	6.27	3427.43	
58R-7, 88-90	539.35	21.48	c	9.77	6.77	3172.82	0.07
59R-1, 23-25	540.33	21.37	a	9.51	6.51	3282.64	
59R-1, 23-25	540.33	21.89	b	9.67	6.67	3281.86	
59R-1, 23-25	540.33	21.49	c	9.57	6.57	3270.93	0
59R-2, 65-67	542.25	20.25	a	6.92	3.92	5165.82	
59R-2, 65-67	542.25	21.48	b	7.01	4.01	5356.61	
59R-2, 65-67	542.25	21.44	c	6.83	3.83	5597.91	-0.06
59R-2, 84-86	542.44	20.60	a	6.98	3.98	5175.88	
59R-2, 84-86	542.44	21.58	b	7.07	4.07	5302.21	
59R-2, 84-86	542.44	21.37	c	6.88	3.88	5507.73	-0.05
59R-3, 40-42	543.04	19.40	a	9.23	6.23	3113.97	
59R-3, 40-42	543.04	21.14	b	9.82	6.82	3099.71	
59R-3, 40-42	543.04	21.35	c	9.95	6.95	3071.94	0.01
59R-4, 76-78	544.86	21.41	a	8.81	5.81	3685.03	
59R-4, 76-78	544.86	21.43	b	9.55	6.55	3271.76	
59R-4, 76-78	544.86	21.38	c	9.49	6.49	3294.30	0.05
59R-5, 37-39	545.67	21.25	a	9.89	6.89	3084.18	
59R-5, 37-39	545.67	21.27	b	9.57	6.57	3237.44	
59R-5, 37-39	545.67	21.39	c	9.64	6.64	3221.39	-0.02
59R-5, 49-51	545.79	21.74	a	6.98	3.98	5462.31	
59R-5, 49-51	545.79	21.36	b	7.28	4.28	4990.65	
59R-5, 49-51	545.79	21.48	c	6.96	3.96	5424.24	-0.04
59R-6, 44-46	546.78	21.43	a	8.79	5.79	3701.21	
59R-6, 44-46	546.78	20.73	b	8.91	5.91	3507.61	
59R-6, 44-46	546.78	21.32	c	9.22	6.22	3427.65	0.05
59R-7, 38-40	548.13	21.62	a	9.84	6.84	3160.82	
59R-7, 38-40	548.13	21.36	b	9.46	6.46	3306.50	
59R-7, 38-40	548.13	21.36	c	9.69	6.69	3192.83	0.01
59R-7, 70-72	548.45	12.24	a	6.87	3.87	3162.79	
59R-7, 70-72	548.45	20.55	b	6.58	3.58	5740.22	
59R-7, 70-72	548.45	11.95	c	5.26	2.26	5287.61	-0.17
60R-1, 64-66	550.44	21.22	a	9.22	6.22	3411.58	
60R-1, 64-66	550.44	21.36	b	8.84	5.84	3657.53	
60R-1, 64-66	550.44	21.39	c	9.78	6.78	3154.87	0.11
60R-1, 67-69	550.47	19.75	a	8.09	5.09	3880.16	
60R-1, 67-69	550.47	21.39	b	7.30	4.30	4974.42	
60R-1, 67-69	550.47	21.47	c	7.39	4.39	4890.66	-0.10
60R-1, 127-129	551.07	18.04	a	8.86	5.86	3078.50	
60R-1, 127-129	551.07	21.33	b	9.79	6.79	3141.38	
60R-1, 127-129	551.07	21.30	c	10.08	7.08	3008.48	0.03
60R-1, 132-134	551.12	19.23	a	7.39	4.39	4380.41	
60R-1, 132-134	551.12	19.04	b	7.38	4.38	4347.03	
60R-1, 132-134	551.12	21.45	c	7.39	4.39	4886.11	-0.11
60R-2, 60-62	551.77	21.32	a	9.45	6.45	3305.43	
60R-2, 60-62	551.77	16.73	b	8.28	5.28	3168.56	
60R-2, 60-62	551.77	21.36	c	9.67	6.67	3202.40	0.01
60R-3, 106-108	553.67	21.32	a	9.30	6.30	3384.13	
60R-3, 106-108	553.67	20.58	b	9.27	6.27	3282.30	
60R-3, 106-108	553.67	21.40	c	9.57	6.57	3257.23	0.02
60R-4, 116-118	554.94	21.39	a	9.59	6.59	3245.83	
60R-4, 116-118	554.94	18.95	b	8.66	5.66	3348.06	
60R-4, 116-118	554.94	21.34	c	9.54	6.54	3263.00	0.01
60R-5, 63-65	555.67	20.28	a	8.57	5.57	3640.93	
60R-5, 63-65	555.67	21.21	b	9.06	6.06	3500.00	
60R-5, 63-65	555.67	21.29	c	9.36	6.36	3347.48	0.06
61R-2, 13-15	560.84	21.54	a	9.75	6.75	3191.11	
61R-2, 13-15	560.84	21.29	b	9.29	6.29	3384.74	
61R-2, 13-15	560.84	21.32	c	9.29	6.29	3389.51	-0.03
61R-3, 67-69	562.88	8.22	a	4.78	1.78	4617.98	
61R-3, 67-69	562.88	21.50	b	7.52	4.52	4756.64	
61R-3, 67-69	562.88	21.52	c	7.50	4.50	4782.22	-0.02
61R-4, 96-98	564.63	21.98	a	10.38	7.38	2978.32	
61R-4, 96-98	564.63	21.37	b	10.04	7.04	3035.51	
61R-4, 96-98	564.63	21.29	c	10.38	7.38	2884.82	0.04
61R-5, 88-89	566.01	12.17		8.04	5.04	2414.68	
61R-6, 121-123	567.67	21.97	a	8.87	5.87	3742.76	

Table 13 (Continued).

Core, section, interval (cm)	Depth (mbsf)	Distance (mm)	Axes of measurement	Traveltime (μ m)	Corrected traveltime (μ m)	Measured velocity (m/s)	Velocity anisotropy index
144-878A- (cont.)							
61R-6, 121-123	567.67	21.31	b	8.43	5.43	3924.49	
61R-6, 121-123	567.67	21.33	c	8.34	5.34	3994.38	-0.04
62R-1, 18-20	568.88	21.49	a	9.29	6.29	3416.53	
62R-1, 18-20	568.88	24.57	b	10.64	7.64	3215.97	
62R-1, 18-20	568.88	21.23	c	10.01	7.01	3028.53	0.09
62R-2, 78-80	570.59	20.79	a	9.27	6.27	3315.79	
62R-2, 78-80	570.59	21.31	b	9.36	6.36	3350.63	
62R-2, 78-80	570.59	21.36	c	9.51	6.51	3281.11	0.02
62R-2, 122-124	571.03	21.39	a	7.32	4.32	4951.39	
62R-2, 122-124	571.03	20.43	b	6.99	3.99	5120.30	
62R-2, 122-124	571.03	21.42	c	7.04	4.04	5301.98	-0.05
62R-4, 46-48	573.26	22.08	a	9.53	6.53	3381.32	
62R-4, 46-48	573.26	21.34	b	9.40	6.40	3334.38	
62R-4, 46-48	573.26	21.30	c	9.67	6.67	3193.40	0.05
62R-6, 75-77	576.34	21.42	a	6.59	3.59	5966.57	
62R-6, 75-77	576.34	21.84	b	6.67	3.67	5950.95	
62R-6, 75-77	576.34	21.91	c	6.72	3.72	5889.79	0.01
62R-7, 34-36	577.43	21.45	a	8.78	5.78	3711.07	
62R-7, 34-36	577.43	21.16	b	8.74	5.74	3686.41	
62R-7, 34-36	577.43	21.35	c	8.54	5.54	3853.79	-0.04
63R-1, 77-79	578.87	21.42	a	8.72	5.72	3744.76	
63R-1, 77-79	578.87	21.33	b	8.69	5.69	3748.68	
63R-1, 77-79	578.87	21.28	c	8.72	5.72	3720.28	0.01
63R-1, 131-133	579.41	21.22	a	8.71	5.71	3716.29	
63R-1, 131-133	579.41	21.41	b	8.89	5.89	3634.98	
63R-1, 131-133	579.41	21.55	c	8.95	5.95	3621.85	0.01
63R-4, 42-44	582.96	21.39	a	8.42	5.42	3946.49	
63R-4, 42-44	582.96	21.56	b	8.70	5.70	3782.46	
63R-4, 42-44	582.96	21.35	c	8.31	5.31	4020.72	-0.04
63R-4, 68-70	583.22	21.55	a	6.93	3.93	5483.46	
63R-4, 68-70	583.22	20.73	b	6.98	3.98	5208.54	
63R-4, 68-70	583.22	21.31	c	7.19	4.19	5085.92	0.05
63R-6, 37-39	585.36	21.56	a	9.22	6.22	3466.24	
63R-6, 37-39	585.36	21.42	b	9.06	6.06	3534.65	
63R-6, 37-39	585.36	21.31	c	9.27	6.27	3398.72	0.03
64R-1, 13-15	587.73	18.32	a	8.15	5.15	3557.28	
64R-1, 13-15	587.73	21.35	b	8.72	5.72	3732.52	
64R-1, 13-15	587.73	21.31	c	8.92	5.92	3599.66	0.01
64R-1, 69-71	588.29	16.46	a	6.06	3.06	5379.09	
64R-1, 69-71	588.29	21.45	b	6.81	3.81	5629.92	
64R-1, 69-71	588.29	19.43	c	6.49	3.49	5567.34	-0.01
64R-2, 58-60	589.68	21.40	a	8.10	5.10	4196.08	
64R-2, 58-60	589.68	21.50	b	8.58	5.58	3853.05	
64R-2, 58-60	589.68	21.53	c	8.44	5.44	3957.72	0.02
64R-5, 77-79	594.24	21.21	a	9.56	6.56	3233.23	
64R-5, 77-79	594.24	21.47	b	9.35	6.35	3381.10	
64R-5, 77-79	594.24	21.40	c	8.86	5.86	3651.88	-0.10
65R-1, 13-16	597.23	17.53	a	8.55	5.55	3158.56	
65R-1, 13-16	597.23	21.41	b	9.40	6.40	3345.31	
65R-1, 13-16	597.23	21.31	c	10.02	7.02	3035.61	0.07
65R-1, 51-54	597.61	18.05	a	8.36	5.36	3367.54	
65R-1, 51-54	597.61	21.51	b	9.51	6.51	3304.15	
65R-1, 51-54	597.61	21.38	c	9.64	6.64	3219.88	0.04
65R-3, 70-72	600.78	20.60	a	8.43	5.43	3793.74	
65R-3, 70-72	600.78	21.31	b	8.78	5.78	3686.85	
65R-3, 70-72	600.78	21.40	c	8.78	5.78	3702.42	0.01
65R-5, 73-75	603.31	20.43	a	6.67	3.67	5566.76	
65R-5, 73-75	603.31	21.52	b	6.94	3.94	5461.93	
65R-5, 73-75	603.31	21.23	c	6.94	3.94	5388.33	0.02
65R-5, 84-86	603.42	21.87	a	9.12	6.12	3573.53	
65R-5, 84-86	603.42	21.34	b	8.49	5.49	3887.07	
65R-5, 84-86	603.42	16.44	c	8.11	5.11	3217.22	0.15
65R-6, 41-45	604.49	18.95	a	7.94	4.94	3836.03	
65R-6, 41-45	604.49	21.48	b	8.81	5.81	3697.07	
65R-6, 41-45	604.49	16.65	c	7.45	4.45	3741.57	0.01
66R-1, 10-15	606.70	10.88		7.31	4.31	2524.36	
66R-1, 10-15	606.70	12.51		7.95	4.95	2527.27	
66R-1, 10-15	606.70	21.32		10.66	7.66	2783.29	
67R-1, 31-37	616.61	20.48	a	8.63	5.63	3637.66	
67R-1, 31-37	616.61	18.03	b	8.14	5.14	3507.78	
67R-1, 31-37	616.61	19.37	c	8.40	5.40	3587.04	0
68R-1, 40-45	626.30	13.62		6.81	3.81	3574.80	
68R-1, 40-45	626.30	17.59		8.05	5.05	3483.17	
68R-1, 40-45	626.30	20.69		8.86	5.86	3530.72	
69R-1, 37-42	635.97	16.98		7.79	4.79	3544.89	
69R-1, 37-42	635.97	21.04		9.90	6.90	3049.28	
69R-1, 37-42	635.97	24.97		10.01	7.01	3562.05	
70R-1, 45-51	645.65	17.82		7.82	4.82	3697.10	
70R-1, 45-51	645.65	17.69		8.09	5.09	3475.44	
70R-1, 45-51	645.65	26.15		9.81	6.81	3839.94	
71R-1, 65-67	655.55	21.56	a	9.63	6.63	3251.89	
71R-1, 65-67	655.55	22.98	b	10.12	7.12	3227.53	
71R-1, 65-67	655.55	20.28	c	8.39	5.39	3762.52	-0.15
72R-1, 18-22	664.78	15.47		8.88	5.88	2630.95	

Table 13 (Continued).

Core, section, interval (cm)	Depth (mbsf)	Distance (mm)	Axes of measurement	Traveltime (μm)	Corrected traveltime (μm)	Measured velocity (m/s)	Velocity anisotropy index
144-878A- (cont.)							
73R-1, 41-49	674.61	18.08		9.10	6.10	2963.93	
73R-1, 41-49	674.61	19.97		9.23	6.23	3205.46	
73R-1, 41-49	674.61	22.68		11.03	8.03	2824.41	
74R-1, 23-29	684.13	16.48		9.42	6.42	2566.98	
74R-1, 23-29	684.13	17.76		8.38	5.38	3301.12	
74R-1, 23-29	684.13	22.37		12.73	9.73	2299.08	
75R-1, 122-124	694.72	21.42		9.09	6.09	3517.24	
75R-1, 122-124	694.72	24.53		10.29	7.29	3364.88	
75R-1, 122-124	694.72	21.40		9.54	6.54	3272.17	
75R-2, 27-30	695.27	21.34	a	8.44	5.44	3922.79	
75R-2, 27-30	695.27	22.70	b	8.84	5.84	3886.99	
75R-2, 27-30	695.27	20.86	c	7.89	4.89	4265.85	-0.09
76R-1, 12-14	703.12	21.37	a	9.38	6.38	3349.53	
76R-1, 12-14	703.12	20.74	b	9.80	6.80	3050.00	
76R-1, 12-14	703.12	21.46	c	9.35	6.35	3379.53	-0.05
78R-2, 71-73	724.19	18.09	a	6.84	3.84	4710.94	
78R-2, 71-73	724.19	21.42	b	7.27	4.27	5016.39	
78R-2, 71-73	724.19	21.37	c	7.48	4.48	4770.09	0.02
79R-1, 35-37	732.05	21.16	b	10.74	7.74	2733.85	
79R-1, 35-37	732.05	20.91	c	10.74	7.74	2701.55	0.01
79R-2, 12-14	733.25	13.28	a	5.83	2.83	4692.58	
79R-2, 12-14	733.25	21.31	b	7.27	4.27	4990.63	
79R-2, 12-14	733.25	21.20	c	7.34	4.34	4884.79	-0.01
79R-3, 117-119	735.67	21.30		7.86	4.86	4382.72	
79R-3, 117-119	735.67	21.47		7.80	4.80	4472.92	
79R-3, 117-119	735.67	23.32		8.09	5.09	4581.53	
80R-2, 78-80	743.68	21.37		11.15	8.15	2622.09	
80R-2, 78-80	743.68	18.47		10.19	7.19	2568.85	
80R-2, 78-80	743.68	21.38		11.04	8.04	2659.20	
80R-3, 28-31	744.68	18.99	a	8.94	5.94	3196.97	
80R-3, 28-31	744.68	21.39	b	9.13	6.13	3489.40	
80R-3, 28-31	744.68	21.42	c	9.13	6.13	3494.29	-0.04
81R-1, 15-17	751.15	21.02	a	7.39	4.39	4788.16	
81R-1, 15-17	751.15	21.39	b	7.37	4.37	4894.74	
81R-1, 15-17	751.15	21.34	c	7.37	4.37	4883.30	-0.01
81R-3, 35-38	754.00	23.06	a	7.78	4.78	4824.27	
81R-3, 35-38	754.00	21.41	b	7.57	4.57	4684.90	
81R-3, 35-38	754.00	21.20	c	7.57	4.57	4638.95	0.02
81R-4, 58-60	755.73	21.93	a	8.35	5.35	4099.07	
81R-4, 58-60	755.73	21.48	b	8.35	5.35	4014.95	
81R-4, 58-60	755.73	21.40	c	8.50	5.50	3890.91	0.04
81R-5, 84-87	757.36	21.34	a	7.93	4.93	4328.60	
81R-5, 84-87	757.36	21.33	b	7.64	4.64	4596.98	
81R-5, 84-87	757.36	21.14	c	8.13	5.13	4120.86	0.08
82R-2, 81-83	762.85	23.39	a	8.94	5.94	3937.71	
82R-2, 81-83	762.85	21.32	b	8.18	5.18	4115.83	
82R-2, 81-83	762.85	21.41	c	8.18	5.18	4133.21	-0.03
84R-1, 13-15	780.03	25.19	a	9.01	6.01	4191.35	
84R-1, 13-15	780.03	21.37	b	7.83	4.83	4424.43	
84R-1, 13-15	780.03	21.36	c	7.83	4.83	4422.36	-0.03
84R-5, 67-69	786.48	22.60	a	7.46	4.46	5067.27	
84R-5, 67-69	786.48	21.60	b	7.19	4.19	5155.13	
84R-5, 67-69	786.48	21.41	c	7.08	4.08	5247.55	-0.03
84R-6, 70-72	787.93	21.22	a	8.13	5.13	4136.45	
84R-6, 70-72	787.93	21.44	b	7.96	4.96	4322.58	
84R-6, 70-72	787.93	21.42	c	8.29	5.29	4049.15	0.04
85R-2, 90-92	791.70	20.64	a	7.54	4.54	4546.26	
85R-2, 90-92	791.70	21.34	b	7.43	4.43	4817.16	
85R-2, 90-92	791.70	21.50	c	7.43	4.43	4853.27	-0.04
86R-3, 43-45	801.69	20.92	a	8.73	5.73	3650.96	
86R-3, 43-45	801.69	21.33	b	8.19	5.19	4109.83	
86R-3, 43-45	801.69	21.37	c	8.64	5.64	3789.01	0.02
89R-3, 80-82	831.01	25.28	a	8.00	5.00	5056.00	
89R-3, 80-82	831.01	21.96	b	7.29	4.29	5118.88	
89R-3, 80-82	831.01	21.36	c	6.88	3.88	5505.16	-0.08
90R-6, 49-51	844.85	20.08	a	7.50	4.50	4462.22	
90R-6, 49-51	844.85	21.34	b	7.20	4.20	5080.95	
90R-6, 49-51	844.85	21.59	c	7.20	4.20	5140.48	-0.07

Notes: a = direction perpendicular to split core plane, b = direction transverse to split core plane, and c = core axis; all axes are orthogonal.

apparently poorly recognized or not recovered during coring. For example, the upper 30 m of the carbonate platform appears from resistivity, density, caliper, and calcium measurements to have a progressive upward increase in average cementation and density.

Fluctuations among the bulk density, resistivity, drilling rate, and sonic velocity measurements were observed to correspond within the majority of the lithologies (Fig. 42). The limited core recovery indicates that these common fluctuations are mainly controlled by the abundance

of lime mud and the degree of cementation (see discussion in "Down-hole Measurements and Seismic Stratigraphy" section, "Site 871" chapter, this volume) rather than by mineralogic changes. Because of the enlarged borehole diameter, resistivity measurements depended on the penetration depth of the different resistivity sondes, and we consider that the medium-penetration resistivity measurements provide the more reliable values and detail (see "Explanatory Notes" chapter, this volume). The FMS imagery was not processed in time for this

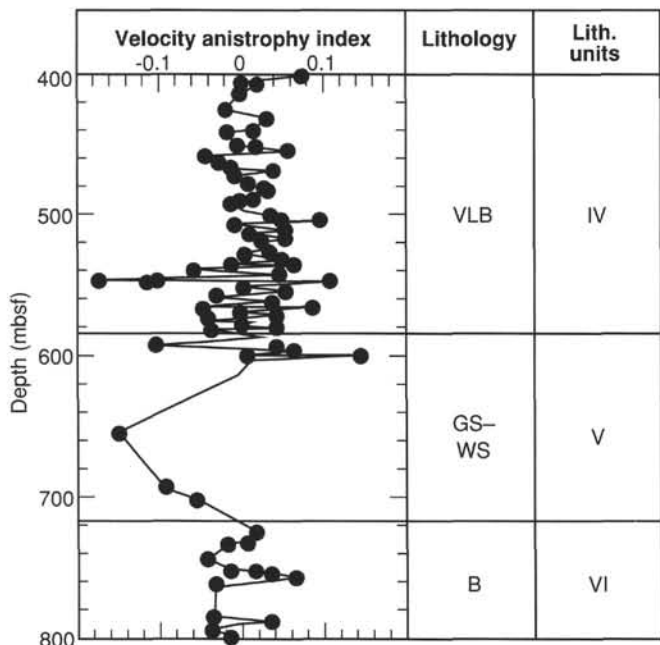


Figure 40. Plot of velocity anisotropy index vs. depth, Hole 878A. VLB = volcanic limestone breccia, GS-WS = grainstone/wackestone, and B = basalt.

volume, but we expect that it will show that many of the short-wavelength features have internal complexity, such as groupings of thin beds or irregular patterns of cementation, whereas the distinct resistivity spikes are caused by well-cemented horizons.

Pelagic Ooze with Manganese Nodules

Lithologic Unit I

Interval: Core 144-878A-1R
Assigned depth from logs: 0–4 mbsf(?)
Age: latest Albian to early Pleistocene

The pelagic cap (Lithologic Unit I) was characterized by rapid drilling penetration rates and was recorded by natural gamma-ray and geochemistry logs through the drill pipe, which will require post-cruise processing. Curiously, the condensed manganese-rich pelagic sedimentation above the carbonate platform does not display any significant increase in natural gamma rays (Fig. 43), suggesting that phosphatization or dissolution associated with the drowned upper surface of the platform is minor. This lack of uranium-thorium concentration is in contrast to the hardground observed at Site 871 on Limalok Guyot (see “Downhole Measurements and Seismic Stratigraphy” section, “Site 871” chapter, this volume), but it is similar to the low gamma-ray signature of the drowning surface at Sites 873 and 874 on Wodejebato Guyot (see “Downhole Measurements and Seismic Stratigraphy” section, “Site 871” chapter, this volume). Calcium content decreases significantly above 2.5 mbsf (Fig. 44). Drilling rates indicate a much harder lithology below about 4 mbsf, as shown by a change from <5 min/m of penetration to slower than 10 min/m, followed by rates slower than 30 min/m at 4.5 through 6.5 mbsf, which is possibly a well-cemented cap to the carbonate platform (Fig. 42).

Upper Carbonate Platform

Lithologic Units II and III

Nature: wackestone to grainstone
Interval: Cores 144-878A-2R through lower -43M
Assigned depth from logs: 4–404 mbsf
Age: late Aptian to Albian

The upper carbonate platform was subdivided into two lithologic units and seven subunits on the basis of variable ratios of lime mud to skeletal grains and of different compositions of the skeletal grains. Most of the lithologic subunits are not distinguished by significant changes in the physical properties measured by the logs. Therefore, some of the subunit interpretations may be artifacts of the selective recovery, which averaged only 2% in this interval, rather than representative of actual bulk lithologic variations. More detail will be available when the two FMS passes have been processed.

The uppermost 30 m (approximately 4 through 35 mbsf) appears to be a series of thick lithified beds with an upward trend of increasing lithification. Even though physical logs were obtained only from the lower portion of this interval, drilling rates and calcium measurements indicate that these characteristics continue through the uppermost limestones, with high calcium contents attained at 3.2 mbsf, the top of the carbonate platform (Fig. 44). Bulk density is approximately 2.3 to 2.45 g/cm³ in most of the upper 45 mbsf, as compared to approximately 2.0 to 2.1 g/cm³ within most of the underlying Lithologic Unit II below this depth (Fig. 41). The resistivity log displays two broad peaks greater than 6 Ωm in this interval, in contrast to the 2- to 3-Ωm resistivity values characteristic of the lower part of Unit II. Recovery in corresponding Cores 144-878A-2R through -4R consisted of wackestone, rich in gastropod molds, and bacteria-produced concretions of *Ortonella* with an average grain size that is coarser than in the underlying portion of Lithologic Subunit IIA. One interpretation is that this uppermost part of Unit II is a progressive shallowing-upward sequence of beds and lithification horizons preceding a possible emergence of the platform, similar to that observed in the upper Maastriichtian of Site 874 (see “Downhole Measurements and Seismic Stratigraphy” section, “Site 874” chapter, this volume).

The lower 210 m (35–245 mbsf) of Lithologic Unit II is characterized by several features. An overall progressive downward increase in average bulk density from 2.0–2.1 to 2.3 g/cm³ is seen (Fig. 41). This trend was also observed in shipboard measurements of physical properties (see “Physical Properties” section, this chapter). Density and resistivity display significant meter-scale variability, suggesting that this unit is medium bedded by alternating minor lithologic fluctuations. Core recovery indicates that these alternations may have been produced by skeletal wackestone of relatively higher density-resistivity, interbedded with packstone-grainstone of relatively lower bulk density. This contrast in interbedding is greatest in both the upper (~35–85 mbsf) and the lower (195–245 mbsf) 50 m of this interval. This meter-scale variability in physical properties is the main distinguishing characteristic between the wackestone-dominated Lithologic Unit II and the grainstone-dominated Lithologic Unit III.

Within Lithologic Unit II, three narrow peaks in resistivity occur at 71, 77, and 140 mbsf. All these peaks are associated with density increases, and the lower peak corresponds to a slower drill penetration rate (Fig. 42). The upper two peaks correspond to Core 144-878A-8R, in which a peloidal packstone, interbedded with peloid algal wackestone, represents a peritidal environment (see “Lithostratigraphy” sections, this chapter). The lower peak corresponds to Core 144-878A-15R, from which 10 cm of relatively denser mudstone was recovered and may be associated with an upward trend from restricted to more open-marine environments (see “Biostratigraphy” section, this chapter). A broader resistivity-density increase and a slower drilling rate occurs from 165 to 175 mbsf, which coincides with a minor peak in uranium. The corresponding interval of Core 144-878A-18R contains a changing benthic foraminifer assemblage that has been interpreted to represent the onset of restricted paleoenvironmental conditions (see “Biostratigraphy” section, this chapter).

The interval from 210 to 245 mbsf displays a general uranium concentration of approximately 1 ppm, which is double the uranium concentration in the overlying 200 m. Recovered pieces in corresponding Cores 144-878A-23M through -25M are very pale brown in color and contain coralline algae, in contrast to the overlying 200 m of white wackestone to grainstone with peloids and mollusks and

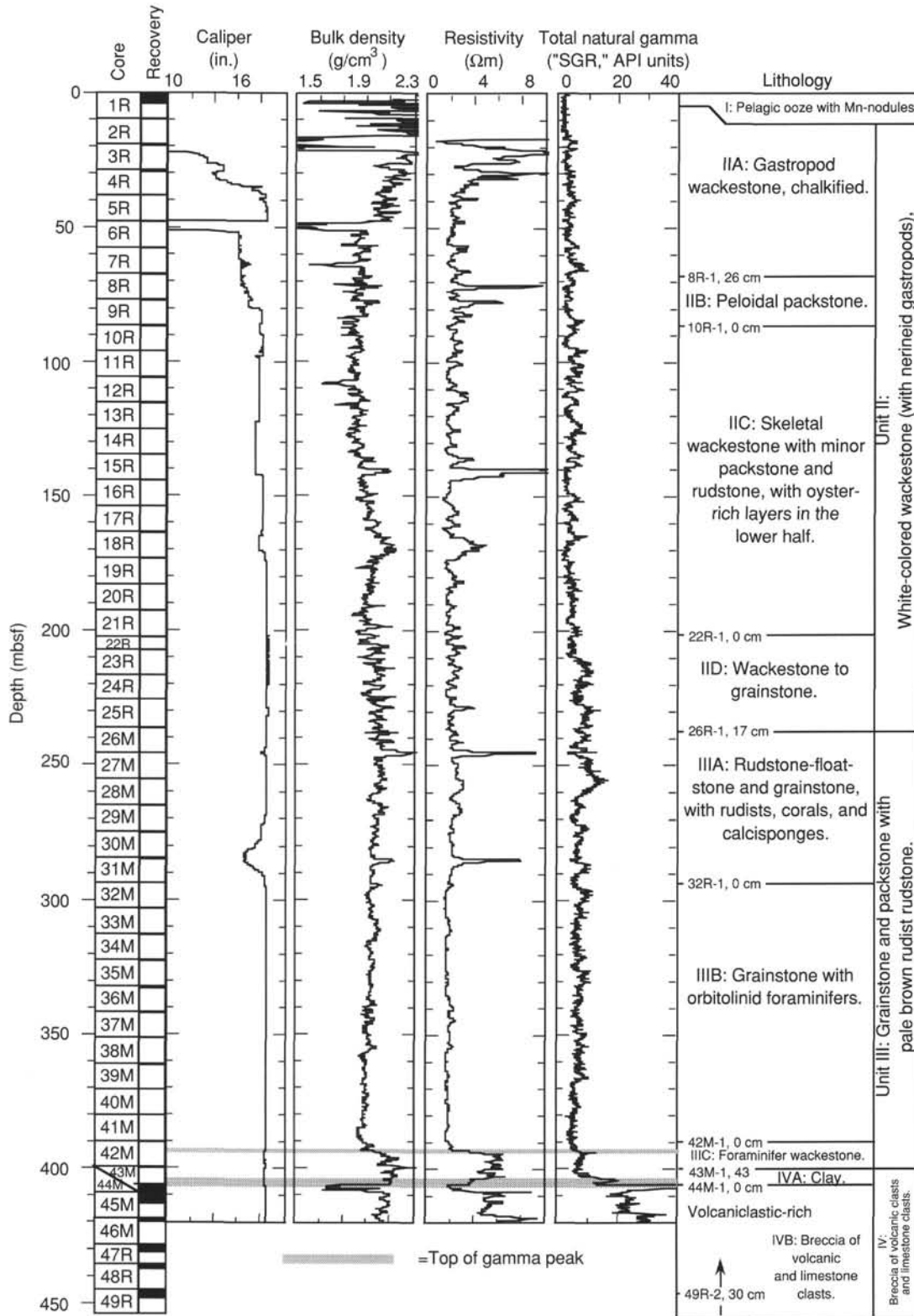


Figure 41. Stratigraphy of Hole 878A from selected geophysical logs compared to cored intervals and lithostratigraphy. Resistivity is from the medium-penetration phasor-induction (IMPH) tool. The natural gamma intensity measurements are from the geochemistry run. Caliper, or apparent hole diameter, does not record values greater than 19 in. (48 cm); drill-bit diameter is 9.9 in. (25 cm). Fluctuations in density and resistivity generally coincide within the carbonate platform; therefore, these variations provide a record of relative porosity of different limestone beds. Peaks in total natural gamma are marked by shaded lines. In the carbonate platform facies, these peaks in total natural gamma mainly result from concentrations of uranium and may be associated with condensed sedimentation, exposure surfaces, or redox front precipitation of uranium. Both uranium and thorium are abundant within the volcanoclastic-rich breccia and clay of Lithologic Unit IV. Meter levels of key stratigraphic horizons are based on the identification of the lithologic units in logs or on measurements of drilling rates.

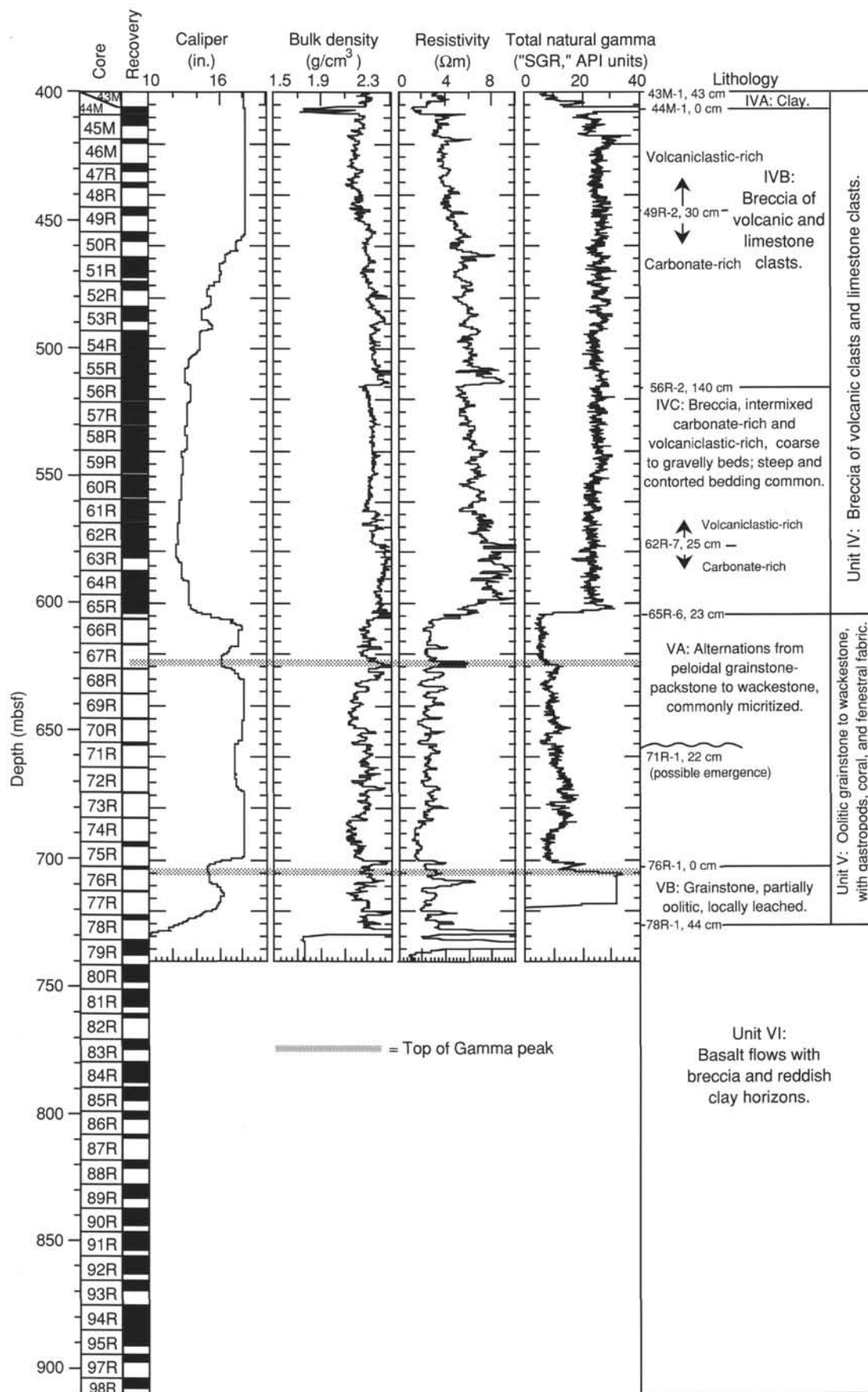


Figure 41 (continued).

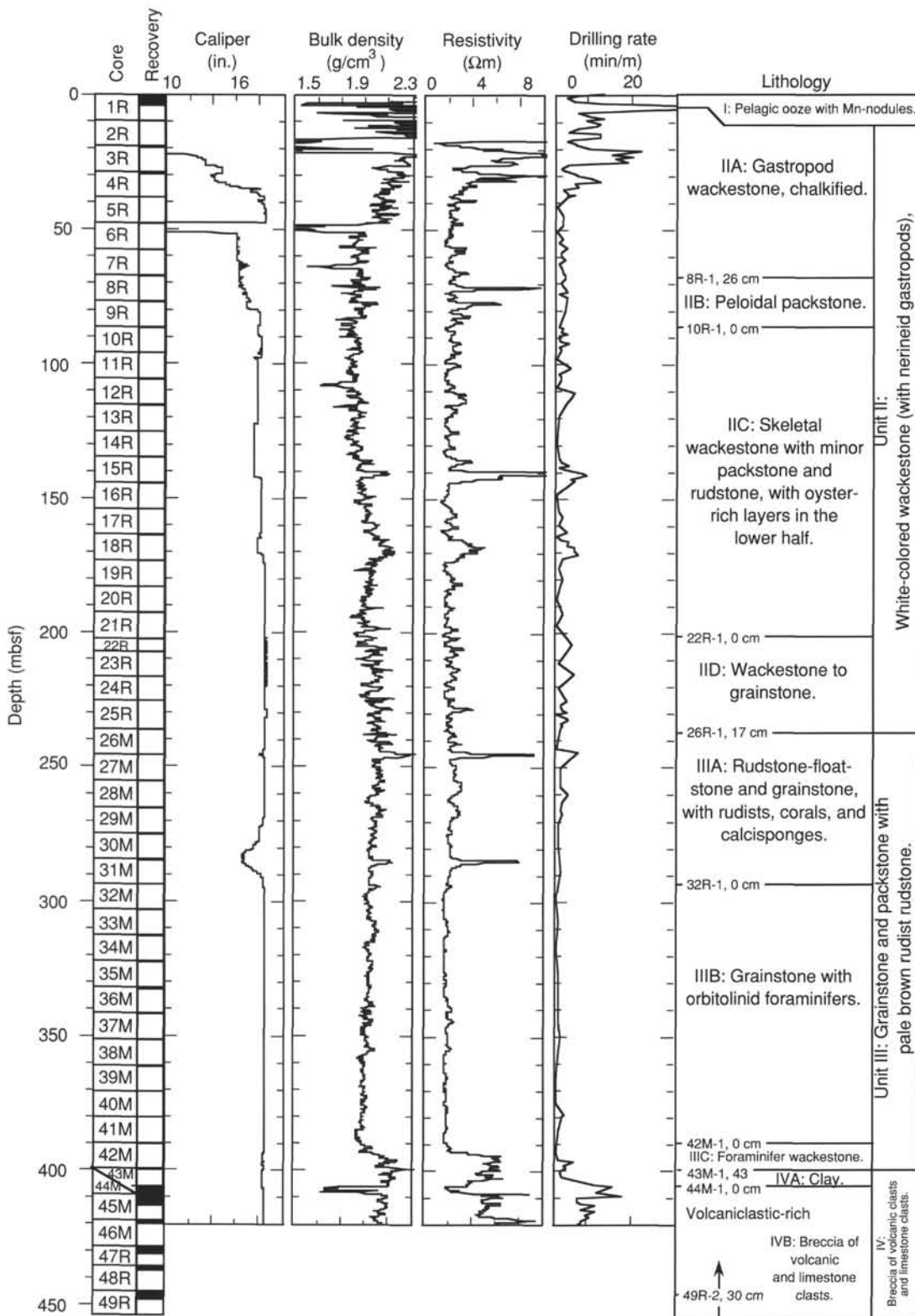


Figure 42. Geophysics logging measurements in Hole 878A. Individual peaks generally correlate among these logs and probably correspond to variations in porosity and cementation within the carbonate platform facies and to intervals of clay-enrichment in the volcanic edifice succession. Drilling penetration rates were recorded at about 1-m intervals. The density and resistivity tools are within the drill pipe from 0 to 17 mbsf.

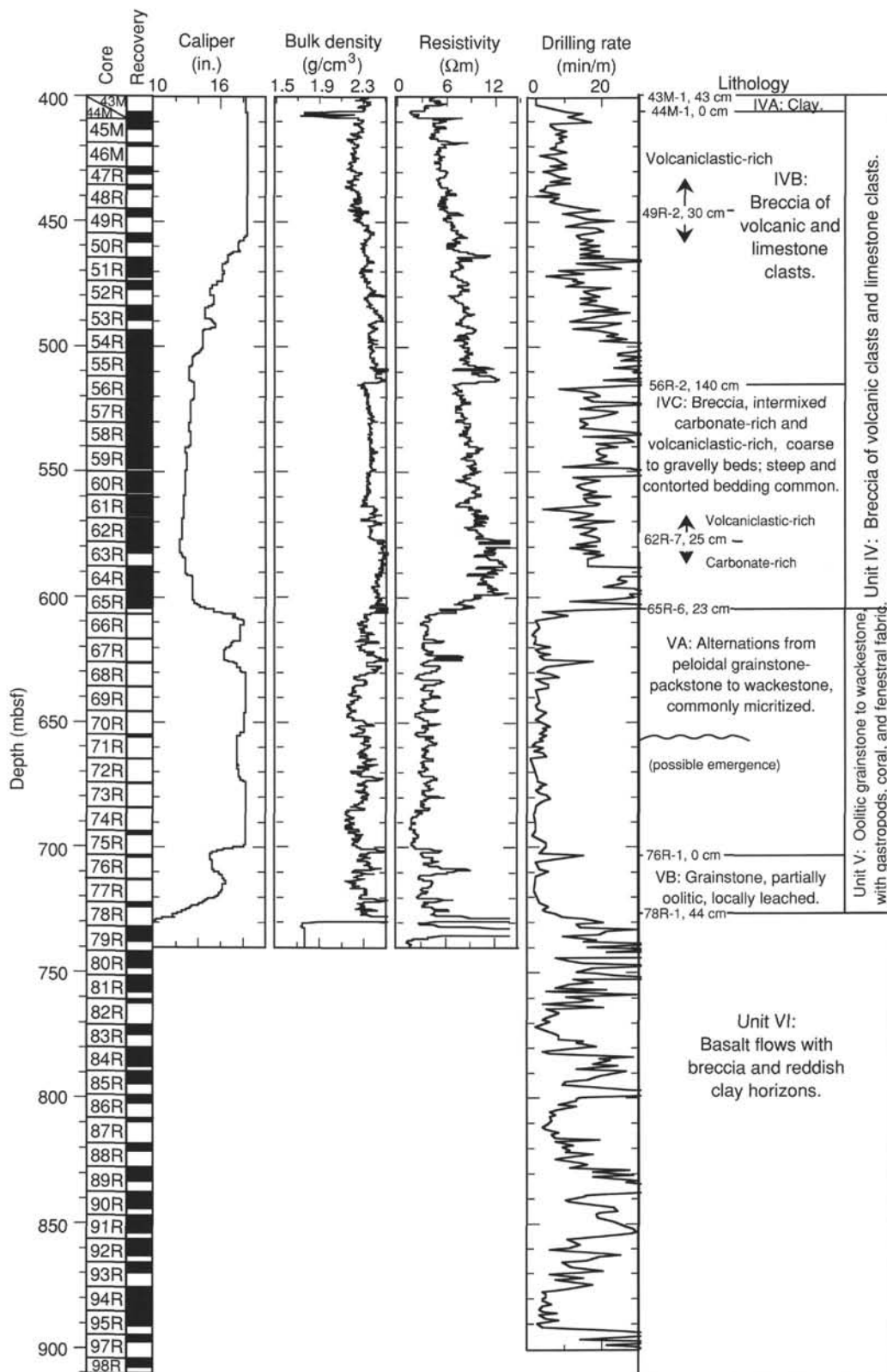


Figure 42 (continued).

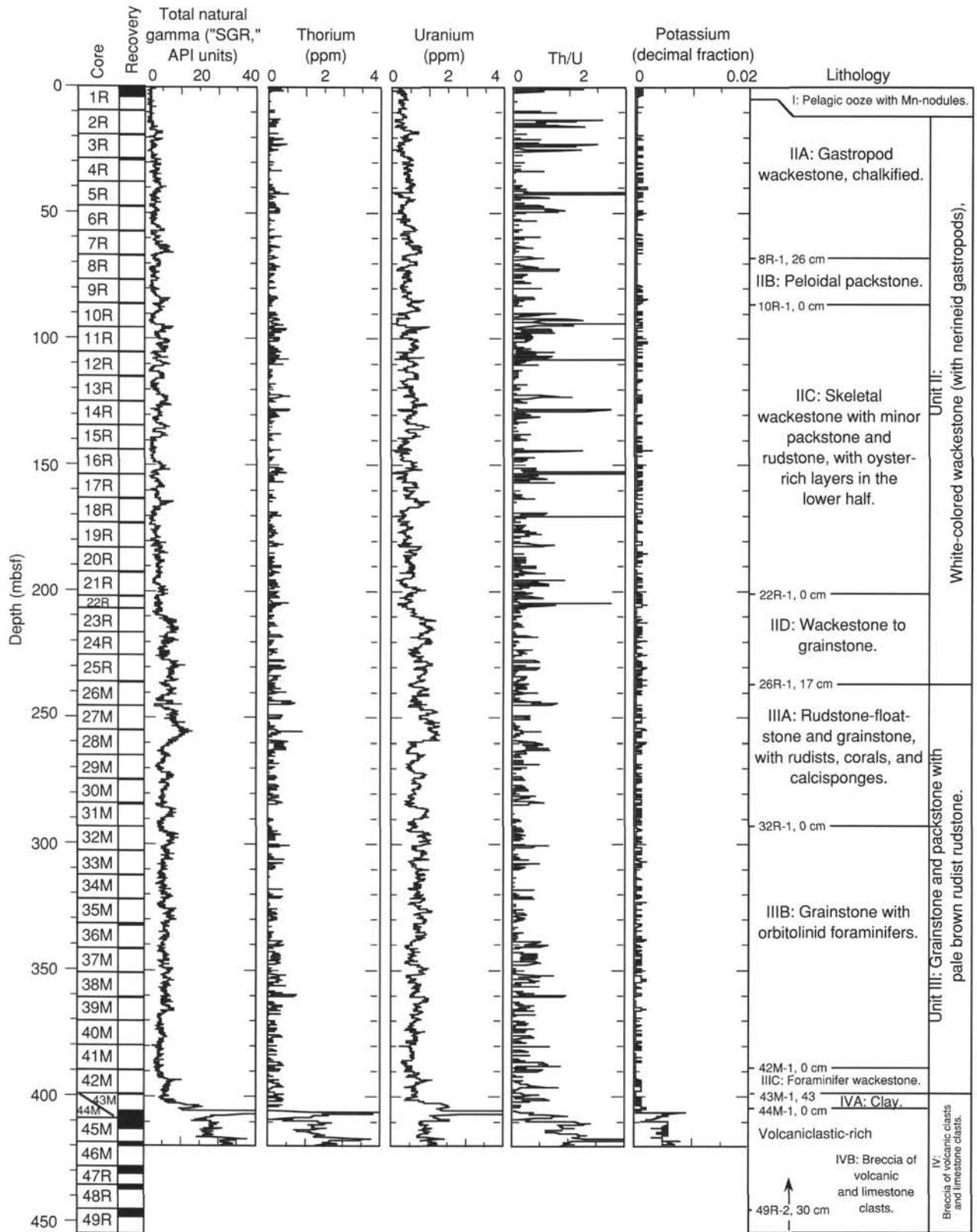


Figure 43. Radioactive element concentrations within the carbonate platform in Hole 878A as recorded by the natural gamma-ray tool on the geochemical tool string. Potassium concentrations remain near the noise level of the measurements within the limestone units with very low concentrations within the volcanoclastic-rich breccia.

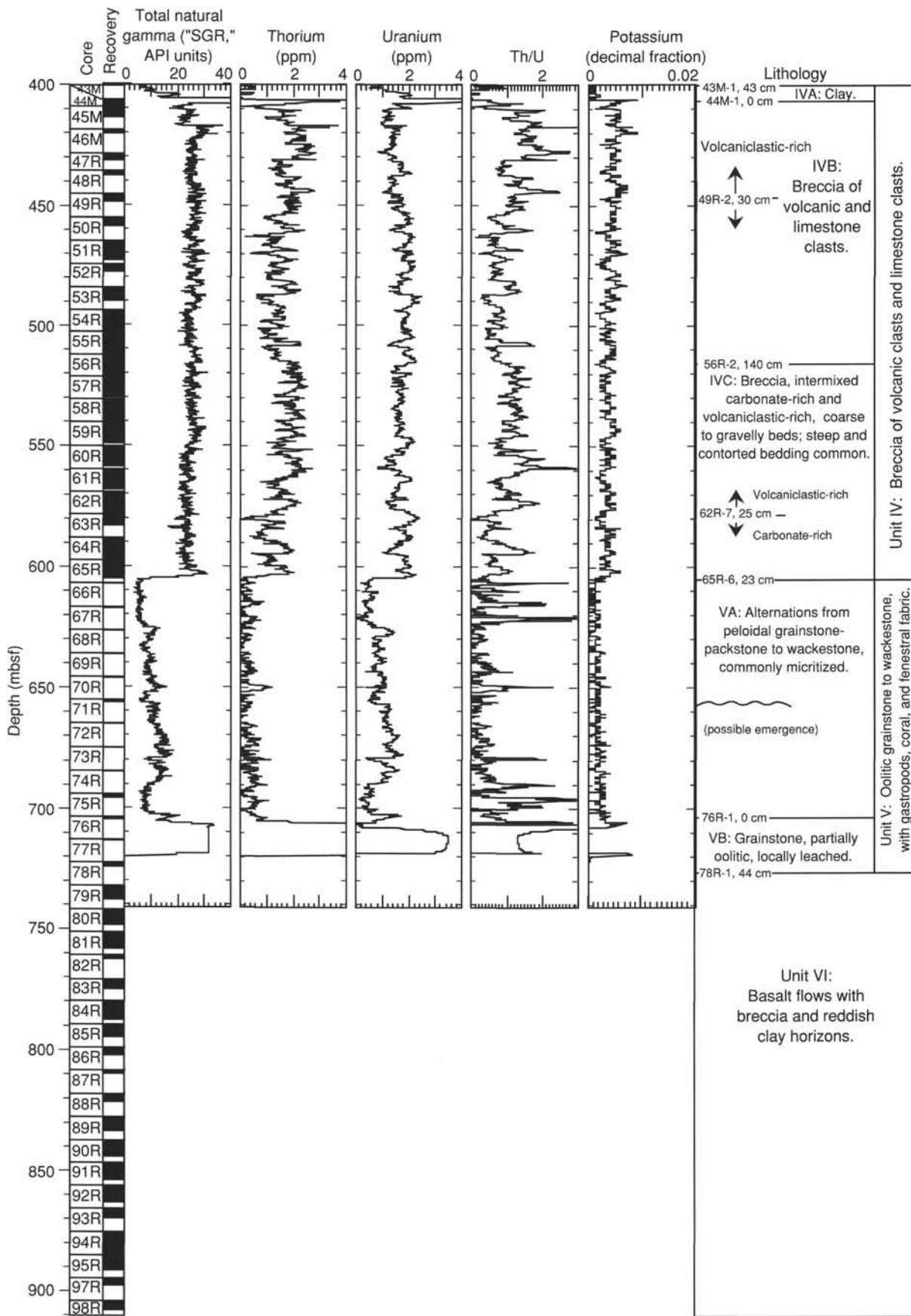


Figure 43 (continued).

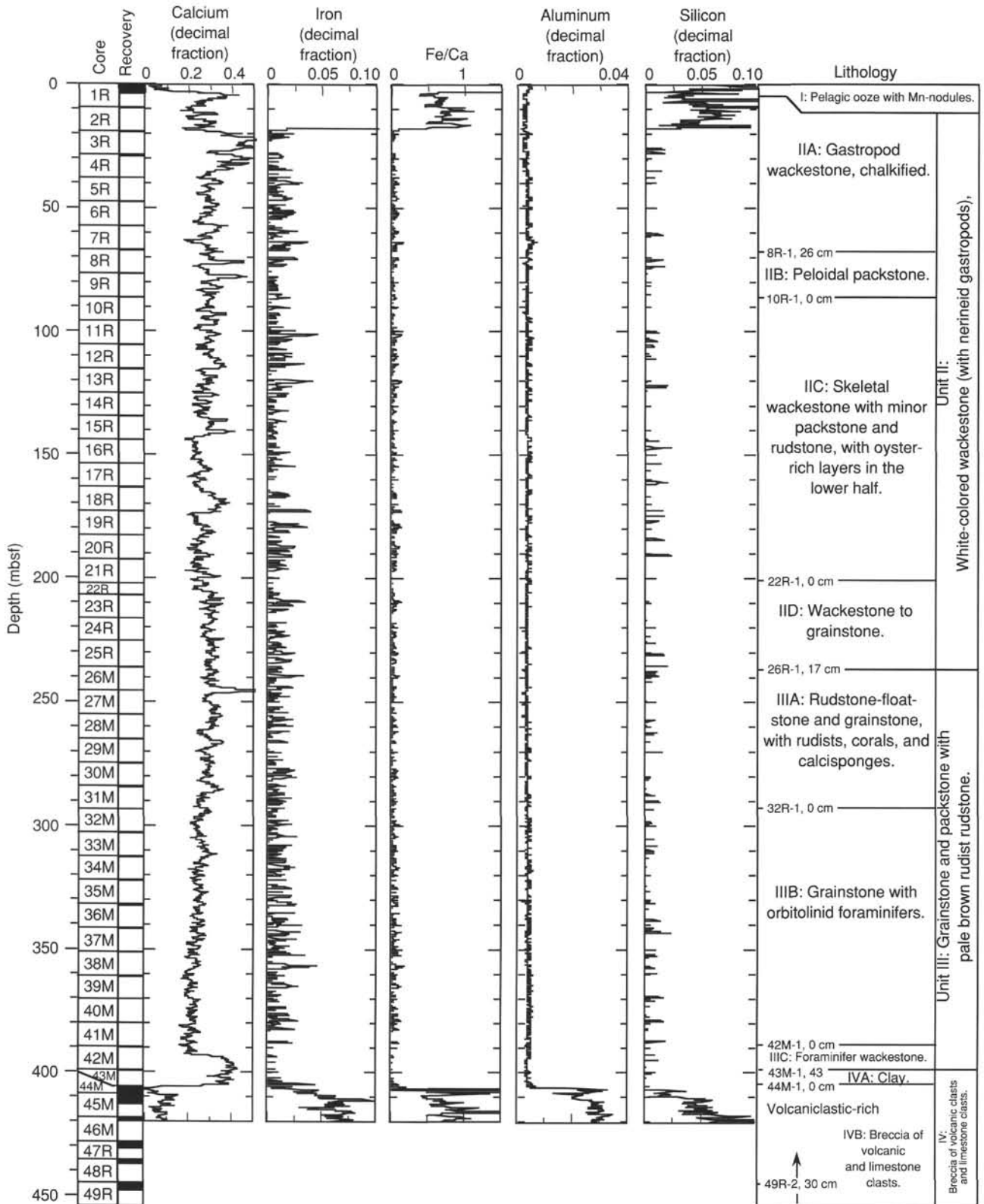


Figure 44. Relative stable elements (calcium, silicon, aluminum, iron, and sulfur) within the carbonate platform in Hole 878A. Values are given in relative proportions and have not been adjusted for porosity variations. Except for calcium, all other elements are in trace amounts within the shallow-water carbonates. Iron, silica, and aluminum are important constituents within the volcanoclastic-limestone breccia of Lithologic Unit IV. Anomalous readings above 17 mbsf for these elements result from logging through the drill pipe, but the upward increase in calcium content is probably produced by increasing cementation.

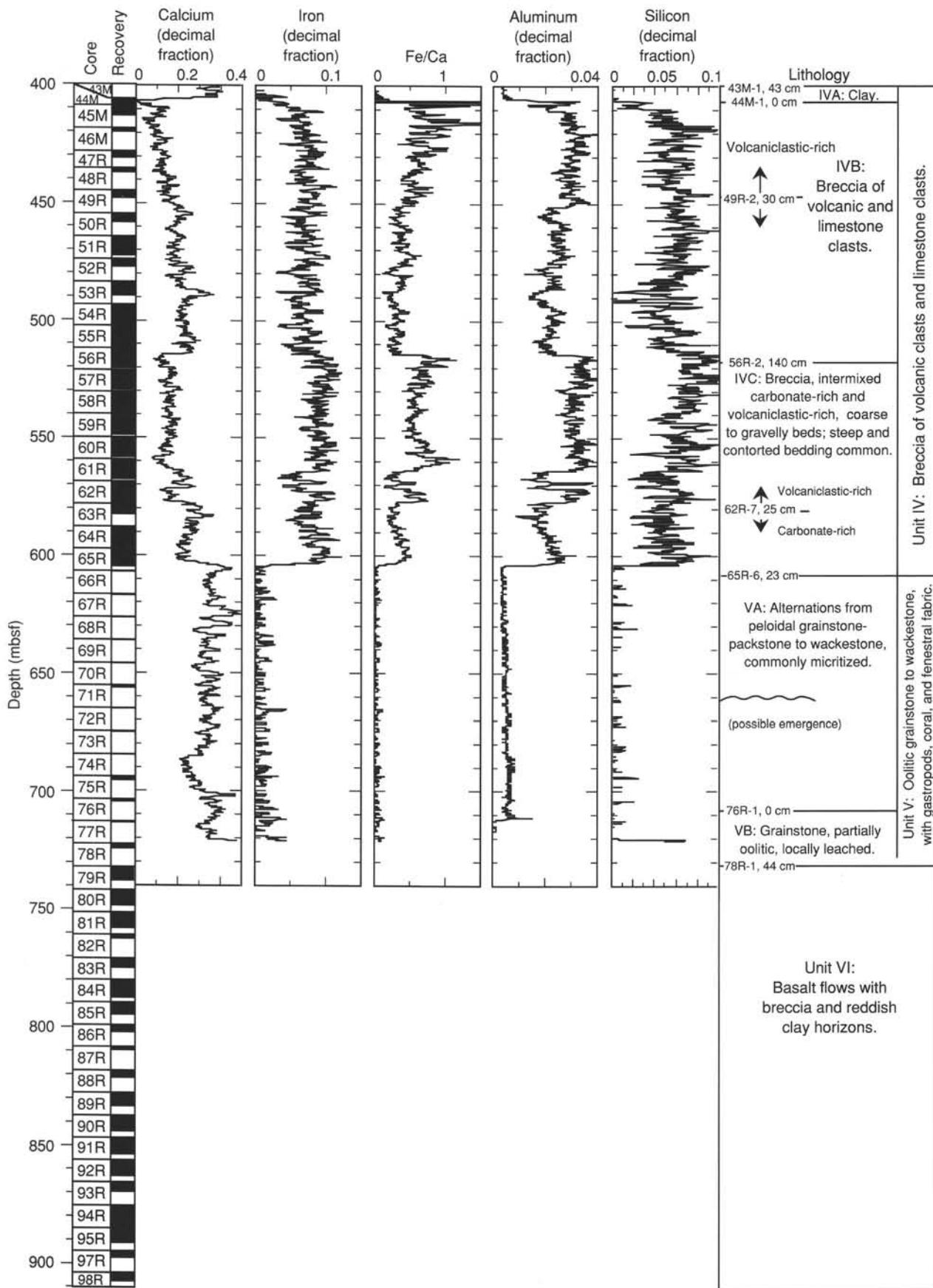


Figure 44 (continued).

no coralline algae. At other sites, the presence of coralline algae and rhodoliths also coincided with sustained uranium concentrations (see discussion in "Downhole Measurements and Seismic Stratigraphy" sections of "Site 871" and "Site 874" chapters, this volume). The resistivity-density logs in these intervals do not display unambiguous indications of shallowing- or deepening-upward sequences, as is observed at the top of Lithologic Unit II or within Lithologic Unit III (~245 to ~400 mbsf).

The lower 159 m (Lithologic Unit III) of the upper carbonate platform is dominated by grainstone. Except for the lowermost 10 m, most of this interval is characterized by (1) featureless curves of resistivity (averaging 2 Ω m) and bulk density (averaging 2.1 g/cm³) without indications of significant interbedding; (2) rapid drilling penetration rates (typically 1–3 min/m); (3) a minor but unexpected downward decrease in both density and resistivity; and (4) a higher average uranium content than in overlying Lithologic Unit II (Figs. 41–43). Most of these features are consistent with a fairly homogeneous grainstone facies, with perhaps progressively less lime mud toward the base.

Peaks in resistivity and density occur at 245 and 285 mbsf. The 245-mbsf event effectively marks the upper boundary of the logging characteristics of Lithologic Unit III and is underlain by 15 m of limestone having a relatively high uranium concentration. Recovery in corresponding basal Cores 144-878A-26M through -27M consists of 26 cm of coarse grainstone to rudstone with rudist and coral fragments and containing pelagic foraminifers, in contrast to the underlying peloid-rich grainstone facies, which lacks significant coarse skeletal fragments. On the basis of the pelagic microfossils, this interval has been interpreted as an open-marine incursion (see "Biostratigraphy" section, this chapter). The 285-mbsf event probably is associated with an interval of coral- and rudist-rich rudstone-floatstone recovered in corresponding Core 144-878A-31R. The interval containing these two rudist-rich horizons was identified as a separate lithologic subunit (IIIA); however, the grainstone sediment between these horizons has the same logging signature and general lithologic characteristics as the underlying grainstone of Lithologic Subunit IIIB.

The lowermost 10 m (394–404 mbsf) of the upper carbonate platform sequence consists of a dense (2.3 g/cm³), high-resistivity (5 Ω m), high-calcium bed of well-lithified skeletal foraminifer grainstone and mudstone (Lithologic Subunit IIIC; Cores 144-878A-42M to -43M). As will be explained later, this layer produces a local seismic reflector.

Volcanic Limestone Breccia

Lithologic Unit IV

Interval: lower Core 144-878A-43M through lower -65R
Assigned depth from logs: 404–604 mbsf
Age: early to late Aptian

A 4-m-thick clay layer overlies approximately 200 m of volcanic limestone breccia. The thickness of the uppermost clay (Lithologic Subunit IVA) has been interpreted by the width of a zone of very low resistivity and slow sonic velocity (Fig. 41) and from its claylike drilling characteristics (G. Foss, written comm., 1992); it may also include some of the clay-rich upper volcanoclastic layers recovered in Core 144-878A-44R. The thickness of the associated peak in natural gamma rays (100 API units), which is caused by a high concentration of uranium (6–8 ppm) and a lesser concentration of thorium (4 ppm), is only 1.2 m thick (405.8–407.1 mbsf). We interpret this uranium-enrichment horizon as having been partially caused by the redox precipitation of uranium at the interface between the more reducing diagenetic environment of the sulfide-rich clay (see "Organic Geochemistry" section, this chapter) and the oxidizing conditions of the overlying limestone.

The main breccia unit is characterized by (1) high resistivity (6 Ω m increasing downward to 12 Ω m); (2) high density (2.3 increasing downward to 2.5 g/cm³); (3) slow drilling penetration rates (averaging

about 15 min/m); (4) high natural gamma-ray radiation (20–25 API units) from abundant uranium (1.5–2 ppm) and thorium (2 ppm); and (5) high abundances of iron, aluminum, and silicon relative to calcium (Figs. 41–44). This breccia unit displays progressive downward increases in calcium content, resistivity, density, and sonic velocity. An interruption (60-m-thick) at 515–575 mbsf of a lithology with a reduced calcium content and lower values of these geophysical parameters enabled us to subdivide the breccia body into two 100-m-thick cycles.

The Fe/Ca ratio within these breccia cycles provides a measure of the relative abundances of volcanoclastic vs. carbonate components (Fig. 44), although the absolute values of these elements will require post-cruise processing. A sharp compositional break is apparent between the two breccia cycles at 514 mbsf, similar to the placement of the boundary between Lithologic Subunits IVB and IVC. The upper cycle displays a progressive upward increase in Fe/Ca, implying a progressive increase in the proportion of volcanoclastics; the lower cycle, on the other hand, appears to have irregular pulses with variable Fe/Ca ratios superimposed on an implied general upward increase in volcanoclastics. Based upon the geochemical abundances, the "carbonate-rich/volcanic-rich" subdivisions of these lithologic subunits appears to be arbitrary to a large degree (Figs. 42 vs. 44). A general correlation of increasing carbonate content with increasing bulk density is seen. Even though the relative proportion of volcanoclastics to limestone varies by a factor of 2 to 3, the uranium and thorium abundances and ratios have no significant variation within or between the breccia cycles (Fig. 43).

The lower breccia cycle contains steeply dipping crossbedding and possible slump deposits. The orientation of these features will be examined in the FMS imagery.

The base of the breccia unit is marked by a sharp downward decrease in resistivity, natural gamma-ray radiation, and Fe/Ca ratio, with the midpoint of this transition located at approximately 604 mbsf, identical to the shipboard placement of the base of Lithologic Unit IV within lower Core 144-878A-65R.

Lower Carbonate Platform

Lithologic Unit V

Nature: grainstone to wackestone
Interval: lower Core 144-878A-65R through middle -78R
Assigned depth from logs: 604.0–727.5 mbsf
Age: early Aptian

The lower carbonate platform comprises three distinct subdivisions with different logging characteristics. The upper 19 m (604–623 mbsf) consists of a low-resistivity (4 Ω m) and low gamma-ray (5 API units) limestone with only a single lithified bed at 617 mbsf with higher resistivity. The uppermost 1 or 2 m of this facies has increased lithification (higher resistivity), which may be partially a contact-diagenetic cementation feature to the overlying polymictic breccia unit. Corresponding Cores 144-878A-66R and -67R are skeletal and oolitic grainstone.

The main portion of the lower carbonate platform (623–700 mbsf) is characterized by interbedded, higher (5–8 Ω m) and lower resistivity (3–4 Ω m) lithologies that are spaced approximately 5 m between the relatively more resistive beds (Fig. 41). The contrast between high- and low-resistivity beds increases uphole; this trend may be related to increasing cementation in high-resistivity beds overlain by low-resistivity (weakly cemented) lithologies. Limestone fragments recovered from this interval include fenestral wackestone with possible intertidal sedimentary structures, peloidal-oolitic grainstone, stromatoporoids, and a piece of recrystallized limestone or dolomite. These logging and lithologic features suggest the presence of a series of shallowing-upward cycles and possible emergent surfaces separated by deepening episodes, with an upward trend toward shallower facies. This succession is similar to shallowing-upward cycle se-

quences observed in logs and cores in Hole 874A (see “Downhole Measurements and Seismic Stratigraphy” section, “Site 874” chapter, this volume) and in other “highstand” shallow-water, back-reef carbonate environments (reviewed in Serra, 1989; Tucker and Wright, 1990). Second-order shallowing and deepening trends are superimposed on this overall shallowing trend (see “Lithostratigraphy” section, this chapter), but the logging data to support this detailed interpretation are ambiguous. The uppermost and most pronounced of the high-resistivity beds is associated with a relative concentration in uranium.

The lowermost 27 m (700–727 mbsf) of the carbonate platform has a higher average bulk density and resistivity, relative to the overlying cyclic facies, and is characterized by elevated abundances of uranium (3 ppm) and thorium (4–5 ppm) (Figs. 42–43). This interval corresponds to Lithologic Subunit VB, which is comprised of well-cemented, coarse-grained, skeletal grainstone with minor coral rudstone and which contains small rounded clasts of altered volcanics. The presence of the volcanic fragments probably contributes to the abundances of thorium and uranium. The sharp upward transition from this high-uranium grainstone to a low-uranium wackestone coincides with the incursion of pelagic microfossils in Core 144-878A-75R (see “Biostratigraphy” section, this chapter), and it has a logging signature consistent with an interpretation of flooding surface.

The contact between the carbonate platform and the underlying basalt is indicated by a sharp downward increase in resistivity and bulk density and a slower rate of drilling at 727.5 mbsf. The resistivity and density measurements appear to indicate a sharp contact of limestone upon basalt with no intervening clay-rich horizon.

Alkalic Basalt

Lithologic Unit VI

Interval: lower Core 144-878A-65R through -78R
Assigned depth from logs and drilling penetration: 727.5–910.0 mbsf
Age: early Aptian or older

The FMS and natural gamma-ray logs were obtained from the uppermost few meters (727–737 mbsf) of the basalt flow complex and from 807 to 885 mbsf. Drilling rates were obtained from the entire basalt complex (Fig. 42). The upper 10 m displays two high-resistivity peaks, separated by 1 m of low-resistivity material. These features correspond to the two basalt flows, separated by a clay-rich alteration or weathering layer recovered in Core 144-878A-79R.

Downhole Magnetometer Measurements

A three-axis fluxgate magnetometer is part of the FMS tool string. Data about the orientation and strength of the magnetic field within the borehole was collected at 15-cm (0.50-ft) intervals, in contrast to the 2.5-mm sampling rate of the FMS resistivity image data. The three-component magnetic data (the horizontal “x” component parallel to the FMS Pad 1 direction, the horizontal “y” component perpendicular to the Pad 1 direction, and the vertical “z” component) enable calculation of horizontal and vertical intensities, inclination, and relative declination of the magnetic field with depth. The magnetic direction is used to orient the FMS traces with respect to magnetic north. Within rocks that have a strong natural remanent magnetization (NRM) different in direction from the present-day magnetic field, the FMS orientation will be slightly distorted, but we still acquire valuable information about the NRM directions of the magnetization within those rocks.

Two intervals of Hole 878A were measured with the FMS tool. The first set of the measurements (two passes; Runs 1 and 2) were made within the lower igneous complex from 806.7 (the end of the drill pipe, 2144.3 mbrf) to 885 mbsf, corresponding to Cores 144-878A-87R through -94R. The second set of FMS logs was through

the carbonate platform succession (two passes; Runs 3 and 4) from 10 to 735 mbsf.

Measurements of the total magnetic field within the upper carbonate platform series is similar to those expected from the ambient present-day field; however, both the vertical and horizontal components of intensity are offset from the ambient field (Fig. 45). The degree of offset of each component displays long-period drifts of 500 nT or greater over depth intervals of hundreds of meters. In addition, the horizontal component has several short-period peaks in intensity. The general pattern of long-period drift in the vertical and horizontal intensities is duplicated between Runs 3 and 4, whereas the peaks in the horizontal component intensity are not. We interpret the peaks in the horizontal component as artifacts of the instrument, but the long-period trends in the horizontal and vertical components may be associated with variations in the in-situ magnetic field within the carbonate succession. According to modeling of borehole magnetometer responses (e.g., Pozzi et al., 1988; Gallet and Courtillot, 1989), the magnetic intensities of the carbonate and breccia sediments, as measured on board the ship (see “Paleomagnetism” section, this chapter), are too weak to cause magnetic anomalies of this magnitude.

Intensities of the total and of the vertical and horizontal components of the magnetic field within the basaltic basement (810–880 mbsf) are generally smaller than the ambient present-day field intensity, except for two depth intervals: 835–840 mbsf and 850–855 mbsf (Fig. 45). The fine-scale variations with depth in the observed magnetic field of the basaltic complex were duplicated on the two FMS passes and are probably associated with individual flows. These magnetic field observations are consistent with the paleomagnetic measurements in the recovered basalt samples (see “Paleomagnetism” section, this chapter). Cores below about 790 mbsf, corresponding to Core 144-878A-85R, generally have reversed magnetic polarity, whereas overlying Cores 144-878A-78R through -84R have normal polarity. In addition, Core 144-878A-88R (approximately 850 mbsf) has normal polarity.

Post-cruise analyses, including calculations based on a disk geometry, will be necessary to model these magnetic field observations by using alternating normal and reversed magnetization and variable NRM intensities of different layers (e.g., Pozzi et al., 1988; Gallet and Courtillot, 1989; Hamano and Kinoshita, 1990).

Sonic Traveltime Calculations

The sonic log was used to produce a curve of traveltime vs. depth by examining the long- (LSSTT) and short-spaced (SSSTT) sonic transit times. The LSSTT is the time difference in microseconds per foot between *P*-wave velocity arrivals at the 12- and 10-ft receivers, whereas the SSSTT is the comparable time difference between the 10- and 8-ft receivers. The inverse of these traveltimes is actual velocity estimates within the formation being logged (feet/per microsecond). If these velocities ranged between 1500 and 5600 m/s, they were averaged together, and the resulting plot of velocity vs. depth is illustrated in Figure 46. Any velocities outside these ranges were rejected. The resulting velocities then were summed down the hole to produce the curve of traveltime vs. depth shown in Figure 47.

The traveltime vs. depth curve was correlated with core recovery and other logging data to calculate interval velocities among prominent seismic reflection events. The first of these prominent horizons correlates to the top of a 10-m-thick layer at 394 mbsf (Lithologic Subunit IIIC; Fig. 46), where seismic velocity increases suddenly from 2700 to 3900 m/s, and then returns to the original, lower velocity. This level corresponds to a prominent increase in resistivity and bulk density (Figs. 41–42) associated with the top of a 10-m-thick, well-lithified, foraminifer wackestone (Lithologic Subunit IIIC), which overlies approximately 4 m of clay (weathered volcanic ash?), which in turn overlies the 195-m-thick breccia sequence. The horizon at 394 mbsf corresponds to a two-way traveltime of 2.11 s, which is 0.32 s below the seafloor reflection at 1.79 s TWT. This seafloor reflection time required a small extrapolation up from the base of pipe set at 17

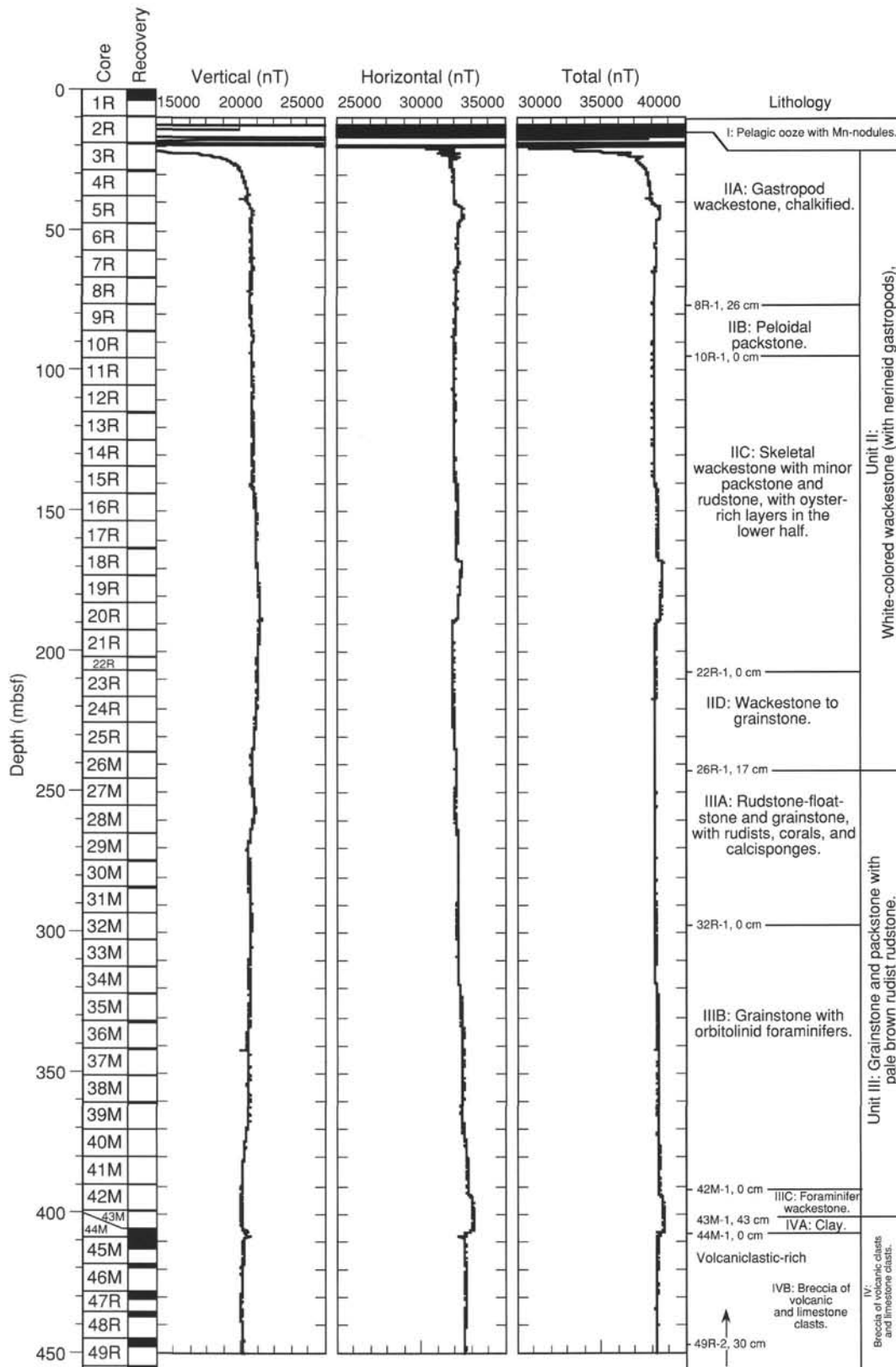


Figure 45. Downhole magnetic field measurements in Hole 878A obtained with the Formation MicroScanner (FMS) three-axis fluxgate magnetometer instrument. The three-component magnetic data (FX is the horizontal “x” component, parallel to the FMS Pad 1 direction; FY is the horizontal “y” component, perpendicular to the FMS Pad 1 direction; and FZ is the vertical “z” component) enable one to calculate horizontal intensity, inclination, and relative declination.

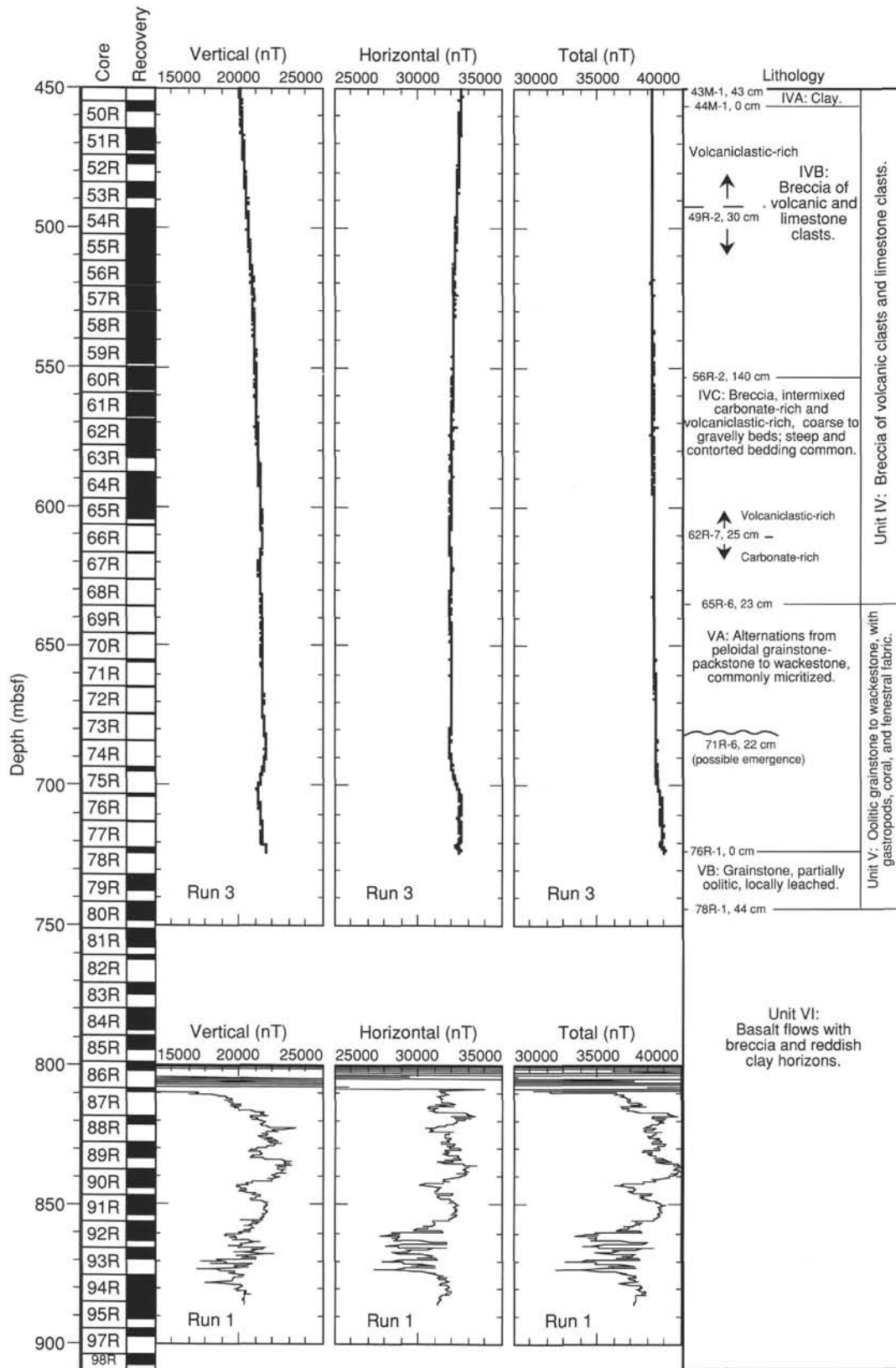


Figure 45 (continued).

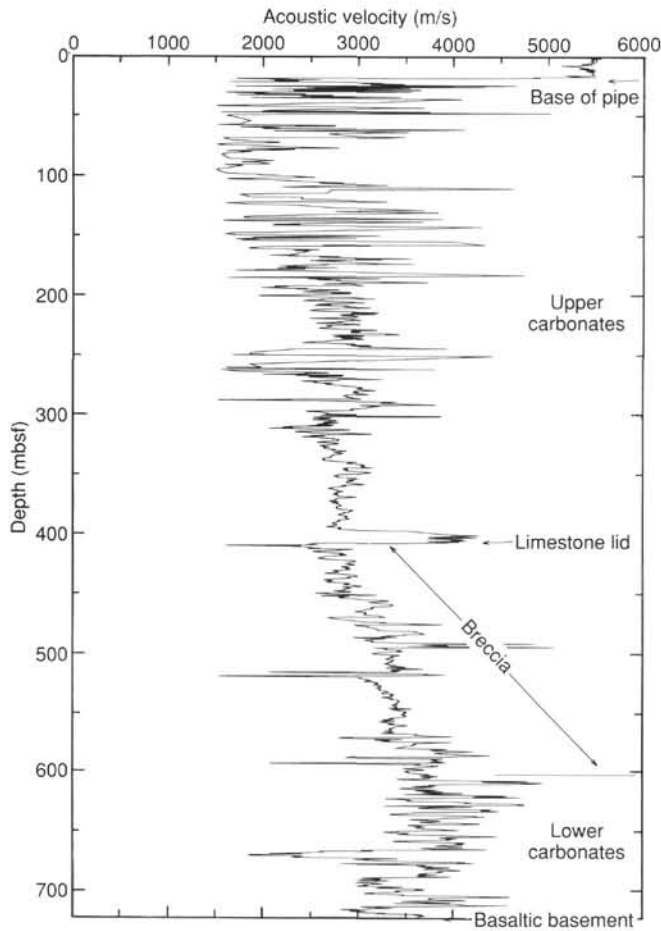


Figure 46. *P*-wave sonic velocity vs. depth in the carbonate and breccia successions in Hole 878A. Velocities were obtained by averaging all the velocity measurements between 1500 and 5600 m/s calculated from sonic log transit-time differences. The “Limestone lid” at 394–404 mbsf is a well-lithified skeletal foraminifer wackestone (Lithologic Subunit IIC) above the clay rich top of the breccia unit. The top of the velocity spike produced by this limestone lid corresponds to the top of an increase in bulk density that, unlike the velocity spike, continues down into the breccia sequence (Fig. 41). The acoustic impedance contrast formed by the combination of these two parameters produces the seismic reflector at 2.11 s TWT (see Fig. 48).

mbsf during the geophysical logging. This extrapolation effectively straightens the “dogleg” that occurs in the traveltme/depth curve so that the extrapolated curve intersects the *y*-axis at 1.79 instead of 1.80 s TWT. Division of 394 mbsf by 0.32 s TWT results in the average interval velocity down to the top of the well-lithified wackestone of 2.45 km/s, similar to velocities determined in similar formations at other Leg 144 sites.

No other prominent seismic events occur in the velocity log, as the log stopped just as it entered basaltic basement. However, the velocity log extends to within only a few meters of the recovery of the top of basalt; thus, a second interval velocity calculation was attempted. The top of basement was identified at 727 mbsf on the basis of the first large increase in resistivity (Fig. 42) that occurs within Core 144-878A-78R, the first core from which basalt was recovered. The velocity log extends to 722 mbsf and was easily extrapolated to 727 mbsf. This corresponds to 2.31 s TWT (Fig. 47), 0.20 s below the upper seismic horizon at 2.11 s. Thus, the average interval velocity from the top of the limestone “lid” that caps the breccia platform to the top of basement (394–727 mbsf) is 3.33 km/s.

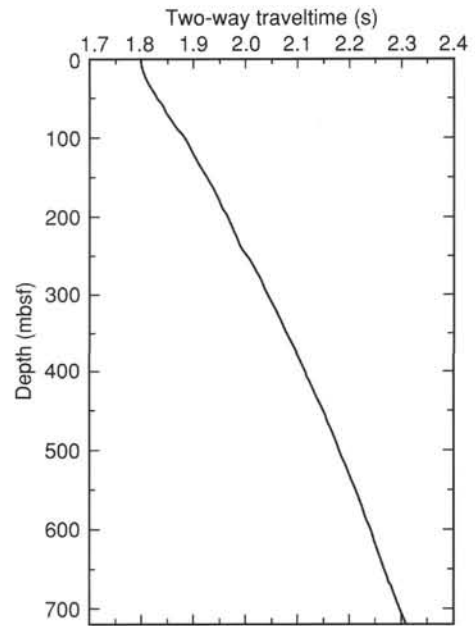


Figure 47. Integrated sonic two-way traveltme vs. depth in the carbonate and breccia sequences in Hole 878A. The upper end of the curve was extrapolated slightly from the bottom of the pipe at 17 mbsf to obtain an estimated traveltme to the seafloor of 1.79 s. The lower end of the curve was extrapolated slightly from 722 to 727 mbsf to obtain a traveltme to the top of basalt of 2.31 s.

Seismic Stratigraphy

Single-channel seismic profiles were obtained during three crossings of Site 878 before occupation of the site using a 200-in.³ water gun as a sound source. These data were partially recorded on a Masscomp computer, but after the survey we discovered that the computer had not recorded a significant number of shots for an undetermined reason. Thus, a single line was run across the site after all downhole activities were concluded. That line was recorded correctly, filtered, and redisplayed (Fig. 48). These data are barely adequate for seismic definition at Site 878, but they are superior to all data obtained before Leg 144, which were inadequate for seismic definition of this deep-penetration, multiple-reentry drilling program.

The right side of Figure 48 shows two gently undulating reflections that intersect Hole 878A at 2.11 and 2.31 s TWT, respectively. Neither of these reflections can be correlated on the left side of the record, which shows little, if any, coherent sub-bottom reflections. However, these two reflections are relatively persistent, if discontinuous, features in the more extensive analog data recorded during the pre-site survey and in the continuation of the digital data shown in Figure 48. The upper reflection corresponds exactly to the increases in *P*-wave velocity and density that mark the top of the limestone lid at 394 mbsf that caps the 195-m-thick breccia sequence (Fig. 47). The lower reflection corresponds exactly to the top of basalt at 727 mbsf, which has an extrapolated two-way traveltme of 2.31 s. Thus, the integrated *P*-wave velocities of 2.45 km/s down to 394 mbsf and 3.3 km/s from 394 to 727 mbsf are in exact agreement with the seismic reflection record. In Figure 48, the 3.3-km/s velocity has been divided into 3.2 km/s for the breccia sequence and 3.5 km/s for the lower carbonate sequence for illustrating this boundary in the lithology column. This boundary is not apparent in the seismic record in this illustration, nor can it be seen in any of the other data available to us.

Because the interval velocities calculated from both the seismic reflection record and the velocity log match exactly, we conclude that this is a good estimate of the velocity structure of the thick carbonate cap of MIT Guyot at Hole 878A and that it can be used with other

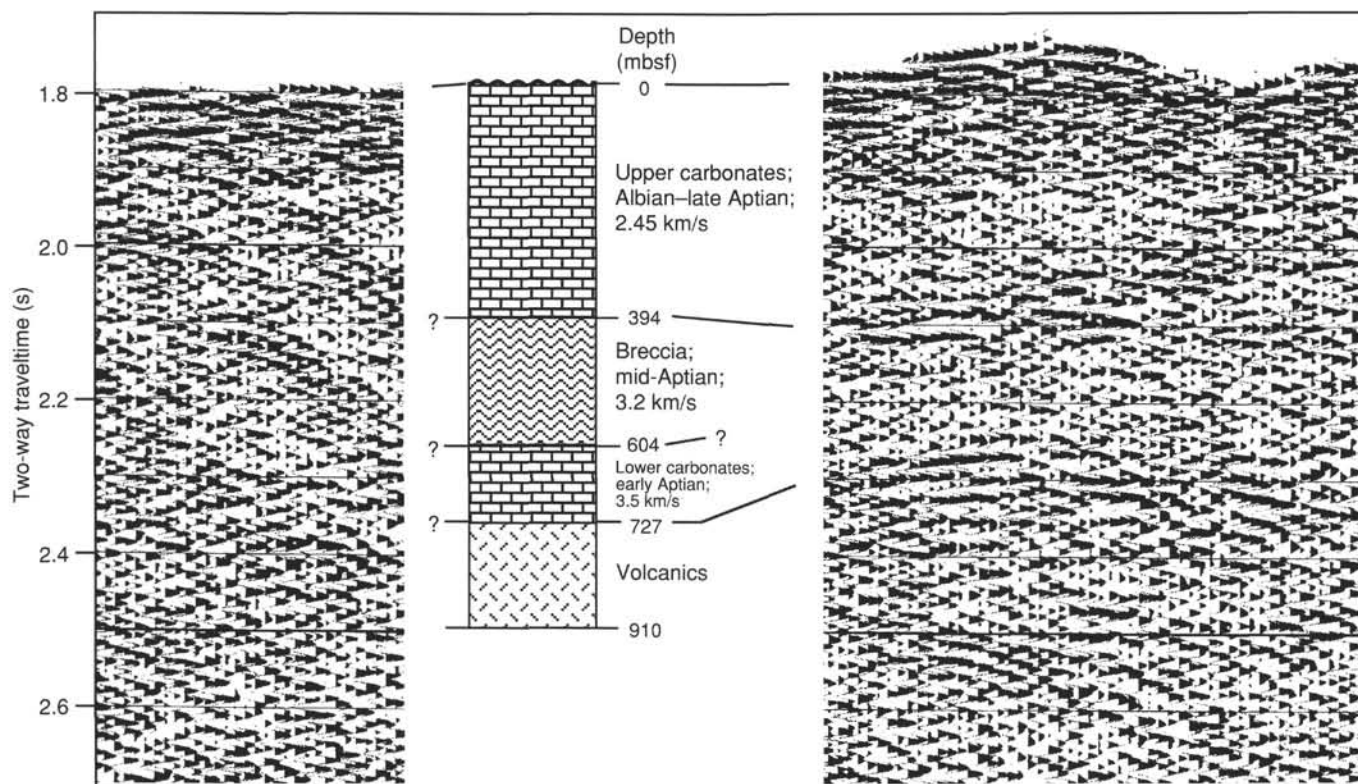


Figure 48. Lithostratigraphic correlations to the seismic stratigraphy section crossing Site 878. The seafloor reflection is at 1.79 s two-way traveltime (TWT). A major seismic reflector at 2.115 s TWT corresponds at 394 mbsf to the top of a well-lithified, 10-m-thick limestone unit that overlies the volcanoclastic-rich breccia. The reflector at 2.31 s TWT corresponds to the top of the basaltic basement at 727 mbsf. These reflectors are apparent only on the right side of the seismic reflection record. The boundary between the breccia and the lower carbonate sequence at 604 mbsf is illustrated on the lithology column, but it is not apparent in the seismic reflection record.

seismic reflection data to produce a more extensive seismic stratigraphy for the entire guyot platform.

SUMMARY AND CONCLUSIONS

Initial interpretation of the cores obtained at Site 878 indicate that the upper portion of the igneous basement of MIT Guyot was formed by numerous lava flows of alkalic affinity, more likely associated with the constructional phase of volcanism rather than with a later rejuvenated phase. The presence of well-defined vesicular and/or brecciated flow tops suggests that these flows are probably subaerial in origin, although indications of significant weathering are missing. Some of the tuffs appear to have been subaqueously deposited.

The overlying sequence records the development of a carbonate platform in the early Aptian. The contact between the carbonate platform and the basement rocks was not recovered; however, a few fragments of highly altered basalt are present within the lowermost coarse-grained skeletal grainstone. The combination of the basalt fragments and the fossil evidence suggests that marine deposition was initiated in a fully oxygenated, high-energy environment, such as an open-marine shoal. This was followed by at least one episode of pelagic influence, and then by a period of slightly less oxygenated, marine conditions. Sedimentation evolved toward upward-coarsening cycles as the environment fluctuated from open-marine to more restricted lagoonal conditions.

The development of the carbonate platform was abruptly interrupted during the late early Aptian by a volcanic eruption through the carbonate platform, which resulted in a 200-m-thick sequence of polymictic breccia. The breccia contains clasts of shallow-water

platform deposits whose origins are still uncertain and whose ages are poorly constrained. There is no apparent depositional trend related to the carbonate lithoclasts. The rare fragments of woody plant material in the breccia are of sub-bituminous rank, implying the presence of a nearly island at some point in the development of the ancient carbonate platform. The maturity level of the organic matter cannot be explained from burial depth alone.

Two distinct cycles are observed within the volcanoclastic succession. Each of these cycles most likely represents a short-lived eruptive episode from a single vent. It is suggested that, at the beginning of each cycle, the eruptive products were dominated by lithoclasts from preexisting volcanic flows and the carbonate platform. As the vent became established, progressively more material derived from new lava was incorporated into the eruptive products. The breccias may represent the evidence for short-lived, very late stage, phreatomagmatic eruptions through a carbonate platform. The resulting mixed basalt/limestone debris was probably redeposited by slumping and gravity flows down the flank of the platform. The perimeter of the platform may have been constructional or down-faulted along the margin. This difference may be resolvable if the relative ages of the limestones above, below, and within the breccia sequence can be established.

The topmost part of the breccia unit is rich in euhedral pyrite, which may indicate that reducing conditions characterized the final deposition of the breccia. Carbonate platform deposition resumed by the late Aptian in a low-energy, restricted, and poorly oxygenated lagoonal environment. The lagoonal environment rapidly changed to an oxygenated and open-marine environment, with a pelagic influence at the beginning of this open-marine, well-oxygenated phase. Later in the late Aptian, this open-marine platform gave way to the growth of one or

more bioherms near Site 878, which was terminated by another flooding event, as inferred from the recovered planktonic foraminifers.

A significant change occurred in the late Aptian with the onset of alternating poorly oxygenated marine and restricted environmental conditions. These alternating conditions evolved into a low-energy, fully restricted environment that was occasionally interrupted by storm deposits, possibly during the Albian. The recovery at Site 878 indicates that the platform was dominantly a restricted environment before its demise. Iron-oxide staining associated with some vugs may indicate that the top of the platform was very briefly subaerially exposed before drowning. It is uncertain if any of the uppermost carbonate platform sequence was removed by erosion or dissolution.

Manganese nodules within and below the ooze sequence contain nuclei that record several episodes of calcareous pelagic sedimentation. The oldest material consists of phosphatized pelagic limestone, with planktonic foraminifers of latest Albian age. This assemblage establishes a minimum age for the drowning of the underlying carbonate platform. Other intervals represented in the manganese nodules are late Santonian to early Campanian, latest Paleocene, and middle early Eocene in age, based on the calcareous microplankton recovered at this site. The age distribution of these microfossils suggests that, for several millions of years, the guyot experienced prevailing nondepositional conditions in an active current regime.

A thin (3 m) manganese-bearing nannofossil ooze of latest Miocene, late Pliocene, and early Pleistocene age was recorded at the upper surface of Site 878. The upper Miocene ooze contains well-preserved nannofossils but severely dissolved planktonic foraminifers. In addition, it contains manganese nodules and micronodules, echinoderm fragments, fish otoliths, and benthic foraminifers, including common *Uvigerina*. This indicates deposition in a low-oxygen environment at, or near, the late Miocene oxygen minimum. The Pliocene-Pleistocene ooze contains well-preserved diatoms, radiolarians, and dinoflagellates in addition to calcareous microplankton, implying a relatively high local productivity during its deposition.

REFERENCES*

- Arnaud-Vanneau, A., 1980. Micropaléontologie, paléocéologie et sédimentologie d'une plate-forme carbonatée de la marge passive de la Téthys: l'Urgonien du Vercors septentrional et de la Chartreuse (Alpes occidentales). *Geol. Alp.*, 11.
- Backman, J., Duncan, R.A., et al., 1988. *Proc. ODP, Init. Repts.*, 115: College Station, TX (Ocean Drilling Program).
- Boillot, G., Winterer, E.L., et al., 1987. *Proc. ODP, Sci. Results*, 103: College Station, TX (Ocean Drilling Program).
- Bukry, D., 1978. Biostratigraphy of Cenozoic marine sediment by calcareous nannofossils. *Micropaleontology*, 24:44–60.
- Coccioni, R., Erba, E., and Premoli Silva, I., 1992. Barremian-Aptian calcareous plankton biostratigraphy from the Gorgo Cerbara section (Marche, central Italy) and implications for plankton evolution. *Cretaceous Res.*, 13:517–537.
- Gallet, Y., and Courtillot, V., 1989. Modeling magnetostratigraphy in a borehole. *Geophysics*, 54:973–983.

- Hamano, Y., and Kinoshita, H., 1990. Magnetization of the oceanic crust inferred from magnetic logging in Hole 395A. In Detrick, R., Honnorez, J., Bryan, W.B., Juteau, T., et al., *Proc. ODP, Sci. Results*, 106/109: College Station, TX (Ocean Drilling Program), 223–229.
- Harland, W.B., Armstrong, R.L., Cox, A.V., Craig, L.E., Smith, A.G., and Smith, D.G., 1990. *A Geologic Time Scale*: Cambridge (Cambridge Univ. Press).
- Holland, H.D., 1984. *The Chemical Evolution of the Atmosphere and Oceans*: Princeton, NJ (Princeton Univ. Press).
- Hydrographer of the Navy, 1991. *Admiralty Tide Tables* (Vol. 3): *Pacific Ocean and Adjacent Seas*: London (Hydrographer of the Navy).
- Larson, R.L., Steiner, M.B., Erba, E., and Lancelot, Y., 1992. Paleolatitudes and tectonic reconstructions of the oldest portion of the Pacific Plate: a comparative study. In Larson, R.L., Lancelot, Y., et al., *Proc. ODP, Sci. Results*, 129: College Station, TX (Ocean Drilling Program), 615–631.
- McNutt, M.K., and Fischer, K.M., 1987. The South Pacific Superswell. In Keating, B.H., Fryer, P., Batiza, R., and Boehlert, G.W. (Eds.), *Seamounts, Islands, and Atolls*. Am. Geophys. Union, Geophys. Monogr. Ser., 43:25–34.
- Mutterlose, J., 1991. Das Verteilungs- und Migrationsmuster des kalkigen Nannoplanktons in der borealen Unterkruste (Valangin-Apt) NW-Deutschlands. *Palaeontographica, Ser. B*, 221:27–152.
- Nakanishi, M., Tamaki, K., and Kobayashi, K., 1992a. Magnetic anomaly lineations from Late Jurassic to Early Cretaceous in the west-central Pacific Ocean. *Geophys. J. Int.*, 109:701–719.
- , 1992b. A new Mesozoic isochron chart of the northwestern Pacific Ocean: paleomagnetic and tectonic implications. *Geophys. Res. Lett.*, 19:693–696.
- Pozzi, J.-P., Martin, J.P., Pocachard, J., Feinberg, H., and Galdeano, A., 1988. In situ magnetostratigraphy: interpretation of magnetic logging in sediments. *Earth Planet. Sci. Lett.*, 88:357–373.
- Sager, W.W., Duncan, R.A., and Handschumacher, D.W., in press. Paleomagnetism of the Japanese and Marcus-Wake seamounts, Western Pacific Ocean. In Pringle, M.S., Sager, W.W., Sliter, W.V., and Stein, S. (Eds.), *The Mesozoic Pacific*. Am. Geophys. Union, Geophys. Monogr. Ser.
- Serra, O., 1989. 6.8 shallow water carbonate environment. *Sedimentary Environments from Wireline Logs* (2nd ed.): Houston, TX (Schlumberger Well Services), 199–211.
- Tucker, M.E., and Wright, P.V., 1990. *Carbonate Sedimentology*: Oxford (Blackwell Sci. Publ.).
- van Waasbergen, R.J., and Winterer, E.L., in press. Summit geomorphology of Western Pacific guyots. In Pringle, M.S., Sager, W.W., Sliter, W.V., and Stein, S. (Eds.), *The Mesozoic Pacific*. Am. Geophys. Union, Geophys. Monogr. Ser.
- Winterer, E.L., Duncan, R.A., McNutt, M.K., Natland, J.H., Premoli Silva, I., Sager, W.W., Sliter, W.V., van Waasbergen, R.J., and Wolfe, C.J., in press. Cretaceous guyots in the northwest Pacific: an overview of their geology and geophysics. In Pringle, M.S., Sager, W.W., Sliter, W.V., and Stein, S. (Eds.), *The Mesozoic Pacific*. Am. Geophys. Union, Geophys. Monogr. Ser.

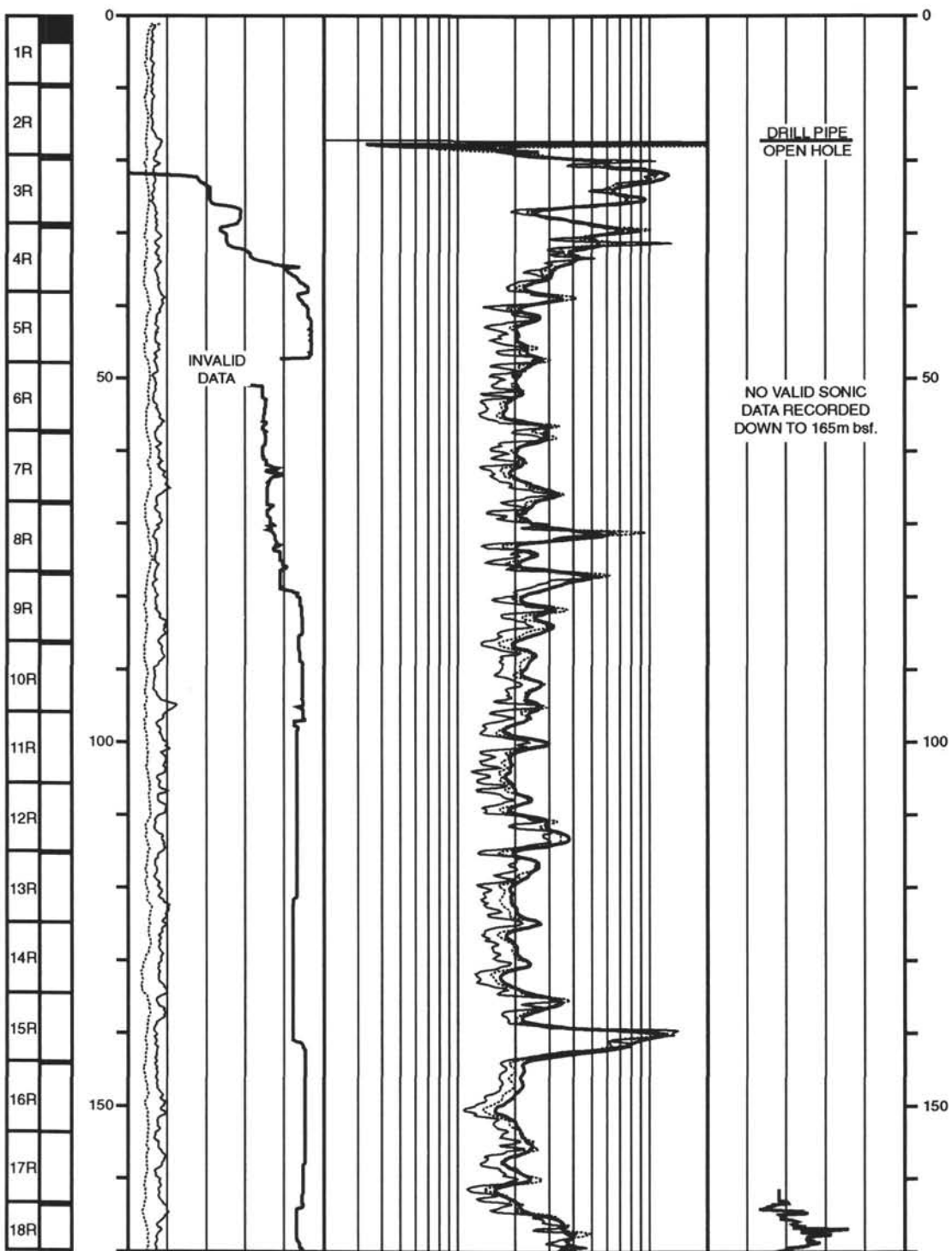
* Abbreviations for names of organizations and publication titles in ODP reference lists follow the style given in *Chemical Abstracts Service Source Index* (published by American Chemical Society).

Ms 144IR-111

NOTE: For all sites drilled, core-description forms (“barrel sheets”) and core photographs can be found in Section 3, beginning on page 453. Forms containing smear-slide data can be found in Section 4, beginning on page 1017. Thin-section data are given in Section 5, beginning on page 1037. Conventional log, FMS, dipmeter, and geochemical log (element and oxide weight %) data can be found in CD-ROM form (back pocket).

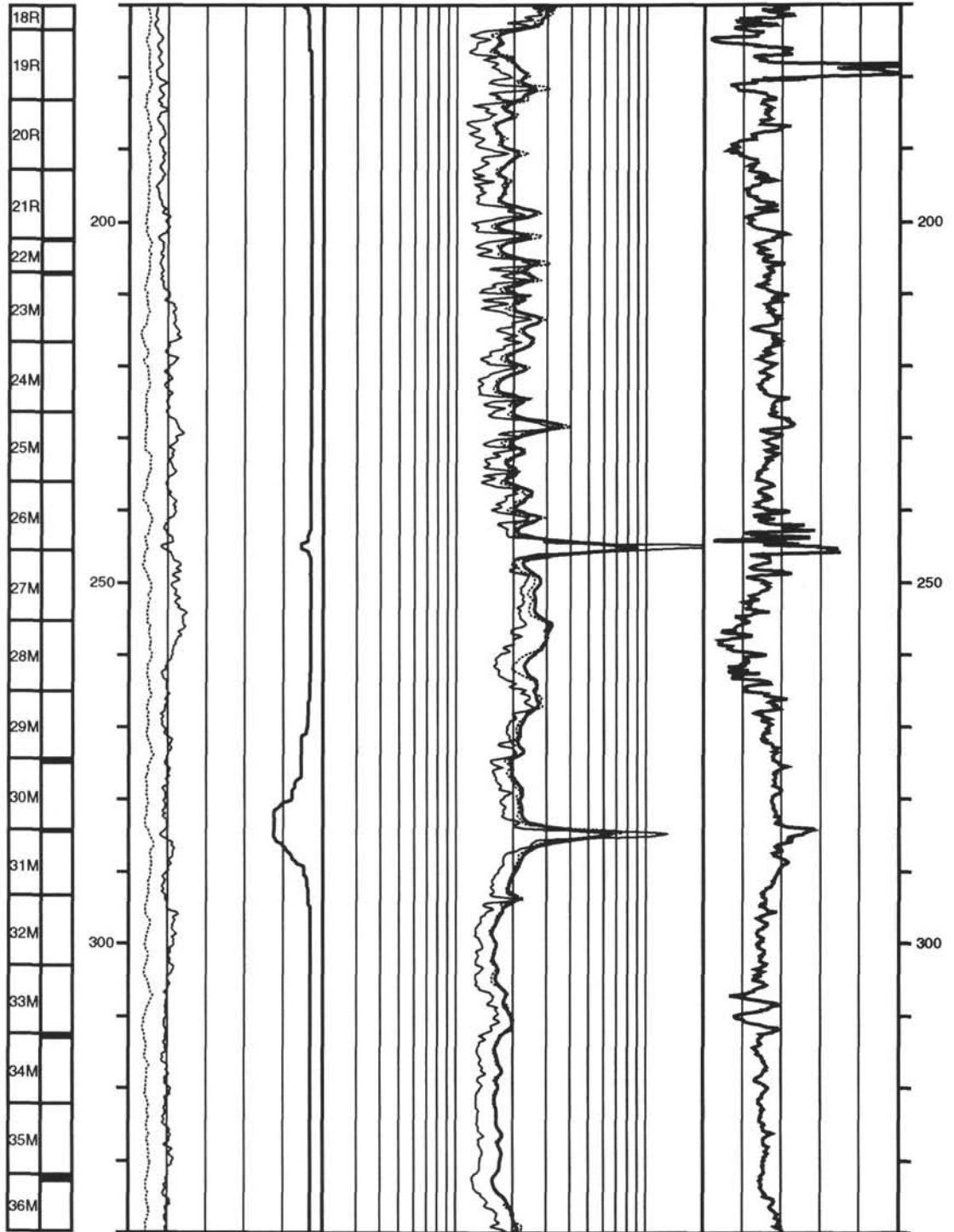
Hole 878A: Resistivity-Velocity-Natural Gamma Ray Log Summary

CORE RECOVERY	SPECTRAL GAMMA RAY				RESISTIVITY			DEPTH BELOW SEA FLOOR (m)
	TOTAL				FOCUSED			
	-10	API units	90	.2	ohm-m	20		
	COMPUTED				MEDIUM			
	-10	API units	90	.2	ohm-m	20		
	CALIPER				DEEP		VELOCITY	
	9	in	19	.2	ohm-m	20	1.5 km/s	5.5



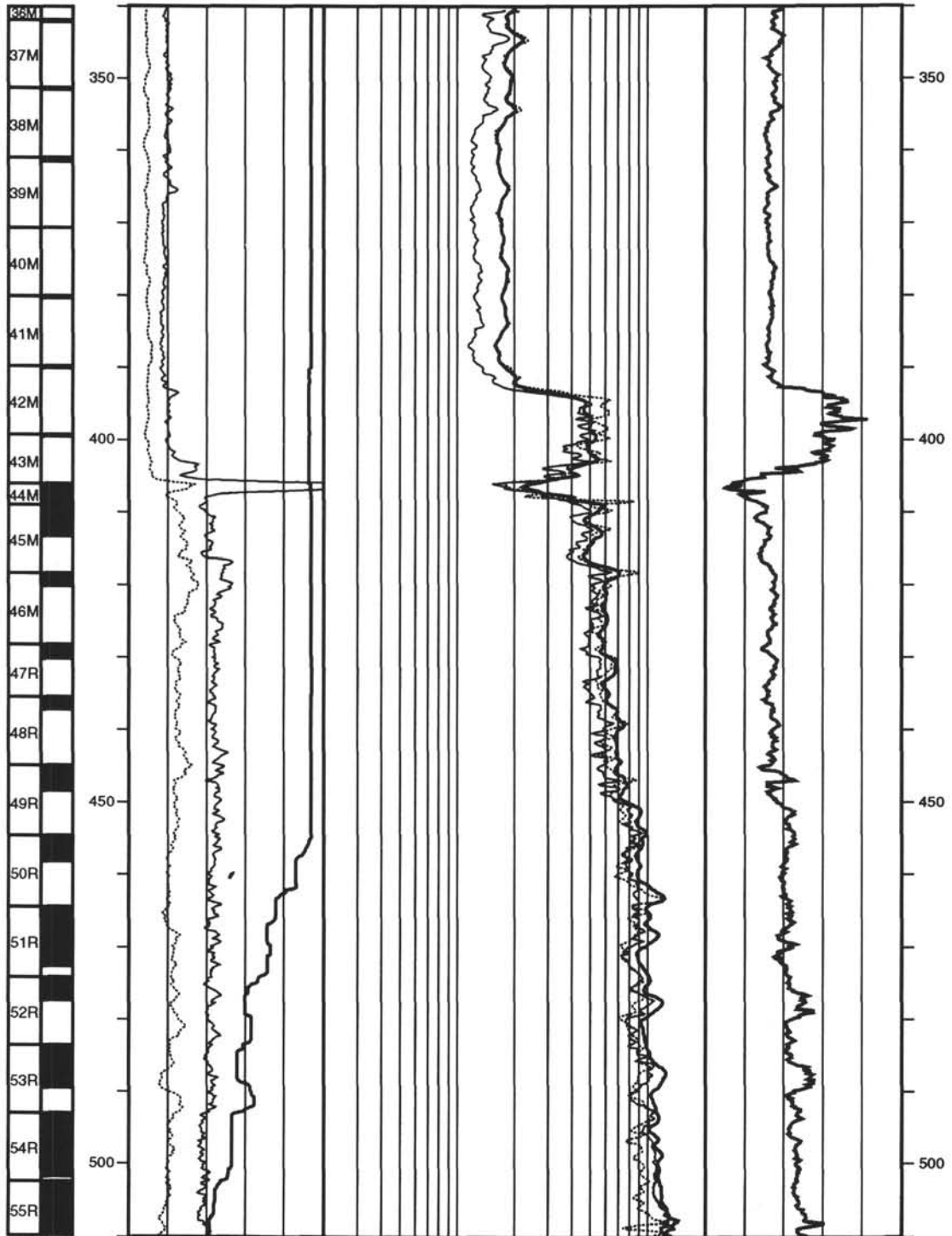
Hole 878A: Resistivity-Velocity-Natural Gamma Ray Log Summary (continued)

CORE RECOVERY	SPECTRAL GAMMA RAY				RESISTIVITY FOCUSED			DEPTH BELOW SEA FLOOR (m)
	TOTAL				FOCUSED			
	DEPTH BELOW SEA FLOOR (m)	API units	90	.2	ohm-m	20		
	COMPUTED				MEDIUM			
	DEPTH BELOW SEA FLOOR (m)	API units	90	.2	ohm-m	20		
	CALIPER				DEEP		VELOCITY	
	9	In	19	.2	ohm-m	20	1.5 km/s	5.5



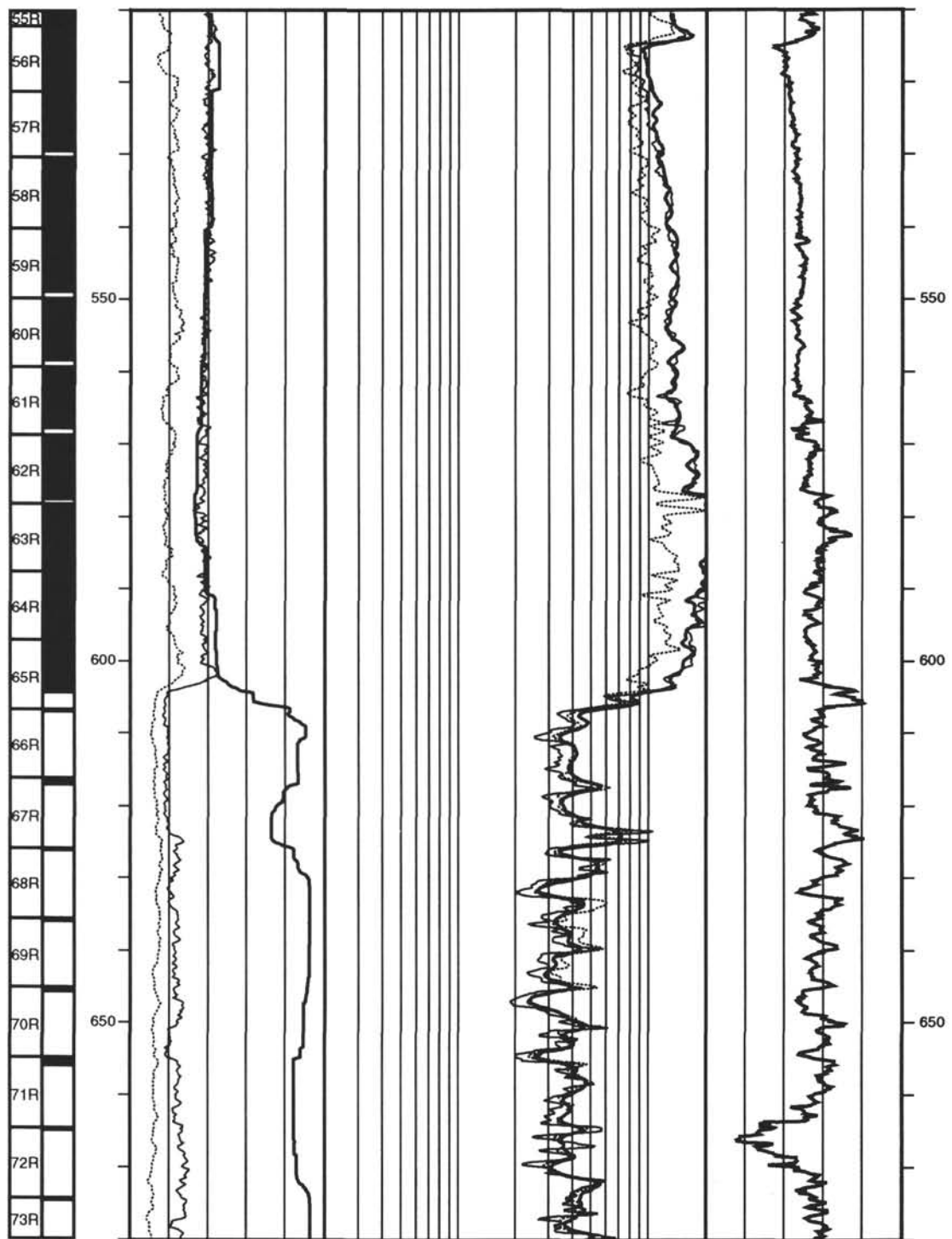
Hole 878A: Resistivity-Velocity-Natural Gamma Ray Log Summary (continued)

CORE RECOVERY	SPECTRAL GAMMA RAY				RESISTIVITY		VELOCITY		
	TOTAL				FOCUSED				
	API units				ohm-m				
	DEPTH BELOW SEA FLOOR (m)								
	-10	90	.2	20					
	COMPUTED				MEDIUM				
	API units				ohm-m				
	-10	90	.2	20					
	CALIPER				DEEP		VELOCITY		
	In				ohm-m		km/s		
	9	19	.2	20	1.5	5.5			



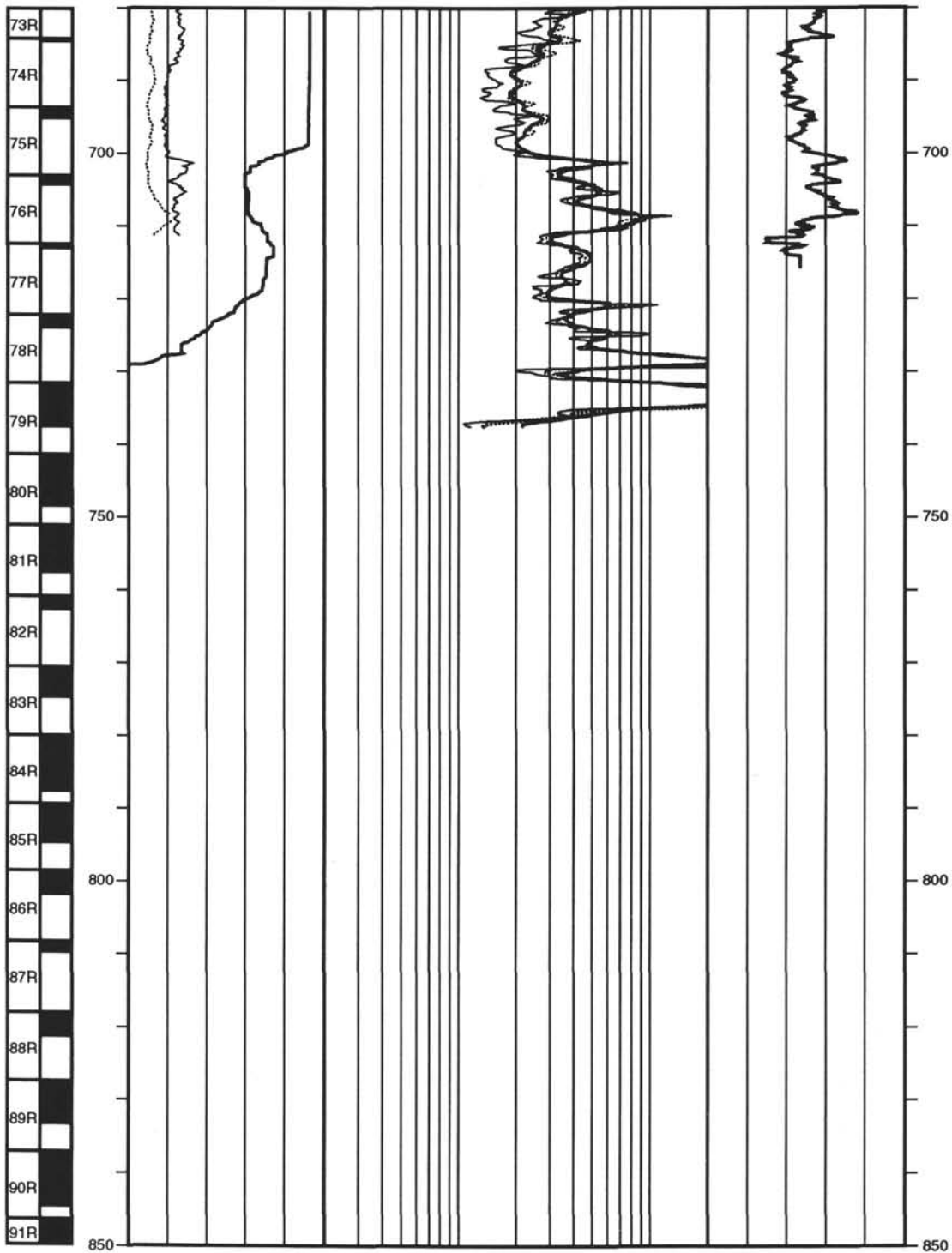
Hole 878A: Resistivity-Velocity-Natural Gamma Ray Log Summary (continued)

CORE RECOVERY	SPECTRAL GAMMA RAY TOTAL				RESISTIVITY FOCUSED		VELOCITY			DEPTH BELOW SEA FLOOR (m)
	-10	API units	90	.2	ohm-m					
	COMPUTED				MEDIUM					
	-10	API units	90	.2	ohm-m					
	9	in	19	.2	ohm-m		20	1.5	km/s	5.5

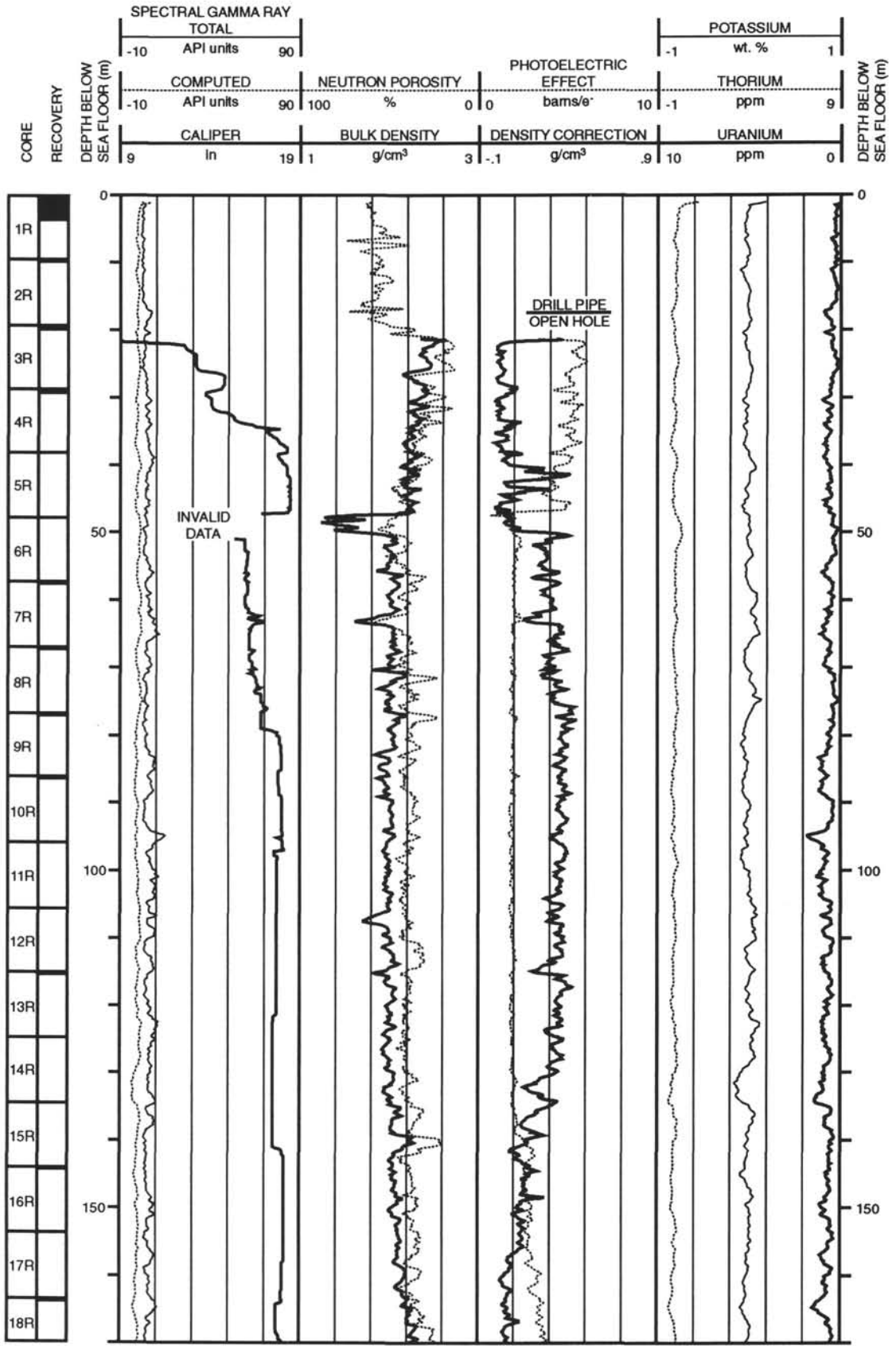


Hole 878A: Resistivity-Velocity-Natural Gamma Ray Log Summary (continued)

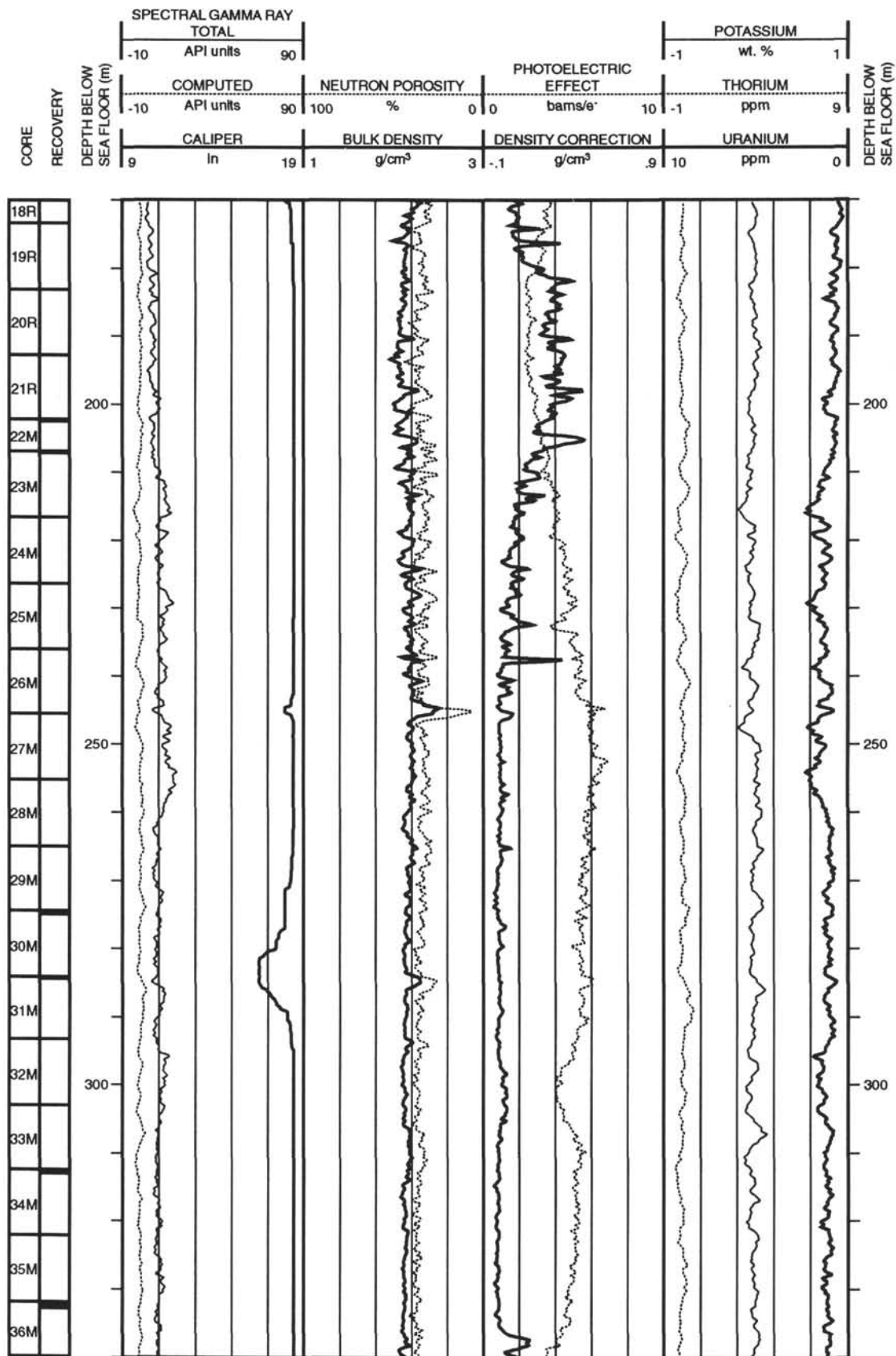
CORE RECOVERY	SPECTRAL GAMMA RAY				RESISTIVITY		VELOCITY		
	TOTAL				FOCUSED				
	DEPTH BELOW SEA FLOOR (m)	API units	90	.2	ohm-m	20			
	COMPUTED								
	DEPTH BELOW SEA FLOOR (m)	API units	90	.2	ohm-m	20			
	CALIPER				DEEP		VELOCITY		
	9	in	19	.2	ohm-m	20	1.5	km/s	5.5



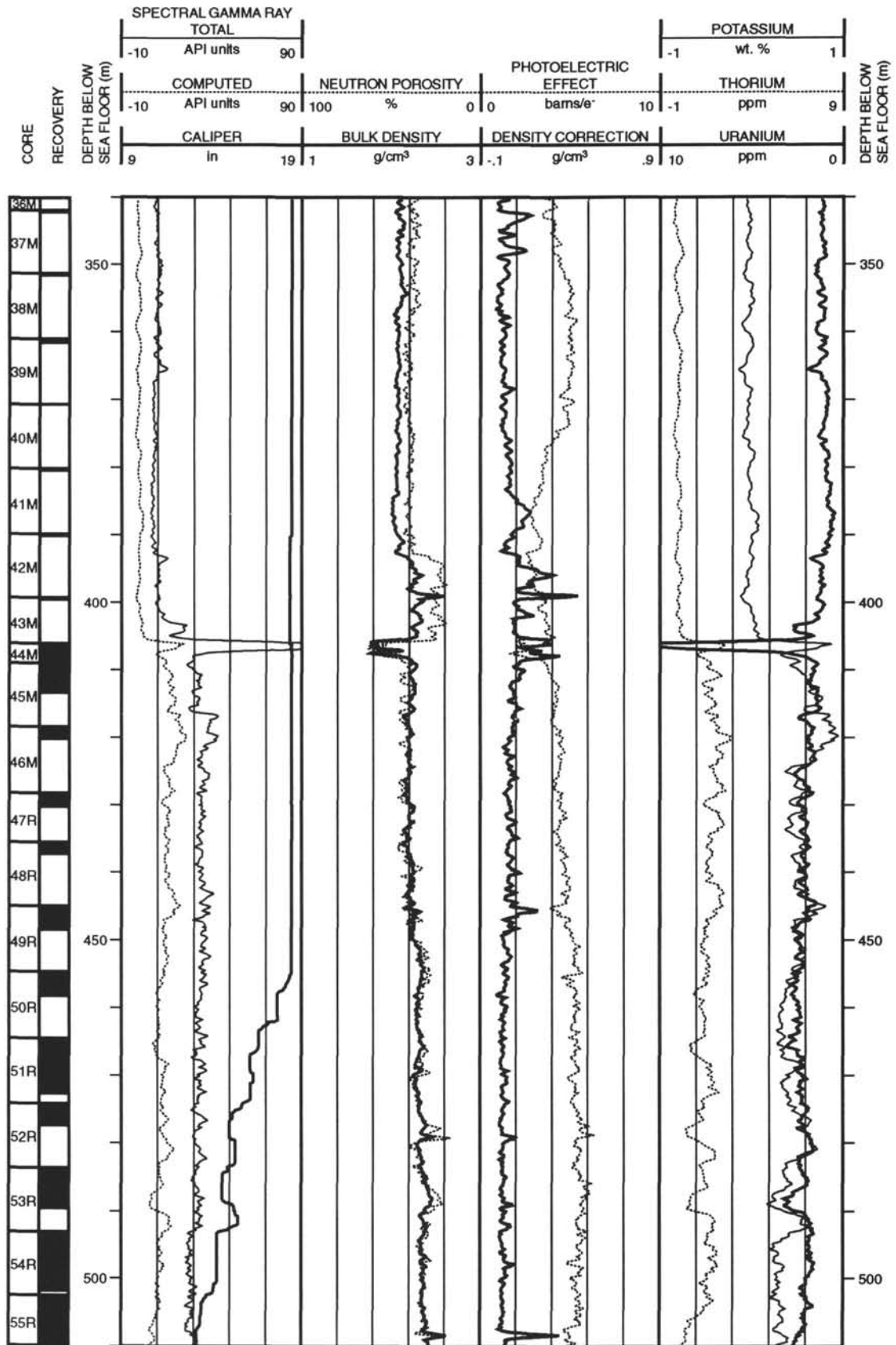
Hole 878A: Density-Porosity-Natural Gamma Ray Log Summary



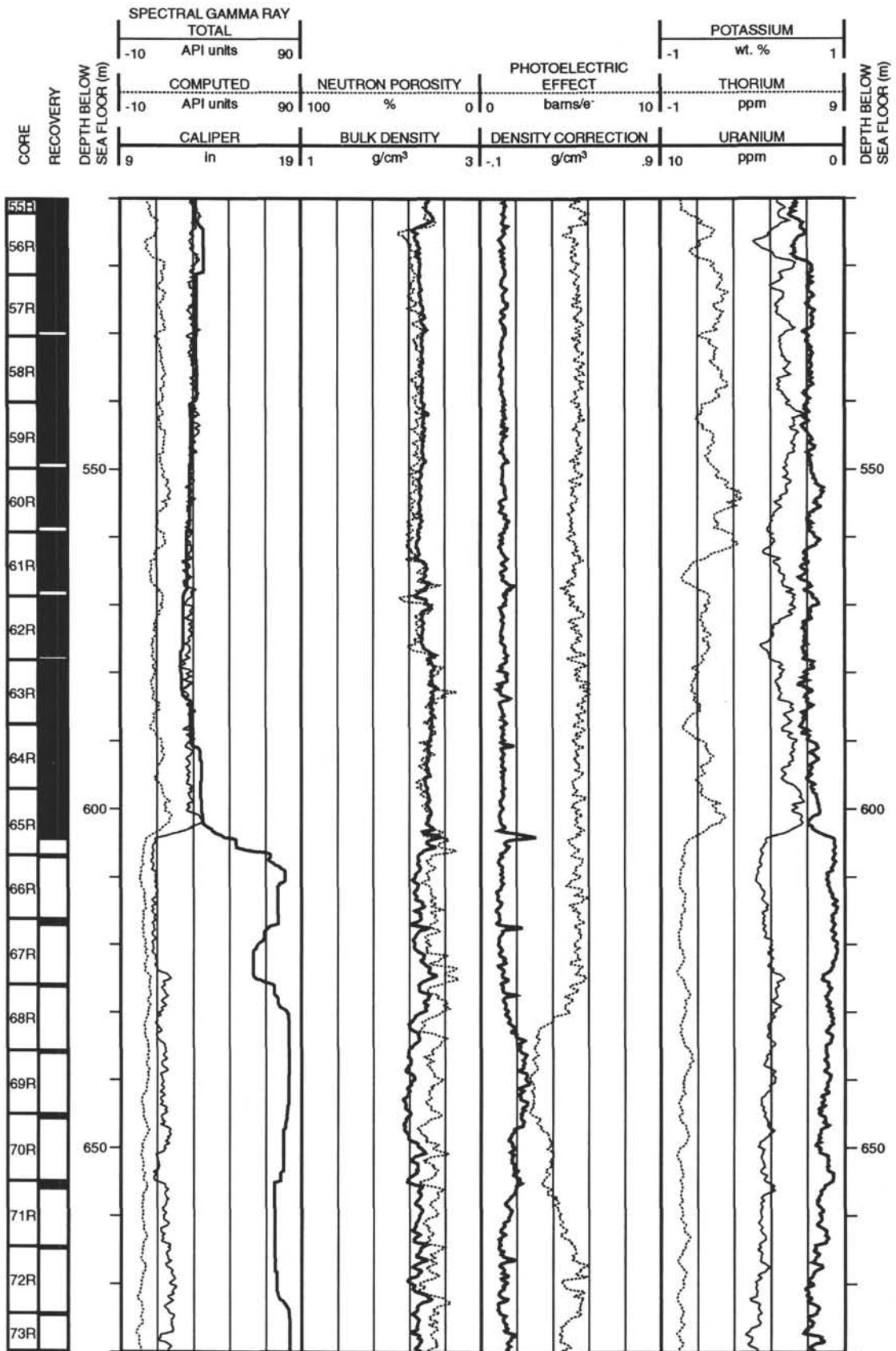
Hole 878A: Density-Porosity-Natural Gamma Ray Log Summary (continued)



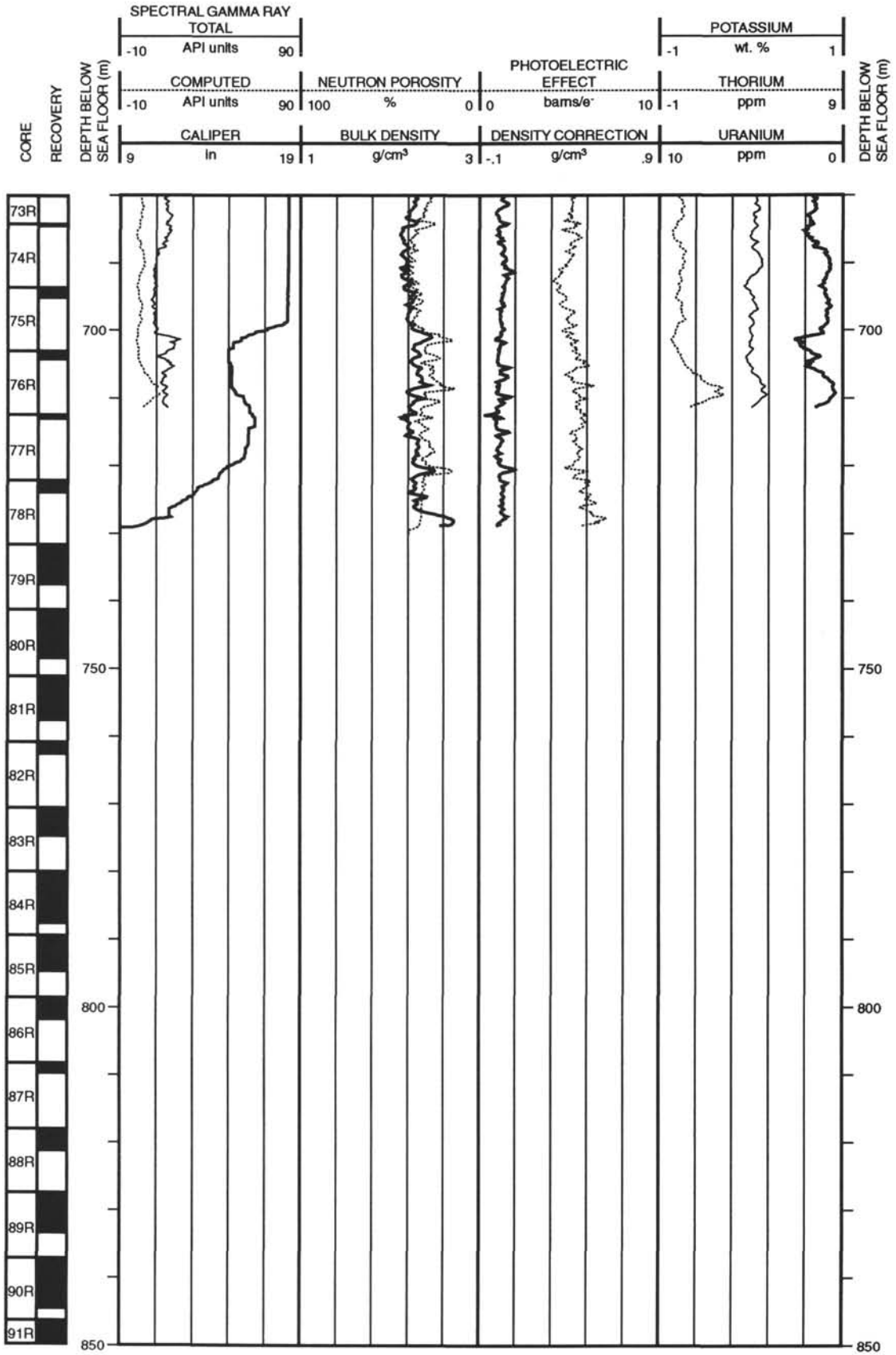
Hole 878A: Density-Positivity-Natural Gamma Ray Log Summary (continued)



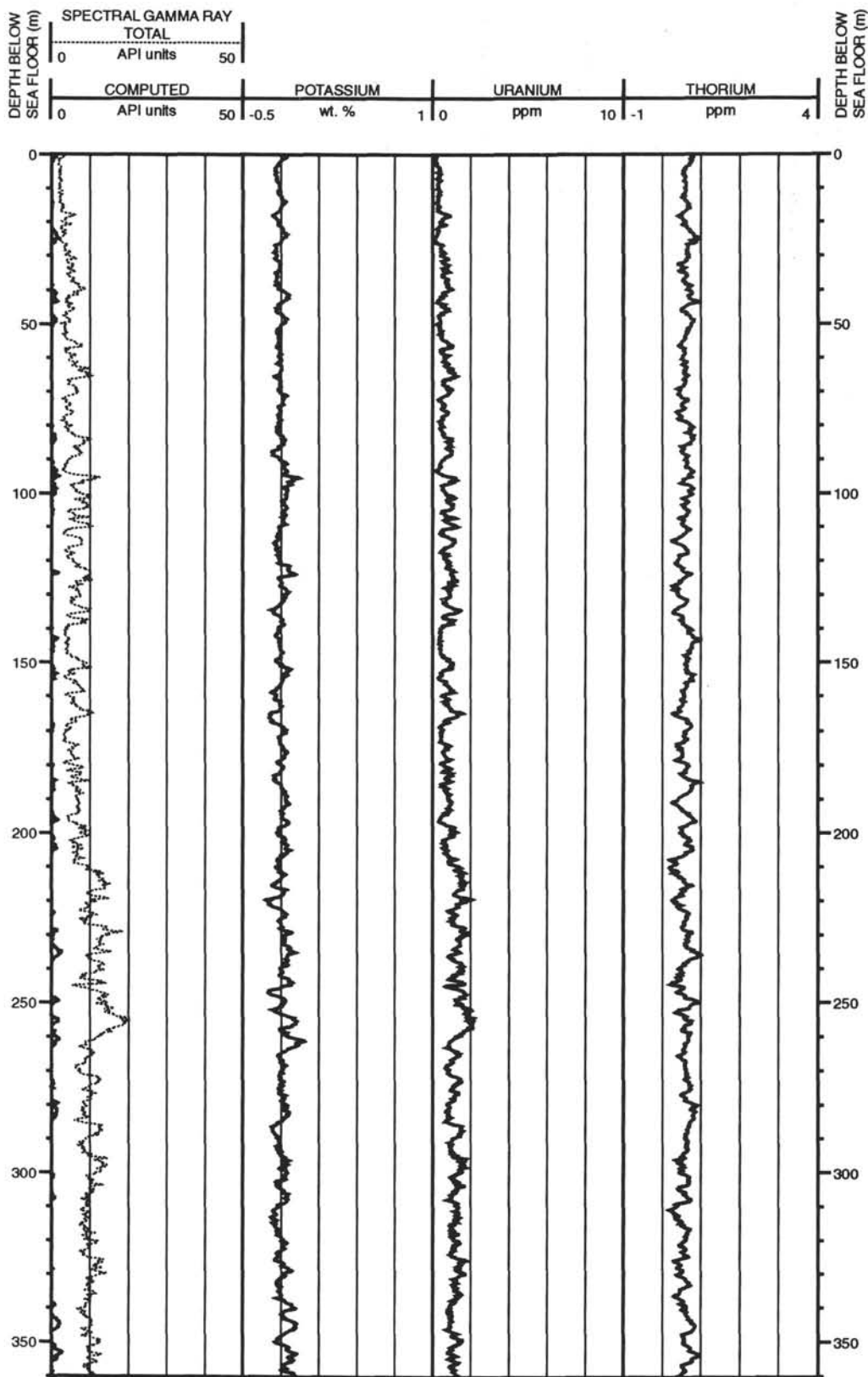
Hole 878A: Density-Porosity-Natural Gamma Ray Log Summary (continued)



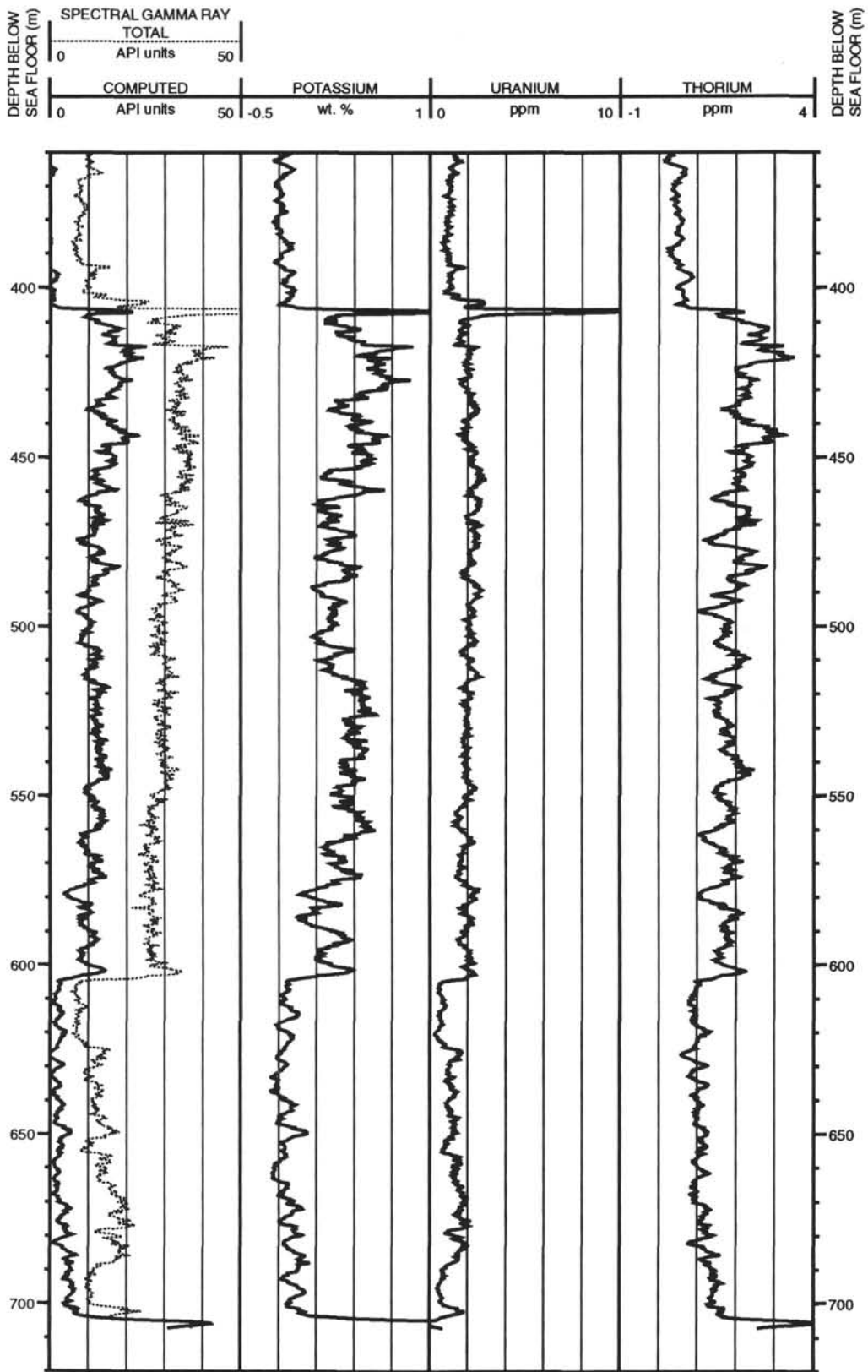
Hole 878A: Density-Porosity-Natural Gamma Ray Log Summary (continued)



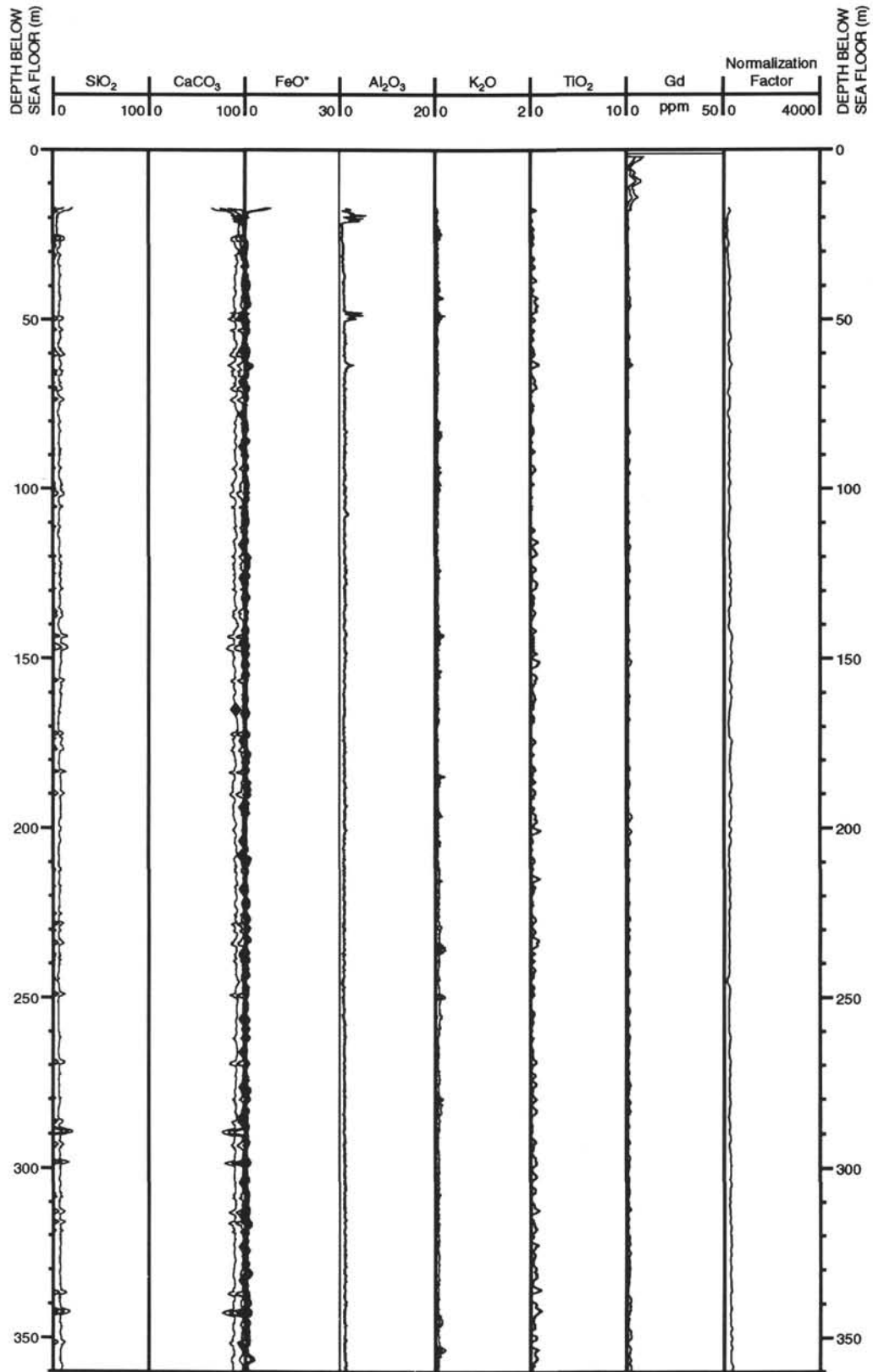
Hole 878A: Geochemical Log Summary



Hole 878A: Geochemical Log Summary (continued)



Hole 878A: Geochemical Log Summary



Hole 878A: Geochemical Log Summary (continued)

